Analysis and design of side-by-side mooring arrangements for LNG transfer

Frequency And Time Domain Hydrodynamics

M.V. Popiniuc

TU Delft

Analysis and design of side-by-side mooring arrangements for LNG transfer

Frequency And Time Domain Hydrodynamics

by

M.V. Popiniuc

to obtain the degree of Master of Science
at the Delft University of Technology

Student number:	4751094	
Project duration:	April 1, 2019 – January 20, 2020	
Thesis committee:	Prof. dr. ir. M.L. Kaminski,	TU Delft, chairman
	Dr. ir. J.H. den Besten,	TU Delft, daily supervisor
	Dr. ir. S.A. Miedema,	TU Delft
	Dr. ir. G. Gkikas,	SBM Offshore, daily supervisor
	ir. J. Pinkster,	SBM Offshore, supervisor

This thesis is confidential and cannot be made public until January 31, 2025.

TU Delft

Preface

This research project is part of the Master Program of Maritime Technology within the 3ME department of TU Delft University.

The thesis report represents the ending of a chapter from my student life and starting-up my carrier in this fascinating domain. The entire forming period of two years consisted of hard working, challenging projects and courses, which helped me to achieve knowledge and personal experiences and to shape myself as an engineer.

First of all I would like to thank to my professors Mirek Kaminski and Henk den Besten for the guidance and motivation during the project. A special thanks to the entire hydrodynamic department from SBM offshore for critical and brainstorm sessions. In particular to my daily supervisor Georgios Gkikas, Jessus Navarro Rodriguez and Hilmi Sukri for sharing their experience and regular guidance which helped me to contour this project.

I would also like to acknowledge my former professor from Romania, Dan Obreja who inspired and motivated me to continue my studies with the master degree at TU Delft.

Last but not least I would like to thank to my partner George for all his support and encouragement during this intense journey. Furthermore special thanks to family and relatives, friends and colleagues which helped me to overcome the challenges during this period in the Netherlands.

M.V. Popiniuc
Delft, January 2020

Abstract

The aim of this study is to conclude which parameters are influencing the most the hydrodynamic interaction between the two moored vessels in side-by-side configuration using frequency and time domain simulations. Furthermore to show what is the added value of the hydrodynamic input used in time domain investigations using 2 different integration schemes. Ultimately identify what is the impact on the mooring arrangements and what it needs to be done to ensure safe offloading operations.

During the offloading process (18 to 24 hours), the transfer equipment needs to accommodate the relative motions between the two vessels. There are several parameters which might influence the operations, which are dependent on the location (i.e. environmental conditions) and on the mooring system (i.e. vessels size, draft, mooring arrangements, etc.).

The side-by-side mooring system analyzed consists of a turret moored FLNG and various size of off-take carriers. A sensitivity analysis is done with respect to the physical parameters (i.e ship dimensions, loading conditions and separation distance) and modelling parameters (i.e parameters dependent on damping factor) in order to determine the effects on the first and second order quantities using frequency domain analysis. This represents the input for time domain numerical investigations in order to assess the relative motions and line tensions under certain environmental conditions.

It is known that the diffraction-radiation tools overestimate the results in the gap region. This is an effect of using potential flow which do not count for viscous effects. To overcome this problem and to describe in a realistic mode, multiple methods or numerical techniques has been proposed. With this regard a detailed numerical investigation has been carried out to conclude what is the impact of varying the dissipation factor (i.e between 0 and 0.4) on first and second order quantities.

Traditionally, the relative motions are determined using experimental tests which might be time-consuming. In particular for sensitivity analysis, numerical investigations are preferred in order to shape a main conclusion. Ultimately some of the results can be validated thorough experiments.

The hydrodynamic interaction revealed important aspects, especially with respect to the off-take carrier. If the carrier is smaller the impact is higher due to the presence of the FLNG. Such that the carrier rolls significantly when there are head or following seas. Furthermore decrease in heave motion of the FLNG at the resonance frequency due to the roll of the carrier has been noticed. The same phenomena occur for heave of the carrier. Thus, this represents a strong coupling between heave-roll motion of the two vessels. Another important aspect revealed is with the respect to the shielding effects under beam conditions. In general FLNG is slightly influenced by the presence of the carrier. In particular, it can be noticed only when it is in ballast condition due to the fact that the draft and thus the displacement of the carrier is considerably higher.

The sensitivity analysis points out that the modelling parameters (i.e dissipation factor) does hardly influence the response of the vessels even if it is considered or not. On the other hand drift forces are highly dependent on these parameters as a consequence of sharp changes of the wave elevations between the vessels. Such that if there is no dissipation factor to damp the wave elevation the resulted forces are extremely high compare to the cases where the dissipation factor is different than 0. This occurs only at the wave gap resonance and towards higher frequency region when diffraction effects are important. This is emphasized by the time domain analysis which prove that under the sea-states close to the gap resonance the lines and fenders tension reaches extreme magnitudes. Outside the gap resonance the relative motions and tensions are not influenced by the variation of the dissipation factor.

The moored system (i.e FLNG-LNGC or FLNG-LPGC) is governed relatively by long crested waves. Thus it is expected to have higher line loads under these sea-states. The actual mooring design shows that under squall conditions (i.e Tp of 14s) the mooring lines exceeds the

safe working limit for the FLNG-LNGC, while for FLNG-LPGC exceeds the minimum breaking load. In terms of relative motions for the same environmental conditions, the criteria is not satisfied.

The proposed optimization of the mooring lines does bring reduction in the mooring line tensions, but not enough to drop below safe working limit for FLNG-LPGC configuration. On the other hand for FLNG-LNGC, the line tension is within the limits, but the relative motions still exceeds the criteria. Therefore choosing the optimum mooring configuration is a trade-off between line stiffness and location of the connection points of the mooring lines which sometimes may lead to unpractical solutions.

Contents

1

Introduction

On the last few years due to the new regulations and restrictions from the environmental organizations and classification societies became stricter. Therefore the demand for clean energy, such as LNG (liquefied natural gas) became higher. The prospects about the LNG consumption-demand are expected to grow really fast across the world. The forecast for the natural gas and LNG demand for the next few years is presented in the table below [12].

Figure 1.1: Side-by-side offloading operation[41]

	since 2000 (per year)	until 2035 (per year)
Natural gas	2.7%	1.6%
LNG	7.6%	5-6%

Table 1.1: Global demand of Natural Gas and LNG [12]

Therefore the offshore companies triggered the attention toward the gas fields - extracting, processing and delivering. To cover such demand on the market, the offloading process and the transport facilities need to be efficient.

The import of the LNG can be done directly using subsea tieback to onshore terminals or either offshore system configurations. The downside of the onshore terminals is that are not flexible, especially in the areas where significant amount of resources were found and the subsea infrastructure facility is not feasible neither economical. Therefore in this sense, the offshore offloading systems are preferred and the gas assets to be delivered to the shore location.

In general, the offloading process can be done by various methods such as: tandem, side by side, catenary anchor leg mooring, soft mooring.

The offloading operation from an LNG should be done very carefully because the flow lines have to overcame an extremely low temperature. Furthermore the gap distance and arrangement is restricted by the arm-length of the off-loading arms. Taking into account those restrictions, the most feasible option for offloading is side by side arrangement (Figure 1.1).

The shuttle tanker(LNG carrier) approaches slowly from astern the FLNG, then the fenders are released and placed between the ships in order to absorb the impacts. When the shuttle tanker is parked in close proximity and parallel to the berthed LNG-FPSO, they are moored in side by side configuration. Usually the separation distance between the two vessels is directly proportional to the designed fender diameter.

1.1. Research problem

The major interest is to ensure a safe and reliable transfer operations. Therefore the hydrodynamic interaction between the two-vessels needs to be evaluated in order to determine the criteria for a safe operation and designing the optimum mooring system. Usually, the cryogenic manifolds are very sensitive and the offloading process is limited only to benign weather conditions such that to be able to conduct safely transfer operations (upon a certain level of workability in function of the field location, but even though the interaction effects cannot be neglected.) Moored vessels in open sea are subjected to wave loading at various frequencies, which induce motions on the floating body and implicit its mooring system. The hydrodynamics of two vessels in side-by-side configuration is a problem more complex than for a single body. The challenge is due to the strong hydrodynamic coupling effects, the shielding effects and the wave gap resonance that occurs between the two floating bodies. To solve the hydrodynamic interactions is required a coupled 12 by 12 system of dynamics equations which make the. The first order wave forces and wave drift forces are influenced by the resonance phenomenon which are reflected into vessels and mooring system motions. Furthermore, the relative position of the vessels changes continuously (draft variation) during offloading operations. Another important aspect are the shielding effects and non-liniearities due to the mooring system. In order to be evaluated, time domain analysis is required. Furthermore a good prediction of hydrodynamic interaction, ensure safe and efficient offloading operations. Good estimation of horizontal drift forces helps to reduce the DP power and tension in lines.

To quantify all the effects on the mooring system configuration, a parametric investigation with respect to gap parameters(dissipation factor, length and separation distance), vessel's loading conditions and size needs to be carried out. In general, to asses the sensitivity of multiple parameters, numerical simulations are preferred because requires lower cost and are faster compare to the experimental tests or full scale measurements, especially in the basic design stage. To indicate the (environmental) loading conditions on the moored vessel and shuttle tanker, the environmental site location specifications are used. The hydrodynamic numerical solutions of the system configuration is investigated with the help of a panel method solver (Hydrostar). This consists in a 3D frequency domain diffraction-radiation potential theory for wave-body/multi-body interaction problem. First order and second order wave loads, motions of the floating bodies can be evaluated in deep or finite water depth considering forward speed or not or tanking into consideration the dynamic effects given by the liquid motion in the tanks [36]. However the non-linear effects (non-linear restoring forces) of the mooring systems are not included within this method, therefore a time-domain mooring analysis solver is recommended to be used.

Considering the potential flow theory, design parameters and environmental conditions, can drive to multiple uncertainties. In order to define/establish the optimum mooring arrangement and the effects of the parameters mentioned before needs to be quantified.

1.2. Research question and objectives

The main goal of this research study is to establish the:

- effects of hydrodynamic interaction between two vessels
- parameters which are sensitive for side-by-side operations considering first and second

order response

In order to asses the main goals of the study, the following question is formulated:

What are the sensitive parameters and what are the effects on side-by-side mooring system configurations (analyzed in time domain), considering that the potential theory is used in order to estimate the first and second order response?

In order to answer the research question, the following objectives are established:

- analyze and investigate the hydrodynamic coupling between side-by-side vessels;
- analyze and investigate the shielding effects and draft variation during offloading operations;
- analyze and investigate the influence of the resonance gap and gap parameters (dissipation factor, separation distance and gap length) between the two vessels on the hydrodynamic coupling response;
- conclude what are the effects of hydrodynamic input on time domain analysis;
- quantify the differences between time domain decoupled and coupled analysis;
- investigate the influence of the design parameters of the mooring lines (length, material, orientation/position) with respect to the loading response.
- to establish an optimum mooring configuration arrangement for side-by-side offloading operations using the numerical method approach based on coupled and decoupled scheme

Achieving these objectives, the maximum limiting response can be determined and it will allow to determine and select the most appropriate mooring system configuration from safety and operational perspective.

2

Literature review

2.1. Introduction

In order to establish the required equipment that is necessary to perform safe operations (i.e fenders, mooring lines,tugs, etc) is important to understand the hydrodynamic interactions between the vessels. This provides a feasible design for certain sea states (i.e site location of the moored system) and helps to establish a plan for safe offloading operations.

In the recent years, this subject was treated with great interest as this concern a complex hydrodynamic problem, exposed to open seas, which faces many challenges. The main important parameters that needs to be predicted are: the relative motions between the vessels, tension in the mooring lines, gap flow which forms between the two vessels. These will be detailed in the next sections.

2.2. Side by side hydrodynamics

Kim et. al [28] in their paper found out that the interaction between the vessels is strongly coupled such that in head waves sway and roll motion is no longer zero as for single vessel. Furthermore the resonance peak for sway motion appears to be towards the higher frequencies (relatively short waves). Regarding the carrier, this experiences lower motions on the lee-side than on the weather side due to sheltering effects. Another important aspect mentioned by them is that the FLNG experiences the same motions with or without in presence of the carrier, with few exceptions (for few frequencies) which causes the hydrodynamic interaction between them.

Hohn Gould [17] investigated also the shielding effects on the carrier. This phenomena can influence the response of the LNG carrier, but is strongly depended on the wave heading. The main observation made is that the shielding effects for lower frequencies are not visible, while for the resonant frequency a lower peak response can be identified. The reason behind is that swell wave energy (waves with frequencies<0.55 rad/sec) passes easily under the FLNG vessel. Above the resonance frequency, towards higher frequencies, the shielding effects are 100%.

During offloading operations, the monitoring system measures continuously the relative motions between the vessels such that to avoid any collision impact or damage of the loading arm systems. Prior to site operations, in the project design stage, the relative motions represents one of the governing parameter which determines the operability of the offloading operations and avoid any undesirable extreme relative motions. According to Kim et. al [28] the relative motions does not appear neither on low nor on high frequency region if the vessels are on phase. this most likely happens if the vessels motions are out of phase. Usually in beam waves is expected to have the highest relative motions, in particular on carrier's weather side and significant longitudinal relative motions governed by head and bow-quartering waves as observed also by Kim et. al [28] their paper. However the probability of beam waves occurrence is small as the FLNG is turret moored and has capability to control the bow-heading angle against the incoming waves.

Brun et al. [5] divide the interaction between two vessels in side by side configuration as follows: mechanical interactions - due to the mooring-fender system and hydro-aerodynamic interactions - influence of wind, wave and current.

Zhao et. al [46] performed numerical analyses of multiple bodies moored in closed proximity. The separation distance between them is equal to the fender diameter (4m) and the system is analysed in irregular waves system with a 2.5m wave height and a peak period of 10s approaching from stern, with current and steady wind. The main conclusions on their study is that hydrodynamic interactions between the two vessels can affect the phase of the low frequency motions (i.e surge, sway, yaw), while the phase of wave frequency motions (i.e roll, heave, pitch) are less influenced. Generally the stern mooring lines are more loaded than the ones in the bow of the vessels. Regarding the fenders, it seems that the loads which are acting on the fenders are similar to impulses rather than continuous series. Furthermore, Brun et. al [5] emphasis that the mooring lines are not sensitive to the in-phase motions bu to the out-of-phase motions.

It has been proven that the hydrodynamic interactions have an effect on relative phase for the low frequency motions, while for wave frequency motions can be considered negligible. Moreover the interactions between 2-body system bring an increase in hawser loads.

Wang et. al [39] carried out numerical simulations for different separation distances (i.e from 4m to 20m) and also single vessel only in order to determine the hydrodynamic influences of multi-body system, especially for forces from horizontal plane(i.e surge,sway,yaw). The main conclusion of their study is that there is a strong hydrodynamic coupling such that the yaw and sway for a symmetrical vessel wrt. XoZ plane is no longer zero as for single vessel case. Furthermore, by decreasing the gap between the two vessels, yaw motions becomes larger while the peak frequencies tend to be higher. The worse case scenario is defined by the beam waves due to the severe fluid motion (reflection and radiation) which occur between the vessels. Regarding the drift forces, they showed that at high frequencies, the drift forces for multi-body case can experience large sharp peaks, especially when the natural period of the incoming wave is close to the resonant gap. In particular, seeing from sway drift forces, the ships are pushed away from each other. Therefore the most important parameters of side-by-side moored vessels are the gap distance and the incoming wave direction. In operations the governing incoming wave should be stern or head waves.

The side-by-side offloading system does not have a great impact on the pitch motions because the power spectral densities are close to their natural frequency [44].

Yan et al. [42] investigated the interaction between two floating structures moored in side-by-side configuration using a fully nonlinear potential theory. They used oblique monochromatic waves field for various wave amplitudes, frequencies and angle of incidence. Their results show how important are the nonlinearities and how the wave loads change with the wave direction. This confirm that a fully nonlinear theory may capture the high order components which are considerably large. However their study has not been validated yet with experimental tests.

2.3. Side-by-side modelling and validation

The wave fluctuations between the two vessels moored in side-by-side configuration is really important to be accurately estimated. It is known that this affects both the first and second order wave forces which consequently may alter the prediction of the vessel motions, especially the relative ship motions and the mooring line tensions. The diffraction-radiation tools overestimate the results in the gap region. This is an effect of using potential flow which do not count for viscous effects. To overcome this problem and to describe in a realistic mode, multiple methods or numerical techniques has been proposed. First method was proposed by Huijsmans et al.(2001) [18], by implementing a rigid lid condition to the free surface analogous to the irregular frequency suppression technique. The free surface condition is by imposing zero wave elevation in the gap region. In contrast to this method, Newman(2003)[22] introduced a linear damping coefficient in order to control the wave amplitude over the gap region. Another method, was proposed by Chen(2005)[8] who formulated a boundary condition for this area including a linear dissipation term. An advantage of this

method is that there is no extra degree of freedom added to the model and the effect of lid damping is included in all hydrodynamic coefficients. Extensive research has been done with this respect.

Kim et. al [28] developed a tool based on three-dimensional potential theory and three-dimensional source distribution technique which is validated using the well-known experimental and numerical results. The validation regards the vessels motions response and the relative motion between vessels under regular and irregular waves (i.e Jonswap spectrum). Their tool presents good correlation between experimental results and the other available diffraction tools.

Buchner et al. [3] performed model tests in order to validate a numerical time domain model. They introduced a rigid lid on the free surface within the multi-body diffraction analysis such that to suppress the unrealistic resonant wave oscillations. The main conclusion of their work is that the quality of numerical results strictly depends on the use of appropriate damping factor which can suppress the unrealistic wave phenomena. However the use of surface lid shown important improvement on the drift forces and relative sway and yaw moments. Furthermore a good prediction of the low frequency motions in numerical simulation needs to have an input of viscous damping in horizontal plane based on experimental tests.

Since there is no theoretical solution that can establish the required value of damping parameter for each specific configuration(i.e different separation distance) ,Pauw et al. [40] carried out experimental tests in order to determine this value. They replace the rigid lid with a numerical damping lid. For experiments they considered one carrier positioned parallel to a wall in order to simulate the presence of the other vessel. While for numerical configurations, they used a symmetric side-by-side configuration (two identical carriers) has been proposed with a separation distance of 4m. The main conclusion was that there is no unique value for dissipation factor (ϵ) does fully cover the comparison with the measured results for gap distances smaller than 25 meters. Furthermore they suggest that the tunning of the damping value should be with done with respect to second order quantities (i.e bigger impact) and not first order loads.

Naciri et. al[27] has performed a numerical study using three different diffraction programs (i.e AQWA, LIFSIM, aNySIM) for a side-by-side moored system in intermediate water depth. Their results gives similar values in all three both from statistical point of view and also time trace. However differences in the extreme load lines can be observed. This is explained by the smaller differences between numerical solvers such as: interpolation of the wave forces, fender friction model,etc. However the relative motions are very sensitive to these small variations.

Fournier et. al [20] investigated the gap resonance through experimental and numerical simulations using diffraction tools (i.e Wamit and Hydrostar). Experimental tests has been carried out using 20m and 25m separation distance between vessels. The measured wave elevations between the two vessels shows that this can be two times higher than the incident wave height. Furthermore the gap resonance affects both the first order motion response and second order loads. Thus is most likely to affect the relative motions at the loading arm and the mooring line loads. They identified a single value of dissipation factor(i.e 0.1) that can be used for both quantities first and second order loads which gives good agreement with the experimental tests in spite the fact that this factor is applied at the water surface only (away from the dissipation actually takes place, near the bilge keels). This is a lack of diffraction tools which does not account for viscous dissipation such that linear damping coefficients needs to be determined from experiments.

Chen et. al [43] analyzed the effect of dissipation factor against measurements. They proved that the numerical computations gives good agreement with experimental results. Furthermore they showed that away from resonance the free surface dissipation is not affecting the sway, heave motion response. They also found out that the gap resonance is not only affecting the wave field but also the 1st order motion response (i.e for certain degrees of freedom) and sway mean drift. Furthermore they investigated the effect of liquid motion in tanks for vessel with single row tank arrangement under beam waves condition. The filling rate is 30% of of the height of the prismatic tanks. At low frequencies, this can be treated as a solid mass. However at the resonant frequency, the inertia increases rapidly without

limitation and is creating the so-called ”sloshing effect”. Such that this variation of inertia modify the roll response of the vessel. Towards higher frequencies, the large negative values of the inertia due to motion in tanks yield to a second peak in the roll response of the vessel which is a resultant between total inertia force and the stiffness force of the vessel. Thus, by considering the dynamic effects of liquid motion there are expected two peaks: one considering the peak response of the vessel itself and the other one caused by tank resonance which is slightly reduced. This phenomena can highly influence the second order low-frequency loads of the vessels.

Diebold et. al [26] investigate the effect of sloshing for double row tank arrangement with 50% filling rate of their height. They used diffraction solver and show that the coupling effect between sway-roll motion does not affect the motion response. Furthermore an extensive research did with respect to regular and irregular excitation forces for prismatic tanks using CFD tools (OpenFoam), experiments and semi-analytical solutions (Wagner). Their main conclusion of the study is that the global flow inside the tank can be predicted accurately with the means of CFD tools for various amplitudes and harmonic or irregular excitations. Good agreement between peak impact pressure (drop test) for smooth wedge (ie. dead rise angle of 10deg.) calculated with CFD and Wagner solution has been found.

Another research regarding the sloshing phenomena inside the tanks is made by Hohn [17]. He shows that this affects the roll motions of the LNGC, especially in beam seas with 10% filled tanks, roll motion is considerably higher. Furthermore, due to the coupling effects, the roll response has two natural period peaks, one represented by the in phase roll-sloshing motion and the other one out of phase. With regards the coupling effects between vessels and sloshing in the tanks, the results, show that the more extreme case is or bow-quartering waves, where the highest roll-sloshing out-of-phase occur.

Gkikas [16] validate time domain simulations (ie. Ariane7) with experimental tests for a twin-hull LNG-FPSO in side by side offloading operations. Two sea states were considered: short waves (7s) and long waves (17s). For both of them, good agreement between measured and simulations results has been found. Regarding the wind and current coefficients for vessels based on measurements an empirical formulation can be used in order to account for the shielding effects. This shows that provides better estimates for mean heading and yaw motion.

The friction of the fenders represent a source of damping which may affect the estimation of horizontal motions, especially for surge. For relative sway, beside the effect of fender friction, the water moving in and out of the gap results in a dissipation of energy. This is an important aspect mentioned by Gkikas [16] in his paper. According to him the stick-slip phenomena results in non-negligible forces along the longitudinal axis. However the time domain tool does not take into account this friction effect of the fenders and it can overestimates the horizontal excursions. A solution can be by implementation of a viscous damping which can accounts for both the hull viscous damping and fender friction based on experimental tests.

2.4. Offloading arms limitations

Cryogenic loading arms are used on floating terminals, generally in pair of 4 16inch are required on board. Three of them are used for loading the cryogenic liquefied natural gas and one for vapor return. In general the maximum allowable criteria for safe side-by-side operations is governed by the allowable motion envelope of the loading arms. Naciri et. al [27] presents the the criteria under side-by-side offloading operations can be safely conducted based on Van der Valk studies: low frequency horizontal relative motions $\pm 4m$ wave frequency horizontal and vertical relative motions $\pm 2m$.

Kim et. al [28] establish a lateral and vertical motion criteria of 1.7m and 2m respectively. While the lateral and vertical acceleration a criteria up to $0.5\text{m}/s^2$.

According to American Petrolium Institute(2001) the side-by-side offloading operation is restricted only for head seas condition with a significant wave height up to 2.4m

Arjan et. al [1] showed that the offloading is possible for significant wave height more than 3m in collinear environmental conditions for almost head on.

Conventional side-by-side mooring is possible for waves up to 2.5m significant height and

wind speed up to 30knots. However, Naciri et. al [27] proved that is possible for significant wave height above 3m due to higher nylon tail lengths (i.e 25m).

2.5. Side-by-side mooring lines and fenders

Jeong et.al [35] carried out mooring analysis using time domain simulations with the aid of SIMO software (Kaasen and Mo [25]. The results are validated using another commercial software (Shuttle developed by Bunnik et.al [40]) where both tension in lines and fender loads are in good agreement. They showed that by decreasing the angle with the longitudinal axis of the breast line, the dynamic tension also decrease. However, regarding the fenders it shows the opposite trend. Thus an optimized mooring arrangement with respect to site-specific environmental conditions is a trade off between all the systems involved (ie mooring lines, fenders, loading condition of the vessels, etc) and it requires a complex design loop. In general breast lines tends to affect sway and yaw motions more than the spring lines.

Arjan et. al [1] investigate the on-site offloading operations measurements and feedback from mooring masters into simulation models. The effect of heading of the vessel on roll and breast line loads was analyzed for a 3m Hs and Tp of 12s. The results show that if the angle between current and wind direction is increasing, then the vessel's roll and the breast line load will increase as well. Furthermore they used the operational data from Liberdade in order to check with their developed tool. This shows that the loads in the line exceed the operational criteria for a significant wave height of 2.5m with a peak period of 7seconds or either 3m significant wave height and a peak period of 10 seconds.

Kim et. al [45] carried out a numerical study with respect to side-by-side mooring system optimization. They varied the stiffness of the mooring lines and showed that the relative motions are not sensitive to these variations.

Naciri et. al [27] gives as initial stiffness and line pretension in the neutral position in calm water at 15 tons. OCIMF also recommends an initial pretension of 5-15 tons. For their analysis used a 44mm steel wire with a SWL of 681kN which represents 55 % of MBL. Nylon tails which are used in order to introduce elasticity in high modulus wire lines(low stretch) which reduce the peak stresses, extends the service life and also provides safer operations. They considered a nylon tail length of 25m for each mooring line Pneumatic fenders are used wrapped in tyres with a 4.5m diameter (SWL = 2492kN at 55% of MBL).

3

Side-by-side hydrodynamics

3.1. Potential flow theory

In this chapter general aspects regarding the potential flow theory, starting from the laws of fluid mechanics, environmental loads(wave, wind,current) and ship response are presented, followed by the theoretical background of the numerical tools used for this project (Hydrostar, Ariane, Orcaflex). Simulations with numerical models are often referred as numerical experiments by analogy to classical experimental towing tests. In general, numerical calculations are performed to determine the response/behaviour of the analyzed case where multiple parameters are varied as a function of the interest problem. Numerical simulations are faster and less expensive compare to the experimental tests, especially when the number and complexity of parameters is relatively high. On the other side in both cases errors can appear due to multiple factors such as: how accurate is the set-up of the model, assumptions made, limitations (space, time, resources) of the model, etc.

In the figure below it is presented the inflow and outflow mass through the faces.

general continuity equation/mass conservation:

$$\begin{aligned} x: \frac{\partial m}{\partial t} &= [\rho u + \frac{\partial \rho u}{\partial x} dx] dz dy - \rho u dy dz = \frac{\partial \rho u}{\partial x} dx dy dz \\ y: \frac{\partial m}{\partial t} &= [\rho v + \frac{\partial \rho v}{\partial y} dy] dx dz - \rho v dx dz = \frac{\partial \rho v}{\partial y} dx dy dz \\ z: \frac{\partial m}{\partial t} &= [\rho w + \frac{\partial \rho w}{\partial z} dz] dx dy - \rho w dx dy = \frac{\partial \rho w}{\partial z} dx dy dz \end{aligned} \tag{3.1}$$

it reduces to:

$$\begin{aligned} x: \frac{\partial m}{\partial t} &= \frac{\partial \rho u}{\partial x} dx dy dz \\ y: \frac{\partial m}{\partial t} &= \frac{\partial \rho v}{\partial y} dx dy dz \\ z: \frac{\partial m}{\partial t} &= \frac{\partial \rho w}{\partial z} dx dy dz \end{aligned} \tag{3.2}$$

The continuity equation becomes:

$$\frac{\partial \rho}{\partial t} + \frac{\partial (\rho u)}{\partial x} + \frac{\partial (\rho v)}{\partial y} + \frac{\partial (\rho w)}{\partial z} = 0 \tag{3.3}$$

For an incompressible flow, where the density is constant, the above equation reduces to:

$$\frac{\partial u}{\partial x} + \frac{\partial v}{\partial y} + \frac{\partial w}{\partial z} = 0 \quad or \quad \nabla \cdot \vec{v} = 0 \tag{3.4}$$

And implicit Laplace equation, where the velocity potential $\Phi(x,y,z,t)$ is a function depended on space and time, and its property is that the velocity component in a point in the fluid in any chosen direction is simply the derivative of this potential function in that point to that chosen direction:

$$\nabla^2\Phi = \frac{\partial^2\Phi}{\partial x^2} + \frac{\partial^2\Phi}{\partial y^2} + \frac{\partial^2\Phi}{\partial z^2} \tag{3.5}$$

General momentum balance:

Newton's second law defines the rate of change of momentum of a fluid particle which is equal to the forces acting on that particle of fluid:

$$m\vec{a} = \sum \vec{F} \tag{3.6}$$

$$\rho dxdydz\frac{D\vec{u}}{Dt} = \sum \vec{F} \tag{3.7}$$

Where the acceleration of a fluid particle is given by the Lagrangian of the fluid velocity:

$$\frac{D\vec{u}}{Dt} = \frac{\partial u}{\partial t} + \frac{\partial u}{\partial x}u + \frac{\partial v}{\partial y}v + \frac{\partial w}{\partial z}w = \frac{\partial u}{\partial t} + (\vec{u}\cdot\nabla)\vec{u} \tag{3.8}$$

$$\begin{aligned} x: \rho dxdydz\frac{Du}{Dt} &= \left(\frac{\partial \rho u}{\partial t} + \frac{\partial \rho uu}{\partial x} + \frac{\partial \rho uv}{\partial y} + \frac{\partial \rho uw}{\partial z}\right)dxdydz \\ y: \rho dxdydz\frac{Dv}{Dt} &= \left(\frac{\partial \rho v}{\partial t} + \frac{\partial \rho uv}{\partial x} + \frac{\partial \rho vv}{\partial y} + \frac{\partial \rho vw}{\partial z}\right)dxdydz \\ z: \rho dxdydz\frac{Dw}{Dt} &= \left(\frac{\partial \rho w}{\partial t} + \frac{\partial \rho uw}{\partial x} + \frac{\partial \rho vw}{\partial y} + \frac{\partial \rho ww}{\partial z}\right)dxdydz \end{aligned} \tag{3.9}$$

Pressure forces:

$$\begin{aligned} F_{px} &= [p]dydz - [p + \frac{\partial p}{\partial x}dx]dydz = -\frac{\partial p}{x}dxdydz \\ F_{py} &= [p]dxdz - [p + \frac{\partial p}{\partial y}dy]dxdz = -\frac{\partial p}{y}dxdydz \\ F_{pz} &= [p]dxdy - [p + \frac{\partial p}{\partial z}dz]dxdy = -\frac{\partial p}{z}dxdydz \end{aligned} \tag{3.10}$$

Viscous forces:

$$\begin{aligned} F_{vx} &= \nabla\cdot\sigma = \nabla\cdot\mu\nabla u = \mu\nabla^2 u \\ F_{vy} &= \nabla\cdot\sigma = \nabla\cdot\mu\nabla v = \mu\nabla^2 v \\ F_{wz} &= \nabla\cdot\sigma = \nabla\cdot\mu\nabla w = \mu\nabla^2 w \end{aligned} \tag{3.11}$$

where the stress tensor is:

$$\sigma_{ij} = \begin{bmatrix} \sigma_{xx} & \tau_{xy} & \tau_{xz} \\ \tau_{yx} & \sigma_{yy} & \tau_{yz} \\ \tau_{zx} & \tau_{zy} & \sigma_{zz} \end{bmatrix} \tag{3.12}$$

External forces:

$$\begin{aligned} F_{gx} &= 0 \\ F_{gy} &= 0 \\ F_{gz} &= -[\rho g]dxdydz \end{aligned} \tag{3.13}$$

The final expression for the total forces becomes:

$$\frac{\partial u}{\partial t} + \vec{u} \cdot \nabla \vec{u} = -\frac{1}{\rho}\nabla p + \frac{\mu}{\rho}\nabla \cdot \nabla \vec{u} + \vec{F}_{ext} \tag{3.14}$$

The potential flow theory has the following assumptions:

- the fluid is inviscid - there is no viscosity considered in the fluid flow, therefore all the friction effects are neglected
- the fluid is irrotational - this is a fact that the fluid is frictionless and therefore the fluid flow is uniform, no vorticity involved
- the fluid is considered homogeneous, where all the particles has uniform properties in the fluid
- the fluid is incompressible, which means that the density is constant in the fluid

Euler equations:
Based on the assumptions stated above, the momentum balance for an ideal flow become:

$$\begin{aligned} x: \left(\frac{\partial \rho u}{\partial t} + \frac{\partial \rho uu}{\partial x} + \frac{\partial \rho uv}{\partial y} + \frac{\partial \rho uw}{\partial z}\right)dxdydz &= -\frac{1}{\rho} \cdot \frac{\partial p}{\partial x} \\ y: \left(\frac{\partial \rho v}{\partial t} + \frac{\partial \rho uv}{\partial x} + \frac{\partial \rho vv}{\partial y} + \frac{\partial \rho vw}{\partial z}\right)dxdydz &= -\frac{1}{\rho} \cdot \frac{\partial p}{\partial y} \\ z: \left(\frac{\partial \rho w}{\partial t} + \frac{\partial \rho uw}{\partial x} + \frac{\partial \rho vw}{\partial y} + \frac{\partial \rho ww}{\partial z}\right)dxdydz &= -\frac{1}{\rho} \cdot \frac{\partial p}{\partial z} - \rho g dxdydz \end{aligned} \tag{3.15}$$

where the velocity fields in each direction is described by the derivative of the potential function:

$$x: u = \frac{\partial \Phi}{\partial x}; \quad y: v = \frac{\partial \Phi}{\partial y}; \quad z: w = \frac{\partial \Phi}{\partial z}; \tag{3.16}$$

and

$$\begin{aligned} u\frac{\partial u}{\partial x} &= \frac{\partial \Phi}{\partial x} \cdot \frac{\partial^2 \Phi}{\partial x^2} = \frac{1}{2} \cdot \frac{\partial}{\partial x}\left(\frac{\partial \Phi}{\partial x}\right)^2 \\ v\frac{\partial u}{\partial y} &= \frac{\partial \Phi}{\partial y} \cdot \frac{\partial^2 \Phi}{\partial x \partial y} = \frac{1}{2} \cdot \frac{\partial}{\partial x}\left(\frac{\partial \Phi}{\partial y}\right)^2 \\ w\frac{\partial u}{\partial z} &= \frac{\partial \Phi}{\partial z} \cdot \frac{\partial^2 \Phi}{\partial x \partial z} = \frac{1}{2} \cdot \frac{\partial}{\partial x}\left(\frac{\partial \Phi}{\partial z}\right)^2 \end{aligned} \tag{3.17}$$

If equation 3.16 and 3.17 is plugged in equation 3.15, then the momentum balance become:

$$\begin{aligned} x: \frac{\partial}{\partial x}\left(\frac{\partial \Phi}{\partial t} + \frac{1}{2}\left[\left(\frac{\partial \Phi}{\partial x}\right)^2 + \left(\frac{\partial \Phi}{\partial y}\right)^2 + \left(\frac{\partial \Phi}{\partial z}\right)^2\right] + \frac{p}{\rho}\right) &= 0 \\ y: \frac{\partial}{\partial y}\left(\frac{\partial \Phi}{\partial t} + \frac{1}{2}\left[\left(\frac{\partial \Phi}{\partial x}\right)^2 + \left(\frac{\partial \Phi}{\partial y}\right)^2 + \left(\frac{\partial \Phi}{\partial z}\right)^2\right] + \frac{p}{\rho}\right) &= 0 \\ z: \frac{\partial}{\partial z}\left(\frac{\partial \Phi}{\partial t} + \frac{1}{2}\left[\left(\frac{\partial \Phi}{\partial x}\right)^2 + \left(\frac{\partial \Phi}{\partial y}\right)^2 + \left(\frac{\partial \Phi}{\partial z}\right)^2\right] + \frac{p}{\rho}\right) + \rho g z &= 0 \end{aligned} \tag{3.18}$$

From equation 3.20 Bernoulli equation can be identified:

$$\frac{\partial \Phi}{\partial t} + \frac{1}{2}\nabla^2\Phi + \frac{p}{\rho} + gz = C(t) \tag{3.19}$$

3.2. Regular Waves and Wave Potential

The ocean waves are governed and generated by multiple factors(heat transfer, mass and momentum flux, etc.), due to the hydrodynamic coupled system between ocean and atmosphere. In general they are classified by their main restoring force as follows [32]:

- **Sound waves:** these types of waves are governed by the compressibility of the water. Since the water cannot be compressed, therefore, the probability of occurrence this type of waves is really small
- **Capillary waves:** these are high frequency waves generated by the turbulence wind where the surface tension play an important role as the restoring force
- **Gravity waves:** when the capillary force (surface tension) of the water become insignificant, the gravity become the main generator factor of waves. They can be splited in two types:

  - surface gravity waves: generally are generated by the wind and can be observed at the water interface

  - internal gravity waves: can be observed at the interfaces of stratified fluids
- **Planetary (Rossby) waves:** due to changes in depth or latitude there is a variation of the equilibrium potential vorticity that creates this type of waves

Figure 3.1 presents a general overview of the wave types and formation as a function of frequency (period). In general for offshore industry, the major interest of research is for gravity waves which cause the biggest influence on the structures.

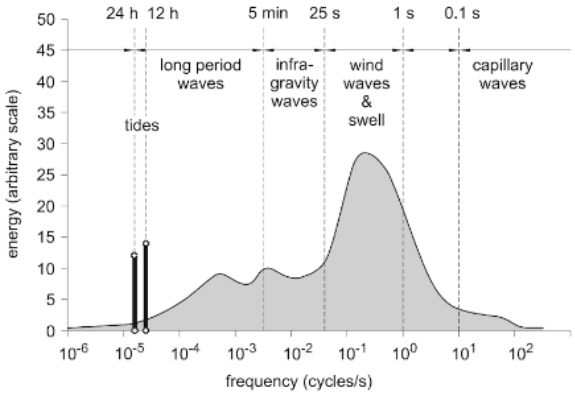

Figure 3.1: Schematic distribution of wave-energy in frequencies[32]

Wind waves can be classified in two categories:

- Sea
- Swell

The linear wave theory (Airy wave theory) can solve for surface gravity waves, where the waves are not steep neither in very shallow waters.

To get the expression that describes the waves it needs to be solved the mass and momentum conservation, explained in more details further in this chapter, where specific boundary conditions (kinematic and dynamic) are applied. The main assumption of this theory is that

the the amplitude of the wave is relatively small compare to the wave length and to the water depth, such that the wave profile can be described as a cosine or sine profile. Furthermore, the linear wave theory is based on potential flow and they are governed by gravity (ie gravity waves).

Therefore the wave potential can be written as a mathematical function as follows:

$$\Phi_w = P(z) \cdot sin(kx - \omega t) \tag{3.20}$$

where P(z) is the unknown function In order to get the function P(z) the velocity potential of the harmonic waves has to fulfil 4 requirements/conditions:

a) Laplace equation/continuity equation

From Laplace equation, it is obtained the homogeneous solution (equation 3.22)

$$\nabla^2\Phi = \frac{\partial^2\Phi}{\partial x^2} + \frac{\partial^2\Phi}{\partial y^2} + \frac{\partial^2\Phi}{\partial z^2} \tag{3.21}$$

$$\begin{aligned} \frac{d^2P(z)}{dz^2} - k^2P(z) = 0 \\ P(z) = C_1e^{+kz} + C_2e^{-kz} \end{aligned} \tag{3.22}$$

therefore the wave potential become a function of 2 constants:

$$\Phi_w(x,z,t) = (C_1e^{+kz} + C_2e^{-kz}) \cdot sin(kx - \omega t) \tag{3.23}$$

In order to get the final expression for the wave potential, the constants C_1 and C_2 has to be identified. Therefore the seabed boundary condition is applied.

b) Seabed boundary condition

$$\begin{aligned} \frac{\partial\Phi_w}{\partial z} = 0 \quad at \quad z = -h \\ k \cdot C_1 \cdot e^{-kh} - k \cdot C_2 \cdot e^{kh} = 0 \quad at \quad z = -h \end{aligned} \tag{3.24}$$

it is used the mathematical notation, in order to get the trivial solutions for C_1 and C_2 as follows:

$$\begin{aligned} C_1 \cdot e^{-kh} - C_2 \cdot e^{kh} = \frac{C}{2} \\ C_1 = \frac{C}{2} \cdot e^{kh} \quad and \quad C_2 = \frac{C}{2} \cdot e^{-kh} \end{aligned} \tag{3.25}$$

Making use of hyperbolic function and the trivial solutions, the wave potential becomes:

$$\Phi_w(x,z,t) = Ccoshk(h+z) \cdot sin(kx - \omega t) \tag{3.26}$$

where C is a constant and is still unknown yet

c) Free surface dynamic boundary condition

At the water surface the pressure is equal to the atmospheric pressure and the linearized (second order terms are considered small, therefore neglected) Bernoulli equation reduces to:

$$\begin{aligned} p = p_0 \quad at \quad z = \zeta \\ \frac{\partial\Phi_w}{\partial t} + g\zeta = 0 \quad at \quad z = \zeta \end{aligned} \tag{3.27}$$

The time depended part is decomposed using Taylor expansion

$$\left[\Phi_w(x,z,t)\right]_{z=\zeta} = \left[\Phi_w(x,z,t)\right]_{z=0} + \zeta \cdot \left[\frac{\partial \Phi_w(x,z,t)}{\partial z}\right]_{z=0} + \dots$$
$$\left[\frac{\Phi_w(x,z,t)}{\partial t}\right]_{z=\zeta} = \zeta \cdot \left[\frac{\partial \Phi_w(x,z,t)}{\partial t}\right]_{z=0} + O(\epsilon^2) \tag{3.28}$$

In equation 3.28 second order terms are considered very small, therefore the surface dynamic boundary condition can be expressed at the mean water level:

$$\frac{\partial \Phi_w}{\partial t} + g\zeta = 0 \quad at \quad z = 0 \tag{3.29}$$

where the wave elevation can be expressed as:

$$\zeta = -\frac{\partial \Phi_w}{\partial t}\frac{1}{g}$$
$$\zeta = \frac{C}{g}\omega coshkcos(kx - \omega t) = \zeta_a \cdot cos(kx - \omega t) \tag{3.30}$$

where the unknown constant C is equal to:

$$C = \frac{\zeta_a g}{\omega coshkh} \tag{3.31}$$

This gives the final expression for the wave potential:

$$\Phi_w(x,z,t) = \frac{\zeta_a g}{\omega}\frac{coshk(k+z)}{coshkh}sin(kx - \omega t) \tag{3.32}$$

d) Free surface kinematic boundary condition

$$\frac{dz}{dt} = \frac{d\zeta}{dt} + \frac{d\zeta}{dx}\frac{dx}{dt} \quad at \quad z = \zeta \tag{3.33}$$

According to the assumption that the wave steepness is small, the equation 3.33 reduces to, where is valid only at the mean water surafce:

$$\frac{dz}{dt} = \frac{d\zeta}{dt} \quad at \quad z = 0 \tag{3.34}$$

Equation 3.34 reduces to the Cauchy-Poisson boundary condition:

$$\frac{dz}{dt} = -\frac{\partial^2 \Phi_w}{\partial t^2}\frac{1}{g} \tag{3.35}$$

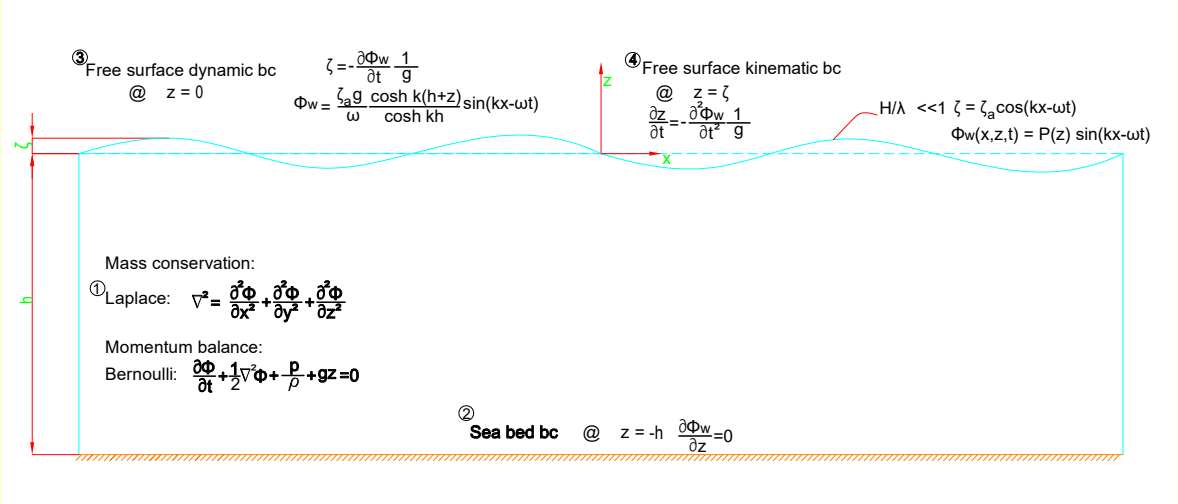

Figure 3.2: Potential theory - boundary conditions

3.3. Irregular Waves

The sea surface is represented by the irregular harmonic waves which can be represented as a linear superposition of a series of wave components. To do this, it is considered that the wave signal repeats itself after each long interval.

The wave elevation, that propagates in x-direction, of a long-crested irregular sea, represented in time domain, can be expressed as a sum of a considerable number of regular wave components:

$$\zeta(t) = \sum_{n=1}^{N} \zeta_{a_n} cos(k_x - \omega_n t + \epsilon_n) \tag{3.36}$$

where: ϵ_n - phase angle of the wave component n k_n - wave number component

To reproduce the entire time record at a certain water level, is needed to have enough Fourier series terms in order to capture all the /amplitudes. The amplitude ζ_{a_n} can be found by a Fourier analysis of the signal.

A wave spectrum describe an irregular sea/wave conditions based on statistics which uses a mean period and a significant wave height based on statistics. In this way, the energy component of each wave frequency can be described. Furthermore, the wave energy can be converted to time domain using Fourier transformations. The response spectrum can be found by multiplying the squared RAOs of the considered with the wave spectrum. This can be used in order to determine the displacements, velocities or accelerations of the considered body in a certain period of time.

It is considered that the wave system (input) is known based on statistics and wave field measurements on the specific location. In principle, a linear behaviour of the system means that the wave input is proportional to the motion output for each frequency. This system can be analyzed in frequency-domain and used to obtain the RAOs. If the wave system consists in an irregular wave field, then it can be still considered as a summation of multiple regular

waves (superposition principle). Therefore the time-domain wave record can be transformed into frequency-domain (wave spectrum) using Fourier transformation. The superposition principle is valid as long as there are no steep waves or shallow water regime neither rough sea conditions.

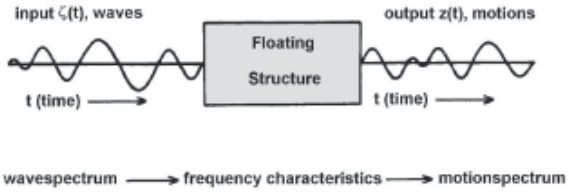

Figure 3.3: Relation between motions and waves[21]

3.4. Side-by-side Boundary conditions

Consider 2 rigid bodies floating (stationary) in an ideal fluid with harmonic waves in a finite water depth domain. The potential of both bodies is given by the definition of the linear potential theory, which is a superposition of the potentials due to the undisturbed incoming wave(Φ_w), diffraction potential(Φ_D) due to the incoming wave on the fixed body and the radiation potential(Φ_R) in still water due to the six body motions. Furthermore, because the two vessels are in close proximity, due to the shielding effects and reflection of the wave, there is a strong hydrodynamic interactions and each vessel suffers additional diffraction and radiation force.

Based on superposition principle, the total potential can be written as:

$$\Phi(x, y, z, t) = \Phi_w + \Phi_D + \Phi_R \tag{3.37}$$

Therefore finding the forces acting on the 2 body system can be divided into two parts as follows:

1. Finding the forces acting on the ship when it is restrained from motion and subjected to regular waves. These are:

   - The Froude–Krylov force, which represents the pressure in the undisturbed waves(Φ_w) integrated over the wetted surface of the ship.

   - The Diffraction forces(Φ_D), which are pressures that occur due to the disturbances in the water because of the ships presence.

2. Finding the forces on the ship when it is forced to oscillate in still water conditions. The forces are divided into:

   - Added mass forces due to the acceleration of the fluid flow around the ship.

   - Damping forces due to the body oscillations which creates outgoing waves which carry energy away from the ship.

   - Restoring forces due to buoyancy/weight of the bodies.

The resultant velocity potentials on each ship ”a” and ”b” can be expressed as:

$$\begin{aligned} \Phi_a &= \Phi_w + \Phi_{Daa} + \Phi_{Dba} + \sum_{j=1}^{6} \Phi_{Rjaa} + \sum_{j=1}^{6} \Phi_{Rjba} \\ \Phi_b &= \Phi_w + \Phi_{Dbb} + \Phi_{Dab} + \sum_{j=1}^{6} \Phi_{Rjbb} + \sum_{j=1}^{6} \Phi_{Rjab} \end{aligned} \tag{3.38}$$

where Φ_w is the incoming undisturbed wave potential(3.32); Φ_{Daa}, Φ_{Dba} are the diffraction potentials of body a due to the presence of ship a and ship b respectively; Φ_{Rjaa}, Φ_{Rjab} are the jth mode(for j = 1…6) radiation potentials of body a and b due to the oscillation of ship a while ship b is restrained; similar for $\Phi_{Dbb}, \Phi_{Dab}, \Phi_{Rjbb}, \Phi_{Rjba}$

Boundary conditions:

a) Laplace equation:

$$\nabla^2\Phi = \frac{\partial^2\Phi}{\partial x^2} + \frac{\partial^2\Phi}{\partial y^2} + \frac{\partial^2\Phi}{\partial z^2} \tag{3.39}$$

b) Seabed boundary condition:

$$\frac{\partial\Phi_w}{\partial z} = 0 \quad at \quad z = -h \tag{3.40}$$

c) Free surface boundary condition:

Combining the dynamic and kinematic boundary condition:

$$\frac{\partial^2\Phi_w}{\partial t^2} + g\frac{\partial\Phi_w}{\partial z} = 0 \quad at \quad z = 0 \tag{3.41}$$

d) Radiation condition:

$$\lim_{y\to\infty} \Phi = 0 \tag{3.42}$$

e) Diffraction potential boundary condition:

for body a:

$$\frac{\partial}{\partial n}\left(\Phi_w + \Phi_{Daa} + \Phi_{Dba}\right) = 0 \tag{3.43}$$

for body b:

$$\frac{\partial}{\partial n}\left(\Phi_w + \Phi_{Dbb} + \Phi_{Dab}\right) = 0 \tag{3.44}$$

f) Radiation potential boundary condition:

for body a:

$$\begin{aligned} \frac{\partial}{\partial n}\Phi_{Rjaa} &= -i\omega n_j \quad on \quad S_a \\ \frac{\partial}{\partial n}\Phi_{Rjab} &= 0 \quad on \quad S_b \end{aligned} \tag{3.45}$$

for body b:

$$\begin{aligned} \frac{\partial}{\partial n}\Phi_{Rjbb} &= -i\omega n_j \quad on \quad S_b \\ \frac{\partial}{\partial n}\Phi_{Rjba} &= 0 \quad on \quad S_a \end{aligned} \tag{3.46}$$

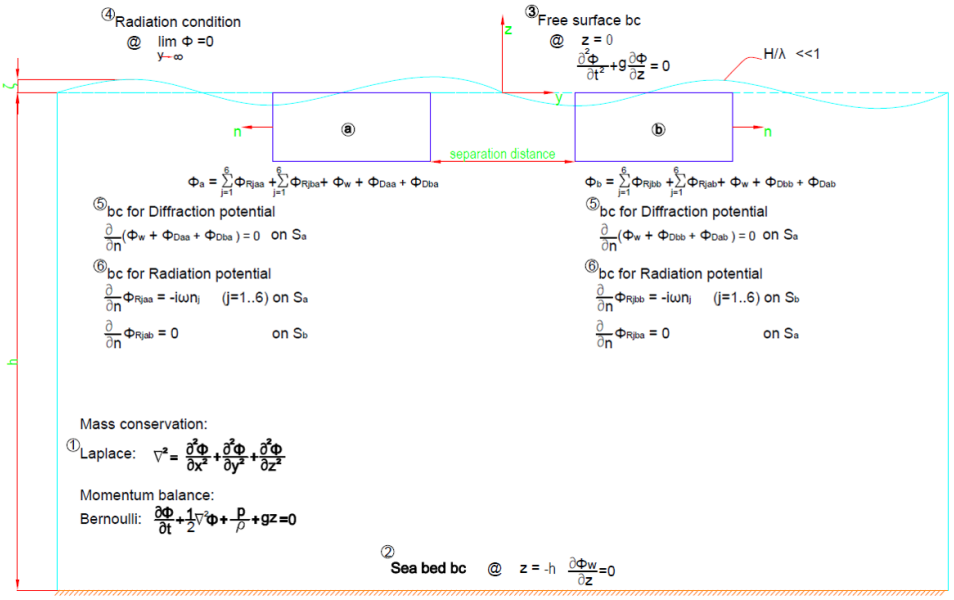

Figure 3.4: Potential theory - boundary conditions

3.5. First order loads and coupled equation of motions

Once the potentials are known, the forces and moments follow from the integration of pressure which is acting over the submerged body surface. The pressure formulation comes from linearized Bernoulli equation, where the second order term is neglected:

$$p = -\frac{\partial \Phi}{\partial t} - \rho \frac{1}{2} \nabla^2 \Phi - \rho g z \tag{3.47}$$

$$F_a{}^{(1)} = \iint_{S_a} (p \cdot n)\, dS = -\rho \iint_{S_a} \left(\frac{\partial \Phi_w}{\partial t} + \frac{\partial \Phi_{Daa}}{\partial t} + \frac{\partial \Phi_{Dba}}{\partial t} + \sum_{j=1}^{6} \frac{\partial \Phi_{Rjaa}}{\partial t} + \sum_{j=1}^{6} \frac{\partial \Phi_{Rjba}}{\partial t} + gz \right) n\, dS$$

$$F_b{}^{(1)} = \iint_{S_b} (p \cdot n) dS = -\rho \iint_{S_b} \left(\frac{\partial \Phi_w}{\partial t} + \frac{\partial \Phi_{Dbb}}{\partial t} + \frac{\partial \Phi_{Dab}}{\partial t} + \sum_{j=1}^{6} \frac{\partial \Phi_{Rjbb}}{\partial t} + \sum_{j=1}^{6} \frac{\partial \Phi_{Rjab}}{\partial t} + gz \right) n\, dS \tag{3.48}$$

And moments:

$$M_a{}^{(1)} = \iint_{S_a} p(r \times n)\, dS$$
$$M_b{}^{(1)} = \iint_{S_b} p(r \times n)\, dS \tag{3.49}$$

where: $F_a{}^{(1)}$, $M_a{}^{(1)}$, $F_b{}^{(1)}$, $M_b{}^{(1)}$ are the wave induced forces and moments respectively on ship A and on ship B; n represents the outward normal vector on the body surface.

The hydrodynamic coefficients: added mass and damping coefficient of the radiation forces are given by:

$$
\begin{aligned}
A_{jkaa} &= -Re\{\rho \iint_{S_a} \Phi_{Rjaa} n_k \, dS\} \\
A_{jkba} &= -Re\{\rho \iint_{S_a} \Phi_{Rjba} n_k \, dS\} \\
A_{jkbb} &= -Re\{\rho \iint_{S_a} \Phi_{Rjbb} n_k \, dS\} \\
A_{jkab} &= -Re\{\rho \iint_{S_a} \Phi_{Rjab} n_k \, dS\}
\end{aligned}
\tag{3.50}
$$

$$
\begin{aligned}
B_{jkaa} &= -Re\{\rho \iint_{S_a} \Phi_{Rjaa} n_k \, dS\} \\
B_{jkba} &= -Re\{\rho \iint_{S_a} \Phi_{Rjba} n_k \, dS\} \\
B_{jkbb} &= -Re\{\rho \iint_{S_a} \Phi_{Rjbb} n_k \, dS\} \\
B_{jkab} &= -Re\{\rho \iint_{S_a} \Phi_{Rjab} n_k \, dS\}
\end{aligned}
\tag{3.51}
$$

Where A and B represents the added mass and damping coefficients respectively (for example the component A_{jkba} stands for the added mass of ship A due to the motion of ship B in j direction)

Once the potentials are solve, respectively the hydrodynamic coefficients, the coupled equation of motions for two body system can be written as:

$$
\begin{aligned}
\sum_{j=1}^{6} \{(-\omega^2(M_a + A_{jkaa}) - i\omega B_{jkaa} + C_a)j_a + (-\omega^2 A_{jkba} - i\omega B_{jkba})j_b\} &= -\rho \iint_{S_a} \left(\frac{\partial \Phi_w}{\partial t} + \frac{\partial \Phi_{Daa}}{\partial t} + \frac{\partial \Phi_{Dba}}{\partial t} n \, dS \right) \\
\sum_{j=1}^{6} \{(-\omega^2(M_b + A_{jkbb}) - i\omega B_{jkbb} + C_b)j_b + (-\omega^2 A_{jkab} - i\omega B_{jkab})j_a\} &= -\rho \iint_{S_b} \left(\frac{\partial \Phi_w}{\partial t} + \frac{\partial \Phi_{Dbb}}{\partial t} + \frac{\partial \Phi_{Dab}}{\partial t} n \, dS \right)
\end{aligned}
\tag{3.52}
$$

Where M and C represents the mass of the ship and restoring force with the suffix a(ship A) and b(ship B) with the jth mode of ship A(j_a) and mode of ship B(j_b) with j=1..6.

Solving the equation of motions, the Response Amplitude Operator for each degree of freedom can be derived. RAOs are transfer functions used to determine the hydrodynamic behaviour for a specific sea state.

3.6. Second order loads

Moored vessels in irregular waves are subjected to large first order wave forces and moments which are proportional to the wave height and contain the same frequencies as the waves.The second order wave forces are smaller than the first order wave loads but they can be observed in particular on the behaviour of anchored or moored structures. Usually the second order loads are proportional to the squared wave amplitude and the frequency of the these forces is close to the low resonant frequency of the moored ship. For lower frequencies, the moored system has a little damping which can lead to large excursions of the system.

Three main components of the horizontal motions for moored or anchored floating structures can be identified:[1]

1. A mean displacement of the structure - caused by the constant load component due to sources: current and wind. Likewise additional components are the effects of the non-linear wave potential (mean wave drift forces) together with the mooring system
2. An oscillating displacement of the body at frequencies corresponding to those of the waves. This is caused by the first order wave loads.
3. An oscillating displacement of the structure at frequencies that are much lower than those of the irregular waves. These motions are caused by the low-frequency wave drift forces together with the spring characteristics of the mooring system.

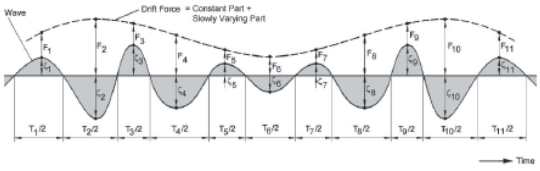

Figure 3.5: Drift force[1]

As it was mentioned previously, the superposition principle is still valid for irregular waves and thus the loads can be determined using the complete form of Bernoulli equation. In order to have an overview of each component of second order forces, the mathematical expressions are detailed below:

Starting from complete form of Bernoulli equation:

$$p = -\frac{\partial \Phi}{\partial t} - \rho \frac{1}{2} \nabla^2 \Phi - \rho g z \tag{3.53}$$

To understand from where it comes the mean, sum and difference frequency parts, it is shown the expansion of the quadratic velocity term in x direction:

$$-\rho \frac{1}{2} |\nabla \Phi|^2 = -\frac{\rho}{2} [U_x^2 + U_y^2 + U_z^2] \tag{3.54}$$

where the x-component of the velocity of two regular wave components can be written as:

$$U_x = \zeta_1 cos(\omega_1 t + \epsilon_1) + \zeta_2 cos(\omega_2 t + \epsilon_2) \tag{3.55}$$

therefore the mean square velocity become:

$$\begin{aligned} \frac{\rho}{2} U_x^2 = -\frac{\rho}{2} \Big[& \frac{\zeta_1^2}{2} + \frac{\zeta_2^2}{2} + \\ & + \frac{\zeta_1^2}{2} cos(2\omega_1 t + 2\epsilon_1) + \frac{\zeta_2^2}{2} cos(2\omega_2 t + 2\epsilon_2) + \\ & + \zeta_1 \zeta_2 cos[(\omega_1 - \omega_2)]t + (\epsilon_1 - \epsilon_2)] \\ & + \zeta_1 \zeta_2 cos[(\omega_1 + \omega_2)t + (\epsilon_1 + \epsilon_2)] \end{aligned} \tag{3.56}$$

The solution of the second order problem is composed by: a constant component, a mean drift component and two oscillating components with difference and sum frequency respectively (Eq.3.56). Generally, second order loads can be assessed using the three available methods:

- Far field (momentum conservation) by Maruo (1960) and Newman (1967) - this is based on momentum conservation over a closed surface away from the ship. This method allows the computation of the mean wave drift only in the horizontal plane. However this method does not gives accurate estimates for drift loads, since the interaction between the vessels is not considered;

- Middle field - involves a surface integral on the control surface at certain distance from the body and a line integral along its intersection with the free surface.

- Near field method - direct pressure integration on the hull and along the waterline. This method is able to capture the hydrodynamic interaction between multiple vessels.

Near Field Method

The theory is developed using perturbation methods. This means that all quantities such as: wave height, motions, potentials, pressures etc are assumed to vary only very slightly relative to some initial static value. Considering that the velocity potential Φ is known, the non-linear pressure equation (Bernoulli) can be expressed as a Taylor expansion in its mean position:

$$p = p^{(0)} + \epsilon p^{(1)} + \epsilon^2 p^{(2)} \tag{3.57}$$

where:

- hydrostatic component:

$$p^{(0)} = -\rho g \vec{X}_3^{(0)} \tag{3.58}$$

- first order component:

$$p^{(1)} = -\rho g \vec{X}_3^{(0)} \tag{3.59}$$

- second order component:

$$p^{(2)} = -\frac{1}{2}\rho(\vec{\nabla}\Phi^{(1)})^2 - \rho\frac{\partial^2\Phi^2}{\partial t^2} - \rho\left(\vec{X}^{(1)} \cdot \vec{\nabla}\frac{\partial\nabla^{(1)}}{\partial t}\right) \tag{3.60}$$

These derivatives needs to be evaluated at the mean position of the calculated point (ie center of gravity). Therefore the instantaneous wetted surface can be splitted into two parts: one constant (S_0) which represents the static wetted surface and an oscillating part (s) which represents the zone between the static waterline and the wave profile along the body. The forces becomes:

-hydrostatic force:

$$\vec{F}^0 = -\iint_{S_0}(p^{(0)} \cdot \vec{n})dS = \rho g \nabla \tag{3.61}$$

-first order oscillatory force:

$$\begin{aligned}\vec{F}^{(1)} &= -\iint_{S_0}(p^{(0)} \cdot \vec{N}^{(1)})dS - \iint_{S_0}(p^{(1)} \cdot \vec{n})dS - \iint_{s}(p^{(0)} \cdot \vec{n})dS \\ &= R^{(1)} \cdot \rho g \nabla - \iint_{S_0}(p^{(1)} \cdot \vec{n})dS\end{aligned} \tag{3.62}$$

-second order fluid force:

$$\vec{F}^{(2)} = -\iint_{S_0}(p^{(1)}\cdot\vec{N}^{(1)})dS - \iint_{S_0}(p^{(2)}\cdot\vec{n})dS - \iint_{s}(p^{(0)}\cdot\vec{n})dS - \iint_{s}(p^{(0)}\cdot\vec{N}^{(1)})dS \iint_{s}(p^{(1)}\cdot\vec{n})dS$$
$$= m\cdot R^{(1)}\cdot\vec{\ddot{X}_g}^{(1)}$$
$$+ \iint_{S_0}\left\{\frac{1}{2}\rho(\vec{\nabla}\Phi^{(1)})^2 + \rho\frac{\partial\Phi^{(2)}}{\partial t} + \rho\vec{X}^{(1)}\cdot\vec{\nabla}\frac{\partial\Phi^{(1)}}{\partial t}\right\}\cdot\vec{n}dS$$
$$- \oint_{wl}\frac{1}{2}\rho g(\zeta^{(1)})^2\cdot\vec{n}\cdot dl \tag{3.63}$$

Thus, the total contribution of the second as it can be seen in the equation from above by: roll and pitch inertia force; pressure drop due to the velocity squared, contribution due to the 2^{nd} order potential, pressure due to the $1^{s}t$ order contribution; and the relative wave height contribution over the waterline.

3.7. Numerical procedure and problems

Potential flow allows to convert the integrals over the fluid domain into integrals over the boundaries of the fluid domain. Therefore the surface of the ships and surrounding water is discretized into elements. Velocity potential at any point in the fluid can be calculated using the distribution of singularities over the vessel's surface elements (source with corresponding sink). This can be done using the Green's function which satisfy the Laplace equation. By imposing the body boundary conditions and boundary conditions for diffraction and radiation potentials, the normal component of the velocity on the body surface can be solved.

Within the potential flow theory solvers there are multiple problems and limitations which could alter the simulation results. In particular the irregular frequencies phenomena that is a numerical problem associated with the solution of eq. for certain frequencies (usually at higher frequencies) which the results are unrealistic described by higher peaks.

Irregular frequencies are associated with the internal eigen mode of the non-physical internal flow of the body and increasing the number of panels (finer mesh) does not help. In order to reduce the effects of irregular frequencies, Malenica and Chen [38] instead a lid on the free surface inside the body improve the simulations results. This phenomena occurs exclusively to the surface piercing bodies, the fully submerged bodies does not encounter these characteristics.

Below it is presented a case where it can be clearly identified the effect of the lid effect on the results.

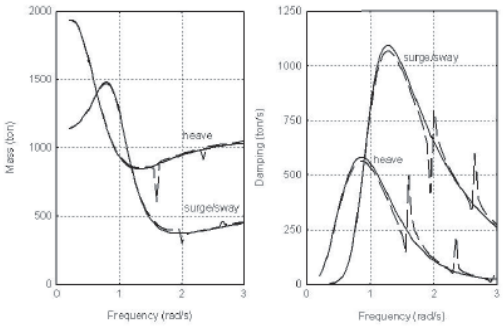

Figure 3.6: Effect of lid on irregular frequencies [21]

4

Frequency domain model setup

4.1. Introduction

This chapter presents the findings after the numerical investigation carried in diffraction code (HydroStar) varying different parameters such as:

- vessel's loading condition
- damping parameter
- separation distance
- carrier and FLNG size

The results are presented in graphs and tables where is needed to emphasis the maximum value/impact. Furthermore in order to support the findings, comparisons with research papers is done. The conclusions of this chapter gives valuable data/information regarding the sensitive parameters for side-by-side mooring arrangements.

Hydrostar is a powerful 3D diffraction/radiation software based on potential theory for wave-body interactions. It is able to evaluate the first and second order wave loads for single or multi-body interaction in deep or finite water depth, effects of forward speed and internal liquid motions. Hydrostar has been extensively tested and validated through comparison with semi-analytical studies, numerical results from recognized tools and experimental data. The software provides numerous advantages and functionalities to meet high-level requirements, including [36]:

- Dynamic coupling between liquid motions in internal tanks and ship motions
- Generalized modes calculation: Hydrostar can solve the hydro-dynamic problem on user-defined modes
- Side-by-side configuration as the software handles multi-body interactions

Second order loads can be solved using the following theories: far field (momentum conservation method); middle field (pressure integration over a control volume near the hull); or near field (pressure integration on the hull surface).

4.2. Main particulars and Stability Data of the FLNGs

Before presenting the results an overview of the vessel characteristics both FLNGs and LNGs are presented in the tables 4.1 and 4.2.

Main particulars of the floating vessls (FLNG) are presented in the table 4.1. Three vessels are used for investigation. As it can be observed in the picture 4.1, the FLNGs are barge shaped, with straight lines at the stern and bow part. This represents an advantage in terms of capability of accommodating large storage tanks.

Loading condition	301.5 m		346 m		371.4 m	
	Min (ballast)	Max (fully loaded)	Min (ballast)	Max (fully loaded)	Min (ballast)	Max (fully loaded)
Length [m]	301.5	301.5	346	346	371.4	371.4
Beam [m]	66	66	66	66	68	68
Draft [m]	13.19	13.47	-	15.69	16	18
Volume [m^3]	2.43e+05	2.48e+05	-	3.32e+05	3.98e+05	4.5e+05
Displacement [kg]	2.49e+08	2.54e+08	-	3.40e+08	4.08e+08	4.61e+08
LCG [m]	153.07	152.99	-	168.081	184.1	184.5
KG [m]	22.89	25.89	-	24.37	20.4	22.4
K_{xx} [m]	26.4	26.4	-	26.4	27.2	25.8
K_{yy} [m]	81.405	81.405	-	100.456	100.5	100.5
K_{zz} [m]	81.405	81.405	-	100.456	100.5	100.5
GM_t [m]	11.82	7.99	-	6.72	11.70	7.90

Table 4.1: FLNGs main characteristics

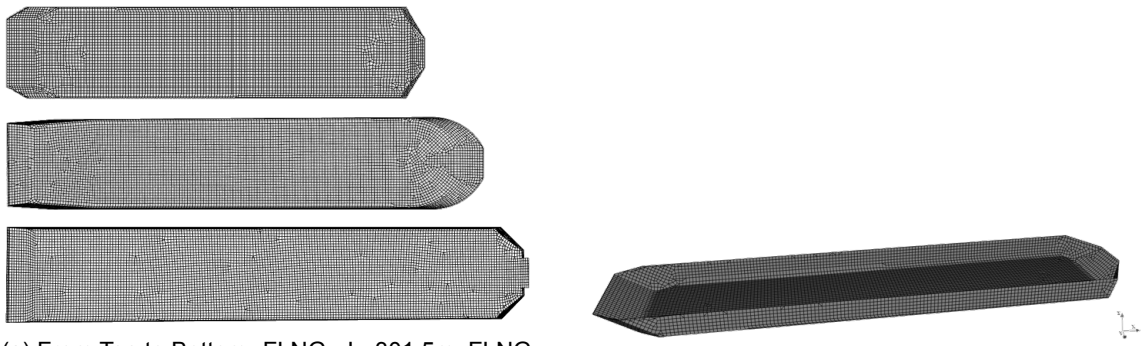

(a) From Top to Bottom: FLNG - L=301.5m; FLNG - L=346m; FLNG - L=371.4m

(b) 3D view of FLNG - L=301.5m

Figure 4.1: FLNG size variation

4.3. Main particulars and Stability Data of the Carriers

Periodical offloading is done with the aid of a carrier of two different sizes, moored in side by side configuration. The main particulars of the carriers are presented in the Table 4.2. As it can be seen the LPGC is almost half than the LNGC length. The geometry of the carriers is defined by having fine lines and bulbous bow (Figure 4.2).

Loading condition	LNGC		LPGC	
	Min (ballast)	Max (fully loaded)	Min (ballast)	Max (fully loaded)
Length [m]	285	285	172	172
Beam [m]	45.8	45.8	28.4	28.4
Draft [m]	9.6	11.5	5.6	9.5
Volume [m^3]	9.41e+04	1.16e+05	1.92e+04	3.44e+04
Displacement [kg]	9.65e+07	1.19e+08	1.97e+07	3.53e+07
LCG [m]	143	141.5	82.5	82
KG [m]	12.45	16.1	9.15	9.55
K_{xx} [m]	17.45	14.95	10.5	9
K_{yy} [m]	71.85	65.75	44.75	39.5
K_{zz} [m]	72.75	66	44.75	39.75
GM_t [m]	7.9	3.55	4.7	2.33

Table 4.2: LNGs main characteristics

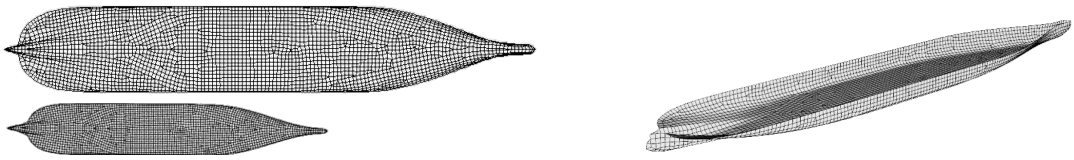

(a) From Top to Bottom: LNGC; LPGC (b) 3D view of LNGC

Figure 4.2: Carrier size variation

4.4. Side by Side Arrangement and Manifold location

In this section the side by side arrangement is shown for different carrier and FLNGs size in order to have an idea how the the carriers are positioned with respect to the FLNG's manifold location. For the case of side by side arrangement between FLNG of 301.5m length and LNGC which has the length comparable to FLNG's length, the bulbous bow of the carrier is un-shielded (Figure 4.3). In each side-by-side configuration shown below, the location of the manifolds with respect to the aft part of the FLNG is given in meters. Absolute wave elevation for each manifold, has been calculated at the mid separation distance between the two vessels.

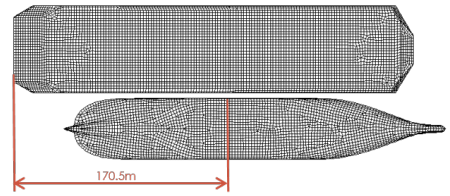

(a) FLNG(L=301.5m) - LNGC

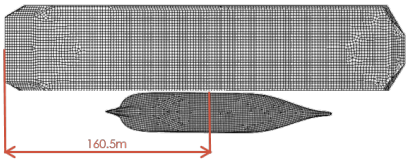

(b) FLNG(L=301.5m) - LPGC

Figure 4.3: Side by Side arrangement for different carrier size and manifold location

The side-by-side arrangement using different size of FLNG is presented in Figure 4.4. It can be seen that for FLNG of 346m and 371m the carrier is completely shielded by the FLNG.

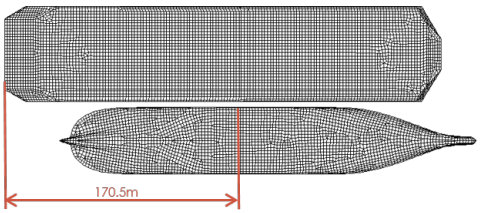

(a) FLNG(L=301.5m) - LNGC

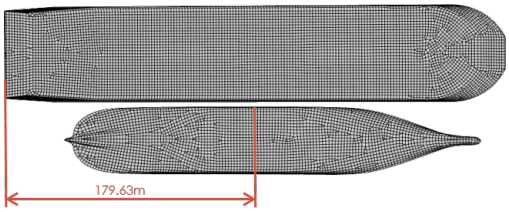

(b) FLNG(L=346m) - LNGC

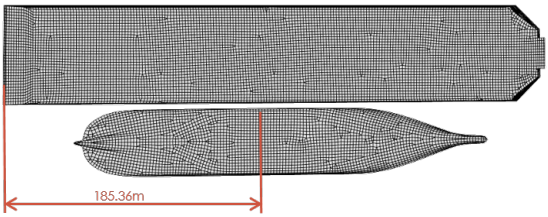

(c) FLNG(L=371m) - LNGC

Figure 4.4: Side by Side arrangement for FLNG of different length and manifold location for each configuration

4.5. Model parameters

This section describe in details the parameters which have been varied, numerical set-up and limitations of the diffraction code. Sensitivity analysis has been performed for the following parameters: variation of the vessels size (both the carrier and the production unit), loading condition (ballast, fully-loaded), separation distance, dissipation factor and length of the damping lid. In the following sections each parameter is described in more details.

4.5.1. Vessels size and loading condition

SBM company possess a huge fleet of various floating platforms, FPSOs and FLNGs with internal or external turret moored (Figure 4.5), able to operate in ultra deep water to shallow water conditions (<50m depth). Majority of them has a length above 300m with a significant storage capacity. The offloading process for FLNGs units is done using the cryogenic loading arms to an LNG carrier parked in close proximity (roughly 4.5 metres, equivalent to the fender diameter) in a side by side vessel configuration.

Three different FLNGs sizes has been chosen (Figure4.1) and two shuttle tankers for the unloading process. When the carrier sails to the FLNG location for the offloading process is considered to be in ballast condition and FLNG fully-loaded. After the off-take process, the FLNG is in ballast condition and the carrier fully loaded and ready to depart. In the tables below are presented the loading conditions and vessels size variation for side by side mooring configuration and single vessels with its corresponding notation that will be used for throughout the report.

Notation	FLNG Length	Loading condition
$SbS_{1.1}$	301.5m	$FLNG_{fully\ loaded} - LNGC_{ballast}$
$SbS_{1.2}$	346m	$FLNG_{fully\ loaded} - LNGC_{ballast}$
$SbS_{1.3}$	371m	$FLNG_{fully\ loaded} - LNGC_{ballast}$
$SbS_{2.1}$	301.5m	$FLNG_{fully\ loaded} - LPGC_{ballast}$
$SbS_{3.1}$	301.5m	$FLNG_{ballast} - LNGC_{fully\ loaded}$
$SbS_{4.1}$	301.5m	$FLNG_{ballast} - LPGC_{fully\ loaded}$

Table 4.3: Side by side vessels and loading condition variation

Notation	Single Vessel	Loading condition
SV_1	FLNG	$FLNG_{fully\ loaded}$
SV_2	FLNG	$FLNG_{ballast}$
SV_3	LNGC	$LNGC_{ballast}$
SV_4	LNGC	$LNGC_{fully\ loaded}$
SV_5	LPGC	$LPGC_{ballast}$
SV_6	LPGC	$LPGC_{fully\ loaded}$

Table 4.4: Single vessel - loading condition variation and notations

Figure 4.5: **Left:** SbS arrangement (FLNG with external turret); **Right:** FPSO - internal turret [33]

4.5.2. Dissipation factor and length of the damping zone

Dissipation factor

As it is presented in Chapter 3 within the potential theory framework there is no limitation for prediction of the resonant wave elevation while in reality there are different mechanisms of dissipation. This cause unrealistic wave elevation between the two bodies. Furthermore breaking waves phenomena which may also have a big contribution to the unrealistic calculation of wave elevation are not counted into the potential flow solvers. For these reasons researchers came up with different solutions such that to suppress the unrealistic effects and to deal with the gap resonant effects.

Chen(2005)[8] proposed a method to solve the limitation of the potential theory, by implementing a damping force at the meshed free surface in between the two floating bodies (Figure 4.7). Considering the assumptions of the potential flow (i.e. rotation free) the damping force affects only the free surface boundary condition. Experimental tests has been carried out in order to validate the numerical sensitivity for damping ratio. Publications by i.e J.R Fournier et. al [20], R.Huijsmans [40] and X.B.Chen [43] shows that the free surface dissipation is much more dominant near the resonance frequency. Away from resonance the dissipation factor does not have any impact. The experimental tests revealed the fact that there is no unique damping factor that can be used for every type of side-by-side mooring configuration. J.R. Fournier et al. [20] found different dissipation factor for first order and second order quantities. For instance if a damping ratio of 0.1 gives good agreement between numerical

and experimental tests for wave elevation and drift forces, on the other side, for the first order forces a damping ratio of 0.2 offers better agreement with the experiment. R.Huijsmans et. al [40] found out that there is no unique value for free surface dissipation parameter which fully cover the comparison with the measured results for separation distances less than 25m. Moreover tunning the damping value of the lid should be based on the second order forces as they are more sensitive and the damping parameter has a greater impact than on the first order quantities. On the other hand, Fournier et al. [23] provide an analytical method to determine an unique value for epsilon parameter for separation distances greater than 25m. Therefore in order to assess the damping ratio effects for the considered side-by-side arrangements a range for ϵ between 0 and 0.4 has been used as follows:

$\epsilon_j[-]$	$\epsilon_1 = 0$	ϵ_2 = 0.1	ϵ_3 = 0.2	ϵ_4 = 0.3	$\epsilon_5 = 0.4$

Table 4.5: Dissipation factor range

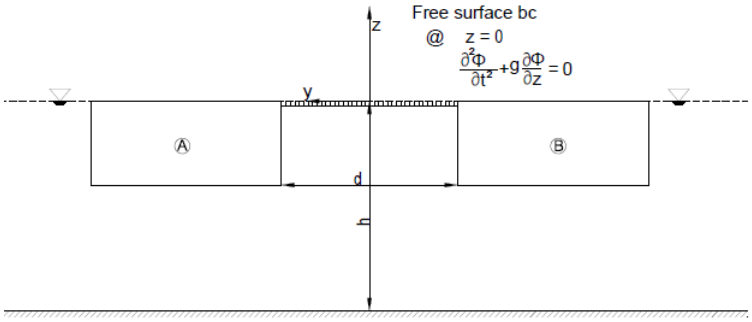

Figure 4.6: Free surface damping lid

Conventional	Rigid lid	Damping lid
Undamped wave elevation	No wave elevation	Damped wave elevation
$\frac{\partial\Phi}{\partial z}-\frac{\omega^2}{g}\Phi=0$	$\frac{\partial\Phi}{\partial n}=0$	$\frac{\partial\Phi}{\partial z}-(1-i\epsilon)\frac{\omega^2}{g}\Phi=0$

Table 4.6: Dissipation factor

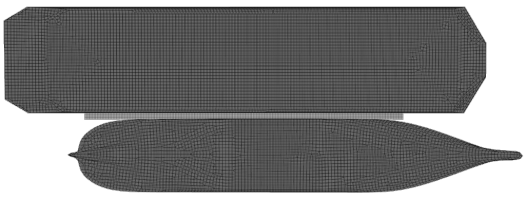

Figure 4.7: Damping zone between vessels

Length of the damping zone

According to the available literature, there is no theoretical method to assess a length of the lid on the gap between vessels. For certain publications (i.e Buchner et al. [3]) the authors used a lid area which covers only the constant width between the two vessels with no further extension towards the bow or stern where the vessel's shape gets finer. In other papers (i.e Huijsmans et. al [40], Buchner et. al [4]), the free surface lid damping is modelled a bit more extended towards the bow and the stern of the carrier. Another example of different area used for the lid damping is presented by Hong-Chao and Lei Wang [39] where they used a length for the lid surface equal to the length of the floating production unit. Furthermore

the superposition of the incoming wave and the diffracted waves results in cancellation in nodes at certain frequencies. This cancellation is dependent on the ratio between the gap dimensions (such as width and length) and the wave length[40]. Therefore in order to quantify the effects on both the FLNG and the carrier, 3 different lengths for the free surface lid has been used as follows:

LD_j	$LD_1 = 160m$	LD_2 = 200m	LD_3 = 285m

Table 4.7: Variation of the damping zone

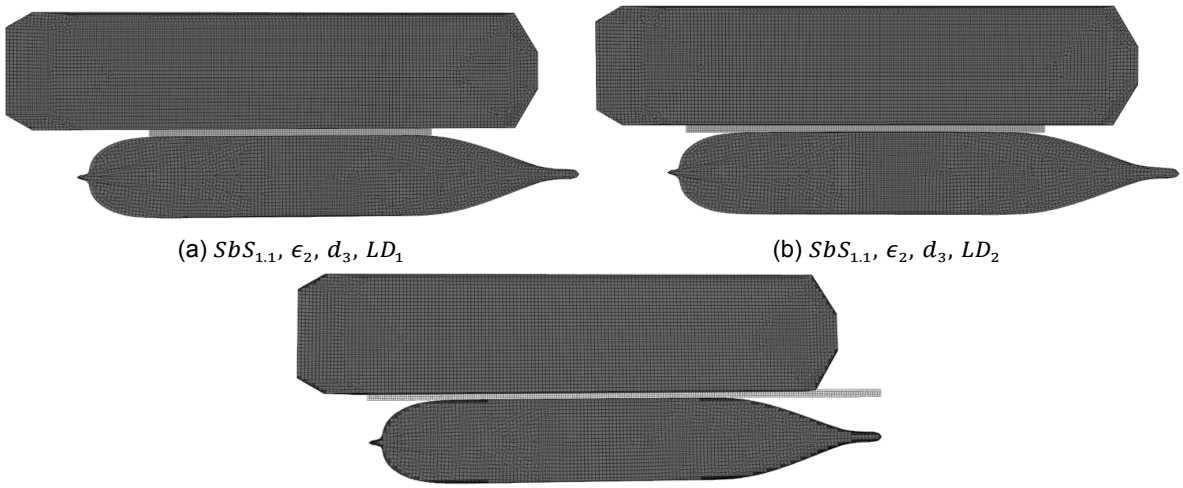

(a) $SbS_{1.1}$, ϵ_2, d_3, LD_1 (b) $SbS_{1.1}$, ϵ_2, d_3, LD_2

(c) $SbS_{1.1}$, ϵ_2, d_3, LD_3

Figure 4.8: Length of the free surface damping lid

4.5.3. Separation distance

The maximum separation distance is governed by the length of the cryogenic loading arms and the diameter of the fender such that to provide enough reaction force and to avoid any potential risks of collision. On the other hand the vessels needs to be as closer as possible to avoid extreme oscillations of the loading arm. For vessels in close proximity, the hydrodynamic interaction is complex and strongly coupled. Over many cycles of the first order oscillatory motions that can be in phase or out of phase (higher impact), the drift forces may cause substantial changes in the relative positions, possibly leading to collisions (striking the fenders). Moreover, the separation distance is essential in deciding the coupled drift forces and the wave formation in between the two vessels which affects the responses. It can be discerned that small decrease in gap distances may result in intense increase of loads. Hong-Chao Wang and Lei Wang [39] investigated the effects of different separation distances and apparently the sway, yaw and sway mean drift force are affected the most. A range of separation distances has been used in order to assess the forces effect when compressed or uncompressed fender is considered. The available fenders that are used for offloading operations have a diameter of 4.5m. Therefore a separation distance of 4.5m will represent the case of uncompressed fender while below 4.5m distance will represent a compressed fender, considering 3m for extreme situations.

d_j	$d_1 = 3m$	d_2 = 3.5m	d_3 = 4m	$d_4 = 4.5m$

Table 4.8: Separation distance variation

4.5.4. Gap resonance

In order to understand the behaviour of the oscillating water in between the vessels is prior to assess the natural periods of the standing wave. Large amplitudes can develop when the

incident wave frequency is close to the natural frequency of the fluid in the gap. At these frequencies extreme motions and line tensions are expected.

In the available literature, the gap resonance is referred to the moonpool resonance which can have different geometry such as: circular, symmetrical wrt. vertical axis or asymmetrical rectangular shape (moonpool with recess), The gap region between two vessels can be treated as a rectangular monopool. Therefore, for the sake of simplicity the gap can be defined as a box with the dimensions: L = length of the damping zone(Figure 4.8); d = separation distance (Table 4.8; D = draft of the carrier (Table 4.2). With this regard, a literature research has been done and the following theoretical and empirical formulations for assessing the natural frequencies are proposed:

Natural frequency - sloshing mode

Sloshing phenomena may occur when there is a resonance between the natural sloshing modes of the moonpool and the pitch or roll period. This characteristic behaviour is usually for large moonpools where the length provides enough time to develop.

The n-th order resonance frequency of sloshing mode is suggested by Newman (1977) [29] as:

$$\omega_n = \sqrt{\frac{n\pi g}{L}} \tag{4.1}$$

where n represents the order of resonance, g gravitational acceleration and L is the moonpool length

Below it is presented the resonant frequencies using Newman formulation (eq. 4.1).

	ω_1 [rad/s]	T_1 [s]
$L = 160m$	0.438	14.316
$L = 200m$	0.392	16.006
$L = 285m$	0.3288	19.107

Table 4.9: Sloshing modes with Newman's formulation

Molin (2001) proposed a quasi-analytical expression for the resonant frequencies of a rectangular moonpool [2]:

$$\omega_{n0} = \sqrt{g\lambda_n \cdot \frac{1 + J_{n0} tanh(\lambda_n D)}{J_{n0} tanh(\lambda_n D)}} \tag{4.2}$$

where $\lambda_n = \frac{n\pi}{L}$ and J_{n0} is a function of moonpool dimensions and can be obtained through numerical integration:

$$J_{n0} = \frac{2}{n\pi^2 r}\left[\int_0^1 \frac{r^2}{u^2\sqrt{u^2+r^2}}\left(1 + (u-1)cos(n\pi u) - \frac{sin(n\pi u)}{n\pi}\right)du + \frac{1}{sin\theta_0} - 1\right] \tag{4.3}$$

where $r = \frac{d}{L}$, $tan\theta_0 = r^{-1}$

In the tables below are presented the resonant frequencies as a function of gap dimensions. The analyzed case consists in side by side configuration of FLNG with each carrier before(i.e FLNGmax-LNGCmin; FLNGmax-LPGCmin) and after offloading (i.e FLNGmin-LNGCmax; FLNGmin-LPGCmin) where the draft of the vessels varies.

Side by Side Configuration	Gap length	d=3m		d=3.5m		d=4m		d=4.5m	
		ω_1[rad/s]	T_1[s]	ω_1[rad/s]	T_1[s]	ω_1[rad/s]	T_1[s]	ω_1[rad/s]	T_1[s]
FLNGmax -LNGCmin draft = 9.6m	L =160m	0.70	9.0	0.66	9.5	0.63	10.0	0.61	10.4
	L =200m	0.61	10.3	0.58	10.9	0.55	11.5	0.53	12.0
	L=285m	0.49	12.8	0.46	13.6	0.44	14.3	0.42	14.9
FLNGmin - LNGCmax draft = 11.5m	L =160m	0.77	8.2	0.72	8.7	0.69	9.1	0.66	9.5
	L =200m	0.67	9.4	0.60	10.4	0.60	10.5	0.57	10.9
	L=285m	0.54	11.7	0.51	12.4	0.48	13.1	0.46	13.7

Table 4.10: Sloshing resonant frequencies for FLNG-LNGC according to Molin(2001)[2]

Side by Side Configuration	Gap length	d=3m		d=3.5m		d=4m		d=4.5m	
		ω_1[rad/s]	T_1[s]	ω_1[rad/s]	T_1[s]	ω_1[rad/s]	T_1[s]	ω_1[rad/s]	T_1[s]
FLNGmax -LPGCmin draft = 5.6m	L =81.5m	0.83	7.6	0.78	8.0	0.75	8.4	0.72	8.7
FLNGmin - LPGCmax draft =9.5m		1.07	5.9	1.02	6.2	0.97	6.5	0.94	6.7

Table 4.11: Sloshing resonant frequencies for FLNG-LPGC according to Molin(2001)[2]

As it can be observed, the natural frequencies estimated using Newman's formulations are significantly low compare to the results based on Molin's formulation which is more elaborated, dependent both on length and draft of the moonpool. Thus, the sloshing resonant frequency would be referred to Molin's equation for both sensitivity analyses in frequency and time domain. This is considered a rough estimation of the resonant periods in order to be able to have a better understanding on the hydrodynamic of the two vessels coupled system. On the other side, according to the recent publications, empirical and theoretical formulations seems to have relatively large discrepancy when it is compared to the numerical results.

Natural frequency - piston mode

This mode is governed by the oscillation of the water column in vertical directions. When waves period enters in resonance with the moonpool natural period. the water column between the vessels can form high wave elevation which ultimately by breaking, pushing the vessels sideways violently.

Starting from the general expression:

$$\omega_n = \sqrt{\frac{c}{m + a_{33}}} \tag{4.4}$$

where, m is mass of moonpool, $m_{33}$is the added mass and c is constant spring

Fukuda(1977) carried out experiments with regards the added mass term for the piston mode oscillation for both rectangular and circular moonpools. He found out that there the added draft of the moonpool is proportional to the root square of the cross-section area. Such that he recommends the following formulation:

$$\omega_0 = \sqrt{\frac{g}{D + D'}} = \sqrt{\frac{g}{D + (0.41 \cdot \sqrt{S})}} \tag{4.5}$$

where D- draft of the vessel, D' is added draft and S-cross section area

Side by Side Configuration	d=3m		d=3.5m		d=4m		d=4.5m	
	ω_1[rad/s]	T_1[s]	ω_1[rad/s]	T_1[s]	ω_1[rad/s]	T_1[s]	ω_1[rad/s]	T_1[s]
FLNGmax -LNGCmin draft = 9.6m	0.91	6.9	0.91	6.9	0.90	7.0	0.89	7.0
FLNGmin - LNGCmax draft =11.5m	0.84	7.5	0.83	7.5	0.83	7.6	0.82	7.6

Table 4.12: Piston resonant frequencies for FLNG-LNGC according to Fukuda(1977)[24]

Side by Side Configuration	d=3m		d=3.5m		d=4m		d=4.5m	
	ω_1[rad/s]	T_1[s]	ω_1[rad/s]	T_1[s]	ω_1[rad/s]	T_1[s]	ω_1[rad/s]	T_1[s]
FLNGmax -LPGCmin draft = 5.6m	1.16	5.4	1.15	5.5	1.14	5.5	1.13	5.6
FLNGmin - LPGCmax draft = 9.5m	0.92	6.9	0.91	6.9	0.90	7.0	0.90	7.0

Table 4.13: Piston resonant frequencies for FLNG-LPGC according to Fukuda(1977)[24]

Molin(2001) [2] proposed the following expression for resonant frequency given in two-dimensions as:

$$\omega_0 = \sqrt{\frac{g}{D + \frac{d}{\pi D}(\frac{3}{2} + ln(d))}} \tag{4.6}$$

where: D-draft of the vessel, d-separation distance

Side by Side Configuration	d=3m		d=3.5m		d=4m		d=4.5m	
	ω_1[rad/s]	T_1[s]	ω_1[rad/s]	T_1[s]	ω_1[rad/s]	T_1[s]	ω_1[rad/s]	T_1[s]
FLNGmax -LNGCmin draft = 9.6m	1.00	6.3	0.99	6.3	0.99	6.3	0.99	6.4
FLNGmin - LNGCmax draft =11.5m	0.92	6.9	0.91	6.9	0.91	6.9	0.91	6.9

Table 4.14: Piston resonant frequencies for FLNG-LNGC according to Molin(2001)[2]

Side by Side Configuration	d=3m		d=3.5m		d=4m		d=4.5m	
	ω_1[rad/s]	T_1[s]	ω_1[rad/s]	T_1[s]	ω_1[rad/s]	T_1[s]	ω_1[rad/s]	T_1[s]
FLNGmax -LPGCmin draft = 5.6m	1.27	4.9	1.27	5.0	1.25	5.0	1.24	5.1
FLNGmin - LPGCmax draft = 9.5m	1.00	6.3	1.00	6.3	1.00	6.3	0.99	6.3

Table 4.15: Piston resonant frequencies for FLNG-LPGC according to Molin(2001)[2]

4.5.5. Frequency range

Offloading is sensitive to variable weather and ocean conditions (e.g. beam and quartering seas), side-to-side rotation of the LNG carrier, wave motions and different filling conditions of a liquid cargo inside the tanks.

For all comparison cases a detail investigation is done with respect to the hydrodynamic coefficients, first order motions and second order forces. The results of hydrodynamic computations are displayed in terms of RAOs as the vessel's motion response of a unit wave amplitude. Moreover for each degree of freedom for first and second order forces, the results are displayed at the same scale. The frequency range is chosen from 0.02 to 1.6 rad/s with a step of 0.02 rad/s for first order motions for multi-body configuration and single vessel both first and second order. Near the peak frequency the integration step is smaller i.e 0.01 rad/s such that to obtain accurate results at those frequencies. The second order forces for multi-body configuration are computed from 0.02 to 2 rad/s due to the fact that the drift forces are very sensitive especially at higher frequencies.

4.5.6. Roll stiffness

In order to correct the roll motion due to the fluid in the tanks, two methods can be used:

- first is by modelling each tank of the vessel and considering the filling level (ballast or fully loaded) with fluid in each tanks
- second method is considering a stiffness coefficient (Table 4.16) for roll direction which corrects the metacentric height with respect to the fluid inside the tanks.

$$C_{44} = \rho g \nabla G M_T \tag{4.7}$$

Roll stiffness coefficient	FLNG		LNGC		LPGC	
	fully loaded	ballast	fully loaded	ballast	fully loaded	ballast
$C_{44}\left[\frac{t \cdot m^2}{s^2}\right]$	2.088E+06	1.122E+06	1.910E+06	2.777E+06	1.037E+05	5.556E+05

Table 4.16: Roll stiffness correction

4.5.7. Linear viscous damping

According to the potential theory the source of dissipation is only due to the radiation potential. In reality, in addition to the radiation damping, there are various sources of damping acting on the floating structures such as: viscosity of the fluid, hull appendages, mooring line and riser systems damping. In Hydrostar is possible to count for the additional damping using a linear or a quadratic approximation which is function of drag coefficient, size of the vessel and appendages. It has been selected the linear damping as a percentage of the critical damping due to the following reasons: less computational effort and gives good estimates. Critical damping represents the amount of damping for which there is no vibration in the system and the motion dies out immediately in the first oscillation. In each numerical simulation, both the carrier and the FLNG, linear damping represents 3% from the critical damping.

4.5.8. Coordinate systems

To describe the motion responses between two floating structures in waves, three sets of right-handed orthogonal coordinate systems are considered (Figure 4.9).O-XYZ is the space fixed coordinate system. $O_A - X_A Y_A Z_A$ and $O_B - X_B Y_B Z_B$ are the oscillatory coordinate systems fixed with respect to ship A and ship B, respectively. The O-XY plane coincides with the undisturbed free surface, the X-axis positive in the direction of the body's forward and the Z-axis positive vertically upward. The Oscillatory coordinate systems $O_A - X_A Y_A Z_A$ and $O_B - X_B Y_B Z_B$ are used to describe the body motion in six degrees of freedom with complex amplitudes ξ_j with j=1,2,... ,12; where j=1,2,3,4,5,6 represent surge, sway, heave, roll, pitch and yaw for

ship A, respectively, and j=7,8,9,10,11,12 represent surge, sway, heave, roll, pitch and yaw for ship B, respectively, as shown in Figure 4.9.

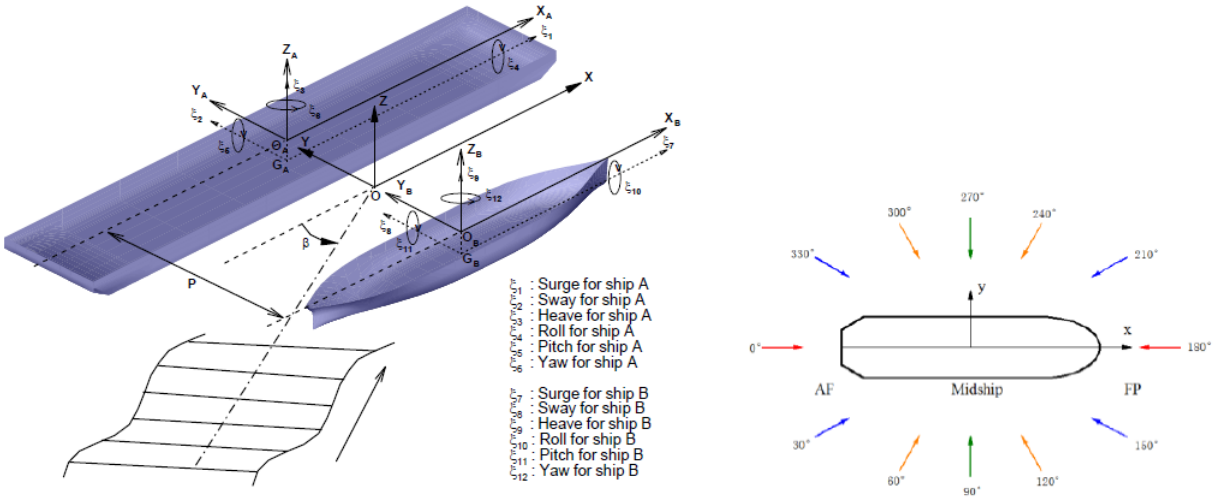

Figure 4.9: **Left:** Definition of coordinate frames [28] **Right:** Direction of incident wave [39]

5

Diffraction results and comparison

5.1. Multi-body vs single body

The aim of this section is to highlight the hydrodynamic interaction effects between the FLNG and carrier in side by side configuration in comparison with the single body case.

5.1.1. FLNG

In order to see the hydrodynamic influence of multi body configuration, the FLNG from side by side configurations (FLNG-LNGC; FLNG-LPGC) is compared to the FLNG fully loaded single body. Below are presented the cases that are analyzed and the list of results.

Cases	$FLNG_{SbS_{1.1},\epsilon_3,d_3,LD_1}$ **vs** $FLNG_{SbS_{2.1},\epsilon_3,d_3,LD_1}$ **vs** SV_1

Table 5.1: Analyzed cases

All the results for this comparison are presented graphically in the Appendix **??**, as follows:

Hydrodynamic coefficients	RAO	QTF	WE
Figure **??**	Figures [**??**...**??**]	Figures [**??**...**??**]	Figure **??**

Table 5.2: List of results

Hydrodynamic coefficients

The first aspect which should be mentioned is that for the moored vessels (zero forward speed), the added mass and damping coefficients stay the same for each wave direction. Moreover, it is noted that the coefficients are exerted only by the radiated wave interactions between the FLNG and the shuttle tanker. For this particular case it can be seen that the hydrodynamic interaction is more obvious for sway, roll and yaw, where sharp variations are observed. Interaction with the LNG carrier has a bigger impact on the hydrodynamic coefficients of the FLNG than the interaction with the LPG carrier. This is logically, because the LNG carrier is twice as long than the LPG carrier and thus the hydrodynamic interaction effects between FLNG-LNGC will have a greater impact on FLNG. Near a particular frequency ($0.78\ rad/s$ for $FLNG_{SbS_{1.1},\epsilon_3,d_3,LD_1}$; $0.98\ rad/s$ for $FLNG_{SbS_{2.1},\epsilon_3,d_3,LD_1}$), the computed added mass respectively the damping coefficient exhibit sharp variation for sway, roll and yaw direction. The radiation potential for these directions in side by side configuration are asymmetric with respect to y axis. For instance, when calculating the radiation potential due to FLNG's roll oscillation, carrier remains fixed, the radiated waves coming from the FLNG encounter the side of the carrier which will reflect back the wave. As the vessel oscillate more (i.e at natural frequency) the radiated wave amplitude becomes higher too. At this frequency, due to the water column between which will form between the two bodies, the added mass for sway, roll and yaw have large peaks, in particular for $FLNG_{SbS_{1.1},\epsilon_3,d_3,LD_1}$ both added mass in sway

and yaw becomes negative (deceleration in the fluid) which means that the vessel is pushed sideways. Due to this phenomena the damping coefficients have huge peak (i.e approx. 4 times higher for $FLNG_{SbS_{1.1},\epsilon_3,d_3,LD_1}$ than single body) at this frequency. Therefore the FLNG is expected to be more sensitive around these frequencies.

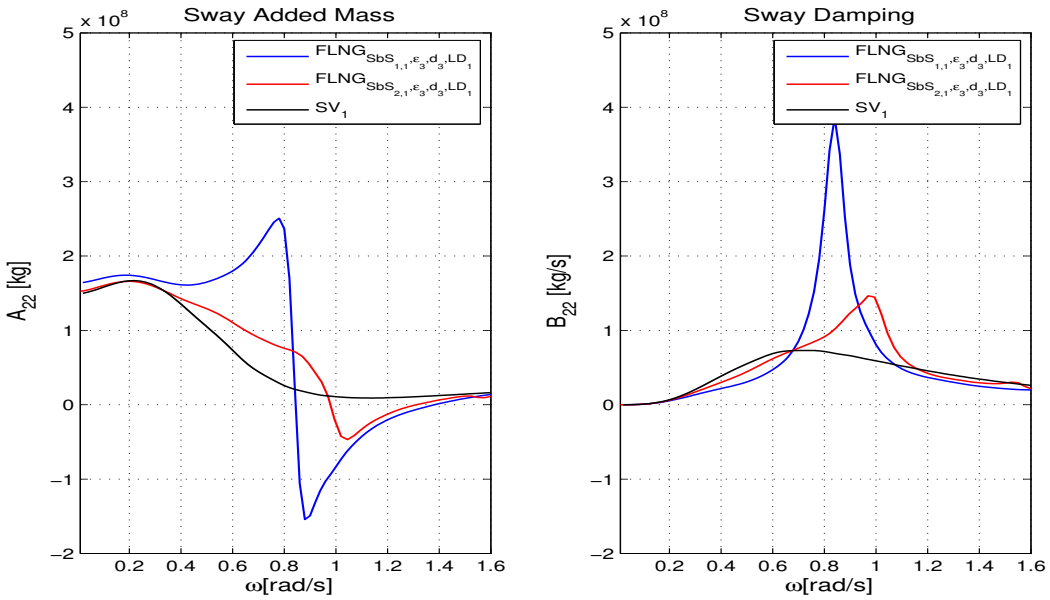

Figure 5.1: Sway hydrodynamic coefficients for FLNGmax single vessel [SV_1] vs FLNGmax multi-body configuration [$SbS_{1.1},\epsilon_3,LD_1$ & $SbS_{2.1},\epsilon_3,LD_1$]

First order motions

As it can be seen throughout the results (Figures [**??**...**??**]) the FLNG responses are slightly affected by the interaction with the carrier(i.e heave, pitch and yaw) near the resonant frequency. However the interaction effects can be visible only for heave in beam waves. Around 0.42 rad/s it can be seen a drop in the heave of FLNG which is caused by the radiated waves from the carrier which oscillate at the roll natural period. It can be considered significant reduction, approx 0.3 m/m in side by side with the LNGC carrier, while with the LPGC is a lot lesser. Pitch and yaw can be considered insignificant ,i.e 0.5 deg/m, for a vessel of 300m. For the other degrees of freedom, no interaction effects can be identified. Especially for roll motion there is no visible shielding effect (90 deg. direction) due to the presence of the carrier. Below it is plotted only the response of the $FLNG_{SbS_{1.1},\epsilon_3,d_3,LD_1}$ and FLNG alone in beam waves. It can be clearly seen that the difference between single vessel and in side by side configuration is insignificantly. Thus it can be considered that there are no shielding effects due to the presence of the carrier for this side by side configuration.

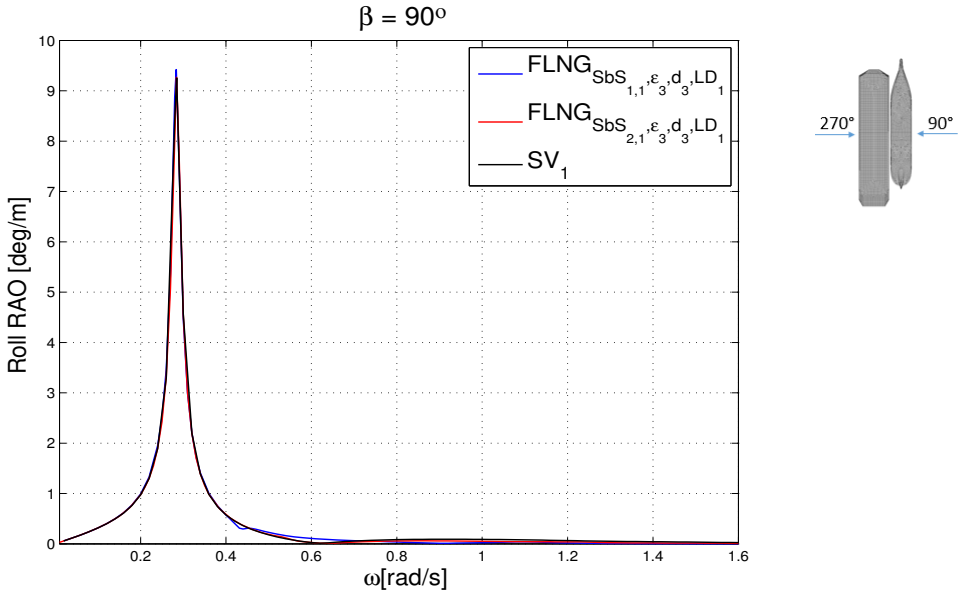

Figure 5.2: FLNGmax single vessel [SV_1] vs FLNGmax in multi-body configuration [$SbS_{1.1}$, ϵ_3, d_3, LD_1 & $SbS_{2.1}$, ϵ_3, d_3, LD_1] in beam waves

Second order forces

The second order forces are shown starting from Figure **??**. Regarding the surge drift forces of the FLNG, it can be observed that between single body and in side-by-side with the LPG carrier there are no significant differences in force magnitude. On the other hand for FLNG-LNG carrier, influences are visible for bow-quartering waves towards higher frequencies. Furthermore the presence of the carrier is reflected by the non-smooth character of the graph after the frequency of 0.5 rad/s which emphasis the interaction effects. Towards really low frequencies there is no impact at all. This is because at very low frequencies, the wave length is very large compare to the ship length and therefore the vessel ”follow” the wave. Furthermore, at this frequencies, the relative wave elevation is zero, thus the drift forces tends to be close to zero. When the FLNG floats alone, sway drift force is nearly zero in head and following waves and surge forces are nearly zero in beam waves. Furthermore, because the FLNG geometry is barge shaped, where the bow tends to be symmetric with the aft part, the yaw drift force for wave directions:0deg, 180deg, 90deg and 270deg. is close to zero when the vessel floats alone. The hydrodynamic interaction effects, can be clearly seen for the forces at the wave directions mentioned before that are non zero when the FLNG is in side by side configuration (Figure5.4).

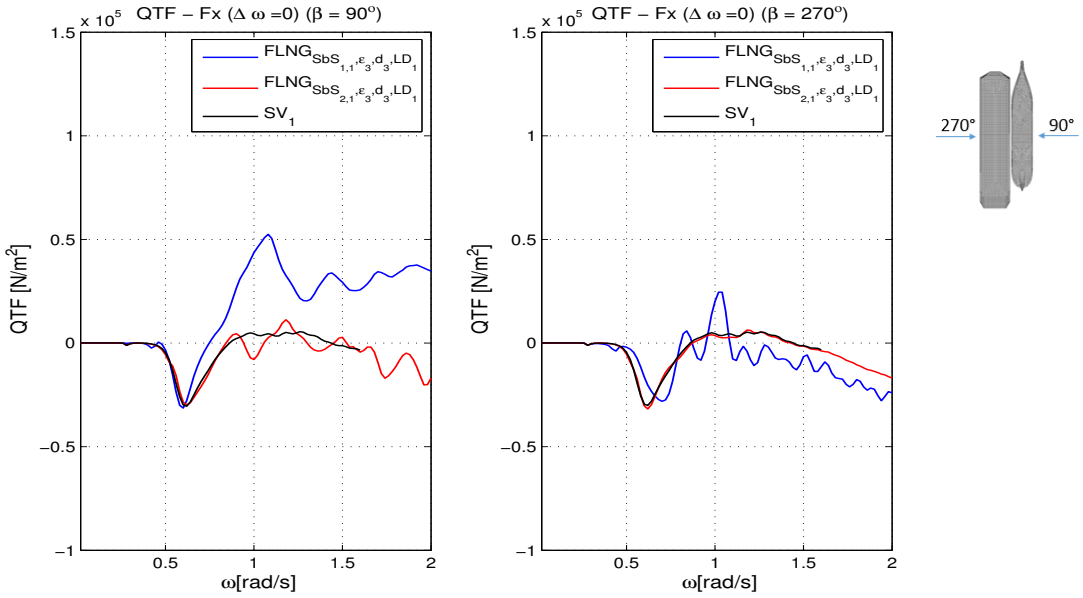

Figure 5.3: Surge mean drift forces for FLNGmax single vessel [SV_1] vs FLNGmax multi-body configuration [$SbS_{1.1}$, ϵ_3, d_3, LD_1 & $SbS_{2.1}$, ϵ_3, d_3, LD_1] - Interaction effects

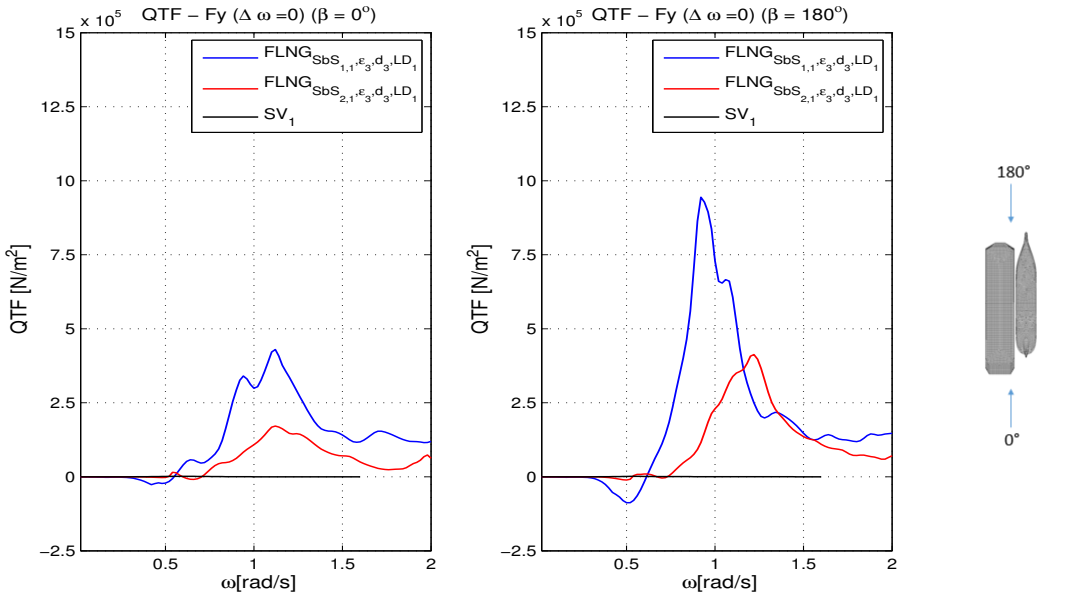

Figure 5.4: Sway mean drift forces for FLNGmax single vessel [SV_1] vs FLNGmax multi-body configuration [$SbS_{1.1}$, ϵ_3, d_3, LD_1 & $SbS_{2.1}$, ϵ_3, d_3, LD_1] - Interaction effects

It is interesting to see that for beam waves, on the shielded side of the FLNG (90 deg.) but as well on the un-shielded side(270 deg.) for lower frequencies (up to 0.5 rad/s) there is a little suction effect for the side by side configuration between FLNG and LNG carrier, where the FLNG tends to drift slowly towards the carrier. After this frequency region, the FLNG is pushed away from the carrier, with a high force in the direction of the incoming wave. As it can be seen in Figure 4.7, the bow region of the FLNG is shielded by the carrier and the effects can be clearly seen, especially for sway mean drift force above 0.6 rad/s, the single body sway mean drift force is higher than for the multi body configuration. On the other side, for un-shielded side (270deg.) an interesting phenomena is remarked. Near the frequency of 1 rad/s, the FLNG is pushed against the wave direction. The physical explanation is that at

this frequency the resonant mode (pumping mode) of the standing wave occur and the FLNG is pushed really violent away from the carrier. This can be emphasized by the wave elevation between the two vessels, which shows that at this frequency, there is a high peak followed by a sharp drop. Similar effects can be noticed for the bow quartering waves (210 deg. and 150 deg.) but with a smaller magnitude. Above this frequency it can be seen that the sway drift force for the single vessel is comparable to the drift force for the FLNG in multi body configuration for the un-shieldied side. On the other side for FLNG-LPGC configuration can be observed that the the drift forces are comparable to the ones when the FLNG floats alone. In particular for surge mean drift force no significant interaction effects could be identified. For sway mean drift forces of FLNG-LPG configuration it can be seen that even the size (i.e wetted surface) of the carrier is small in comparison to the FLNG size, still has considerable shielding effects after certain frequency(i.e 0.6rad/s) when the incoming wave is from 90deg. On the opposite side (270 deg.), the identified effects are due to the high pressure which arise due to the drifting carrier, the FLNG does not experience a violent force opposite to the direction of the incoming wave (move away from the carrier) as for the case when the FLNG floats alongside the LNG carrier.

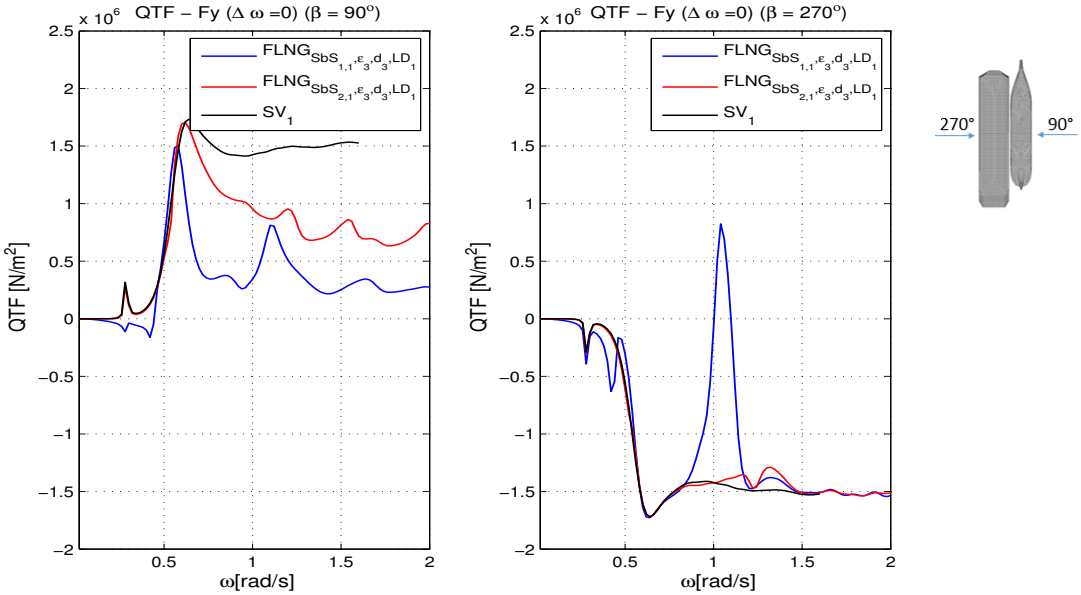

Figure 5.5: Sway drift forces in beam waves for FLNGmax single vessel [SV_1] vs FLNGmax multi-body configuration [$SbS_{1.1}$, ϵ_3, d_3, LD_1 & $SbS_{2.1}$, ϵ_3, d_3, LD_1] - Shielding effects

Yaw drift forces of the single body are nearly zero for beam and stern waves(Figure **??**). However for side by side configuration, the drift forces have very large spikes (near resonance frequency). On the other side, in the low frequency area where the wave length is large, the diffraction effects is obvious and therefore a reduction of the wave force exerted on the vessel can be seen. General conclusion regarding the drift forces for the FLNG in multi-body configuration against the FLNG alone, is that at lower frequencies (up to 0.5rad/s) the forces are the same. Furthermore, the second order forces are more sensitive than first order, thus the shielding effects are visible. By far it is noticed that the beam waves are the most dangerous condition for the side-by-side operations.

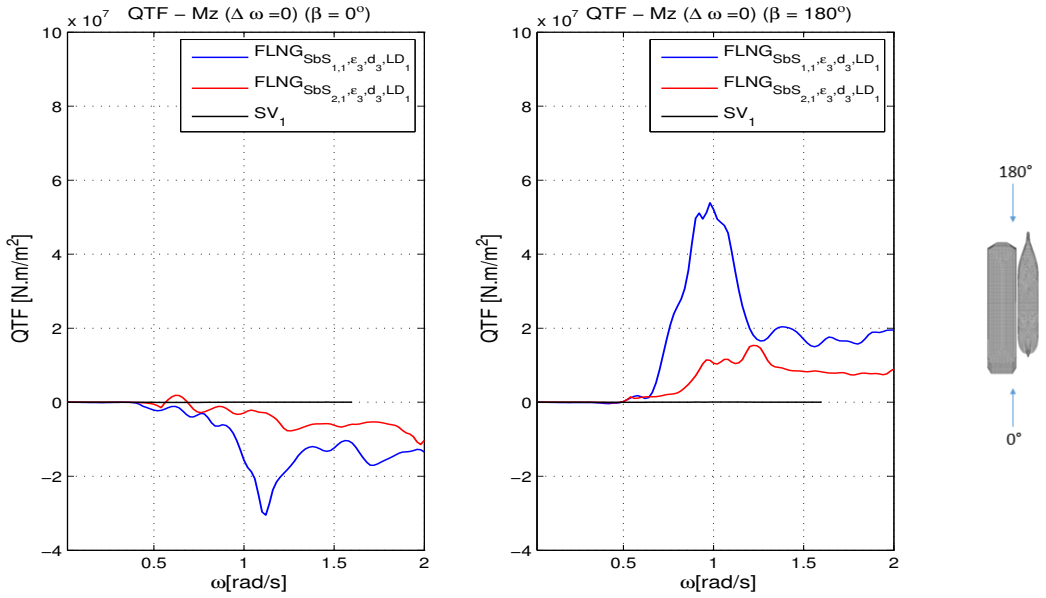

Figure 5.6: Yaw drift forces in head and following waves for FLNGmax single vessel [SV_1] vs FLNGmax multi-body configuration [$SbS_{1.1}$, ϵ_3, d_3, LD_1 & $SbS_{2.1}$, ϵ_3, d_3, LD_1] - Interaction effects

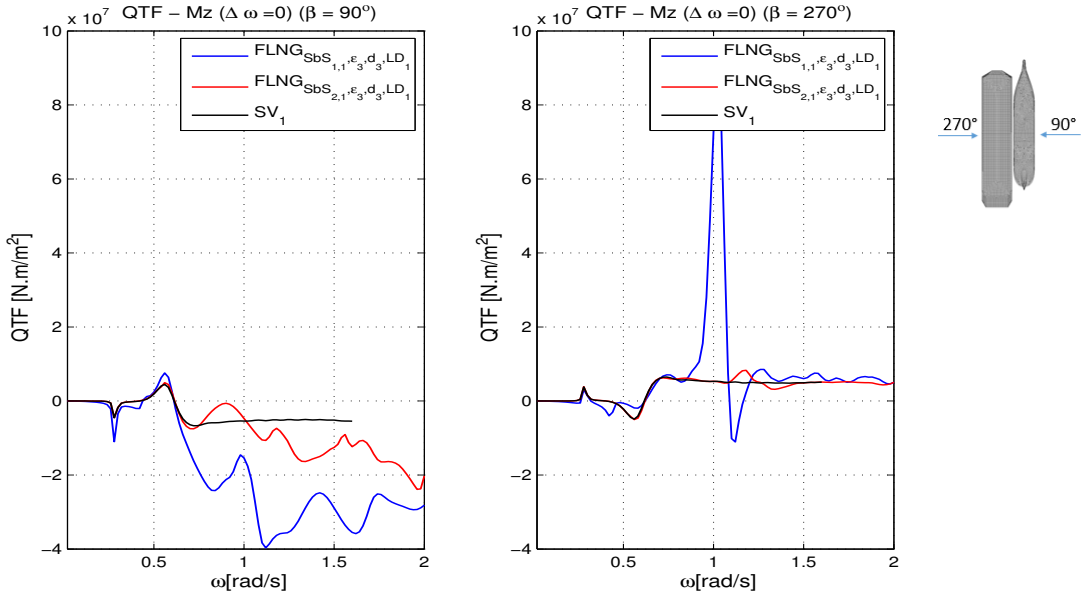

Figure 5.7: Yaw drift forces in beam waves for FLNGmax single vessel [SV_1] vs FLNGmax multi-body configuration [$SbS_{1.1}$, ϵ_3, d_3, LD_1 & $SbS_{2.1}$, ϵ_3, d_3, LD_1] - Interaction effects

Wave elevation

Throughout the graphs it can be seen that the responses for 180 deg. is higher than for 0deg.(stern waves). This is explained the fact that there is more diffraction in the forward part of the side-by-side configuration and it is confirmed by the wave elevation at the manifold location where the highest elevation is reached due to the head waves. Furthermore can be clearly seen the difference of the radiation and diffracted wave due to the presence of the FLNG. When it is considered 270deg. direction (coming from FLNG side), the wave elevation is 1m higher than on the opposite side(from the LNGC's side). In addition can be observed that the wave elevation reaches spikes near the resonance.

5.1.2. LNGC

All the results for this comparison are presented graphically in the Appendix **??**, as follows:

Hydrodynamic coefficients	RAO	QTF
Figure **??**	Figures [**??**...**??**]	Figures [**??**...**??**]

Table 5.3: List of results

Cases	$LNGC_{SbS_{1.1}, \epsilon_3, d_3, LD_1}$ **vs** SV_3

Table 5.4: Analyzed cases

Hydrodynamic coefficients

Hydrodynamic coefficients of the carrier in ballast condition for the multi-body configuration mentioned above, in the Figure **??** are presented. The same conclusions as for the FLNG can be drawn, but the impact of the multi-body system is more evident for the carrier because has smaller volume and finer shape compare to the FLNG. Hydrodynamic coefficients are a function of the vessel size (i.e displacement) are expected to be smaller compare to the FLNG which means that the carrier is expected to be more sensitive in side by side configuration. At lower frequencies (up tp 0.4 rad/s), when the vessel ”follow” the wave, the system is dominated by the restoring term such that the damping of the vessel in multi body configuration is the same as the damping of the single vessel. Furthermore, the added mass are almost equal to the case of the single vessel which means that at lower frequencies, the radiated waves generated by the oscillations of the carrier dies out without reflecting back from the FLNG. For higher frequency region (above 1.2 rad/s), the hydrodynamic coefficients of the side-by-side carrier become close to the vessel alone because the diffraction effects are less. The water column which forms between the vessels at the resonance frequency, influences the hydrodynamic coefficients and implicit the responses results.

First order motions

The effect of multi-body configuration can be clearly seen for the carrier as well. Usually roll, sway and yaw in head and stern waves for single body the response is zero, due to the symmetry with respect to the xOz plane(Figure**??**). When the carrier is moored in close proximity to another vessel, sway and roll in head and following waves is no longer zero (for sway and yaw can be considerable small, but this represents a particularity for side-by-side moored vessels). Moreover, rolling of the carrier appears to be more affected by the strong coupling between vessels and the response is quite considerable (2deg/m).

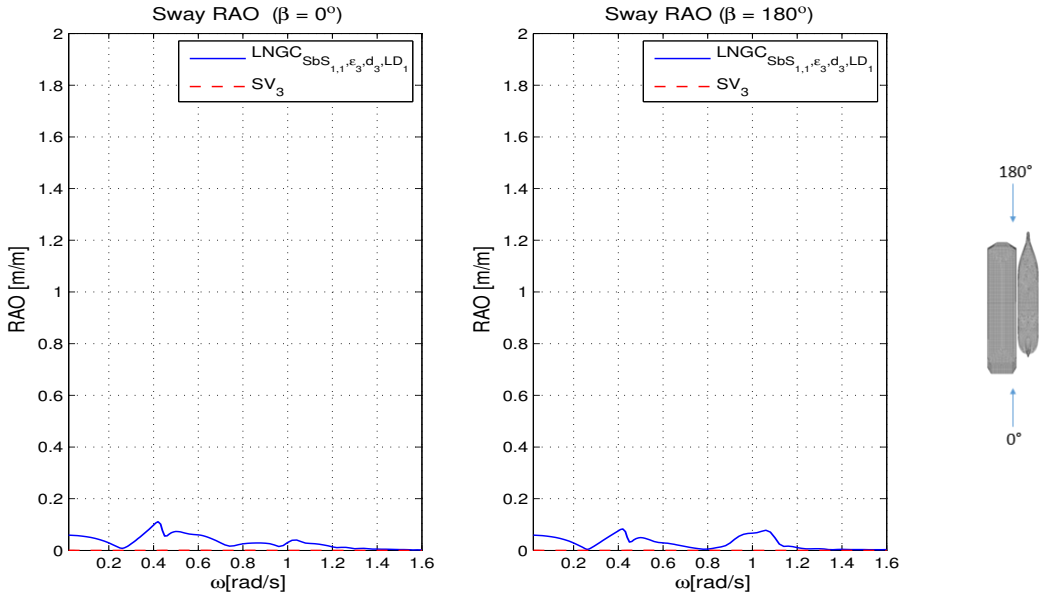

Figure 5.8: Sway for LNGCmin single vessel [SV_3] vs LNGCmin multi-body configuration [$SbS_{1.1}$, ϵ_3, d_3, LD_1]- Interaction effects

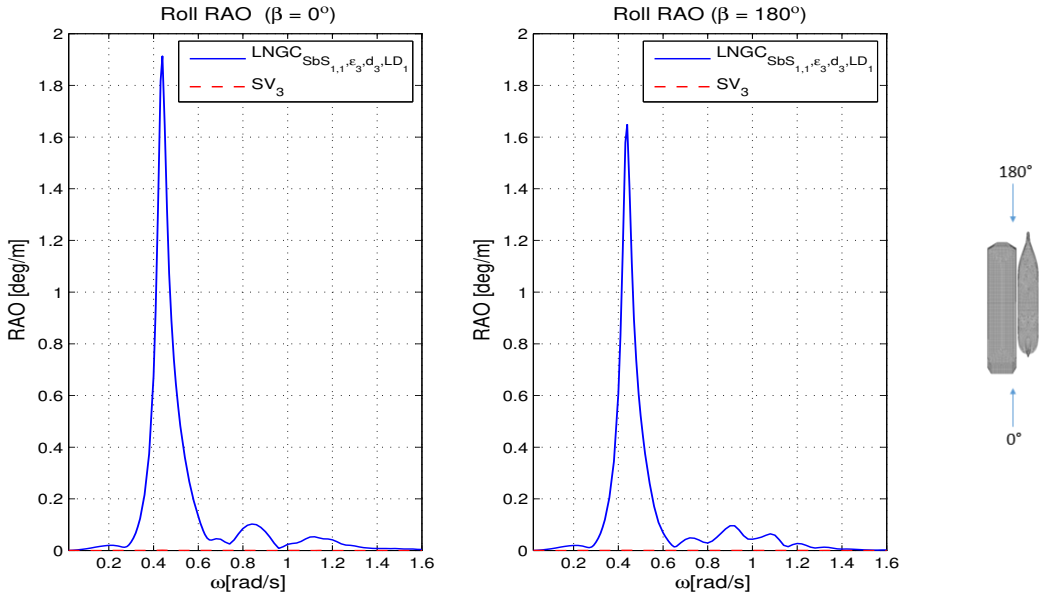

Figure 5.9: Roll for LNGCmin single vessel [SV_3] vs LNGCmin multi-body configuration [$SbS_{1.1}$, ϵ_3, d_3, LD_1] - Interaction effects

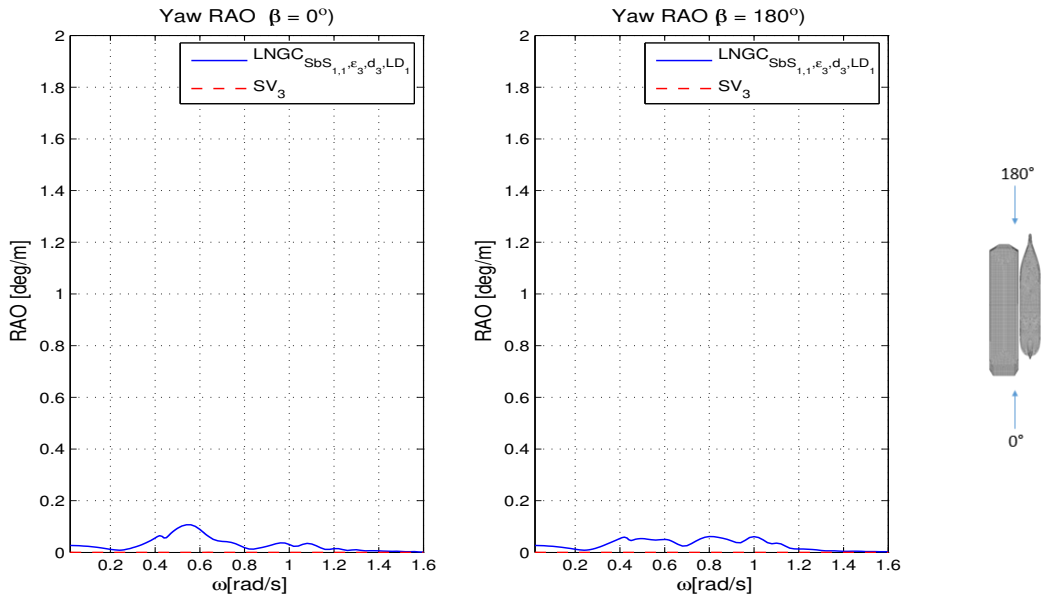

Figure 5.10: Yaw for LNGCmin single vessel [SV_3] vs LNGCmin multi-body configuration [$SbS_{1.1}$, ϵ_3, d_3, LD_1] - Interaction effects

Overall for sway motion from the other wave directions is not influenced at all. Pitch response of the carrier experience the interaction effects starting from natural frequency towards higher frequency limit. On the other hand for roll and heave, the effects of shielding (270deg.) are significant and the motions are considerably reduced (50% for heave; 3deg/m for roll). Furthermore it can be observed from Figure **??** that when the wave is coming from the sheltered area of the carrier, the responses (heave and roll) are smaller than when the vessel floats alone. Moreover the coupling between heave of the carrier and roll of the FLNG is also visible (around 0.25rad/s) where a small drop can be identified.

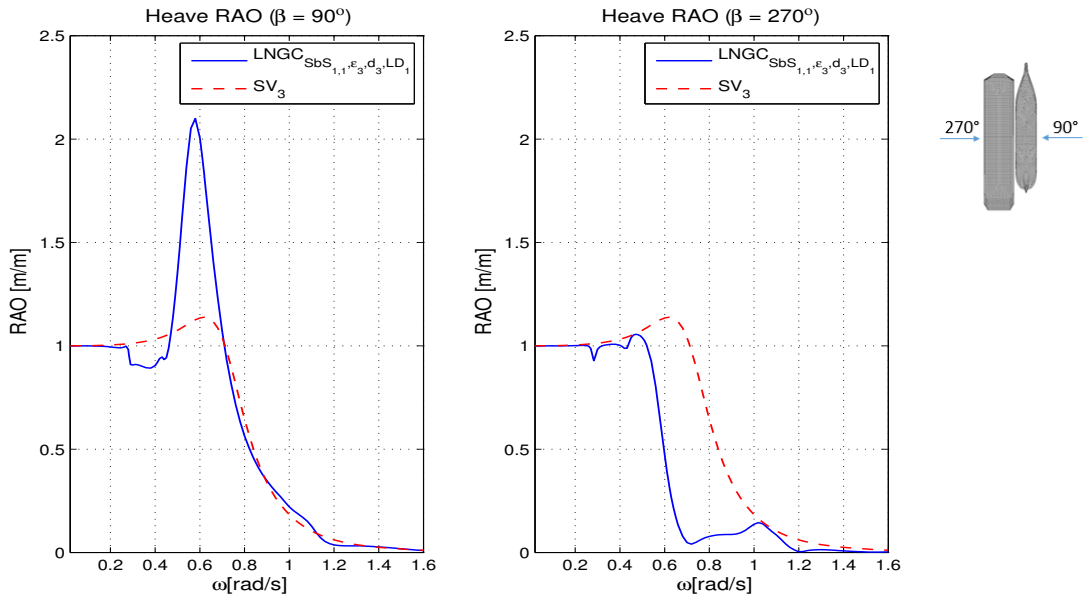

Figure 5.11: Heave for LNGCmin single vessel [SV_3] vs LNGCmin multi-body configuration [$SbS_{1.1}$, ϵ_3, d_3, LD_1] - Shielding effects

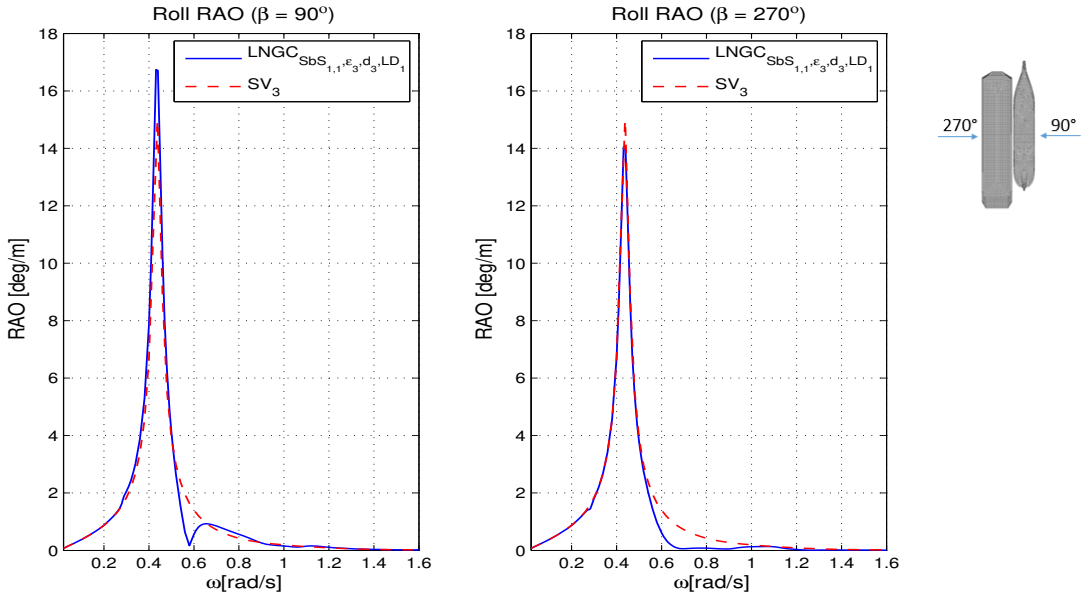

Figure 5.12: Roll for LNGCmin single vessel [SV_3] vs LNGCmin multi-body configuration [$SbS_{1.1}$, ϵ_3, d_3, LD_1] - Shielding effects

An interesting phenomena which should be mentioned is that for 210deg and 330deg (shielded side of the carrier) the carrier appears to be more affected(Figure**??**), thus rolling more than on the opposite side (exposed side). Can be explained by the fact that the radiated and diffracted wave field from the FLNG strikes the carrier which cause ultimately a higher response for the carrier. On the other side, the roll response of the carrier under the exposed area(150deg. and 30deg.) is almost twice smaller than for the carrier alone (Figure**??**). The physical explanation is that the generated wave field from the carrier are reflected back to the carrier which acts on the opposite side of the incoming wave which ultimately damps the roll motion.

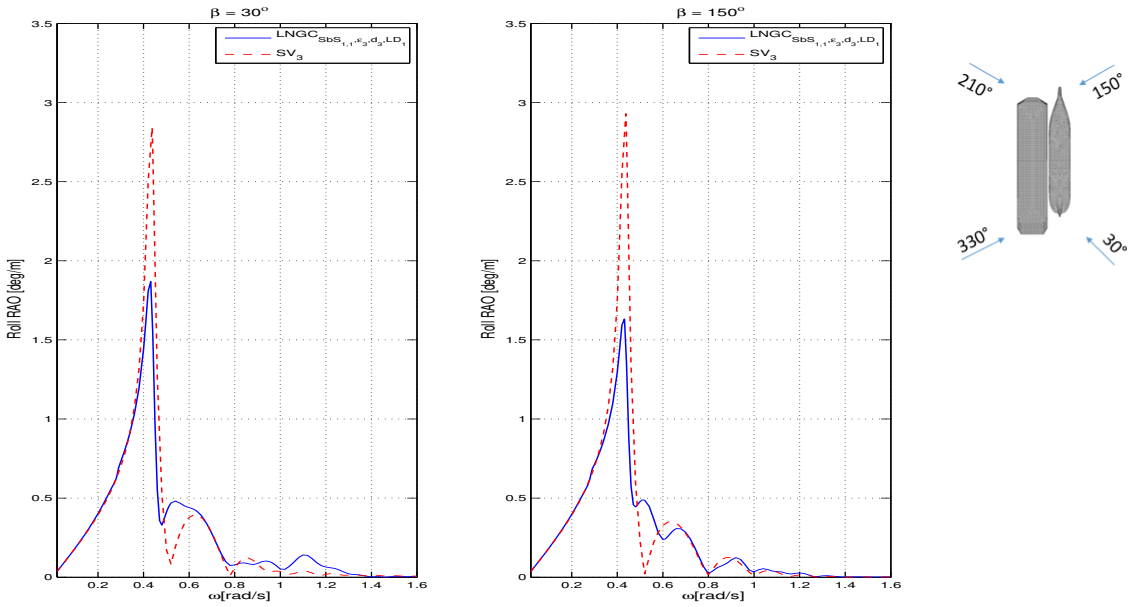

Figure 5.13: Roll in bow and stern quartering waves for exposed side of LNGCmin single vessel [SV_3] vs LNGCmin multi-body configuration [$SbS_{1.1}$, ϵ_3, d_3, LD_1]

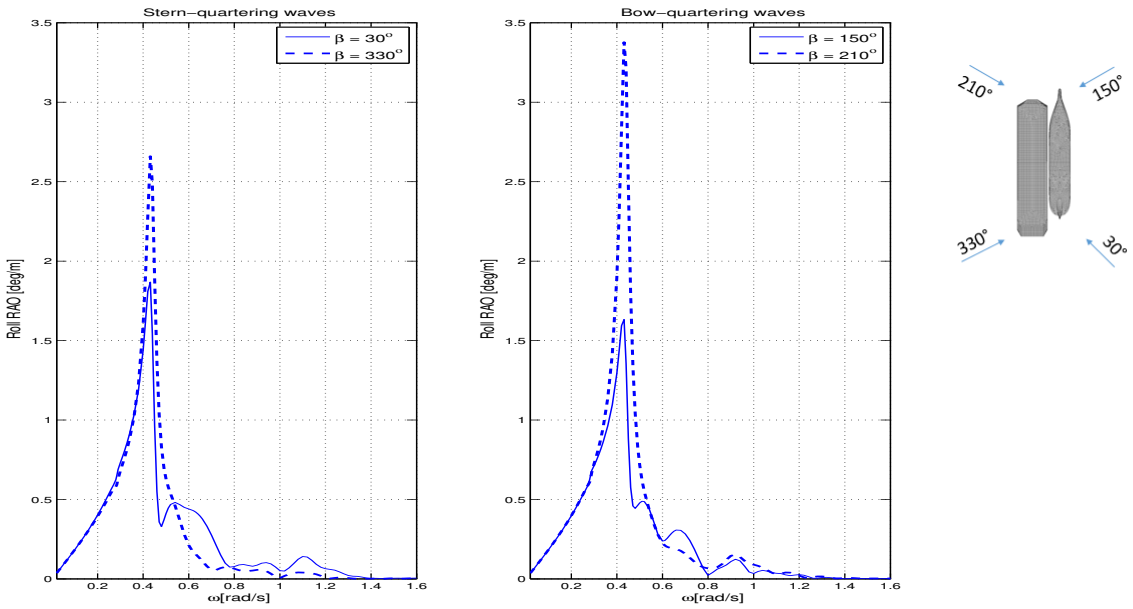

Figure 5.14: Roll in bow and stern quartering waves for exposed and sheltered side of LNGCmin multi-body configuration [$SbS_{1.1}$, ϵ_3, d_3, LD_1]

Second order forces

Second order forces of the carrier alone for head and following waves in sway and yaw direction goes to zero. The interaction effects can be noticed for this specific directions and degree of freedom, such that in side-by-side, the carrier experiences significant drift forces.

For the other wave direction interesting outcome is highlighted. First of all the shielding effects are visible especially for yaw and sway, where the carrier experiences larger forces than in multi body configuration. This is valid for higher frequency region, while for lower frequencies (up to 0.5 rad/s) the force is the same for both cases. This leads to the conclusion that for very low frequencies the multi body interaction effects are not important. For beam seas, for an angle of incidence of 270 deg. which means the shielded part of the LNGC, it can be observed that the sway mean drift is close to zero up to 0.8 rad/s and after this frequency a high spike is remarked, when the carrier is pushed away from the FLNG. The physical explanation is that at the resonance frequency, when the wave elevation becomes larger cause a higher pressure on the port-side of the carrier and consequently the carrier is pushed violently away from the FLNG.

On the exposed side (90 deg.) of the carrier, the same phenomena can be noticed (around 1 rad/s) but with smaller intensity. Compare to the FLNG, it can be noticed, that the carrier in side-by-side configuration is more sensitive due to the interaction with a larger structure.

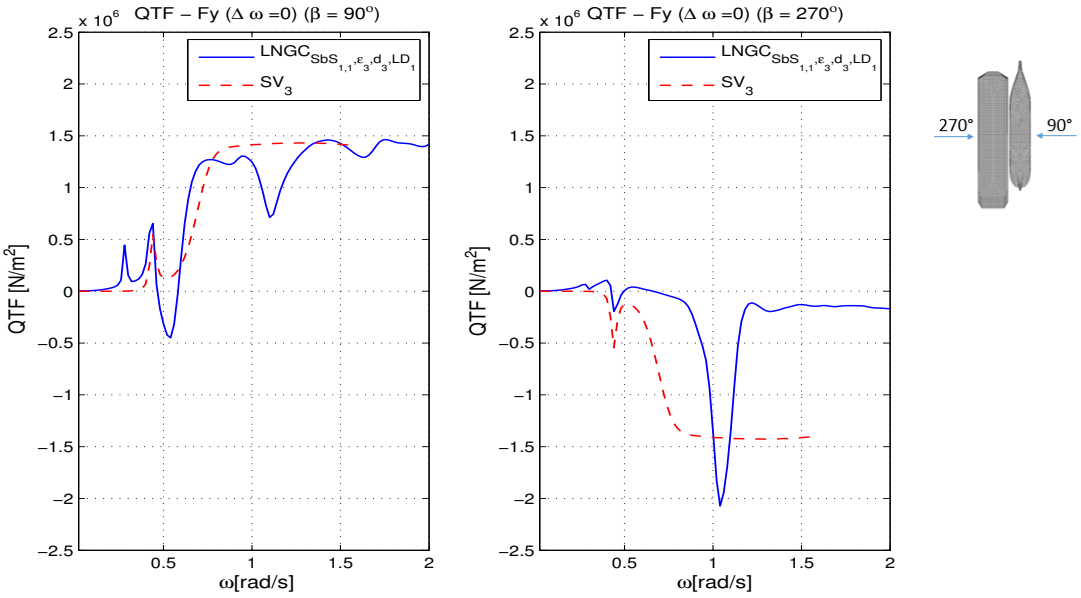

Figure 5.15: Sway drift forces in beam waves of LNGCmin single vessel [SV_3] vs LNGCmin multi-body configuration [$SbS_{1.1}$, ϵ_3, d_3, LD_1]

Regarding the yaw mean drift, it can be seen that the shielding effects are visible for stern-quartering waves (330deg.), while for bow-quartering waves (210deg.) is not valid anymore. This phenomena stands for sway and surge mean drift also.

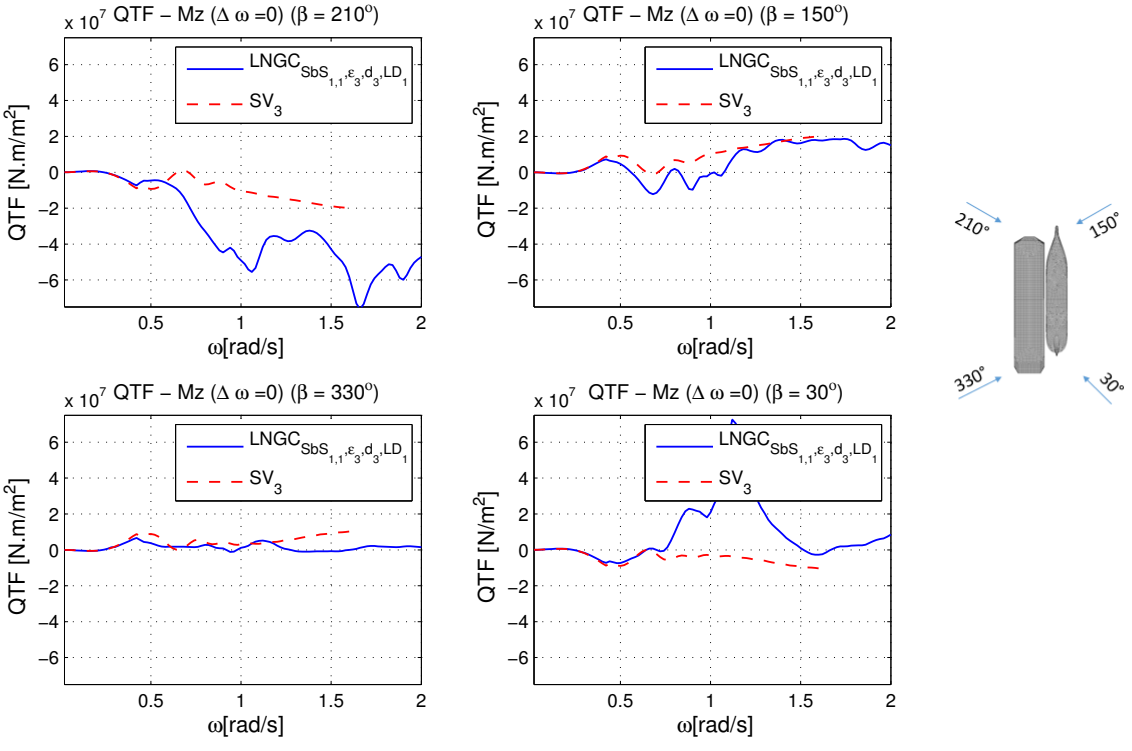

Figure 5.16: Yaw drift forces for bow and stern quartering-waves of LNGCmin single vessel [SV_3] vs LNGCmin multi-body configuration [$SbS_{1.1}$, ϵ_3, d_3, LD_1]

5.1.3. LPGC

All the results for this comparison are presented graphically in the Appendix **??**, as follows:

Hydrodynamic coefficients	RAO	QTF
Figure **??**	Figures [**??**...**??**]	Figures [**??**...**??**]

Table 5.5: List of results

Cases	$LPGC_{SbS_{2.1},\epsilon_3,d_3,LD_1}$ **vs** SV_5

Table 5.6: Analyzed cases

Hydrodynamic coefficients

Hydrodynamic coefficients for the LPG carrier in side-by-side configuration and alone vessel are compared in Figure **??**. It can be observed that the interaction effects are more visible between resonant and higher frequency limit. Near the peak frequency, the hydrodynamic coefficients reach large values. For high frequency region, the hydrodynamic coefficients become smaller than when the carrier floats alone. In general, for higher frequencies, the wave length is shorter and less diffraction effects, but in this case, considering the size of the LPGC, the diffraction effects acts as a dampener and are still considerable for these frequencies.

First order motions

Regarding the first order motion, no significant interaction effects can be identified for surge and sway response, exception makes sway in head and stern waves.

In beam seas(i.e 270deg.), the shielding effect is evident for heave and roll motion especially at the resonant frequency, such that roll of the carrier decrease with 10 deg/m and heave drops to zero. Moreover sheltering effects are reflected in heave, pitch and yaw moment when comparison between bow and stern quartering waves from lee-side (210deg.,330deg.) and the weather side (150deg.,30deg.) of the carrier are done. In particular, it can be seen that for pitch is a visible reduction of 50%. On the contrary, it can be noticed that the rolling of the carrier is higher for the lee-side than the weather side, such that for 150deg is almost zero while for 210deg is approximately 10deg/m. This can be explained by the fact that there is a strong coupling of side-by-side vessels (i.e diffracted wave fields from the FLNG, motion coupling). Therefore, when the incoming wave is from the lee-side direction, the FLNG starts to oscillate such that the radiated waves transports a significant amount of energy which is reflected on the rolling of the carrier. On the weather side, the carrier is excited by the incoming wave and damped by the diffracted waves from the FLNG.

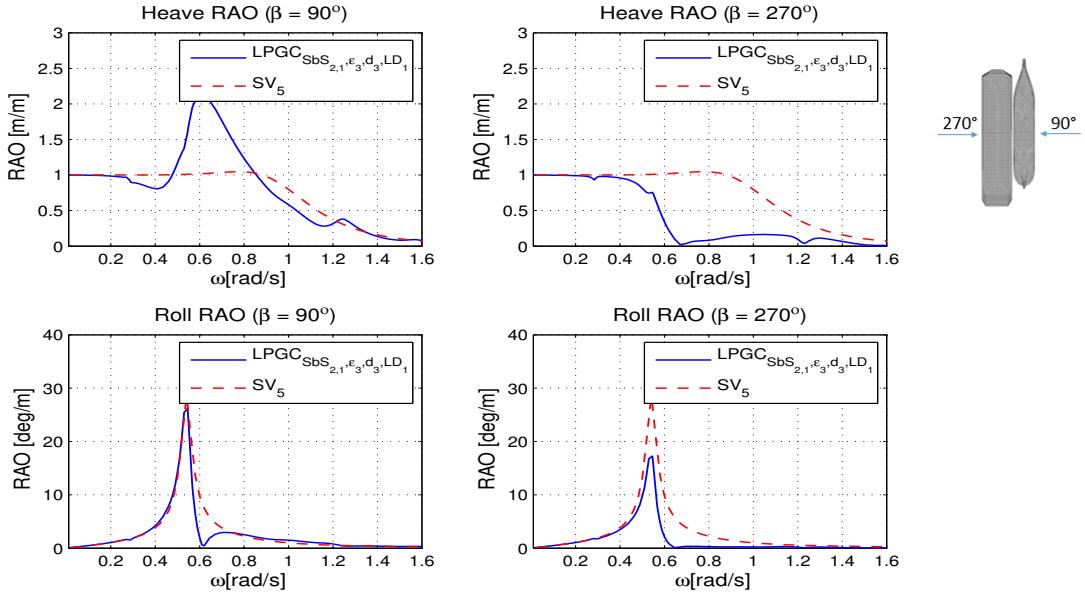

Figure 5.17: Roll and Heave in beam waves of LPGCmin single vessel [SV_5] vs LPGCmin multi-body configuration [$SbS_{2.1}$, ϵ_3, d_3, LD_1]

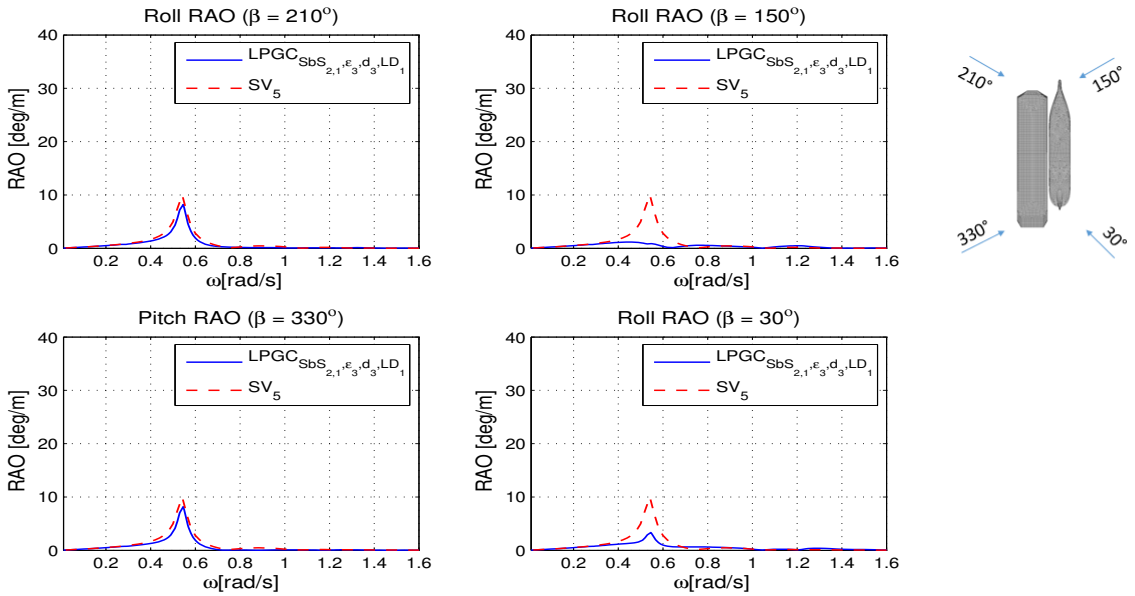

Figure 5.18: Roll for bow and stern quartering waves of LPGCmin single vessel [SV_5] vs LPGCmin multi-body configuration [$SbS_{2.1}$, ϵ_3, d_3, LD_1]

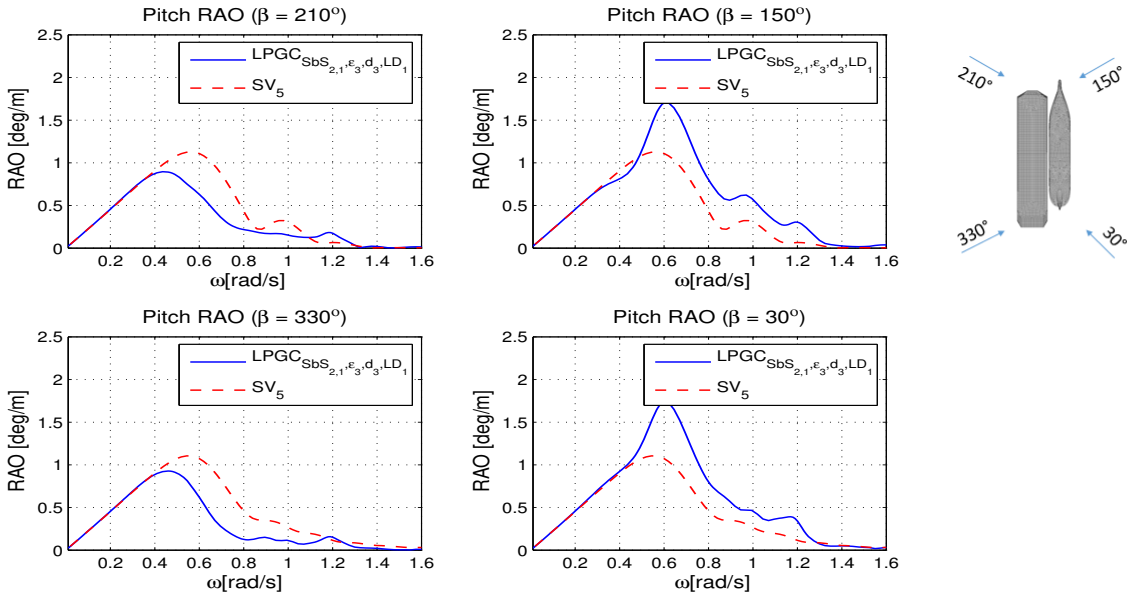

Figure 5.19: Pitch for bow and stern quartering waves of LPGCmin single vessel [SV_5] vs LPGCmin multi-body configuration [$SbS_{2.1}$, ϵ_3, d_3, LD_1]

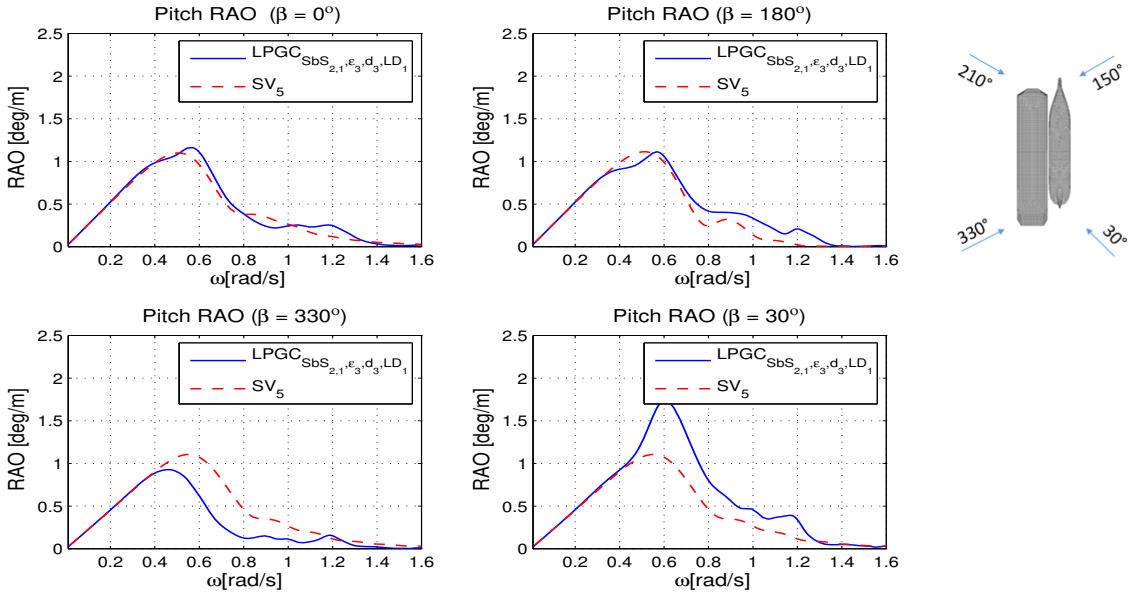

Figure 5.20: Pitch for head and following waves of LPGCmin single vessel [SV_5] vs LPGCmin multi-body configuration [$SbS_{2.1}$, ϵ_3, d_3, LD_1]

Second order forces

Second order drift forces can be checked throughout the Figures [**??**...**??**]. On this section, relevant results are described and shown as figures. Shielding effects are visible between weather side and lee-side, especially for sway mean drift forces. On the other hand, drift forces of the single vessel are very close to the carrier in multi-body configuration. An interesting fact which should be noted is that for stern quartering waves (30deg.), after 0.8 rad/s, sway drift force for the carrier in multi-body system becomes negative. This is the reason of sway-yaw coupling at the pumping resonant frequency which cause a higher pressure on the lee-side than on the weather side and ultimately push the carrier into the opposite side of the incoming wave. Similar behaviour for sway drift forces for bow quartering waves can

be seen.

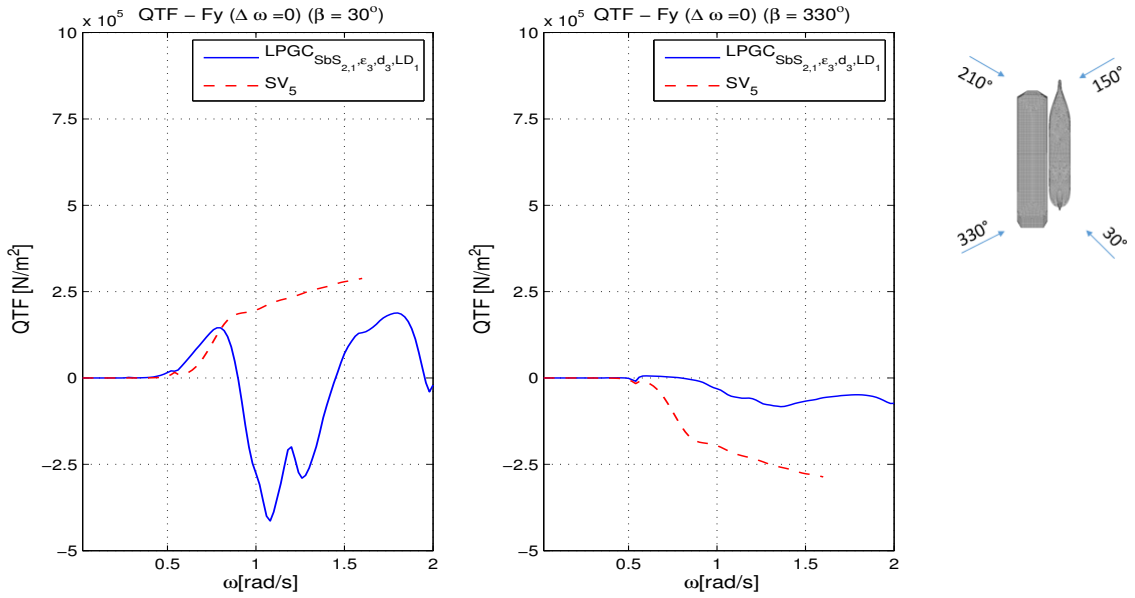

Figure 5.21: Sway drift force for stern quartering waves of LPGCmin single vessel [SV_5] vs LPGCmin multi-body configuration [$SbS_{2.1}$, ϵ_3, d_3, LD_1]

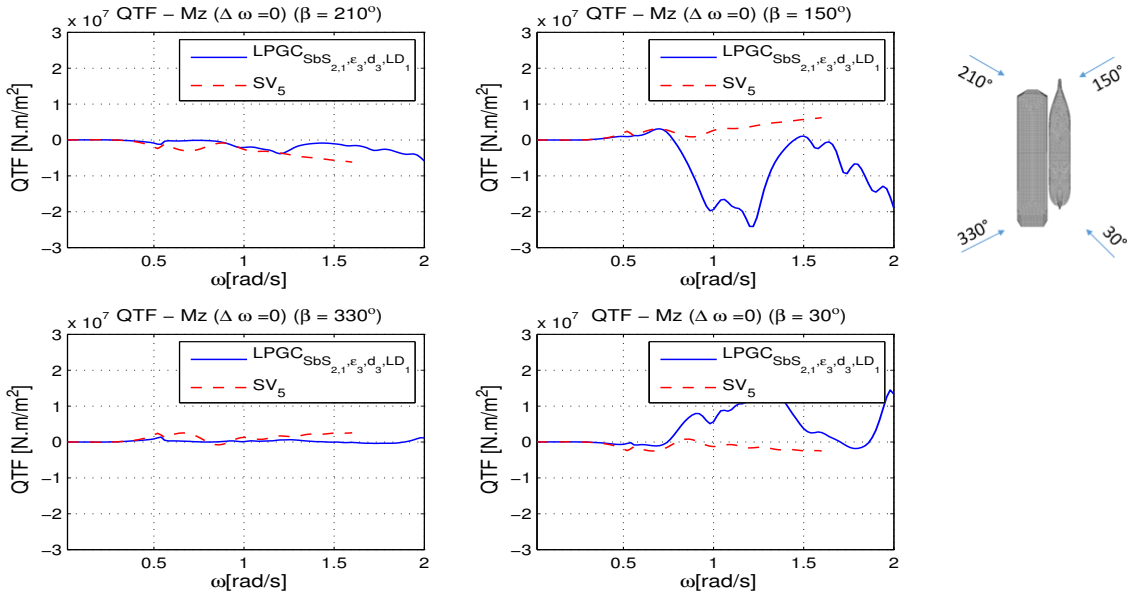

Figure 5.22: Yaw drift force for stern quartering waves of LPGCmin single vessel [SV_5] vs LPGCmin multi-body configuration [$SbS_{2.1}$, ϵ_3, d_3, LD_1]

5.2. FLNG size

All the results for this comparison are presented graphically in the Appendix **??**, as follows:

Hydrodynamic coefficients	RAO	QTF
Figure **??**	Figures [**??**...**??**]	Figures [**??**...**??**]

Table 5.7: List of results

5.2.1. FLNG

For this comparison, only the FLNG size has been varied, while the others parameters remained constants as follows:

Cases	$FLNG_{SbS_{1.1}, \epsilon_3, d_3, LD_1}$ **vs** $FLNG_{SbS_{1.2}, \epsilon_3, d_3, LD_1}$ **vs** $FLNG_{SbS_{3.1}, \epsilon_3, d_3, LD_1}$

Table 5.8: Analyzed cases

Hydrodynamic coefficients

For the FLNG size variation, the hydrodynamic coefficients show that the larger the vessel the larger are the coefficients for all degree of freedom. An exception makes roll damping because of two reasons: firstly, the liquid tank correction has been applied and secondly a larger vessel (quite stiff), will roll less, thus a roll damping smaller. Sway added mass after the natural frequency (0.8 rad/s), for all 3 cases considered, is almost equal.

First order motions

Regarding the first order motions, it can be seen that the sway and surge motions are not affected by the FLNG size variation such that the responses are the same for each case considered. Slightly variations in heave responses could be identified, especially for beam waves. This is caused by the variation in draft of the vessels such that for the FLNG of 371m the B/T is 3.77 while for the FLNG of 301m is 4.89. Therefore a vessel with a smaller B/T ratio will tend to heave more. For roll motions the difference is more evident. Though the difference in magnitude between FLNG of 346m and FLNG of 301.5m is very small. On the other hand compare to the FLNG of 371m, the roll response in beam waves is smaller with 2 degrees/m than for the other cases. The reason behind is that the FLNG of 371.4m is wider than the others, which provides a higher restoring force. Moreover it has a smaller damping which means that is quite stiff and it will tend to oscillate less than for the other FLNG considered. Furthermore, a shifting of the resonance period can be noticed.

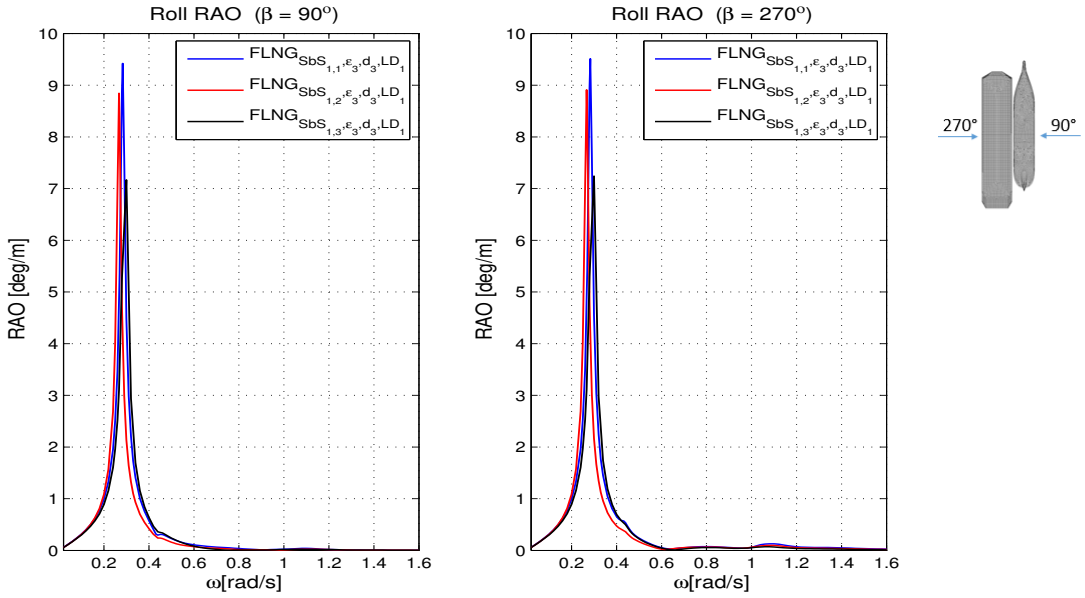

Figure 5.23: Roll in beam waves of FLNGmax with different size in multi-body configuration $[SbS_{1.1},\ \epsilon_3,\ d_3,\ LD_1;\ SbS_{1.2},\ \epsilon_3,\ d_3,\ LD_1;\ SbS_{1.3},\ \epsilon_3,\ d_3,\ LD_1]$

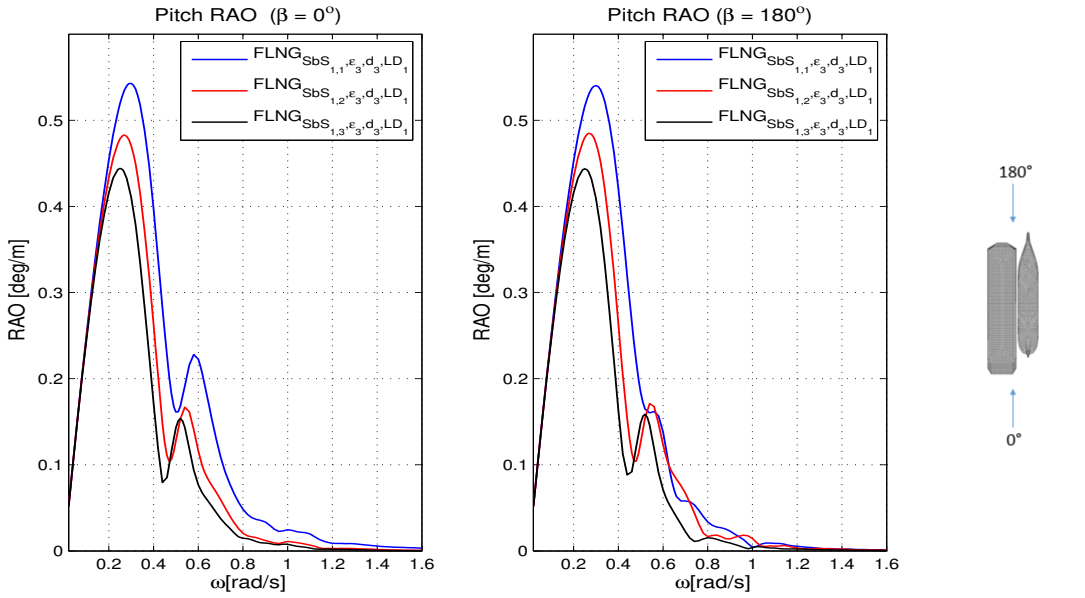

Figure 5.24: Pitch in head and following waves of FLNGmax with different size in multi-body configuration $[SbS_{1.1},\ \epsilon_3,\ d_3,\ LD_1;\ SbS_{1.2},\ \epsilon_3,\ d_3,\ LD_1;\ SbS_{1.3},\ \epsilon_3,\ d_3,\ LD_1]$

Second order forces

In this section the effect of FLNG size variation on the second order drift forces are presented. It is known that the drift force is a function of the wetted surface of the vessel. Such that for a unit wave amplitude, it is expected that the longer the vessel, the higher the drift force, with few exceptions that will be discussed later. It can be observed that for very low frequencies (up to 0.3 rad/s) each FLNG has no drift in any direction. Regarding the surge mean drift force two aspects can be remarked. Firstly, for head waves (180deg.) and bow-quartering waves (210deg.) it can be seen that FLNG of 301.5m length drifts more than the others, especially for high frequency zone. This means that the diffraction effects are still considerable for this side-by-side configuration. Moreover, for the same configuration, can be noticed that the

interaction effects are stronger than for the other cases such that for bow quartering waves, the surge mean drift force is higher than for head waves. For beam waves, surge drift force for FLNG (301.5m) is positive while for the FLNG (371.4m) is negative and for the FLNG(346m) is close to zero.

For sway mean drift force throughout the results no significant differences can be identified, except of beam waves condition. Sway drift force of the FLNG (371.4m) from shielded side (90 deg.) has the highest magnitude. This can be explained by the fact that for this particular size, the starboard side of the FLNG is not fully shielded by the carrier. This is valid on the opposite side also except at the resonant frequency, when the drift force for the biggest FLNG become almost zero, while the other FLNGs are pushed slightly into the opposite direction of the incoming wave.

Overall the yaw mean drift force are very similar, exception makes beam waves coming from the weather side. As it can be seen the moments for FLNG(371m) and FLNG(346m) are almost equal, but for the FLNG(301.5m) the pumping mode resonance is more evident and the yaw moment is almost two times higher than for the other cases.

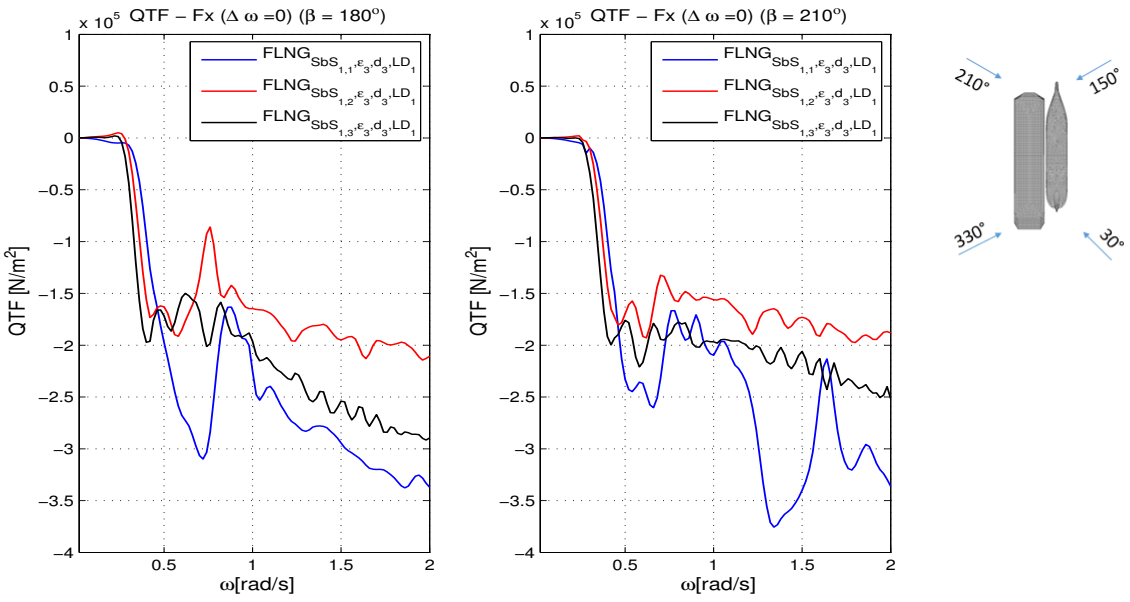

Figure 5.25: Surge drift force for head and quartering waves of FLNGmax with different size in multi-body configuration [$SbS_{1.1}$, ϵ_3, d_3, LD_1; $SbS_{1.2}$, ϵ_3, d_3, LD_1; $SbS_{1.3}$, ϵ_3, d_3, LD_1]

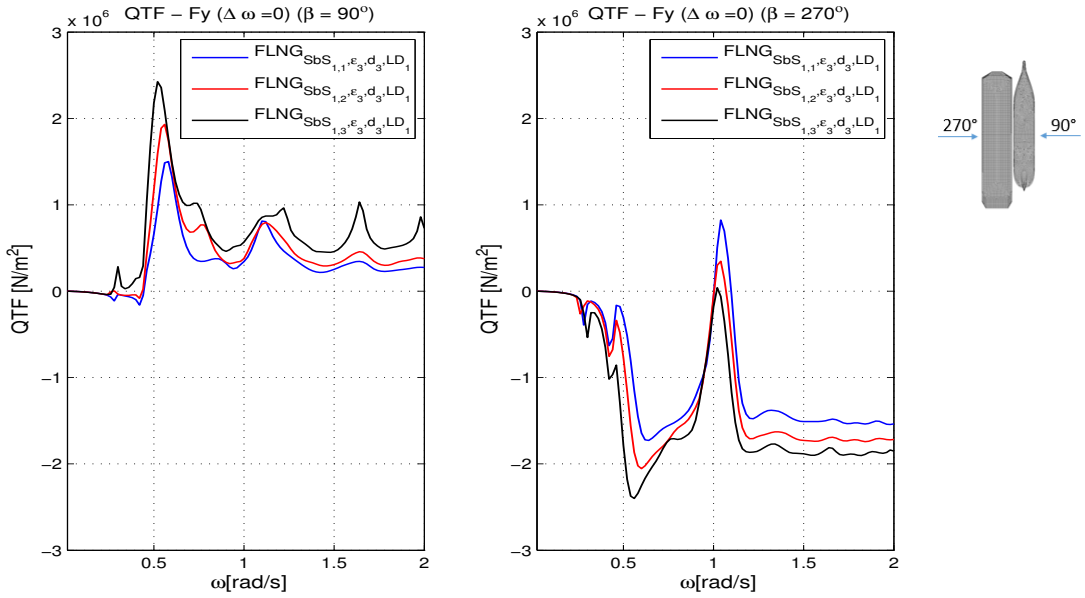

Figure 5.26: Sway drift force in beam waves of FLNGmax with different size in multi-body configuration [$SbS_{1.1}$, ϵ_3, d_3, LD_1; $SbS_{1.2}$, ϵ_3, d_3, LD_1; $SbS_{1.3}$, ϵ_3, d_3, LD_1]

5.2.2. Effect of FLNG size variation on LNGC

Results are presented graphically in the Appendix **??** as follows:

Hydrodynamic coefficients	RAO	QTF	WE
Figure **??**	Figures [**??**...**??**]	Figures [**??**...**??**]	Figure **??**

Table 5.9: List of results

Cases	$LNGC_{SbS_{1.1},\epsilon_3,d_3,LD_1}$ **vs** $LNGC_{SbS_{1.2},\epsilon_3,d_3,LD_1}$ **vs** $LNGC_{SbS_{3.1},\epsilon_3,d_3,LD_1}$

Table 5.10: Analyzed cases

Hydrodynamic coefficients

In side-by-side configuration, as the FLNG length increase, the radiated waves from the carrier can be fully reflected. Such that for the added mass and damping component a small increase in magnitude can be identified. However the overall difference in magnitude for all the considered cases can still be considered small.

First order motions

The influence of the FLNG size variation starts to be visible after a certain frequency (above 0.3 rad/s). In general the bigger the FLNG the greater the impact on the carrier responses.

Responses for surge, sway and yaw moment are equal for all three cases considered. Roll motion of the carrier for each side-by-side configuration considered is very similar. As it was expected for bow-quartering waves (210deg.), roll of the carrier in close proximity to FLNG (301.5m) shows a higher response than for the other configurations, due to the fact that the bow of the carrier is exposed to the incoming wave.

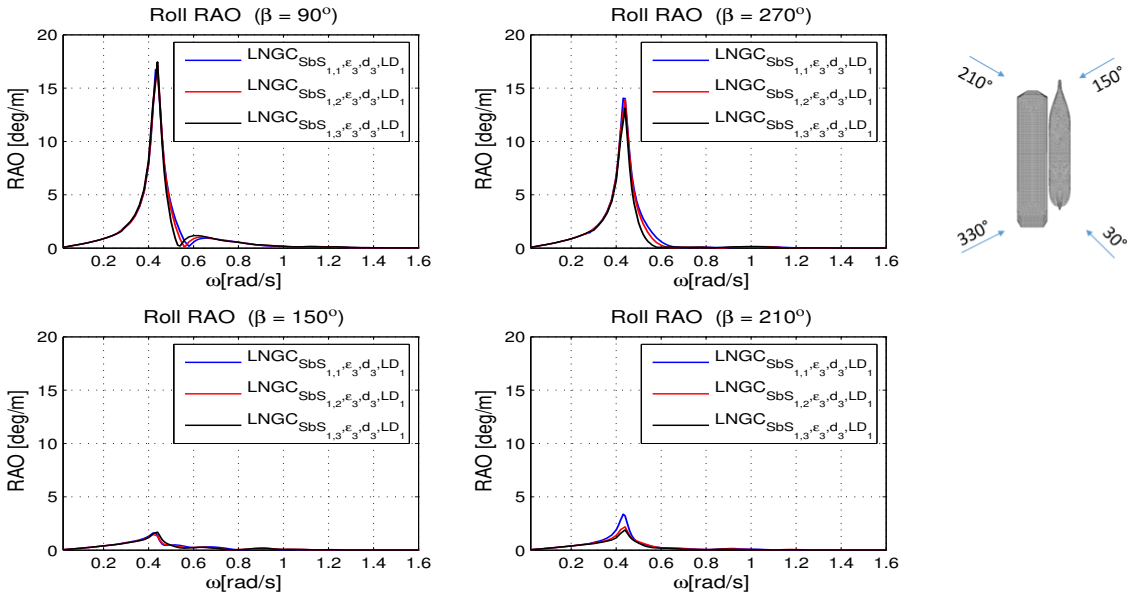

Figure 5.27: Roll in beam and bow quartering waves of LNGCmin in multi-body configuration with different size of FLNG [$SbS_{1.1}$, ϵ_3, d_3, LD_1; $SbS_{1.2}$, ϵ_3, d_3, LD_1; $SbS_{1.3}$, ϵ_3, d_3, LD_1]

Second order forces

The second order forces are presented throughout the Figures [**??**...**??**]. It can be noticed that significant differences are found especially towards the higher frequency region. Shielding effects could be identified, such that the longer the FLNG, the smaller drift forces for bow quartering waves(210deg). For stern quartering waves, no difference could be identified, such that all the forces of the carrier are equal for each side-by-side configuration.

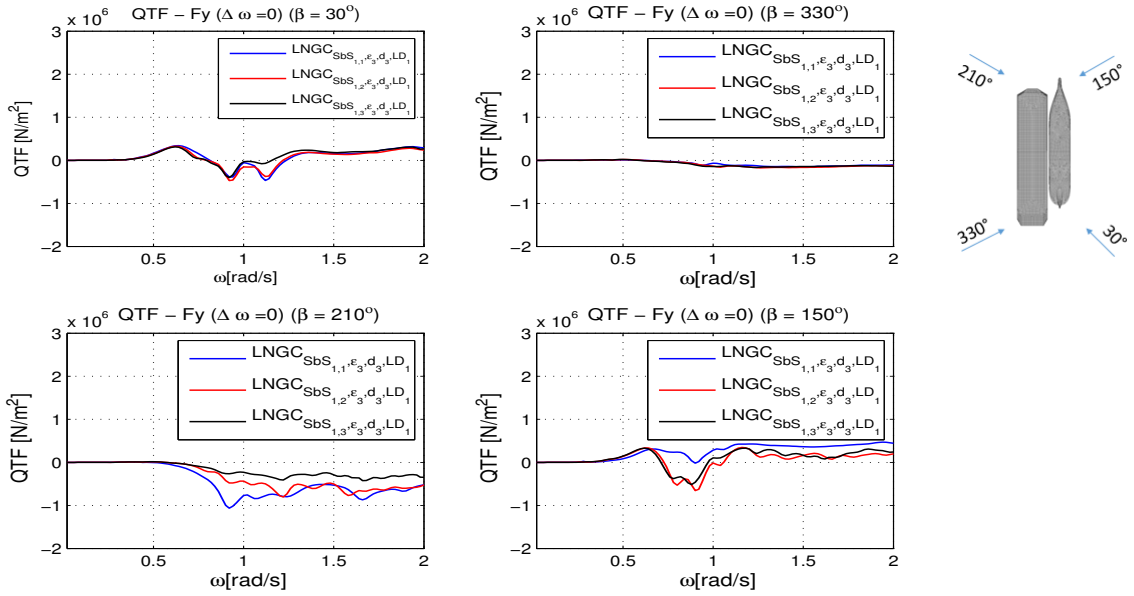

Figure 5.28: Sway drift force in stern and bow quartering waves of LNGCmin in multi-body configuration with different size of FLNG [$SbS_{1.1}$, ϵ_3, d_3, LD_1; $SbS_{1.2}$, ϵ_3, d_3, LD_1; $SbS_{1.3}$, ϵ_3, d_3, LD_1]

5.3. Carrier size

For this comparison two carrier size in ballast condition are considered, while the other parameters are kept constant as is presented below:

Cases	$LNGC_{SbS_{1.1},\epsilon_3,d_3,LD_1}$ **vs** $LPGC_{SbS_{2.1},\epsilon_3,d_3,LD_1}$

Table 5.11: Analyzed cases

The results are presented in the Appendix **??** as follows:

Hydrodynamic coefficients	RAO	QTF
Figure **??**	Figures [**??**...**??**]	Figures [**??**...**??**]

Table 5.12: List of results

5.3.1. Hydrodynamic coefficients

As it can be seen in the Figure 4.2 the difference in size between the LNG carrier and LPG carrier is noticeable. Furthermore the characteristics of each vessel are presented in the Table 4.2. Having a smaller vessel is evident that the added mass and the damping coefficients are significantly lower. Furthermore, for a lighter vessel, the peak frequency tends to shift towards towards higher frequencies. Moreover for particular directions (i.e. surge, sway, pitch and yaw) at frequencies higher than 1 rad/s, the added mass for LPGC becomes close to zero. This means that at this frequency the vessel does not displace any significant amount of water because is lighter compare to the LNGC. Another aspect which should be mentioned is that for certain degree of freedom (i.e surge, heave, sway and yaw) at the frequency of 0.9 rad/s the LNGC and LPGC added mass are equal. The reason behind is that the LNG carrier, for this specific frequency is very well damped.

5.3.2. First order motions

No significant difference for surge, sway and yaw can be identified. For heave and pitch responses significant differences can be remarked. For instance for weather side (30deg. and 150deg.) the heave and pitch of LPGC are higher with 50% than for the LNGC.

Regarding the roll motion it can be observed that the LPGC rolls more than the LNGC because is a tender ship. Furthermore, roll of the LPG carrier in stern waves (0deg.) is equal to the roll on the lee-side (210deg.). This leads to the conclusion that for side-by-side configuration, bow-quartering waves(210deg.) are dangerous as stern and head waves. Moreover, the shielding effects become very important especially for the LPGC case, where roll of the LPGC reduces with 10deg/m compare to the weather side. This makes as the roll of the LPGC to be comparable with roll for LNGC.

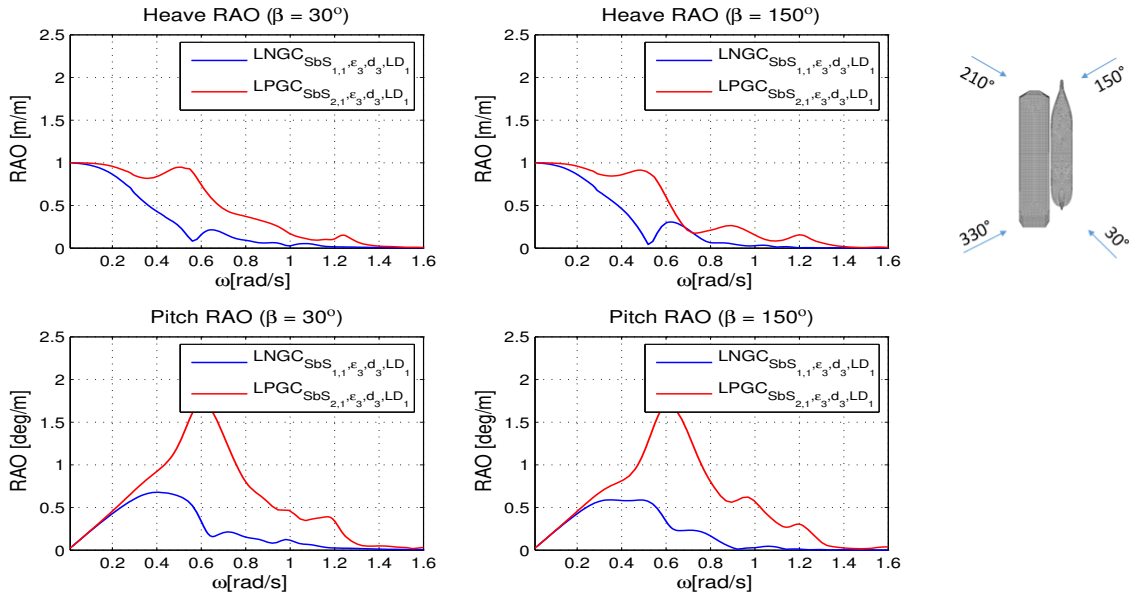

Figure 5.29: Heave and pitch for the exposed side of the carriers in multi-body configuration [LNGCmin - $SbS_{1.1}$, ϵ_3, d_3, LD_1 & LPGCmin - $SbS_{2.1}$, ϵ_3, d_3, LD_1]

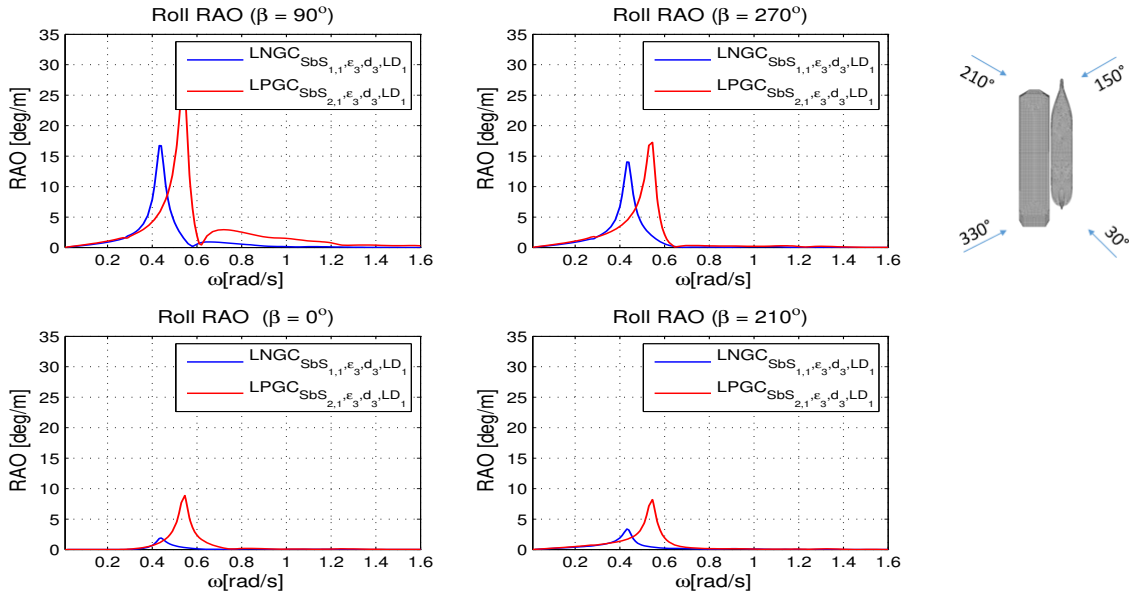

Figure 5.30: Roll for beam, head and bow quartering waves of the carriers in multi-body configuration [LNGCmin - $SbS_{1.1}$, ϵ_3, d_3, LD_1 & LPGCmin - $SbS_{2.1}$, ϵ_3, d_3, LD_1]

5.3.3. Second order forces

The drift force can be scaled with $\rho g \zeta^2 L$, where L-ship length and ζ is the wave amplitude. Knowing that the LPGC is smaller than the LNGC it is expected to have a smaller drift force. Therefore this can be seen starting from Figure **??**. Between LNGC and LPGC a shifting in frequency for seconder order quantities can be noticed (i.e 0.5 rad/s for LPGC; 0.3 rad/s for LNGC). Regarding surge mean drift for bow-quartering waves (150deg.) for both carriers is almost equal. For the same incoming wave direction, sway drift force for the LPG carrier becomes negative (above 0.9 rad/s) and higher in magnitude than for the LNG carrier. The reason behind is that the LPG carrier start to drifts gentle towards the FLNG and it is pushed violent to the opposite side. For sway and yaw moment shielding effects are more visible for

LPGC than LNGC. For instance, considering bow-quartering waves (210deg.) drift forces for the LPG carrier are close to zero while for the LNG are quite significant.

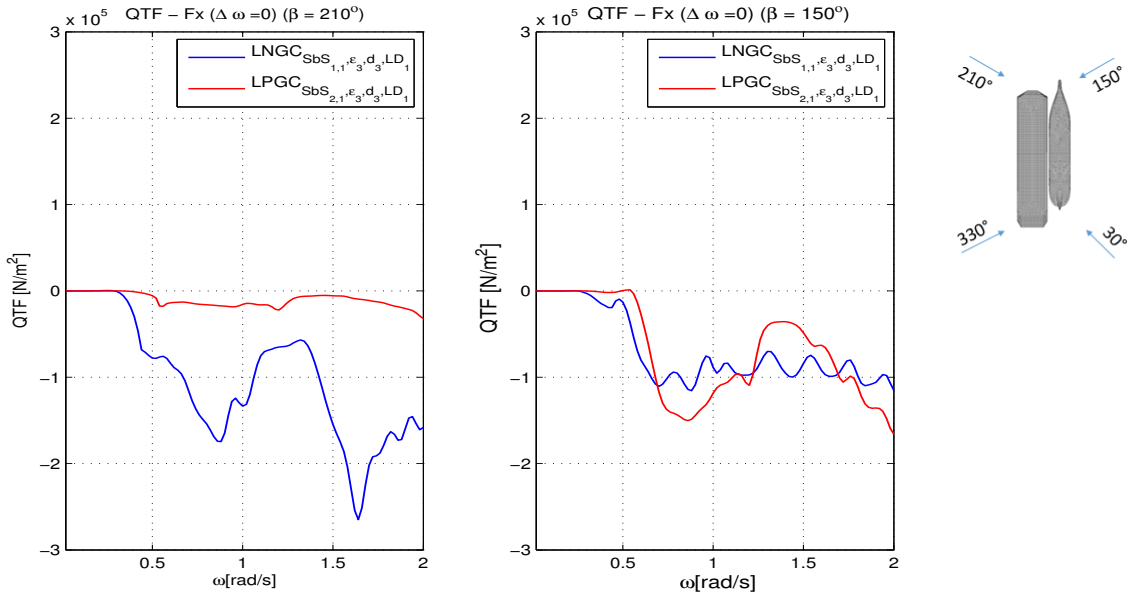

Figure 5.31: Surge drift force for bow quartering waves of the carriers in multi-body configuration [LNGCmin - $SbS_{1.1}$, ϵ_3, d_3, LD_1 & LPGCmin - $SbS_{2.1}$, ϵ_3, d_3, LD_1]

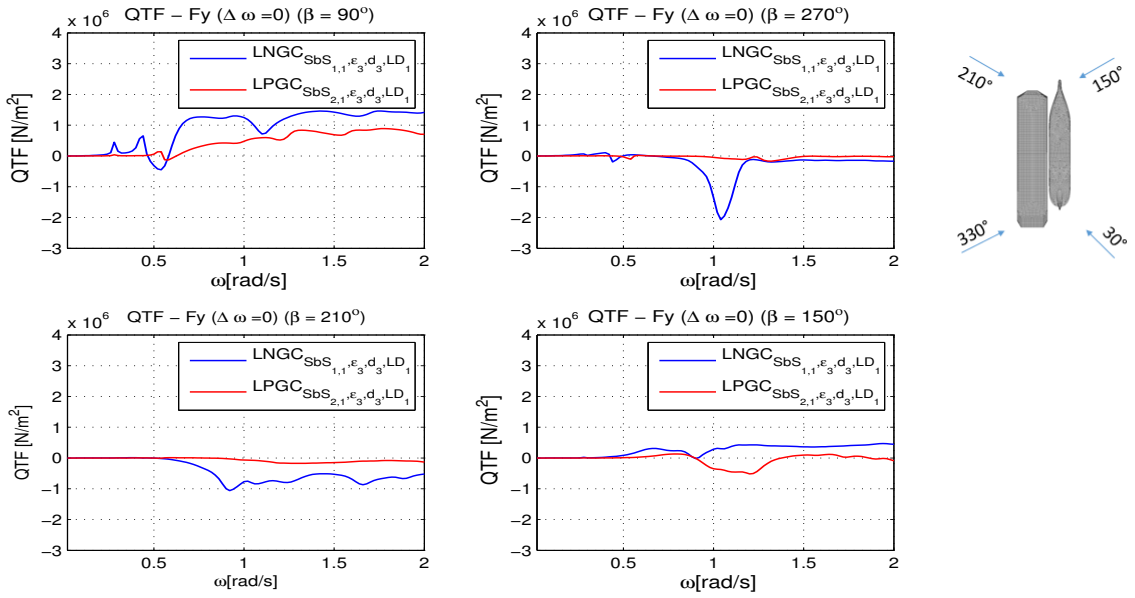

Figure 5.32: Sway drift force for beam and bow quartering waves of the carriers in multi-body configuration [LNGCmin - $SbS_{1.1}$, ϵ_3, d_3, LD_1 & LPGCmin - $SbS_{2.1}$, ϵ_3, d_3, LD_1]

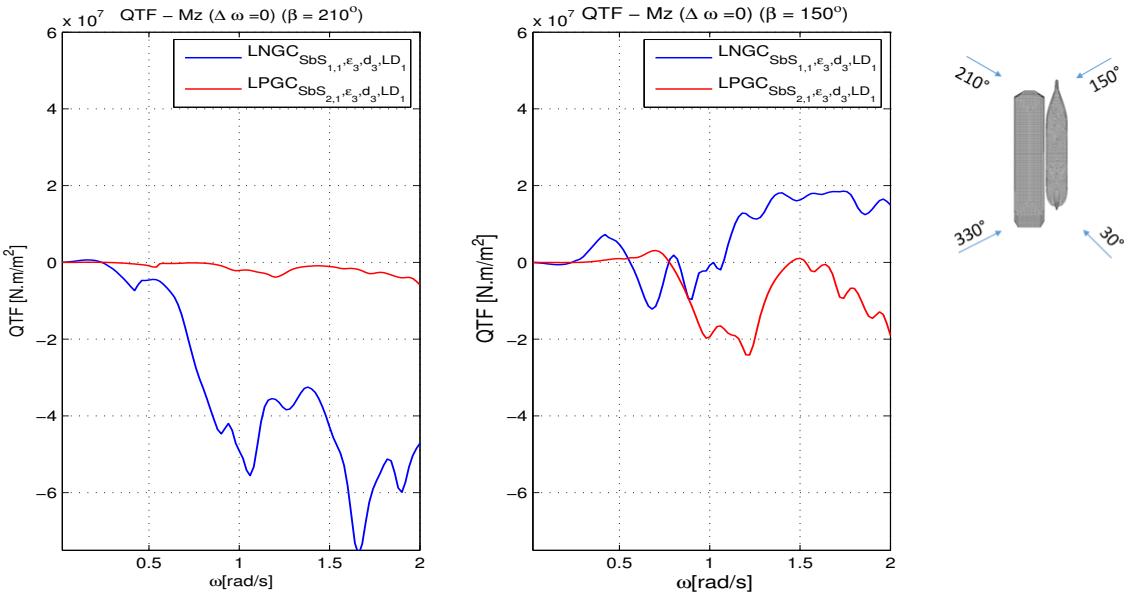

Figure 5.33: Yaw drift force for bow quartering waves of the carriers in multi-body configuration [LNGCmin - $SbS_{1.1}$, ϵ_3, d_3, LD_1 & LPGCmin - $SbS_{2.1}$, ϵ_3, d_3, LD_1]

5.4. Loading conditions

For these comparisons vessels in side by side configuration and single body for fully loaded and ballast loading condition has been considered. In this section, FLNG and carriers are presented.

5.4.1. FLNG

Results are presented graphically in the Appendix **??** as follows:

Hydrodynamic coefficients	RAO	QTF
Figure **??**	Figures [**??**...**??**]	Figures [**??**...**??**]

Table 5.13: List of results

Cases	$FLNG_{SbS_{1.1},\epsilon_3,d_3,LD_1}$ **vs** $FLNG_{SbS_{3.1},\epsilon_3,d_3,LD_1}$ **vs** SV_1 **vs** SV_2

Table 5.14: Analyzed cases

Hydrodynamic coefficients

For this comparison it can be seen that the multi body configuration has a major impact on the hydrodynamic coefficients which turns out in a strong coupling for each degree of freedom, as been mentioned before. On the other side, the effect of variation of the loading condition shows no major impact, except for roll. The reason behind is that the change in volume is not very significant. On the other hand, roll is more sensitive and shows significant impact on the added mass and damping coefficient (the lighter the vessel, the less added mass and damping).

First order motion

It can be seen that the interaction effects becomes important for roll in beam seas for the FLNG in ballast condition.

In particular for beam waves (270 deg.) the roll response for the FLNG in ballast condition for multi body configuration is higher than for the case of the single body for the same loading condition. Usually for ballast condition the ratio B/T increases which lead to an

increase of the metacentric height and a decrease of the roll period. Therefore for ballast condition it is expected to have a higher peak frequency. For the fully loaded condition there is no interaction effect visible. Furthermore, on the shielded side (90 deg.) of the FLNG in ballast condition shielding effect is visible. This favour the response such that is smaller with 2deg/m than the single vessel. For the fully loaded condition no such effects are identified.

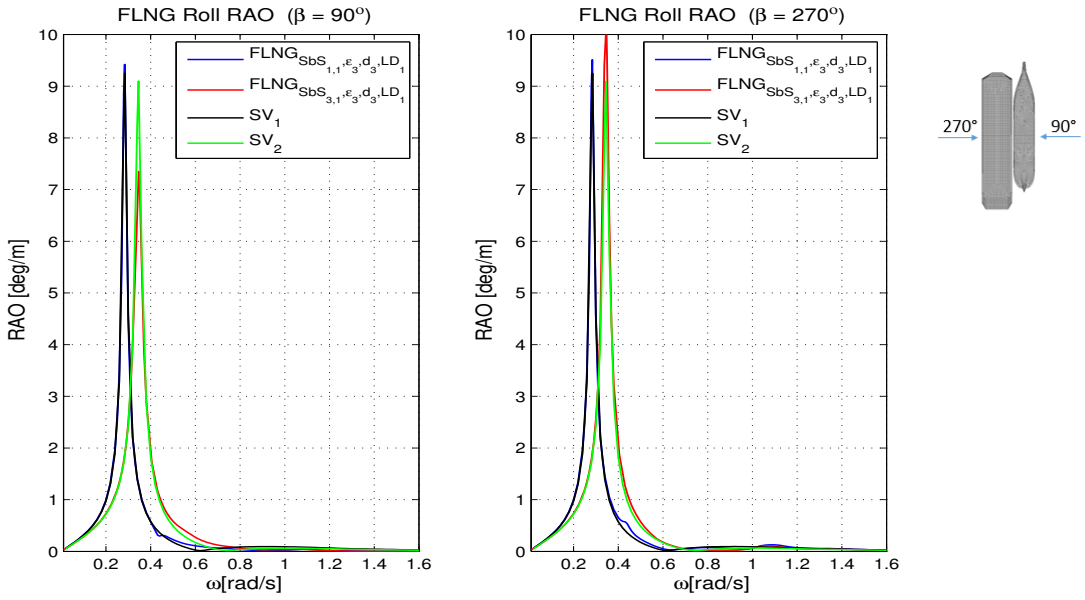

Figure 5.34: Roll for beam waves of the FLNG single vessel and FLNG in multi-body configuration in ballast and fully loaded condition [$SbS_{1.1}$, ϵ_3, d_3, LD_1 & $SbS_{3.1}$, ϵ_3, d_3, LD_1 & SV_1 & SV_2]

Second order forces

The second order forces are presented in Figures starting from **??**. Interesting to see that the loading condition for single body is not influencing the mean drift loads at all and very little for multi body configuration. This is due to the fact that the difference in draft between ballast condition and fully loaded is very small (Table 4.1).

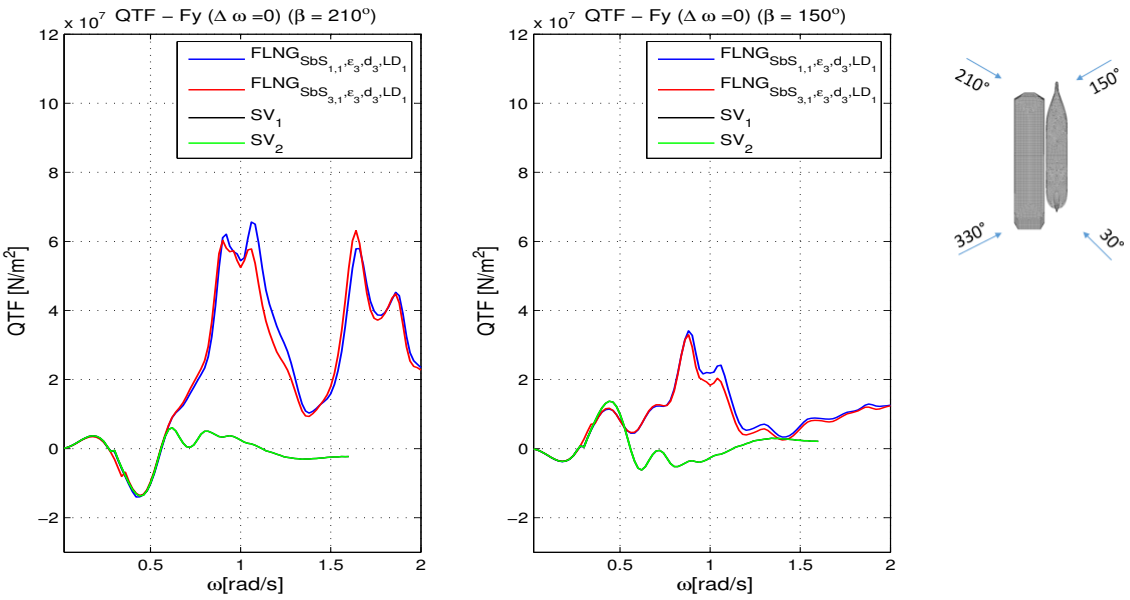

Figure 5.35: Sway drift force for bow quartering waves of the FLNG single vessel and FLNG in multi-body configuration in ballast and fully loaded condition [$SbS_{1.1}$, ϵ_3, d_3, LD_1 & $SbS_{3.1}$, ϵ_3, d_3, LD_1 & SV_1 & SV_2]

5.4.2. Carriers

Results are presented graphically in the Appendix **??** as follows:

Hydrodynamic coefficients	RAO	QTF
Figure **??**	Figures [**??**...**??**]	Figures [**??**...**??**]

Table 5.15: List of results for LNGC

Hydrodynamic coefficients	RAO	QTF	WE
Figure **??**	Figures [**??**...**??**]	Figures [**??**...**??**]	Figure **??**

Table 5.16: List of results for LPGC

Cases	$LNGC_{SbS_{1.1},\epsilon_3,d_3,LD_1}$	**vs**	$LNGC_{SbS_{3.1},\epsilon_3,d_3,LD_1}$	**vs**	SV_3	**vs**	SV_4

Table 5.17: Analyzed cases for LNGC

Cases	$LPGC_{SbS_{2.1},\epsilon_3,d_3,LD_1}$	**vs**	$LPGC_{SbS_{4.1},\epsilon_3,d_3,LD_1}$	**vs**	SV_5	**vs**	SV_6

Table 5.18: Analyzed cases for LPGC

Hydrodynamic coefficients

As it has been explained in the previous sections, in general a heavier vessel (i.e fully loaded) displace more water, thus, the added mass is higher compare to a lighter one (i.e ballast condition). On the other hand for roll motion, a lighter vessel will result in a smaller draft which increase the metacentric height and decrease the rolling period. If a vessel is rolling more often, means that the added mass will be higher.

First order motion

Significant impact can be identified for roll response of the carrier. In particular, the impact for fully loaded carrier is greater, such as: higher interaction and shielding effects. In side-by

side configuration, for beam waves (270deg.) the fully loaded carrier roll less (i.e 5deg/m less) than the single vessel. On the other side (90deg.), the interaction effects are more visible for the fully loaded case, where the roll is higher than the single vessel with 5deg/m. Regarding the other degrees of freedom, there is no significant impact due to the change in the loading condition of the carrier.

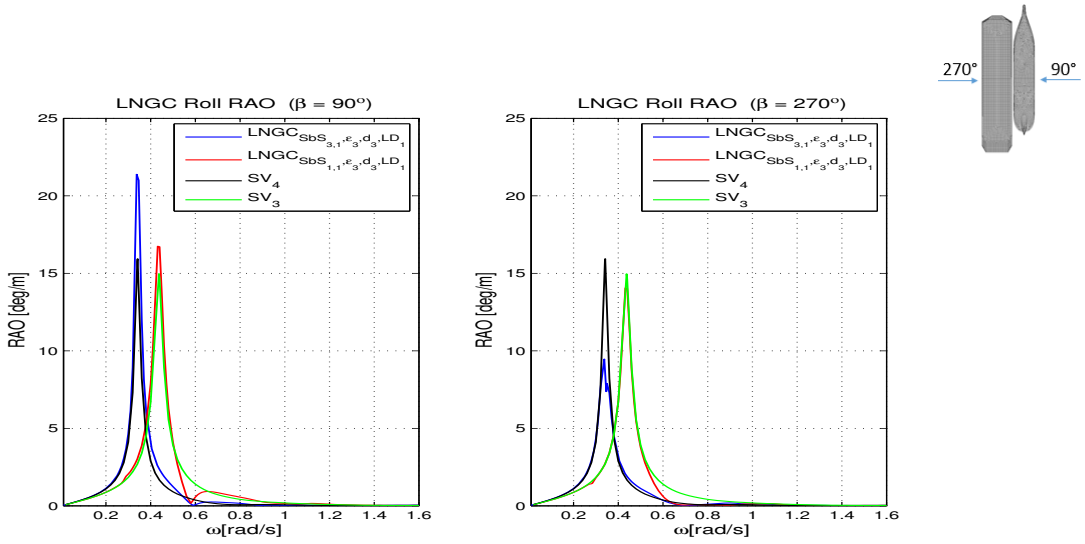

Figure 5.36: Roll for beam waves of the LNGC single vessel and LNGC in multi-body configuration in ballast and fully loaded condition [$SbS_{1.1}$, ϵ_3, d_3, LD_1 & $SbS_{3.1}$, ϵ_3, d_3, LD_1 & SV_4 & SV_3]

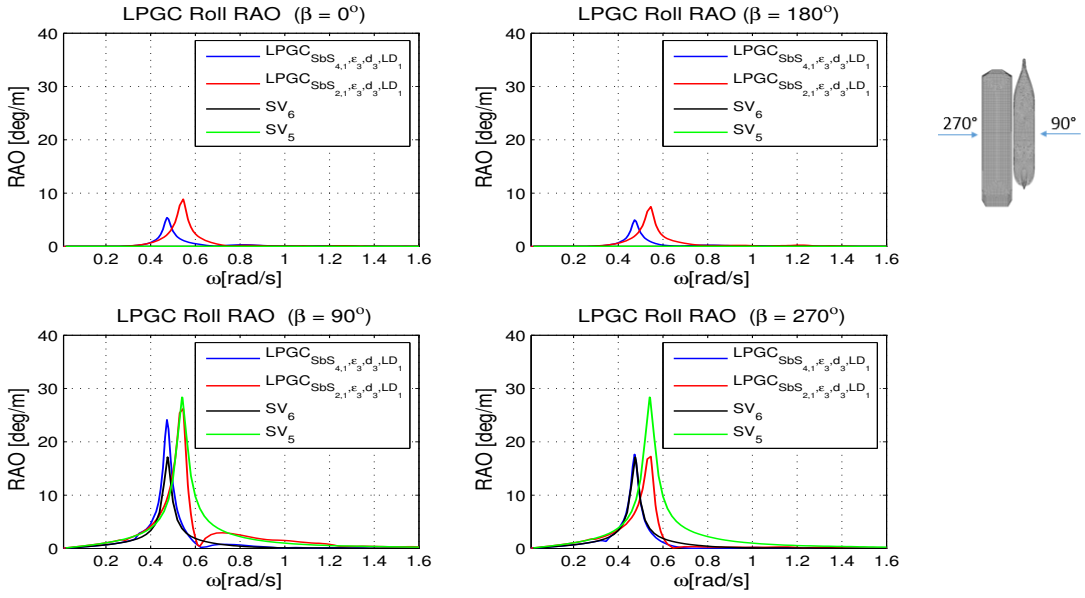

Figure 5.37: Roll for beam, head and following waves of the LPGC single vessel and LPGC in multi-body configuration in ballast and fully loaded condition [$SbS_{2.1}$, ϵ_3, d_3, LD_1 & $SbS_{4.1}$, ϵ_3, d_3, LD_1 & SV_6 & SV_5]

Second order forces

Regarding the second order forces, small influences can be remarked due to the loading condition variation, such that the fully loaded carrier tend to have slightly higher forces due to the increase in draft.

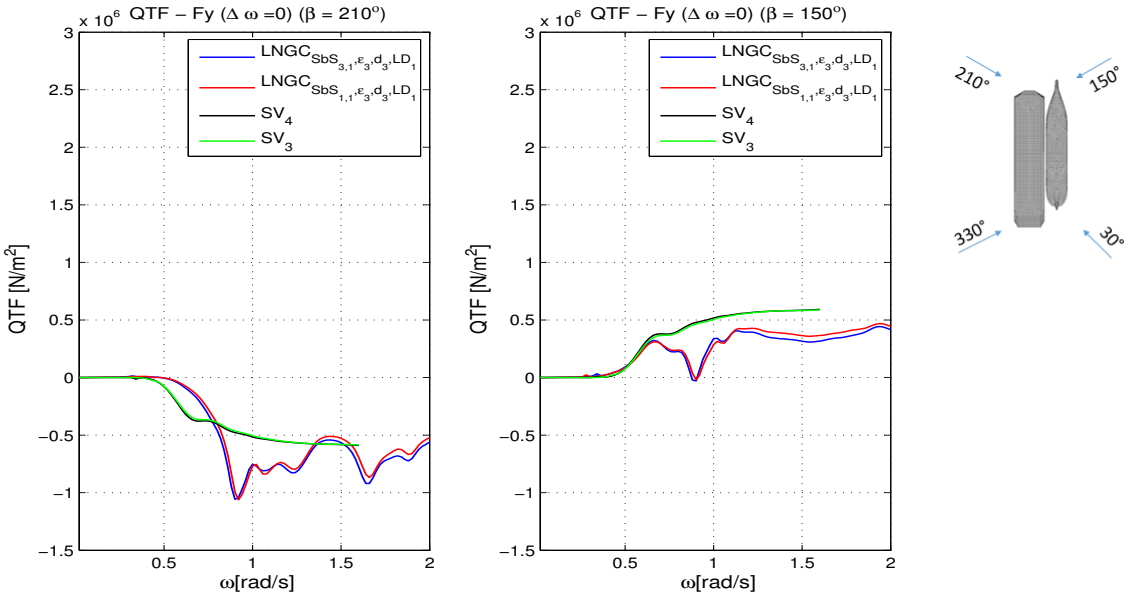

Figure 5.38: Sway drift forces for bow quartering waves of the LNGC single vessel and LNGC in multi-body configuration in ballast and fully loaded condition [$SbS_{1.1}$, ϵ_3, d_3, LD_1 & $SbS_{3.1}$, ϵ_3, d_3, LD_1 & SV_4 & SV_3]

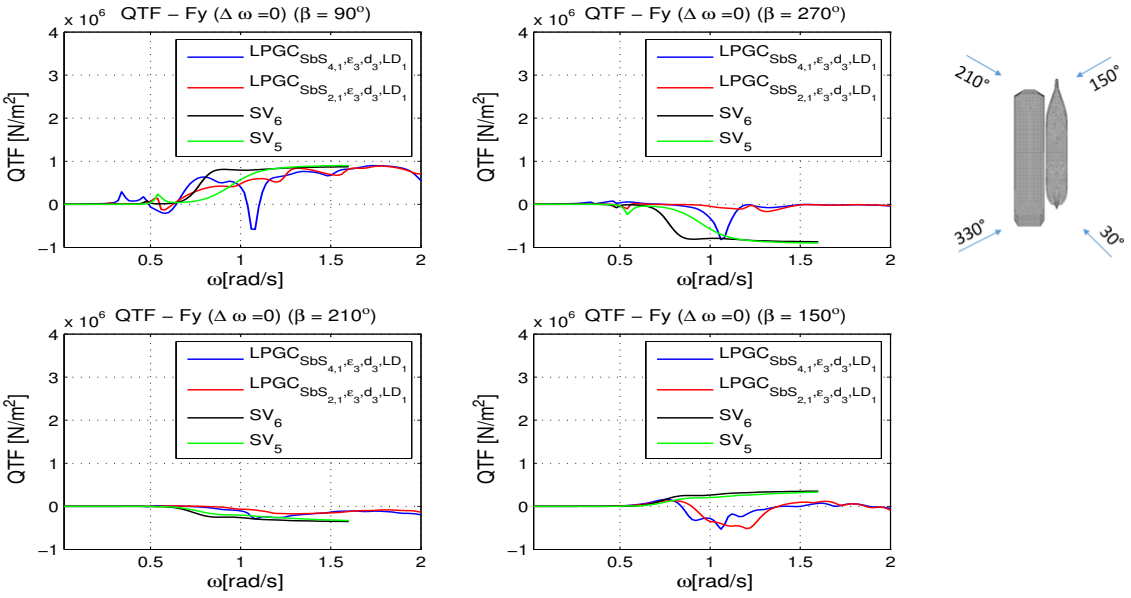

Figure 5.39: Sway drift force for beam and bow quartering waves of the LPGC single vessel and LPGC in multi-body configuration in ballast and fully loaded condition [$SbS_{2.1}$, ϵ_3, d_3, LD_1 & $SbS_{4.1}$, ϵ_3, d_3, LD_1 & SV_6 & SV_5]

5.5. Gap damping length

This comparison has been carried out in order to see the overall influence in the first and second order forces. According to the available literature, there is no theoretical method to assess a length of the lid on the gap between vessels. For certain publications (i.e Buchner et al. [3]) the authors used a lid area which covers only the constant distance between the two vessels with no further extension towards bow/stern where the shape of the vessel gets smoother. In other papers (i.e Huijsmans et. al [40], Buchner et. al [4]), the free surface lid damping is modelled a bit more extended towards the bow and the stern of the carrier.

Another example of different area used for the lid damping is presented by Hong-Chao and Lei Wang [39] where they used a length for the lid surface equal to the length of the floating production unit. Furthermore the superposition of the incoming wave and the diffracted waves results in cancellation in nodes at certain frequencies. This cancellation is dependent on the ratio between the gap dimensions such as width and length and the wave length[40]. Therefore in order to quantify the effects on both the FLNG and the carrier, 3 different lengths for the free surface lid has been used as follows: $L_1 = 160m$, $L_2 = 200m$, $L_3 = 285m$.

The effect of the gap damping area variation on both vessels (FLNG and LNGC) in this section is analyzed.

Results are presented graphically in the Appendix **??** and Appendix **??** as follows:

	Hydrodynamic coefficients	RAO	QTF	WE
FLNG	Figure **??**	Figures [**??**...**??**]	Figures [**??**...**??**]	Figure **??**
LNGC	Figure **??**	Figures [**??**...**??**]	Figures [**??**...**??**]	-

Table 5.19: List of results

Cases	$SbS_{1.1}$, ϵ_3, d_3, LD_1 **vs** $SbS_{1.1}$, ϵ_3, d_3, LD_2 **vs** $SbS_{1.1}$, ϵ_3, d_3, LD_3

Table 5.20: Analyzed cases

Hydrodynamic coefficients

Looking at the hydrodynamic coefficients for both vessels (FLNG and LNGC) it can be noticed that they are influenced near the resonant frequency, where the longest lid applied at the free surface provides the highest damping and a lower added mass as it was expected. Away from resonance, the hydrodynamic coefficients are not affected by the length of the free surface lid between the two vessels. By far the most affected degree of freedom are: roll, yaw and pitch.

First order motion

First order motions seems to be less sensitive to the variation of the lid surface size. If for the hydrodynamic coefficients the most sensitive degrees of freedom are: roll, yaw and pitch, for the first order motions the variation of the lid surface does not show significant differences. A small difference can be identified for yaw moment, where it can be seen that the response is affected in the wave resonant frequency only and the longer the lid the smaller the motion amplitude.

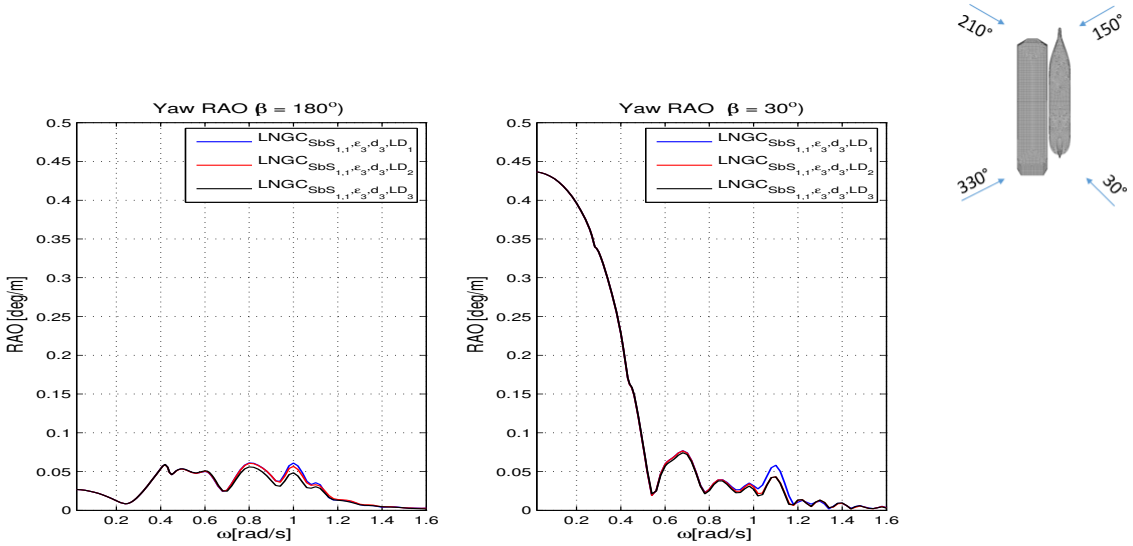

Figure 5.40: Yaw for bow and stern quartering waves of LNGCmin in multi-body configuration for different gap damping length [$SbS_{1.1}$, ϵ_3, d_3, LD_1 & $SbS_{1.1}$, ϵ_3, d_3, LD_2 & $SbS_{1.1}$, ϵ_3, d_3, LD_3]

Second order forces

Second order forces are more sensitive than the first order quantities and not only on the resonant frequency region. Surge drift forces are less affected by the length of the lid. On the other side, the sway and yaw mean drift moment are influenced more by the length of the damping area, starting from the resonant frequency towards higher frequency region. The affected directions are: 180deg., 210deg. and 30deg. where the diffraction effects are more important. Furthermore this can be emphasised by the wave elevation at the manifold location for the directions mentioned.

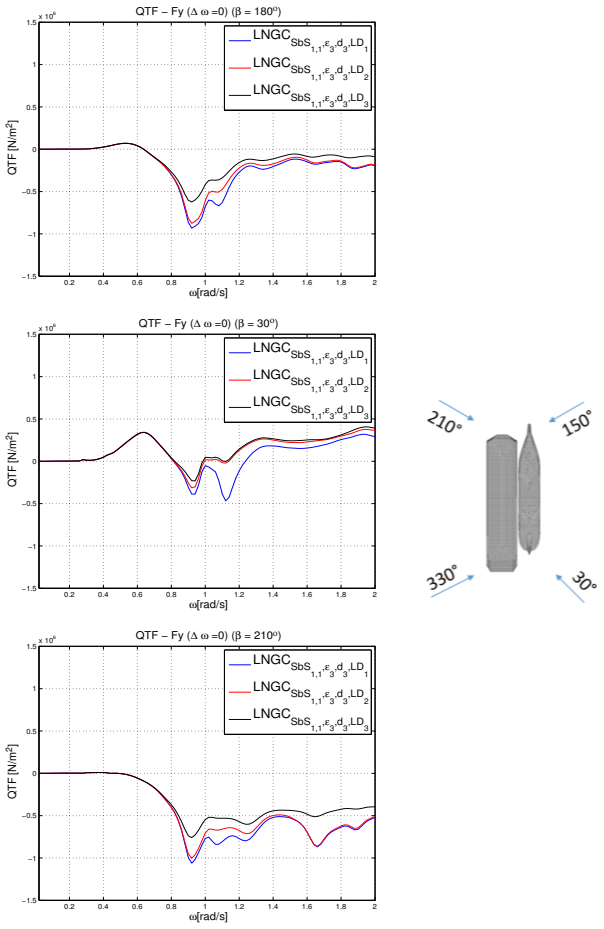

Figure 5.41: Sway drift force in head, stern and bow quartering waves of LNGCmin in multi-body configuration for different gap damping length [$SbS_{1.1}$, ϵ_3, d_3, LD_1 & $SbS_{1.1}$, ϵ_3, d_3, LD_2 & $SbS_{1.1}$, ϵ_3, d_3, LD_3]

5.6. Dissipation factor

This section presents the effect of damping parameter is investigated for FLNG and both carriers.

5.6.1. FLNG

Results are presented graphically in the Appendix **??** as follows:

Hydrodynamic coefficients	RAO	QTF
Figure **??**	Figures [**??**...**??**]	Figures [**??**...**??**]

Table 5.21: List of results

For this section the damping parameter of the free surface between the two vessels has been varied from 0 to 0.4 with step of 0.1, while the other parameters remained constant as follows:

Cases	$FLNG_{SbS_{1.1},\epsilon_1,d_3,LD_1}$ **vs** $FLNG_{SbS_{1.1},\epsilon_3,d_3,LD_1}$ **vs** $FLNG_{SbS_{1.1},\epsilon_2,d_3,LD_1}$ **vs** $FLNG_{SbS_{1.1},\epsilon_3,d_3,LD_1}$ **vs** $FLNG_{SbS_{1.1},\epsilon_4,d_3,LD_1}$ **vs** $FLNG_{SbS_{1.1},\epsilon_5,d_3,LD_1}$

Table 5.22: Analyzed cases

Hydrodynamic coefficients

The hydrodynamic coefficients can be seen in the Figure **??** where for each degree of freedom is shown the added mass and the damping coefficients respectively. The variation of the non-dimensional damping parameter has a major impact for each degree of freedom except of surge, where the results with or without damping parameter are the same. This can be explained by the fact that the damping parameter affects the wave elevation between the vessels and therefore the surge direction is less likely to be affected. However, for the damping parameter of 0.2, 0.3 and 0.4 all the results are really close.

First order motion

The first order motions are presented in the Figures(starting with **??**). It is noticed that near the resonant frequency of the wave, responses are affected. Away from this frequency range, the free surface dissipation is not affecting the motion response of the FLNG. As it has been seen in the previous sections, the most sensitive motion is roll in beam seas. Therefore it has been expected to see significant impact on roll due to variation of damping ratio. It turns out that the roll of FLNG in beam seas with or without damping parameter is the same. For pitch and yaw could be identified a slight difference between the response with damping parameter and the response without. Overall the conclusion is that with or no damping there is no great impact on the first order quantities and where it does, the motions with a damping parameter between 0.2, to 0.4 gives almost equal results for first order motions.

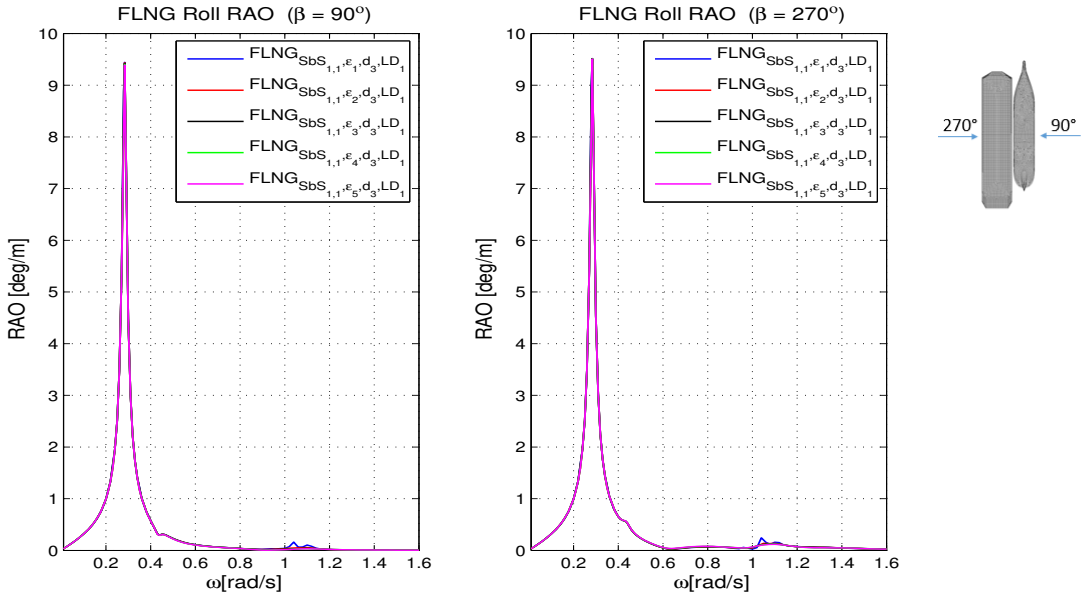

Figure 5.42: Roll in beam waves of FLNGmax in multi-body configuration for different dissipation factors [$SbS_{1.1}$, ϵ_1, d_3, LD_1 & $SbS_{1.1}$, ϵ_2, d_3, LD_1 & $SbS_{1.1}$, ϵ_3, d_3, LD_1 & $SbS_{1.1}$, ϵ_4, d_3, LD_1 , $SbS_{1.1}$, ϵ_5, d_3, LD_1]

Second order forces

Second order drift forces are presented in the Figures **??**. For surge mean drift the influence can be noticed only in the case without the damping parameter near the resonant frequencies. For the other chosen damping values the surge drift force is almost equal. For sway and yaw direction the mean drift force become more sensitive and the difference between with and no dissipation parameter is more evident than for surge mean drift. Moreover forces are also affected towards higher frequency limit. Very close results are given for a dissipation factor between 0.2 to 0.4. It can be seen that the discrepancy between the case without and with damping parameter is very significant, with a yaw mean drift moment (270deg.) 8 times higher than for the case with dissipation factor. It is noticeable that the wave elevation at this frequency reach a huge elevation and without considering the dissipation factor, the potential theory does not give realistic results. These also confirm the importance of the viscous damping effect on the strong hydrodynamic interaction and the validation of the potential method with an appropriate damping parameter is vital.

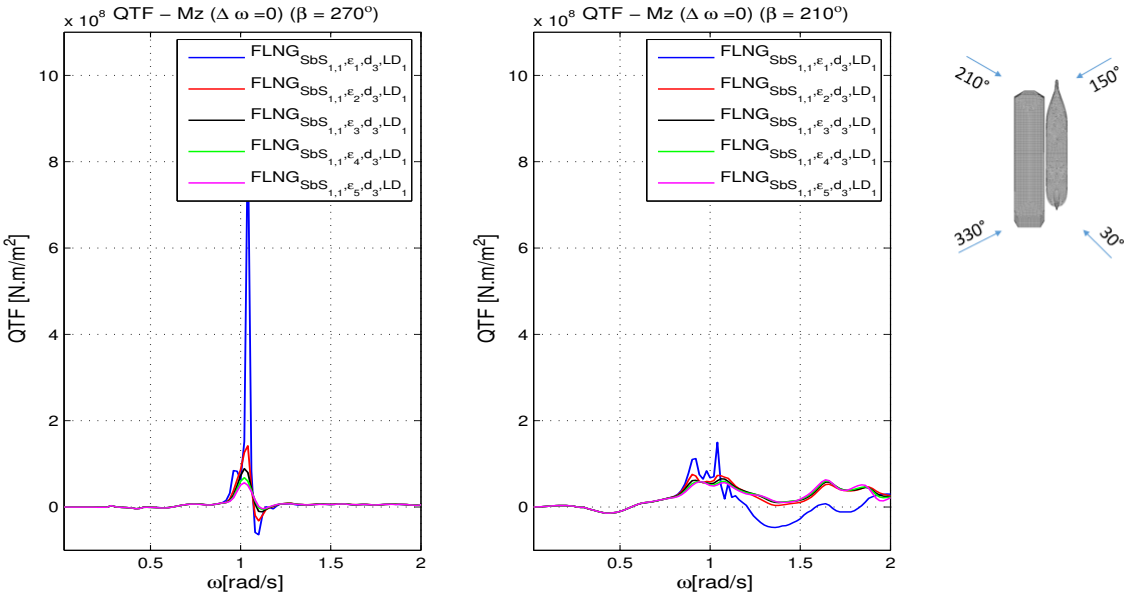

Figure 5.43: Yaw drift force in beam and head quartering waves of FLNGmax in multi-body configuration for different dissipation factors [$SbS_{1.1}$, ϵ_1, d_3, LD_1 & $SbS_{1.1}$, ϵ_2, d_3, LD_1 & $SbS_{1.1}$, ϵ_3, d_3, LD_1 & $SbS_{1.1}$, ϵ_4, d_3, LD_1 , $SbS_{1.1}$, ϵ_5, d_3, LD_1]

5.6.2. Carriers: LNGC and LPGC

Results are presented graphically in the Appendix **??** for LNGC and Appendix **??** for LPGC as follows:

	Hydrodynamic coefficients	RAO	QTF	WE
LNGC	Figure **??**	Figures [**??**...**??**]	Figures [**??**...**??**]	Figure **??**
LPGC	Figure **??**	Figures [**??**...**??**]	Figures [**??**...**??**]	Figure **??**

Table 5.23: List of results

Cases for LNGC	Cases for LPGC
$SbS_{1.1}$, ϵ_1, d_3, LD_1	$SbS_{2.1}$, ϵ_1, d_3, LD_1
vs	**vs**
$SbS_{1.1}$, ϵ_2, d_3, LD_1	$SbS_{2.1}$, ϵ_2, d_3, LD_1
vs	**vs**
$SbS_{1.1}$, ϵ_3, d_3, LD_1	$SbS_{2.1}$, ϵ_3, d_3, LD_1
vs	**vs**
$SbS_{1.1}$, ϵ_4, d_3, LD_1	$SbS_{2.1}$, ϵ_4, d_3, LD_1
vs	**vs**
$SbS_{1.1}$, ϵ_5, d_3, LD_1	$SbS_{2.1}$, ϵ_5, d_3, LD_1

Table 5.24: Analyzed cases for carriers [dissipation factor variation]

Hydrodynamic coefficients

Compared to the FLNG, the carriers appears to be more sensitive and the dissipation factor affects all the degree of freedom and the variation appears to be more evident. Close results are given by the 0.3-0.4 dissipation parameter. Compare to the FLNG, the carriers added mass and damping coefficients without the dissipation term have several spikes after the natural period. On the other hand, in the low frequency region, there is no change in the result, whether is considered or not the dissipation factor.

First order motion

As it can be observed in the Figures **??** the first order motions of the both carriers are affected only near the resonant frequency region, outside of this range, they are not affected at all. Damping effects can be identified only for heave, pitch and yaw moment. The range of 0.2 to 0.4 offers similar results, while for no dissipation a spike around 1.2 rad/s can be seen.

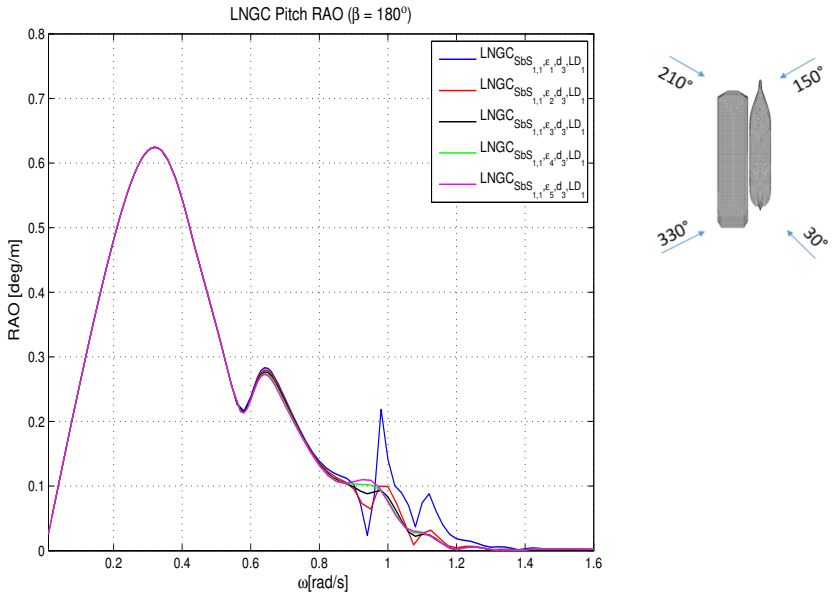

Figure 5.44: Pitch in head waves of LNGCmin in multi-body configuration for different dissipation factors [$SbS_{1.1}$, ϵ_1, d_3, LD_1 & $SbS_{1.1}$, ϵ_2, d_3, LD_1 & $SbS_{1.1}$, ϵ_3, d_3, LD_1 & $SbS_{1.1}$, ϵ_4, d_3, LD_1 , $SbS_{1.1}$, ϵ_5, d_3, LD_1]

Second order forces

Second order drift forces are presented in the Figures **??**. For surge, sway and yaw drift force, for the cases without the damping parameter near the resonant frequencies only significant differences can be observed. It can be seen that the discrepancy between the case without and with damping parameter is very significant. For instance yaw mean drift moment (270deg.) is 4 times higher for the LNGC carrier and 2 times higher for the LPGC carrier compare to the case when the dissipation factor is used. It is noticeable that the wave elevation at this frequency reach a huge elevation and without considering the dissipation factor, the potential theory does not give realistic results.

5.7. Separation distance

For this comparison 4 different separation distances has been used from 4.5m to 3m with step of 0.5m.

Cases	$SbS_{1.1}$, ϵ_3, d_1, LD_1 **vs** $SbS_{1.1}$, ϵ_3, d_2, LD_1 **vs** $SbS_{1.1}$, ϵ_3, d_3, LD_1 **vs** $SbS_{1.1}$, ϵ_3, d_4, LD_1

Table 5.25: Analyzed cases

5.7.1. FLNG and LNGC

Results are presented graphically in the Appendix **??** for FLNG and Appendix **??** for LNGC as follows:

	Hydrodynamic coefficients	RAO	QTF	WE
FLNG	Figure **??**	Figures [**??**...**??**]	Figures [**??**...**??**]	-
LNGC	Figure **??**	Figures [**??**...**??**]	Figures [**??**...**??**]	Figure **??**

Table 5.26: List of results

Hydrodynamic coefficients

From the trend of the hydrodynamic coefficients presented on the Figure **??** and **??** it can be seen that all peak frequencies diminish with increasing the separation distance, exception from this is the yaw added mass.

First order motion

The overall conclusion for both the FLNG and the carrier is that the variation of the separation distance does not influence the first order response. In particular the motion responses (i.e heave, roll, yaw) that are depended on the separation distance are not affected.

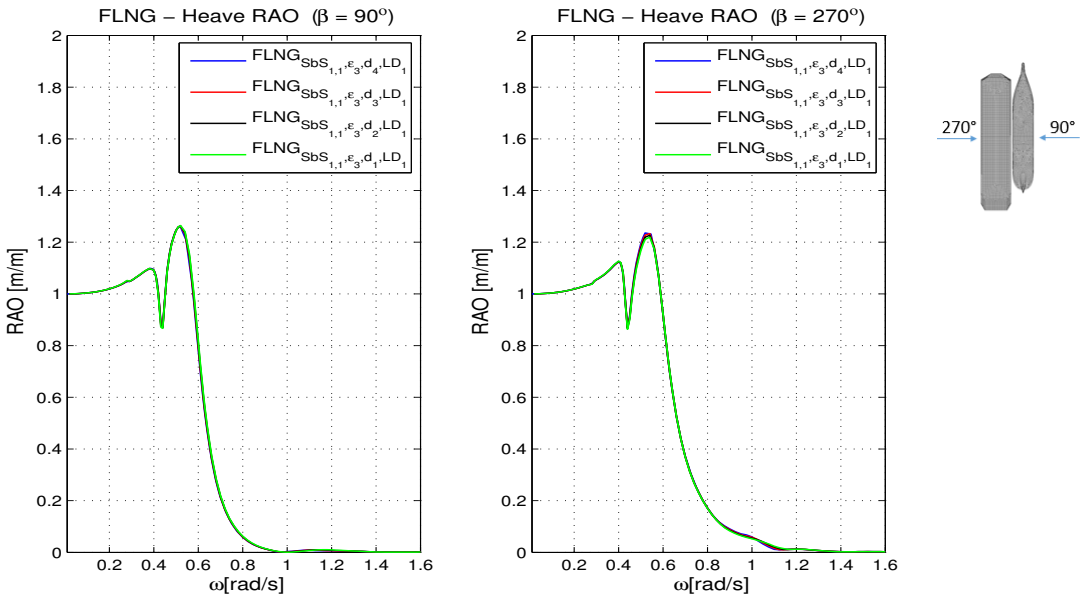

Figure 5.45: Heave in beam waves of FLNGmax in multi-body configuration for different separation distances [$SbS_{1.1}$, ϵ_3, d_1, LD_1 & $SbS_{1.1}$, ϵ_3, d_2, LD_1 & $SbS_{1.1}$, ϵ_3, d_3, LD_1 & $SbS_{1.1}$, ϵ_3, d_4, LD_1]

Second order forces

Regarding the second order motion it can be seen that a smaller separation distance force the vessel to drift more at the higher frequencies. In particular, for lower frequencies, where the wave length is large, the diffraction of waves are important, thus reducing the wave exciting forces on the vessel. This leads to have the same mean drift force for all the distances considered up to 0.75 rad/s. Above this frequency, the separation distance starts to be more visible. The separation distance of 3m for the FLNG in beam waves (270deg.) experience a sway mean drift force and a yaw mean drift moment slightly smaller compare to the other analyzed cases. On the other hand for the same separation distance, the sway mean drift force in beam waves (90deg. and 270deg.) is smaller than for larger separation distances.

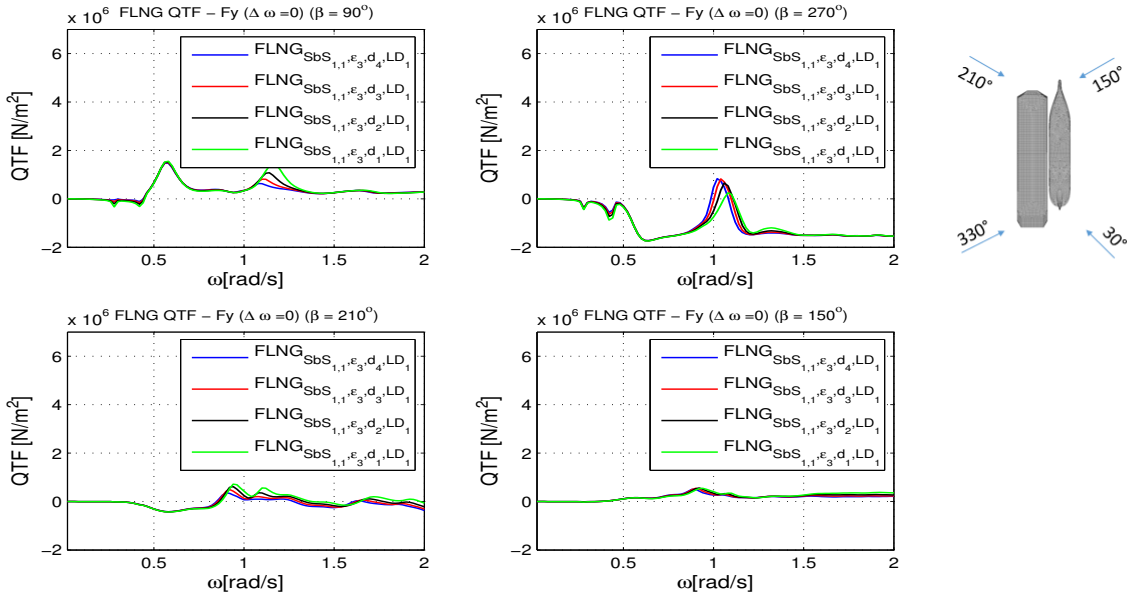

Figure 5.46: Sway drift force in beam and head quartering waves of FLNGmax in multi-body configuration for different separation distances [$SbS_{1.1}$, ϵ_3, d_1, LD_1 & $SbS_{1.1}$, ϵ_3, d_2, LD_1 & $SbS_{1.1}$, ϵ_3, d_3, LD_1 & $SbS_{1.1}$, ϵ_3, d_4, LD_1]

5.8. Sensitivity analysis summary

The diffraction analysis shows that the hydrodynamic interactions effects of the moored systems in side-by-side configuration are complex problems and strongly coupled. A main characteristic of side-by-side system is that the sway added mass become negative at the resonant frequency for both vessels involved. In general the FLNG is less affected by the presence of the carrier. In particular, interaction effects could be identified only for FLNG's heave. It can be clearly identified that there is a heave-roll coupling between FLNG and carrier. Radiated waves from the rolling carrier are travelling towards FLNG's side which cause a significant decrease in FLNG's heave. Regarding the second order quantities the effect is more visible, affecting all degrees of freedom. However, this depends on the carrier's size. As it is presented, when the FLNG is moored in side-by-side configuration with a smaller vessel (i.e LPGC) the interaction is insignificant compare to the single vessel case. Furthermore there are no shielding effects for FLNG in fully loading condition, while for ballast condition they are visible. This is caused by the increase of the carrier volume (LNGC) and respectively the draft which will tend to act like a rigid wall and shelter the FLNG against the incoming waves. The gap resonance highly affects the drifts forces, in particular yaw and sway under beam waves conditions.

The behaviour of the carrier in side-by-side configuration revealed important aspects. In general sway and roll for single vessel is zero for head and following waves due to the symmetry. However in multi-body, the carrier response is significant. For instance rolling of the LNG is 2deg/m while for LPGC approximately 10deg/m. Thus smaller ships are more sensitive due to interaction effect and thus their seakeeping performances become weaker.

An unexpected event regarding roll motions from bow quartering waves has been noticed. Such that the roll of the carrier is two times higher from the lee-side than weather side. This can be explained that the radiated waves from the FLNG have higher amplitudes which impact the bow of the carrier with a higher force than on the opposite side due to the incoming wave (unit amplitude).

The variation of the FLNG sizes does not have a big impact on the first order loads of the carrier. It is notices a small shifting in the resonance period. The same conclusion regarding the roll of the carrier in bow-quartering waves is drawn. This emphasises the statement made above and shows that no matter the size of the FLNG (larger FLNG = higher sheltered area), the roll of the carrier due to the incoming wave from the exposed side is still smaller compare to the sheltered area. On the other hand the drift forces of the carrier are highly influenced by the presence of a the second vessel and its dimensions (length and displacement). The tendency is to expect higher carrier's drift forces when is moored in side-by-side configuration with larger vessel and especially towards higher frequencies.

The variation of the loading condition in terms of drift force no significant difference neither for FLNG nor for carriers has been found. Even though the change in draft for the carrier is not negligible and thus some impact could have been expected.

The variation of the gap damping length shows that there is a small impact, but negligible on the first order quantities, while second order are more sensitive and they are affected towards higher frequencies.

Dissipation factor is not influencing at all the first order loads weather is considering or not. On the other hand the second order forces are extremely affected, except of surge which is not dependent on the pumping mode resonance. Furthermore this shows the importance of the wave heading. Such that if there are beam waves extremely huge peaks can be identified for the case without dissipation factor and important differences between the other values used. However the discrepancies are not that significant if the wave is coming from bow quartering waves due to diffraction effects.

Varying the separation distance between the vessels has no impact on the first order motions. However on the drift loads the effect is visible at the gap resonance mainly. As the distance decrease, the peak frequency is shifted towards higher frequency range.

Overall, in terms of wave loading, beam waves are the most dangerous and needs to be avoided for this kind of moored systems. Due to the turret system which has the capability to weather vane, the bow quartering waves can be considered as the governing sea states.

6

Time domain model setup

6.1. Introduction

This chapter presents the time domain simulations results based on the diffraction database parameters such as: dissipation factor(Table 4.5), gap damping length(Table 4.7), separation distance(Table 4.8), loading condition and carrier size variation. It is important to assess whether the diffraction parameters have or not any effect on the time domain simulations and in which conditions. With this regard, a sensitivity analysis for multiple environmental conditions is carried out. The results are presented in terms of relative motions with respect to the loading arm initial position, maximum line tension and fender loads. Once the effects are highlighted, the next step is to optimize the mooring arrangement. Ultimately a comparison between coupled and quasi-dynamic results is presented.

Ariane is a tool developed by Bureau Veritas which allows to perform quasi-dynamic time domain analysis for single or multi-body mooring systems. Floating structures (ie. ships, semi-submersible, buoys, etc) are considered as rigid body. Mooring lines can be linked to anchor(attached on sea bed) or fairleads. The non-linear properties of the mooring ropes can be defined using a fifth order polynomial curve and the line solution is fully analytic. Drift loads models adapted to any water depth using various approximations, external loads or thruster loads may considered. Additional elements my be modeled such as fenders(based on load compression curve), buoy, sinkers,etc. The sea bed can be defined as single plane with or without inclination or for complex bathymetry with various slopes from external file can be derived. Time domain simulations takes into account all the inertia effects, waves, current, wind, thrusters [36].

6.2. Vessels description and coordinate system

As it is presented in Chapter 4 there are 3 FLNG sizes available, however for time domain analyses, only one hull has been selected (i.e L=301.5m). This vessel has attached an external disconnectable turret, which consists on 3 bundles of 3 catenary lines each, anchored to the ground in a water depth of 50m. This mooring system allows the vessel to freely ”weathervane” 360 degrees, thus controlling the heading in order to limit the motions, especially roll and yaw.

The offloading process is performed via the following configuration:

- FLNG (Floating Liquified Natural Gas unit) and LNGC (Liquified Natural Gas Carrier)
- FLNG (Floating Liquified Natural Gas unit) and LPGC (Liquified Petroleum Gas Carrier)

The size of the carriers varies considerably, as it can be seen in the Table 4.2. Therefore the FLNG shall be designed and equipped with multiple quick release hooks serving different mooring arrangements for various carriers sizes.

Coordinate systems

In numerical models, there are defined two systems of reference such as:

- global reference system (C-North-East) is the space fixed coordinate system which is attached to the center of turret on the mean water line, where z is positive pointing downwards. The environmental conditions and vessel headings are given with respect to this reference system
- local axis system($O - XYZ$) is defined for each individual vessel (i.e subscript A stands for FLNG, while subscript B stands for carrier) and is linked to the vessel's keel, at the longitudinal center of gravity and mid breadth; where X-axis is positive in the direction of the body's forward, z-axis is positive vertically downwards and y-axis is positive towards starboard of the vessel

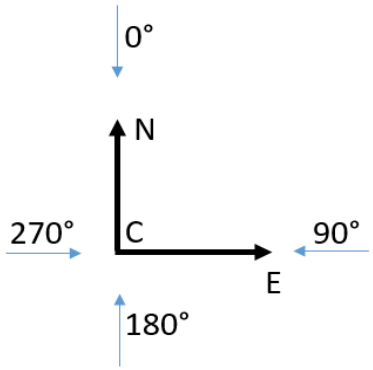

Figure 6.1: Vessel heading convention

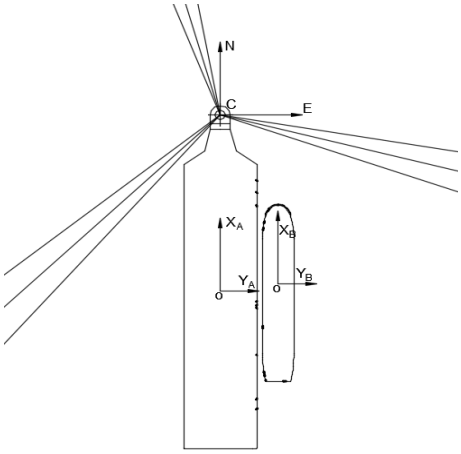

Figure 6.2: Global and local coordinate system

6.3. Mooring layout and Loading arms locations

This section describes the mooring components which concern only the side-by-side configuration and the loading arms location. In general, mooring arrangements needs to accomplish the safety requirements, to be efficient both for anticipated operations or emergency situations(quick mooring and unmooring). Safety criteria is established by the transfer cargo equipment which is predefined by the manufacturer.

Usually, carriers provide oboard mooring arrangements which include the following components: winches, deck fittings (i.e.chokes, bits, fairleads) and mooring lines. Mooring lines from the carrier are headed to the FLNG fairlead and connected to the quick release hook (QRH).

For an efficient/optimum mooring arrangement on FLNG's deck needs to taken into account several parameters such as:

- carrier size: to be capable to fit the number of lines required to conduct safe offloading operations
- loading condition variation - which cause differences in freeboard for both vessels during cargo transfer
- mooring pattern and line locations: needs to minimize the horizontal angle for stern, head and breast lines and also the vertical angle with the horizontal plane such that to maximize the effective force; usually is very difficult to obtain both the optimum mooring pattern and alignment with the loading arm locations, such that most of the time, there is a compromise for reducing effectiveness of the lines in favor of having the loading arms parallel aligned
- stiffness and pretension of the mooring lines: extreme mooring line loads are expected in case if the mooring system resonate at the wave frequency; regarding the pretension in mooring lines, OCIMF [30] recommends to be used an initial pretension between 50 to 150 kN

- environmental conditions and design criteria: investigations shall be done with the site metocean characteristics if there are available, to proof that the system can handle the design criteria which is based mainly on relative motions (loading arms are sensitive); otherwise, DNV [9] propose guidelines to select the environmental conditions(i.e collinear and non-collinear)

6.3.1. Loading arms location

Location of the cryogenic manifolds is given both as table format and drawings. FLNG is equipped with two manifolds: one designated for offloading to LNGC and the other to LPGC. A connection detail between FLNG manifold and carrier's manifold is presented below:

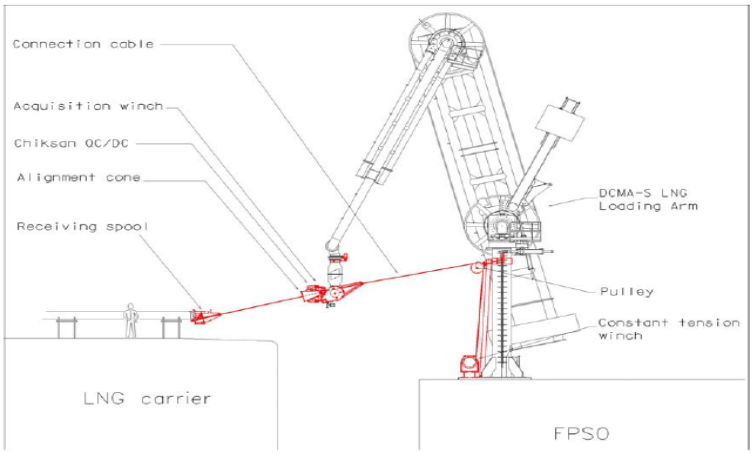

Figure 6.3: Manifold connection via loading arm [34]

The coordinates of the manifolds in longitudinal direction are given with respect to aft of the vessels, for transverse direction with respect to midship of the vessels and in vertical direction with respect to the keel of the vessels.

Relative distances between FLNG and carriers's manifolds are given with respect to initial static position (Table6.3).

Description	Symbol	U.M.	FLNG - LNGC	FLNG - LPGC
Longitudinal distance from aft perpendicular	x_{A-LA}	m	170.5	160.5
Transverse distance from midship	y_{A-LA}	m	31	31
Vertical distance from keel	z_{A-LA}	m	36.6	36.6

Table 6.1: Manifold coordinates for FLNG with respect to LNGC and LPGC

Description	Symbol	U.M.	LNGC	LPGC
Longitudinal distance from aft perpendicular	x_{B-LA}	m	139.56	87.35
Transverse distance from midship	y_{B-LA}	m	18.9	12.2
Vertical distance from keel	z_{B-LA}	m	31	19.7

Table 6.2: Manifold coordinates for shuttle tankers

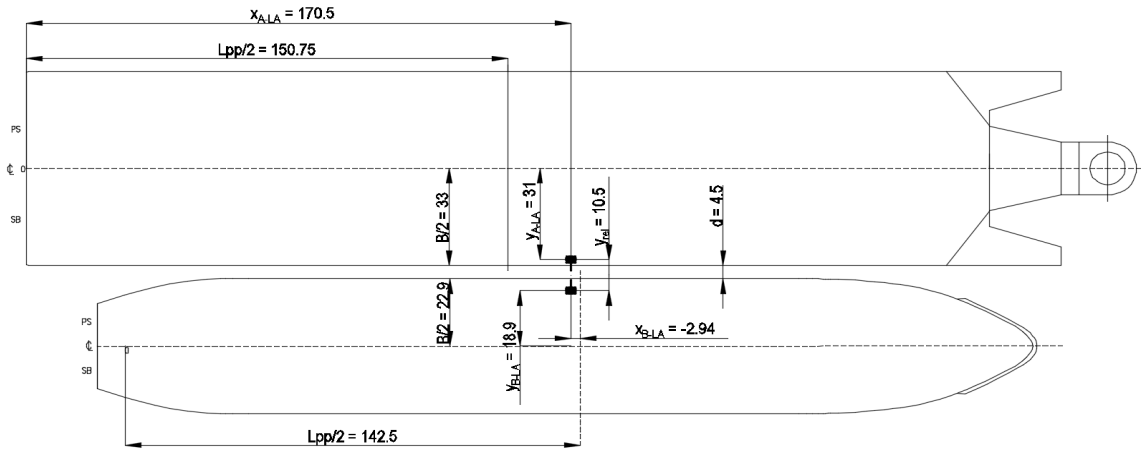

Figure 6.4: Top view of Loading arms for FLNG-LNGC configuration

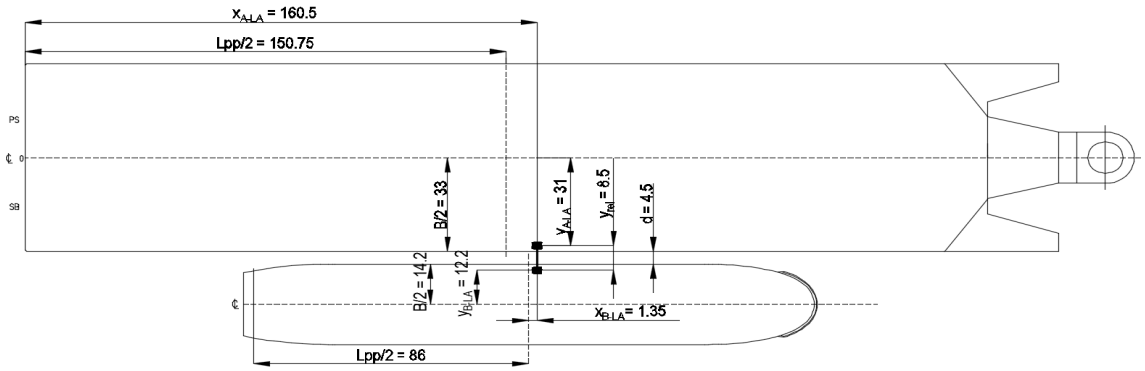

Figure 6.5: Left: Top view of Loading arms for FLNG-LPGC configuration

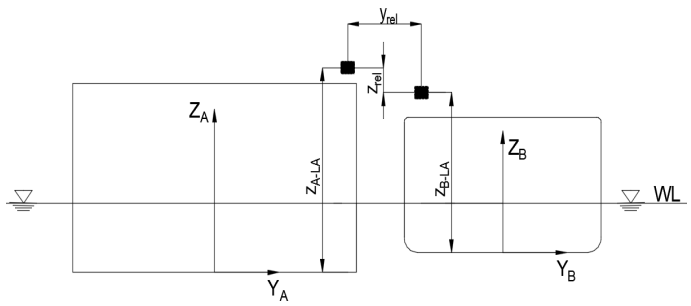

Figure 6.6: Side view: Loading arm relative distances

Description	Symbol	U.M.	FLNG - LNGC	FLNG - LPGC
Relative distance	x_{rel}	m	0	0
	y_{rel}	m	10.5	8.5
	z_{rel} - $FLNG_{max} - Carrier_{min}$	m	4.73	12.03
	z_{rel} - $FLNG_{min} - Carrier_{max}$	m	6.91	16.21

Table 6.3: Relative distances between FLNG and carriers' manifolds

6.3.2. Mooring arrangements

FLNG-LNGC

For sensitivity analysis in time-domain a pre-existing mooring arrangements has been used which are detailed below.

In the Figure 6.7 it is presented the mooring arrangement between FLNG-LNGC which consists in 18 line, numbered from aft to forward, from which: 2 stern lines, 10 brest lines, 4 spring lines and 2 head lines (Table 6.4); They are fitted on deck in bundles of two lines each, except for SbS7 and SbS12; 8 fenders alongside the vessels (4 mid-aft and 4 mid-forward); 12 Quick Release Hooks (QRH) are used from the FLNG's deck which can be double or single hook (Figure **??**) and 18 fairleads onboard of the LNGC for each mooring line.

Stern Lines	Brest Lines	Spring Lines	Head Lines
SbS1; SbS2	SbS3; SbS4; SbS5; SbS6 ;SbS7 SbS12; SbS13; SbS14; SbS15; SbS16	SbS8; SbS9 SbS10; SbS11	SbS17; SbS18

Table 6.4: Side by Side Lines for FLNG-LNGC

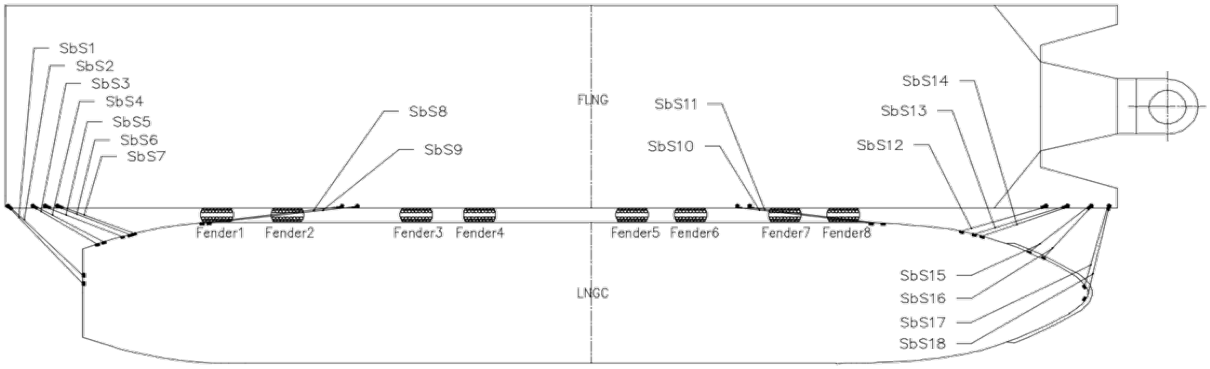

Figure 6.7: Mooring deck arrangement FLNG-LNGC

FLNG-LPGC

In the Figure 6.8 it is presented the mooring arrangement between FLNG-LPGC which consists in 13 line, numbered from aft to forward, from which: 2 stern lines, 6 brest lines, 4 spring lines and 1 head line (Table 6.5); They are fitted on deck in bundles of two lines each, except for SbS7 and SbS12; 8 fenders alongside the vessels (4 mid-aft and 4 mid-forward); 9 Quick Release Hooks (QRH) are used from the FLNG's deck which can be double or single hook (Figure **??**) and 13 fairleads onboard of the LPGC for each mooring line.

Stern Lines	Brest Lines	Spring Lines	Head Lines
SbS1; SbS2	SbS3; SbS4 SbS9; SbS10; SbS11; SbS12	SbS5; SbS6 SbS7; SbS8	SbS13

Table 6.5: Side by Side Lines for FLNG-LNGC

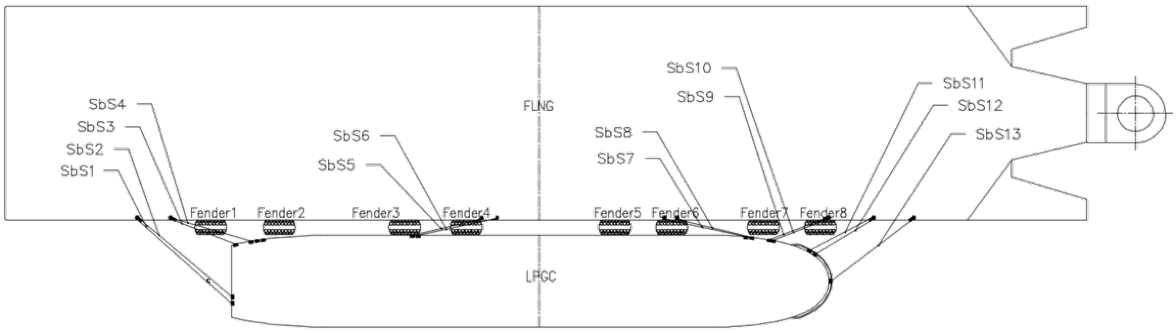

Figure 6.8: Mooring deck arrangement FLNG-LPGC

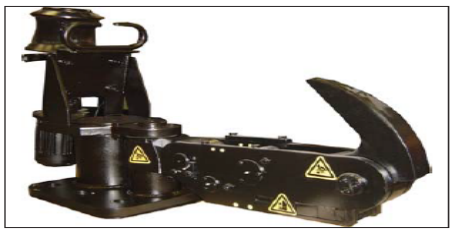

Figure 6.9: Single QRH [19]

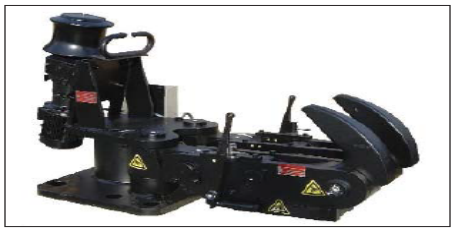

Figure 6.10: Double QRH [19]

6.3.3. Mooring lines - general description and characteristics

In this section a short description of the role of the side by side lines is presented.

Head, stern and spring lines are stabilising the ships alongside. Spring lines provides the greatest holding capacity in the longitudinal direction and they need to be as parallel as possible with respect to the vessels. The function of head ans stern lines are strongly dependent on their angle with the longitudinal axis. For instance a great angle, means that they serve mainly as breast lines, while small angle means that they are able to counteract the longitudinal movements. Brest lines prevent mooring system to break free and they are opposing the transverse movements. Therefore they need to be as perpendicular as possible to the ships longitudinal axis. Overall the vertical angle with the horizontal plane, as per DNV guidelines, should be less as possible (preferably less than 30 degrees), because the effective force is proportional to the cosine of the angle, the smaller the angle the more effective the line.

The efficiency of a mooring rope depends on the following parameters:

- material (steel wire or synthetic -elongation (stiffness) and MBL (Minimum breaking load))
- length and pretension (Short taut lines which can lead to very high tensions with even very small magnitude of motions)
- angles with longitudinal and transverse axis in the horizontal plane
- angles with the horizontal in the vertical vertical plane

In the following there are presented the material and geometrical properties of the lines from each mooring arrangement.

Material properties

For side by side operations, the steel wire mooring lines needs to be fitted with synthetic fibre tail to ensure additional elasticity in the system. According to OCIMF Mooring Equipment Guidelines, tails should be at least 11m long and should have a dry breaking strength at least 25% higher than the wire to which they are attached [30] since they are subjected to more abrasion and fatigue. Thus, it can be seen that for FLNG-LPGC configuration nylon

tail is higher with 25% than wire, while for FLNG-LNCG configuration nylon tail provides 32% higher strength.

For the side-by-side arrangements FLNG-LNGC (Figure 6.7) has been used a nylon tail of 25m while for FLNG-LPGC (Figure 6.8) a nylon tail of 20m length. Material characteristics for each configuration is shown in Tables 6.7 and 6.6 respectively. OCIMF [30] recommends a minimum safety factor of 1.82 for steel and 2.5 for nylon tails. Safety factor for nylon tails are higher due to the fact that in wet conditions, the strength reduces with 10-15 % [30]. Steel wire rope is a ISO 2408 type with 6 strands and steel core (Figure 6.27) and double braided tails (Figure 6.28) . Strength of the mooring winch structure is based on the breaking strength of the lines. The holding capacity requires to be 80% of minimum breaking load of the rope. While in operation, should be no more than 60%.

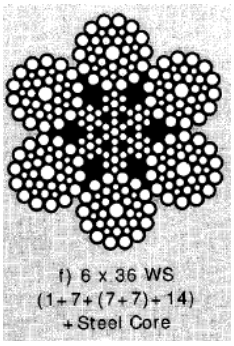

Figure 6.11: Steel wire 6 strands [30]

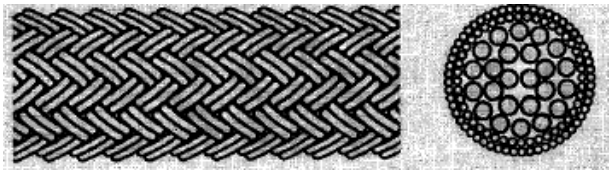

Figure 6.12: Nylon tail (double braided) [30]

Strength criteria

Description	U.M.	Steel wire rope (ISO 2408)	Nylon tail (Double braided)
Diameter	$[m]$	0.03	0.06
Length	$[m]$	220	20
Weight per unit length	$[kg/m]$	3.68	3
Minimum Breaking Load (MBL)	$[kN]$	620	775
Safety factor	$[-]$	1.82	2.5
Safe Working Limit (SWL*)	$[kN]$	340.5	310
Design winch brake capacity (80 % Rope MBL)	$[kN]$	496	620
In-Service winch brake capacity (60 % Rope MBL)	$[kN]$	372	465

*For steel wire wire rope: SWL = 55%MBL; while for nylon tail SWL = 40%MBL as recommended by OCIMF [30]

Table 6.6: Mooring line and winch characteristics and strength criteria for FLNG-LPGC configuration

Description	U.M.	Steel wire rope (ISO 2408)	Nylon tail (Double braided)
Diameter	$[m]$	0.044	0.089
Length	$[m]$	220	25
Weight per unit length	$[kg/m]$	8.4	4.4
Minimum Breaking Load (MBL)	$[kN]$	1240	1638
Safety factor	$[-]$	1.82	2.5
Safe Working Limit (SWL*)	$[kN]$	681	655.2
Design winch brake capacity (80 % Rope MBL)	$[kN]$	992	1310.4
In-Service winch brake capacity (60 % Rope MBL)	$[kN]$	744	982.8

*For steel wire wire rope: SWL = 55%MBL; while for nylon tail SWL = 40%MBL as recommended by OCIMF [30]

Table 6.7: Mooring line and winch characteristics and strength criteria for FLNG-LNGC configuration

Elasticity

Figure 6.13 presents the elasticity of the nylon tails for both configurations.

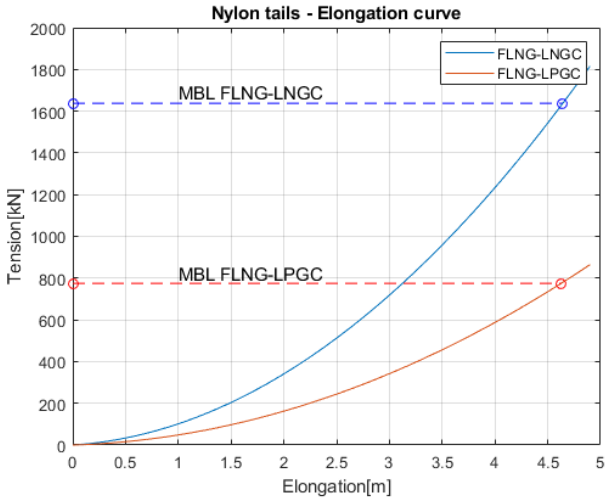

Figure 6.13: Nylon tails elasticity

Methods for connecting the tails

Generally on board of the vessels the wire line is connected with the tail by different methods such as shackles or cow hitch.

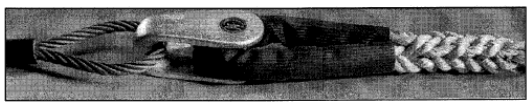

Figure 6.14: Tail-wire connection using shackle [30]

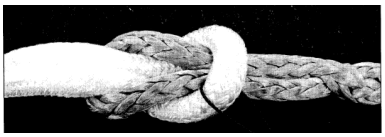

Figure 6.15: Tail-wire connection using 'cow hitch' method [30]

The joining shackles should be equal to or greater than the safe working limit of the mooring line to which it is attached [30]. According to OCIMF [30] if the manufacturer recommends that it is appropriate to attach a synthetic tail directly to wire lines, a 'cow hitch' method can be adopted. However this method reduce the strength of the mooring arrangement with 15%.

However, for the sake of simplicity, in numerical simulations is not used any type of connections mentioned. It is considered as a continuous line with 2 different material properties.

6.3.4. Side by side line position and geometric characteristics

This section presents the location of the quick release hooks (QRH) on FLNG's deck, fairleads (F) on the carrier's decks, together with the mooring line geometric characteristics such as: lengths (horizontal and paid out length) and specific angles: horizontal angle with respect to longitudinal and transverse plane (θ, ϕ) and vertical angle with horizontal plane (α).

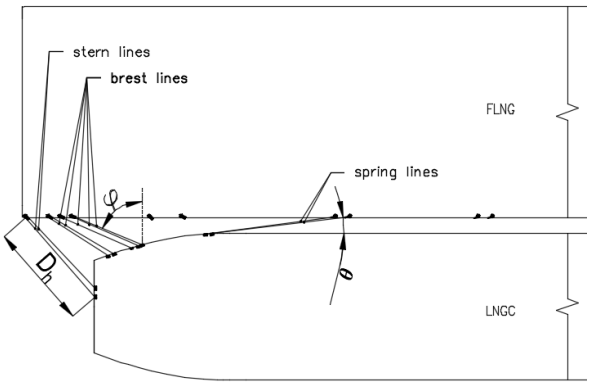

Figure 6.16: Side by side mooring lines - top view (aft part)

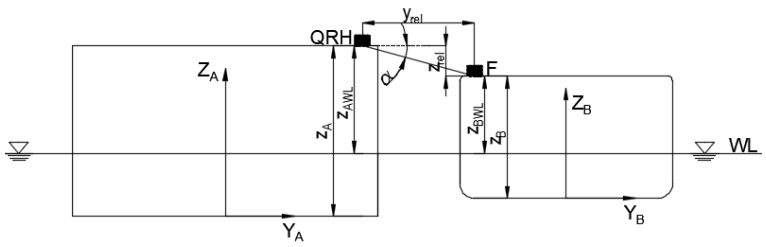

Figure 6.17: Nylon tails elasticity

Nr.crt	FLNG QRH($z_A[m]$)	LNGC F ($z_B[m]$)	LPGC F ($z_B[m]$)
2	24.79	20.7	18.2
2	24.79	20.7	18.2
3	24.79	20.7	18.2
4	24.79	20.7	18.2
5	24.79	20.7	18.2
6	24.79	20.7	18.2
7	24.79	20.7	18.2
8	31.5	26.2	18.2
9	31.5	26.2	18.2
10	31.5	26.2	18.2
11	31.5	26.2	18.2
12	31.5	26.2	18.2
13	31.5	26.2	18.2
14	31.5	26.2	-
15	31.5	26.2	-
16	31.5	26.2	-
17	31.5	26.2	-
18	31.5	26.2	-

Table 6.8: Quick release hooks and fairleads location with respect to main keel for FLNG and carriers

In the following tables there are presented the relative distances and geometric characteristics for side by side lines which corresponds to each configuration and loading condition of the vessels. Paid out length represents the actual length of lines with a pretension in initial position of 100kN. Wire length represents the difference between paid out length and the nylon tail (25m for LNGC and 20m for LPGC). Veritical relative distance represents the difference between QRH location and fairlead location. If this is negative, means that the fairlead on board of the carrier is above the QRH of the FLNG. The vertical angle with respect to the horizontal plane (α) can be seen that is below 15^o, FLNG-LNGC configuration for both loading conditions. On the other side for FLNG-LPGC, the relative height is very large (i.e. maximum of 9.6m) which cause steep angles for side-by side lines. For spring lines, angle θ is more important and needs to be as low as possible for maximizing its holding capacity. On the other side, breast lines are more efficient if angle ϕ is greater.

6.3.5. Location of fenders and material properties

Fenders are placed longitudinally, between vessels in pairs of two, as it can be seen in Figure 6.7 and Figure 6.8. In general for side-by-side offshore operations, pneumatic rubber fenders are used. The selection of type of fenders and number are based on: ship type and size, operational and weather conditions. If the selection is capable to withstand forces from FLNG-LNGC configuration, automatically, the same configuration will bring no problem for the mooring configuration FLNG-LPGC. For both mooring configuration 8 fenders are placed, floated at the water line. The main role of head and stern fender is to prevent contact from rolling of ships due to incoming wave and wind. The rest of them mainly absorb the impact energy and keep the stand-off distance between two ships. Characteristics of the fenders used in the numerical models are based on Yokohama catalogue [6]:

Description	U.M	Value
Diameter	[m]	4.5
Length	[m]	9
Load at 60% deflection(MBL)	[kN]	8041
Safety Factor - OCIMF [30]	-	1.82
Safe Working Load (SWL)	[kN]	4418

Table 6.9: Fender characteristics

Figure 6.18: Pneumatic Fenders placed along the vessel [6]

Figure 6.19: Pneumatic Fender zoom in [6]

Performance curve presents the reaction force and the energy absorption for fenders with an initial internal pressure of 80 kPa Figure **??**.

6.4. Hydrodynamic input

In order to determine the responses in time domain of the moored vessels under the effect of wave, wind and current, the following equation of motions needs to be solved:

$$[M]\{\ddot{X}\} = \sum\{F(t)\} \tag{6.1}$$

where:
-$[M]$ matrix contains the mass and the resonance period added mass
- $\ddot{X}$ acceleration vector
- $F(t)$ external loads applied on the vessels at time instant t, defined as:

$$\sum\{F(t)\} = F_H + F_M + F_B + F_D + F_W + F_C + F_O \tag{6.2}$$

with the following components:
- F_H - hydrodynamic loads;
- F_M - mooring loads;
- F_B - damping loads;
- F_D - wave drift loads;
- F_W - wind loads;
- F_C - current loads;
- F_O for other loads such as: thrusters, risers, fenders etc.

6.4.1. Hydrodynamic loads

The hydrodynamic loads correspond to loads induced by vessels's motions in water and they are determined using the theory of maneuverability. Furthermore, the hydrodynamic interaction between two vessels is represented by the low frequency coupled added mass matrix required as input in Ariane. The coupled hydrodynamic added mass can be written as:

$$[M] = \begin{bmatrix} M_{jj} & M_{kj} \\ M_{jk} & M_{kk} \end{bmatrix} \tag{6.3}$$

for: j=1 and k=2; i.e M_{jj} represents the added mass of ship j due to ship j; while M_{kj} represents the added mass of ship j due to motion of ship k.

where each component consists of horizontal mass matrix (added mass in surge, sway, yaw and sway-way coupling) as can be seen below:

$$M_{jj} = \begin{bmatrix} M_{jj_{xx}} & 0 & 0 \\ 0 & M_{jj_{yy}} & M_{jj_{y\psi}} \\ 0 & M_{jj_{y\psi}} & M_{jj_{\psi\psi}} \end{bmatrix} \tag{6.4}$$

6.4.2. Mooring loads

In this section mooring loads are referred only to mooring lines between two vessels. The axial force in connection point 1 (vessel 1) is equal to the axial force from point 2 which is connected to vessel 2.

In the global axis system the projected forces are:

$$F_x = F \cdot D_h \cdot cos(A) \tag{6.5}$$

$$F_y = F \cdot D_h \cdot sin(A) \tag{6.6}$$

$$M_z = (X_F - X_{East}) \cdot F_y - (Y_F - X_{North}) \cdot F_x \tag{6.7}$$

where:
- D_h - represents the horizontal distance between QRH and F Figure 6.16 and equals to:

$$D_h = \sqrt{\Delta X_{F_{East}}^2 + \Delta X_{F_{North}}^2} \tag{6.8}$$

- X_{East}, X_{North}, Z are the coordinates for each vessel in the global system
- $X_{F_{East}}$, $X_{F_{North}}$, X_F are the coordinates of the fairlead or quick release hook in the global axis system
- A represents the QRH to Fairlead angle (i.e ϕ, Figure 6.16) of side by side lines

6.4.3. Damping loads

In general several damping mechanisms are present for moored systems. Damping contributions acting on a hull may be divided into [7]:

- radiation damping due to wave making
- viscous hull damping;
- wave drift damping;
- mooring line damping.

Radiation damping can be determined from first order potential theory and is proportional to the wave amplitude. This contributes to the wave frequency motions, while for low frequency motions is negligible due to the fact that these have small contribution to wave making.

Viscous effects can be splitted in two components: skin friction and viscous forces due to pressure distribution around the hull (generation of vortices). The latter component is an important contribution in sway and yaw. Roll viscous damping is generated mainly due to bilge keels, while in surge, skin friction is the most significant component to the viscous hull damping. Current loads are the main source of damping effects. In Ariane, they are calculated based on the relative fluid velocity and partly by additional terms which are proportional to the absolute speed of the vessel according to the formulas below:

$$\begin{aligned} F_{Bx} &= -B_{xx}u \\ F_{By} &= -B_{yy}v \\ M_{B\psi} &= -B_{\psi\psi}\dot{\psi} \end{aligned} \tag{6.9}$$

where: B_{xx}, B_{yy}, $B_{\psi\psi}$ are the linear damping coefficients in surge, sway and yaw respectively.

Wave drift damping represents the most important hull damping contribution of low frequency motions. This is caused by the change of vessel's mean drift force when this slowly vary with a speed against or in the direction of the incoming wave. This is proportional to the square of the incoming wave amplitude and slowly varying velocity of the vessel. The associated energy is slow-drift motion damping. In Ariane, this is implemented in drift loads formulation. This consists in calculation at each time step the instantaneous heading of the vessel with respect to the wave and respectively the relative low velocity which depends on the current velocity.

Additional damping in the system is given by the mooring lines which can be significant to the total damping. The magnitude of drag forces increases with increasing the water depth and currents velocity. These forces are proportional to the relative fluid velocity to the body and can be expressed as Morison's equation:

$$F_d = \frac{\rho}{2} C_d D |v_{rel}| v_{rel} \tag{6.10}$$

where C_d is the drag coefficient, D diameter of the mooring line, v_{rel} the relative horizontal velocity between current and mooring line: $V_{rel} = U_c - \dot{r}$

Vessel	Loading condition	$B_{11}[kg/s]$	$B_{22}[kg/s]$	$B_{66}[kg \cdot m^2/s]$
FLNG	ballast(B)	4.04911E+05	1.89260E+06	2.16678E+10
	fully loaded (FL)	4.14009E+05	1.935123E+06	2.2154674195E10
LNGC	ballast (B)	1.20E+06	2.02E+06	1.21E+10
	fully loaded(FL)	1.72E+06	2.38E+06	1.21E+10
LPGC	ballast(B)	9.63E+05	1.33E+06	9.69E+09
	fully loaded(FL)	1.38E+06	1.90E+06	9.69E+09

Table 6.10: Damping Matrix

6.4.4. Wave first order loads

Wave first order loads derive from the Froude-Krylov loads, Chapter 3.

6.4.5. Wave drift loads

In time domain simulations (Ariane), the wave drift loads can be computed using several methods such as [37]:

- Newman approximation (available both on Ariane 7 and 8)
- BV approximation (available both on Ariane 7 and 8)
- Molin approximation (available on Ariane 8)
- Newman current-wave interaction (available both on Ariane 7 and 8)
- QTFC Formulation (available both on Ariane 7 and 8)
- QTFC Formulation with wave-current interaction (Available on Ariane8)
- QTFC 6DOF (available on Ariane 8)

Using Newman approximation, the slow drift loads are derived from the diagonal terms of the Quadratic Transfer Functions (QTFs) of the vessels. This represents the mean loads acting on the vessels when are subjected to bichromatic wave of unitary amplitude. Thus they are proportional to the wave amplitude and may vary with the water depth, direction of the incoming wave relative to the vessel and the two circular frequencies that compose the bichromatic wave. The diagonal terms are obtained when two components of the bichormatic wave are identical and can be determined using diffraction-radiation analysis. This formulation can be used for soft mooring system (i.e. catenary) in deep waters.

Bureau Veritas (BV) approximation introduce a variant in Newman's approximation which give more accurate estimations. This approach consists in introducing a term linearly proportional to the expansion of difference frequency. If this is null, thus the BV approximation becomes Newman approximation. This formulation can be applied to any water depth, but considering only soft mooring systems.

Molin approximation is based on Newman's approximation and involves four summations instead of two in the original formulation. This allows to compute the sign of the loads.

Newman current-wave interaction calculates the slow drift taking into account the current interaction by a correction on the QTF by means of local water velocity, while the current forces are taken into account using the current coefficients.

QTFC formulation has 3 options available in Ariane: QTFC formulation (3DOF), QTFC current-wave formulation and QTFC 6DOF. The standard QTFC formulation is composed from two components: one coming from the quadratic product of the wave fields in the first order and the other is coming from the second order potentials of the oscillating wetted surface of the body. These two components are added to the the second order Froude-Krylov loads. This formulation can be adapted for considering the current-wave interaction or considering all 6 degrees of freedom.

6.4.6. Wind loads

Wind loads are defined using the aerodynamic coefficients in three directions. These coefficients are obtained from wind tunnel tests and includes also the shielding effects. They are function of wind angle of attack. The forces and moment acting on the ships can be calculated as:

$$\begin{aligned} F_{Wx} &= \frac{1}{2}\rho_{air} S_t C_{Wx} \alpha_W V_w^2 \\ F_{Wy} &= \frac{1}{2}\rho_{air} S_l C_{Wy} \alpha_W V_w^2 \\ M_{Wz} &= \frac{1}{2}\rho_{air} S_l L C_{Wz} \alpha_W V_w^2 \end{aligned} \tag{6.11}$$

where: S_t,S_l represents the transverse and respectively longitudinal wind area; C_{Wx},C_{Wy},C_{Wz} represents the longitudinal, lateral and yaw aerodynamic coefficient; V_W represents the wind

velocity at 10m above the water surface; L is length between perpendiculars; α_W is the wind incidence relative to the vessel heading.

In time domain, at each time step, the wind loads are obtained by interpolation between the existing and instantaneous wind angle of incidence. Below there are presented graphically the wind coefficients multiplied by the exposed areas, for both the FLNG and carriers. The wind coefficients are dependent on loading condition of the vessel, such that in ballast condition the wind forces are higher due to the increase in freeboard. It can be seen throughout the figures below, that the difference between fully loaded and ballast condition is significantly especially for carriers where the difference in draft is considerable. The fully exposed areas for both vessels are given in the Table 6.11

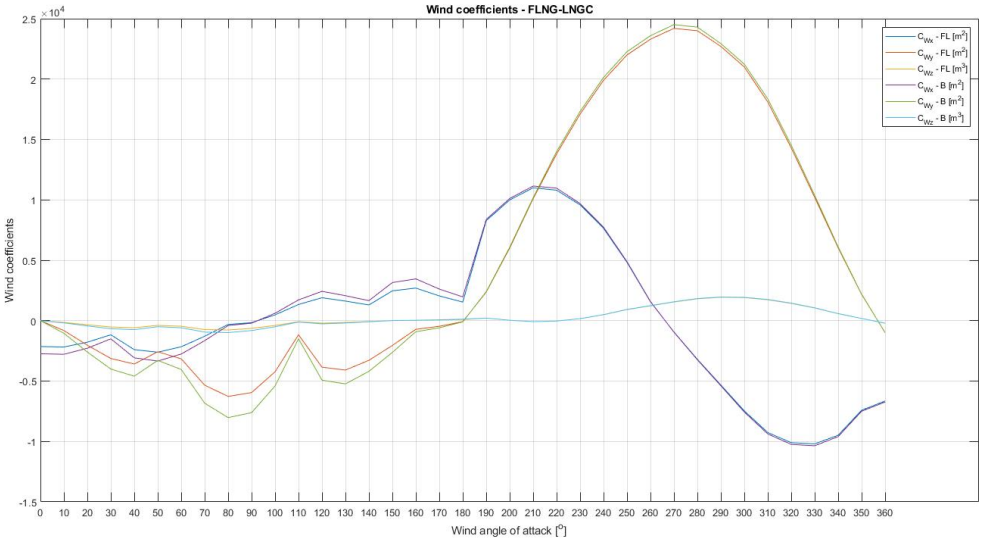

Figure 6.20: Wind coefficients for FLNG based on FLNG-LNGC configuration

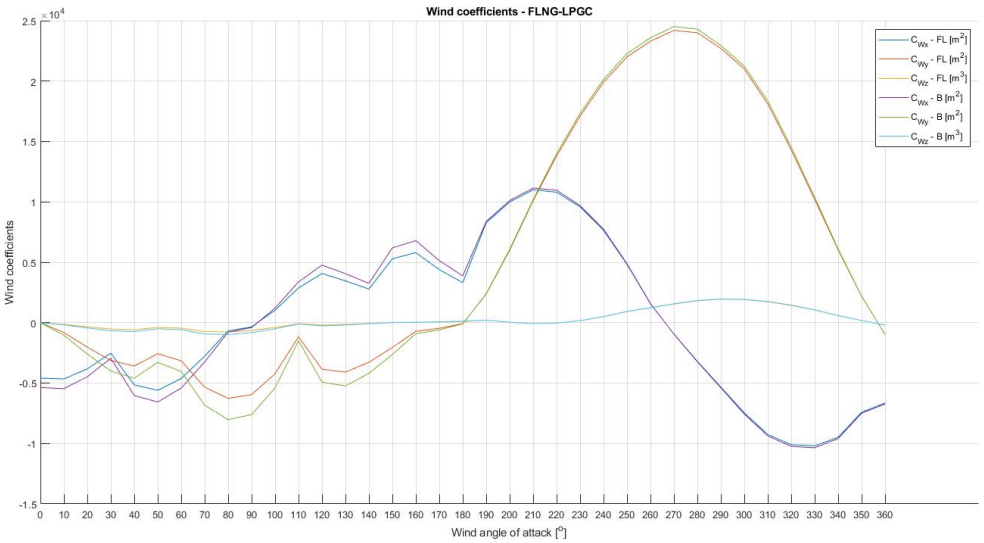

Figure 6.21: Wind coefficients for FLNG based on FLNG-LPGC configuration

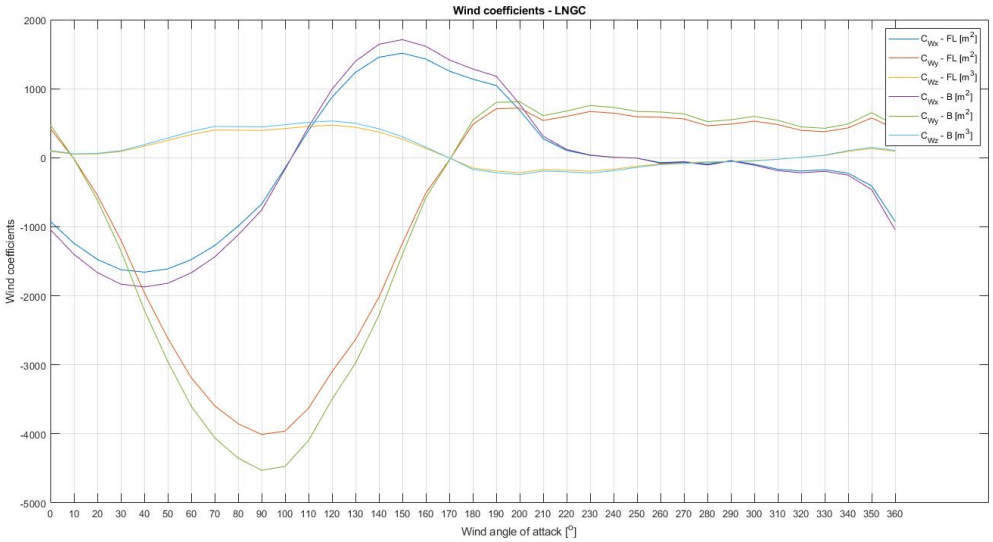

Figure 6.22: Wind coefficients for LNGC based on FLNG-LNGC configuration

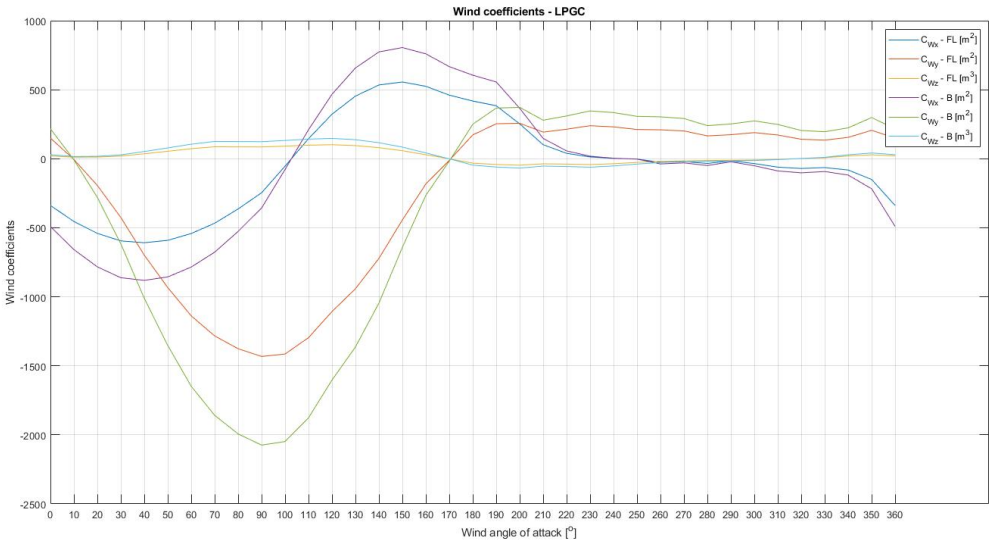

Figure 6.23: Wind coefficients for LPGC based on FLNG-LPGC configuration

Vessel	Loading condition	$S_l[m^2]$	$S_t[m^2]$
FLNG	ballast(B)	7058	1545
	fully loaded (FL)	6973	1526
LNGC	ballast (B)	4731	760
	fully loaded(FL)	4189	673
LPGC	ballast(B)	2167	357
	fully loaded(FL)	1496	247

Table 6.11: Exposed Areas

6.4.7. Current loads

Current loads are due to the relative velocity of the fluid past the vessel. In Ariane they are calculated using hydrodynamic coefficients and the resultant current forces can be expressed as:

$$\begin{aligned} F_{Cx} &= \frac{1}{2}\rho_{water} T_d C_{Cx} \alpha_{current} U_C^2 \\ F_{Cy} &= \frac{1}{2}\rho_{water} T_d C_{Cy} \alpha_{current} U_C^2 \\ M_{Cz} &= \frac{1}{2}\rho_{water} T_d C_{Cz} \alpha_{current} U_C^2 + M_{C\psi Molin/0} \end{aligned} \tag{6.12}$$

where: T_d is the average vessel draft; C_{Cx},C_{Cy},C_{Cz} are respectively the longitudinal, lateral and yaw hydrodynamic drag coefficient; $\alpha_{current}$ is the equivalent incidence of the current with respect to the heading of the vessel; U_C is the relative equivalent current velocity; $M_{C\psi Molin/o}$ is the additional yaw moment applied in the origin of the vessel system

The Molin moment needs to be added to the vessel if the experimental drag coefficients are measured with the vessel considered fixed during model tests. This corrects the yaw moment such that to consider also the yaw viscous damping effects.

Below are presented the drag coefficients for each vessel.

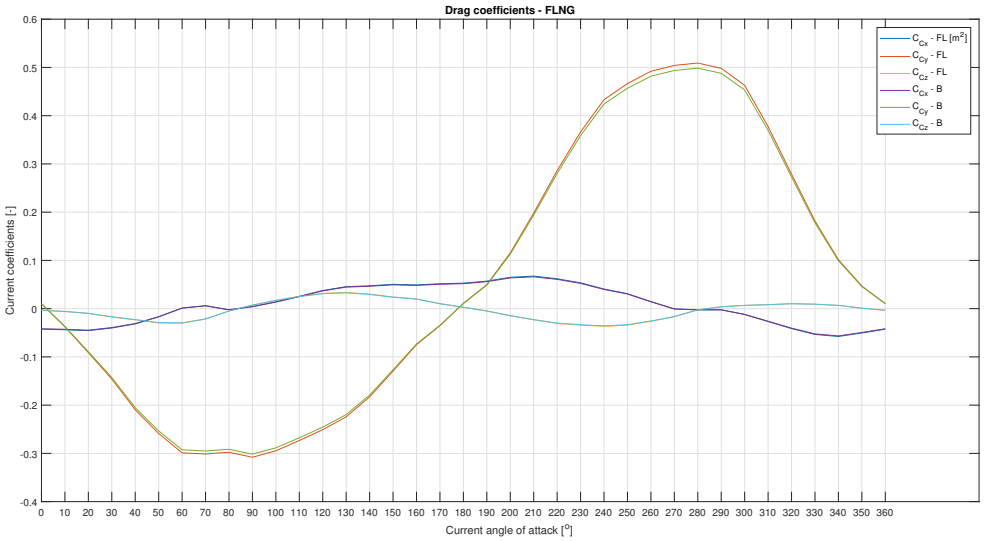

Figure 6.24: Drag coefficients for FLNG in fully loaded (FL) and ballast (B) condition

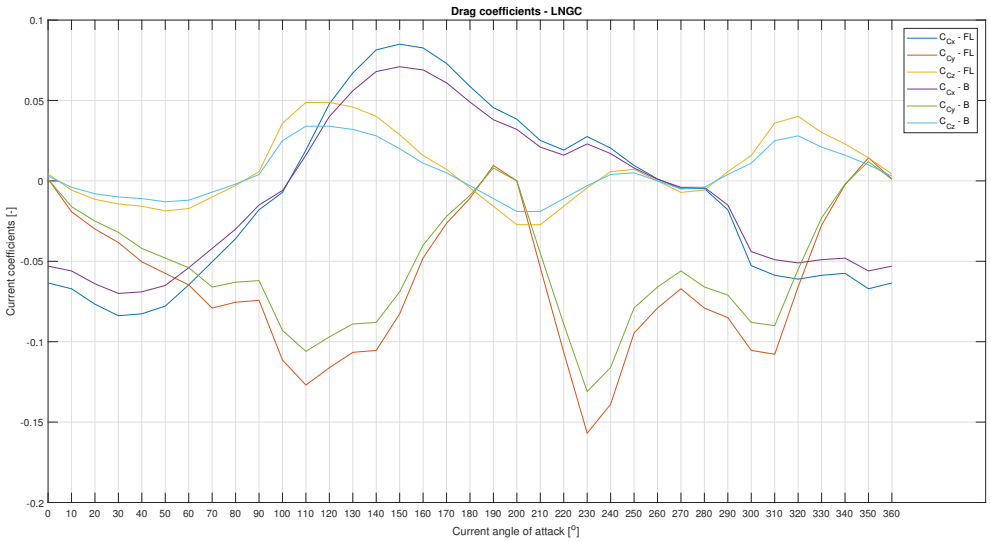

Figure 6.25: Drag coefficients for LNGC in fully loaded (FL) and ballast (B) condition

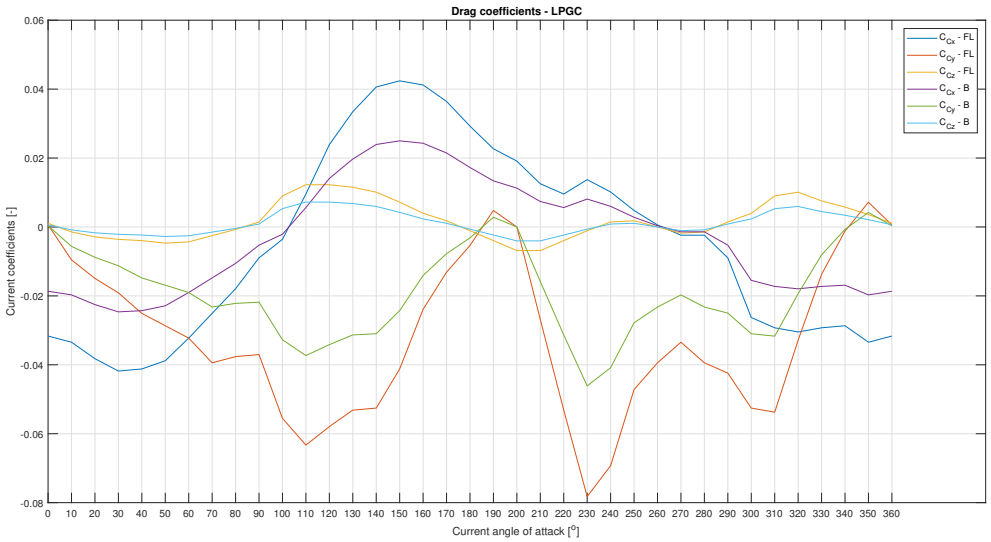

Figure 6.26: Drag coefficients for LPGC in fully loaded (FL) and ballast (B) condition

6.5. Site location and environmental conditions. Offloading criteria

6.5.1. Site location

Vessels are located within the South Atlantic Ocean on the west Coast of Africa, close to the shore, with a specific mean water depth of 50m. This specific zone, between May through October is governed by swell coming from south-westerly direction. These storms are generated in the South Atlantic and travel thousands of miles along the West African coasts which can generate sea-state up to 3m close to equator and 4m in Angola [13]. During October to April, swell approach West African coast from north-westerly directions. Theses storms are generated in North America and travel from North Atlantic towards South Atlantic. The developed wave heights around the West African Coast is up to 0.5m [13]. Below there are presented the statistics for mean wave periods (T_{01}) and significant wave height during 15 years measurements (Angola location) [13]. It can be seen that the highest probability of average period is approximately between 5 and 17seconds, while for waves is from 0.5 up to 2meters.

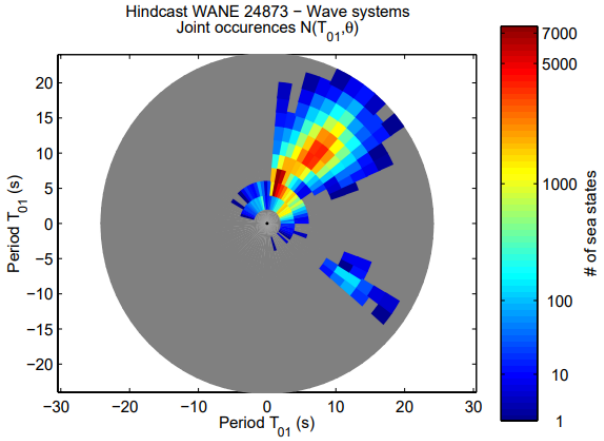

Figure 6.27: Average Wave Period for West African Coast (Angola) [13]

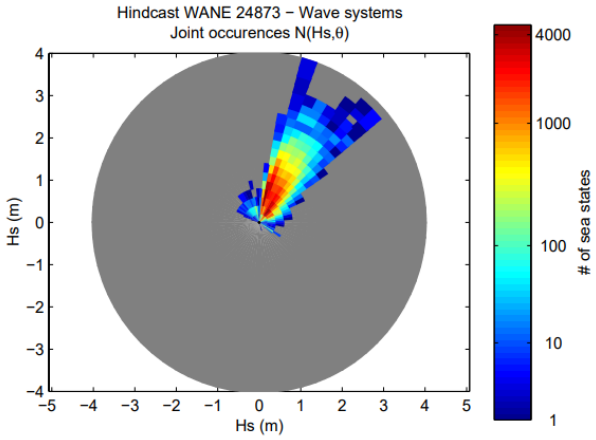

Figure 6.28: Significant Wave Height for West African Coast (Angola) [13]

Besides waves, West Africa is particularly affected by squall phenomena. This is highly unstationary and characterised by sudden and violent windstorm with very rapid changes of wind speed intensity and direction. In particular these events may occur before and after rainy season, i.e from April to June and from September to October [15]. Squall velocity and heading time trace from specific site location are presented in the next subsection.

6.5.2. Environmental conditions

All environmental data are defined with respect to the West African Coast environmental specific. A summary with the environmental conditions for all cases studies are given in the Table 6.12. They are divided into two categories: non-squall cases with significant wave height between 1.9m and 2.5m, constant wind and current loads; squall-cases are governed by a significant wave height of 2m, constant current loads and wind time trace scaled with 25m/s and respectively 30m/s with a initial starting wind direction of 230deg.(south-westerly direction).

	Swell				Wind		Current	
	H_s	T_p	γ	β	U_W	β	U_C	β
Case Nb.	$[m]$	$[s]$	$[-]$	$[^o]$	$[m/s]$	$[^o]$	$[m/s]$	$[^o]$
Non Squall cases								
ME1	2.5	7	2.7	180	8	135	0.7	90
ME2	2.5	14	2.7	180	8	135	0.7	90
ME3	2.5	17	2.7	180	8	135	0.7	90
ME4	2	6.4	1.3	225	12.7	225	0.7	180
ME5	1.9	14.1	2.6	225	7	180	0.7	180
Squall cases								
Squall1	2	14	2.5	225	TS^1	230	0.8	270
Squall2	2	14	2.5	225	TS^2	230	0.8	270

[1] TS-Time series scaled with 25m/s
[2] TS-Time series scaled with 30m/s

Table 6.12: Environmental conditions

The water surface is modelled by a single peaked spectrum for limited fetch, respectively Jonswap spectrum, with a maximum of 2.5m significant wave height. For non-squall cases, wind and current has linear profile, while for squall cases, the wind varies in time and direction, having a starting direction of 230^o. The shape of the spectrum is described by the peakedness γ. Peak enhancement factor, becomes larger as the peak is acute, generally with ranging values between 1-3.3, if 1, this reduces to Pierson-Moscowitz spectrum.

$$S_J(\omega) = \frac{5}{16} \cdot H_s^2 \cdot \omega_p^4 \cdot \omega^{-5} exp\left(-\frac{5}{4} \cdot \left(\frac{\omega}{\omega_p} \right)^{-4} \right) A_\gamma \gamma^{exp\left(-0.5\left(\frac{\omega-\omega_p}{\sigma\omega_p}\right)^2\right)} \tag{6.13}$$

where: $\omega_p = 2\pi/T_p$; γ - nondimensional peak shape parameter; σ - spectral width parameter; A_γ -nonrmalizing factor $(1 - 0.287ln(\gamma))$

Jonswap spectrum is expected to be reasonable model for the following condition: $3.6 < T_p/\sqrt{H_s} < 5$, outside this interval needs to be used with caution [10].

As it can be seen in Figure 6.29, ME1 and ME4 are characteristic to un-developed sea state, governed by short waves with the peak frequency close to the piston frequency of the gap between two vessels.

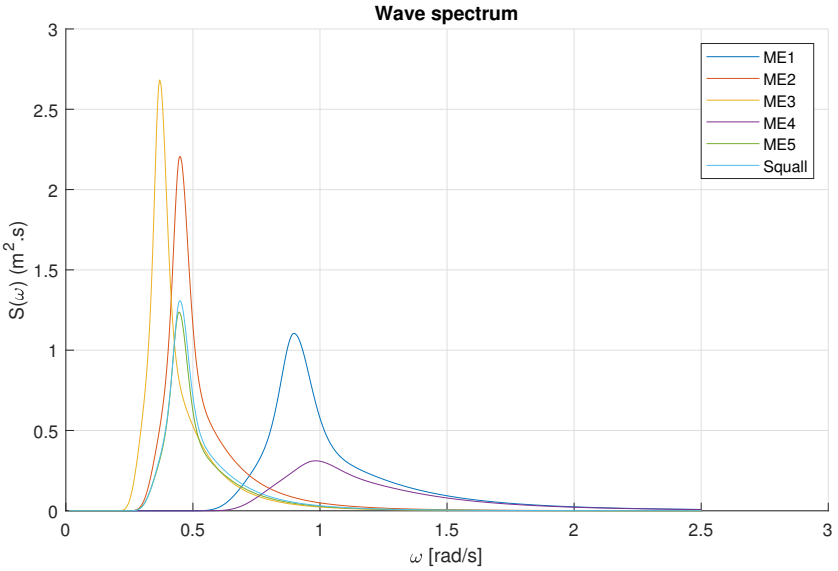

Figure 6.29: Wave energy spectrum

Below there are presented the wind time trace for speed and direction for the both squall cases analyzed. This consists in 3hours wind measurements with a rump-up of 500seconds to have sufficient time for stabilizing the signal. Squall1 is scaled with $25m/s$ while squall2 with $30m/s$. Between 3500-5000seconds there are major changes in wind velocity. It can be seen that the maximum velocity is reached at 4340seconds, while the average is around 0.3 of maximum velocity. Regarding the direction of the wind speed, it can be seen that when the maximum velocity is reached, the direction of the incoming wind is not varying so much (offset of 30 deg. maximum). Between 3000-4000 and 6000-7000 seconds there is a huge difference in wave heading, with an offset of more than 200 degrees.

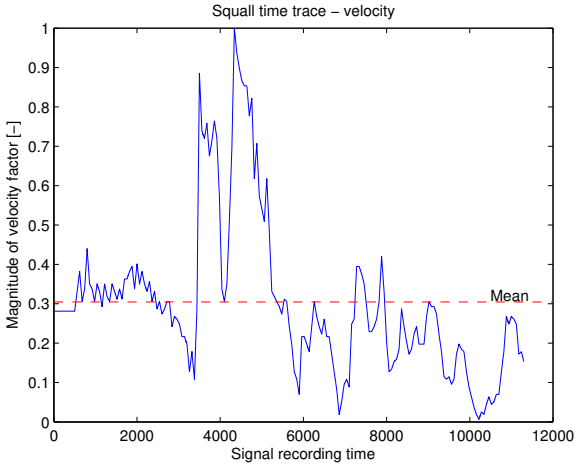

Figure 6.30: Squall wind speed factor

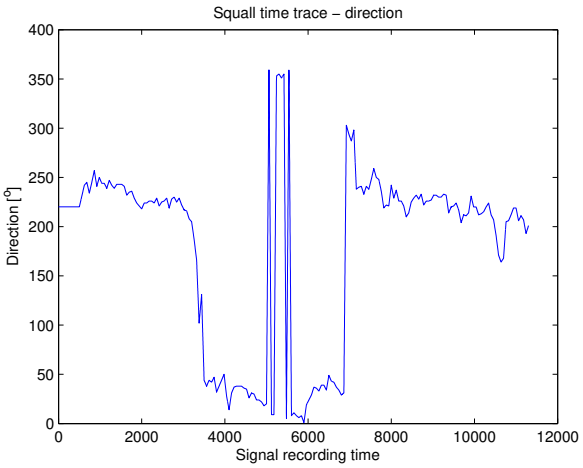

Figure 6.31: Squall direction

6.5.3. Operational criteria and on-site decisions during offloading operations

In general, for side-by-side operations the operational criteria is given by the vendor of the loading arm systems. Typical size used is 16 inch loading arm [27]. Technically feasible motion envelope for operating the loading arms are [27]:

- Low frequency horizontal relative motions: $\pm 4m$
- Wave frequency horizontal relative motions: $\pm 2m$
- Vertical relative motions: $\pm 2m$

According to SBM, the following criteria is proposed:

Parameter		U.M.	Criteria
Max. allowable wave frequency relative	surge	[m]	± 2
	sway	[m]	± 1.5
	heave	[m]	± 1.5
	distance	[m]	± 3
Max. allowable low frequency relative	surge	[m]	± 4
	sway	[m]	± 4

Table 6.13: Maximum allowable relative motions to the manifold location according to SBM

Beside the loading arm criteria which usually is the most sensitive, the mooring line loads criteria is also important. This is given in Table 6.6 (FLNG-LPGC) and Table 6.7 (FLNG-LNGC) for both configurations.

It is hard to anticipate every emergency which could arise in side-by-side offloading operations. However from weather perspective which leads to mooring and fender loads, SBM

based on offshore experience, uses the following actions in case if one of the criteria is exceeded:

Criteria	Actions
25 knots mean wind speed 2m Significant wave height	Consultation between vessels's Master
Forecast ≥ 25knots mean wind speed	Consider stopping the load transfer and disconnecting
≥ 27 knots mean wind speed 2.5m Significant wave height 2^o pitch or roll of carrier	Suspend the cargo transfer Disconnect and retract the mooring lines Consider unberthing
≥ 30knots mean wind speed 3m Significant wave height ≥ 2m relative surge ≥ 1.5m relative sway and heave 3^o pitch or roll of carrier	Unberth the carrier and sail to a sheltered area
Forecast >20knots mean wind speed	Unberth the carrier and sail to sheltered area

Table 6.14: Weather conditions and actions on-site

Under uneven environmental conditions presented above, high loads on the moored system can occur. According to SBM side-by-side guidelines during offloading process, if for one or more mooring lines exceeds five peaks in 3hours of measurements with 50% of its MBL and/or two tension peaks above 50% arise in 2minutes period on the same line in such that and/or the deflection of the fenders is higher than 50%, then the offtake process needs to be suspended, disconnect the manifolds and retract the mooring lines.

6.6. Calculation method

This section presents the calculation method for both Ariane7 and Ariane8 [31], [37].

6.6.1. Quasi-dynamic analysis - Ariane7

For side-by-side moored systems, the best calculation method which Ariane7 can offer is a time domain quasi-dynamic analysis using a de-coupled scheme. The main assumptions of this method is that the mooring lines are considered as non-linear massless springs, which follow their fairlead location. There is no wave, wind or current loads applied to the mooring lines, thus the only load contribution to the vessel is their static spring reaction in the instantaneous vertical plane of the line. The other assumption made is regarding the vessel's motions which are solved in the free surface plane only (surge,sway,yaw) [37]. Calculation procedure is based on the assumption that the wave frequency components does not impact on the low frequency response due to the different time scales. Thus the response of the vessel in time domain is obtained by solving at each time step the low frequency component using vectorial differential Equation 6.1 under environmental conditions (wave, wind and current) plus adding the six wave frequency motions of each vessel. Wave frequency motions are determined by multiplying the amplitude of each wave signal component with RAOs components which are defined with respect to the center of gravity of each vessel. The summation between low and wave frequency components is dependent on time and space phases. Derivation of the mooring line tension is done at the end of each time step from the static catenary response. It is assumed that during simulation the mooring stiffness variation with low frequency motions does not influence the wave frequency response (resonance of mooring system far from wave frequency peak period). Thus, the latter response is computed by taking into account only the average mooring stiffness which corresponds to the mean position of the vessel over the entire simulation. Once having the motion response signal, the instantaneous position between line connection points can be assessed. Thereby, the instantaneous tension line can be computed by interpolating the static catenary response with the obtained vertical positions of line fairleads.

6.6.2. Quasi-dynamic analysis - Ariane8

Compare to Ariane7, Ariane8 provide a quasi-dynamic time domain analysis using coupled scheme (unified method [37]). This method retain the assumptions made in de-coupled scheme such as: lines stay in vertical plane and no environmental loads are applied to them; vessel's motions are calculated in 3D resolution (surge,sway,yaw). The difference between previous and this method is the possibility of solving simultaneously the low and wave frequency responses as shown in the equation below:

$$\big([M] + [M_{a\infty}]\big)\{\ddot{X}(t)\} + \{F_{rad}(t)\} + [B]\{\dot{X}(t)\} = \sum\{F_{LF}(t)\} + \{F_{HF}(t)\} \tag{6.14}$$

where:

- [M] is the vessel mass matrix
- $[M_{a\infty}]$ is the added mass matrix at infinite frequency (explained below)
- $\{\ddot{X}(t)\}$ is the vessel low and high frequency horizontal acceleration vector at time instant t
- $\{F_{rad}(t)\}$ -the radiation memory loads, result of the convolution between the vessel velocity and retardation functions
- $[B]$ is the linear damping matrix
- $\{\dot{X}(t)\}$ the vessel low and high frequency horizontal velocity vector at time instant t
- $\{F_{LF}(t)\}$ and $\{F_{HF}(t)\}$ represents the low and respectively high frequency external loads applied on the vessel at time instant t

This time-domain method has bee proposed by Cummins [11] and Ogilvie [14]. The main idea is that this approach allows non-linearities for all terms in the equation of motion. Thereby, the radiation loads no not only depend on the instantaneous vessel velocity and acceleration, but also due to the presence of the free surface (memory effect). The fluid-memory model needs to be described as a discrete-time approximation of the convolution integral with enough past data. The radiation loads becomes:

$$\{F_{rad}(t)\} = \int_{t-t_{retard}}^{t} \{\dot{X}(t)\}[K(t-\tau]d\tau \tag{6.15}$$

where:

$\dot{X}$ is the vessel instantaneous velocity at time instant t; $[K(t)]$ represents the retardation function; t_{retard} is the time duration for which the convolution with instant velocity and retardation function is calculated.

The hydrodynamic coefficients and the retardation function were established by Ogilvie [14]:

$$[M_a(\omega)] = [M_a(\infty)] - \frac{1}{\omega}\int_0^{\infty} [K(t)]sin\omega t dt \tag{6.16}$$

$$[B(\omega)] = \int_0^{\infty} [K(t)]cos\omega t dt \tag{6.17}$$

Taking the inverse Fourier transform of the above equations, yields the retardation function K(t) as follows:

$$[K(t)] = \frac{2}{\pi}\int_0^{\infty} [B(\omega)]cos\omega t dt \tag{6.18}$$

7

Time domain model results

7.1. Introduction

All the results are presented graphically in Appendix and this section shows only the important aspects with respect to each comparison in terms of relative motions, line tensions and fender loads. The results presented are considered the maximum peak from a duration of 3hours due to one wave realization. Statistically speaking, this is not reliable, but to quantify the effect of diffraction input in time domain should be sufficient. In general most probable maximum of at least 20 realisations is required as per DNV guidelines. In order to keep the same comparison as for diffraction calculations, the results are divided in 3 sections as follows:

1. Gap resonance which depends on the following parameters:
   (a) Dissipation factor
   (b) Gap length
   (c) Separation distance
2. Loading condition and carrier size variation. Mooring line optimization
3. Ariane7 vs Ariane8

7.2. Modal analysis for FLNG-LNGC and FLNG-LPGC

The global stiffness matrix composed from mooring line attached to the sea floor and side-by-side mooring lines, gives important information about the resonant modes of the moored system at its equilibrium position. Prior to time domain analysis under environmental loads is recommended to evaluate the resonant modes of the moored system. This can be assessed in two ways such as: in frequency domain using the calculated stiffness matrix at a specific position of the vessels or in time domain using decay tests around different mean positions [5]. A sensitivity analysis can be done with respect to stiffness matrix in order to determine how much this matrix change for different positions of the vessels.

Below there are presented the stiffness matrix contribution on horizontal plane for both configurations FLNG-LNGC and FLNG-LPGC for two loading conditions: ballast and fully-loaded as the length of side-by-side mooring lines differs for each case. These are calculated for the initial static configuration under the action of pretension without considering any external loads.

In the matrix below there are presented the force or moment in terms of each body and also the mechanical interaction between the two vessels. A remark regarding the stiffness of body 1 (i.e FLNG) is that this incorporates both the anchoring and side-by-side mooring system.

FLNGmin-LNGCmax						
	surge b1	sway b1	yaw b1	surge b2	sway b2	yaw b2
surge b1	1.002E+07	2.803E+04	1.441E+08	-8.933E+06	9.081E+03	2.327E+08
sway b1	2.651E+04	2.082E+06	-8.651E+07	9.083E+03	-1.052E+06	2.445E+07
yaw b1	1.424E+08	-8.558E+07	9.657E+10	5.915E+07	9.250E+07	-5.443E+10
surge b2	-8.933E+06	9.081E+03	5.925E+07	8.933E+06	-9.081E+03	-2.327E+08
sway b2	9.083E+03	-1.052E+06	9.258E+07	-9.083E+03	1.052E+06	-2.445E+07
yaw b2	2.324E+08	2.461E+07	-5.440E+10	-2.324E+08	-2.461E+07	5.745E+10

FLNGmax -LNGCmin						
	surge b1	sway b1	yaw b1	surge b2	sway b2	yaw b2
surge b1	1.005E+07	8.750E+03	1.528E+08	-8.969E+06	2.357E+04	2.372E+08
sway b1	8.311E+03	2.110E+06	-8.958E+07	2.358E+04	-1.079E+06	2.452E+07
yaw b1	1.531E+08	-8.843E+07	9.727E+10	4.820E+07	9.445E+07	-5.534E+10
surge b2	-8.969E+06	2.357E+04	4.797E+07	8.969E+06	-2.357E+04	-2.372E+08
sway b2	2.358E+04	-1.079E+06	9.472E+07	-2.358E+04	1.079E+06	-2.452E+07
yaw b2	2.372E+08	2.460E+07	-5.530E+10	-2.372E+08	-2.460E+07	5.882E+10

FLNGmin -LPGCmax						
	surge b1	sway b1	yaw b1	surge b2	sway b2	yaw b2
surge b1	9.755E+06	-1.114E+04	1.074E+08	-8.673E+06	4.823E+04	1.089E+08
sway b1	-1.525E+04	1.931E+06	-5.623E+07	5.084E+04	-9.012E+05	1.034E+07
yaw b1	1.063E+08	-5.474E+07	8.421E+10	9.528E+07	6.165E+07	-4.336E+10
surge b2	-8.673E+06	4.823E+04	9.598E+07	8.673E+06	-4.823E+04	-1.089E+08
sway b2	5.084E+04	-9.012E+05	6.229E+07	-5.084E+04	9.012E+05	-1.034E+07
yaw b2	1.085E+08	1.048E+07	-4.339E+10	-1.085E+08	-1.048E+07	4.295E+10

FLNGmax -LPGCmin						
	surge b1	sway b1	yaw b1	surge b2	sway b2	yaw b2
surge b1	9.793E+06	-6.982E+04	1.108E+08	-8.712E+06	1.025E+05	1.072E+08
sway b1	-7.358E+04	2.060E+06	-6.685E+07	1.057E+05	-1.029E+06	1.279E+07
yaw b1	1.113E+08	-6.445E+07	8.465E+10	9.000E+07	7.053E+07	-4.372E+10
surge b2	-8.712E+06	1.025E+05	9.002E+07	8.712E+06	-1.025E+05	-1.072E+08
sway b2	1.057E+05	-1.029E+06	7.202E+07	-1.057E+05	1.029E+06	-1.279E+07
yaw b2	1.069E+08	1.272E+07	-4.379E+10	-1.069E+08	-1.272E+07	4.320E+10

Figure 7.1: Stiffness matrix at the equilibrium position for each configuration [N/m, N, N.m]
(body1 = FLNG; body2 = carrier)

Therefore once having the stiffness matrix the eigen modes can be determined. For the configurations mentioned 12 eigen modes are determined based on frequency domain, where first six modes are given by the hydro-static stiffness of the vessels and the last six modes are given by the mooring stiffness of the system. It is hard to assign one mode to a single motion as this can be a result of a coupled motion between the two bodies.

FLNGmin-LNGCmax			
Mode	ω [rad/s]	T [s]	DoF
1	0.653	9.627	pitch b2
2	0.606	10.367	heave b2
3	0.483	13.014	pitch b1
4	0.483	13.014	heave b1
5	0.347	18.131	roll b1
6	0.337	18.630	roll b2
7	0.337	18.644	out-of-phase sway/yaw
8	0.266	23.621	out-of-phase sway
9	0.121	51.927	out-of-phase surge
10	0.083	75.701	in-phase yaw
11	0.042	149.600	in-phase surge
12	0.001	6283.185	in-phase sway

FLNGmax-LNGCmin			
Mode	ω [rad/s]	T [s]	DoF
1	0.620	10.129	pitch b2
2	0.620	10.129	heave b2
3	0.491	12.804	pitch b1
4	0.491	12.804	heave b1
5	0.283	22.165	roll b1
6	0.431	14.573	roll b2
7	0.284	22.124	out-of-phase sway/yaw
8	0.281	22.360	out-of-phase sway
9	0.124	50.671	out-of-phase surge
10	0.089	70.598	in-phase yaw
11	0.043	146.121	in-phase surge
12	0.006	1047.198	in-phase sway

FLNGmin-LPGCmax			
Mode	ω [rad/s]	T [s]	DoF
1	0.793	7.925	pitch b2
2	0.709	8.863	heave b2
3	0.568	11.054	pitch b1
4	0.514	12.217	heave b1
5	0.345	18.194	roll b1
6	0.472	13.310	roll b2
7	0.463	13.571	out-of-phase sway/yaw
8	0.345	18.212	out-of-phase sway
9	0.151	41.610	out-of-phase surge
10	0.110	57.120	in-phase yaw
11	0.052	120.830	in-phase surge
12	0.033	190.400	in-phase sway

FLNGmax-LPGCmin			
Mode	ω [rad/s]	T [s]	DoF
1	0.762	8.242	pitch b2
2	1.232	5.102	heave b2
3	0.567	11.085	pitch b1
4	0.508	12.366	heave b1
5	0.284	22.098	roll b1
6	0.546	11.512	roll b2
7	0.509	12.344	out-of-phase sway/yaw
8	0.285	22.046	out-of-phase sway
9	0.214	29.361	out-of-phase surge
10	0.135	46.542	in-phase yaw
11	0.050	125.664	in-phase surge
12	0.006	1047.198	in-phase sway

Figure 7.2: Resonant modes of the system

In the tables above there are presented the motions which contribute the most to the mode. It can be seen that all the modes due to the mooring system for FLNG-LNGC are outside the range of the wave periods analysed (Table 6.12), while for configuration FLNG-LPGC the out

of phase sway-yaw it is within the range of the wave periods. It is expected to have higher tensions in the mooring lines for the last configuration mentioned. Moreover because the out-of-phase modes are governed by difference frequencies higher than in-phase modes, full QTF is recommended in order to have more accurate estimates of the relative motions. With this respect a comparison between Newman-wave/current formulation and full QTF matrix will be presented.

7.3. Gap parameters

For this section only one mooring configuration has been considered (i.e. FLNGmax - LNGCmin) where the governing parameters which defines the gap between the two vessels has been varied in terms of diffraction input only.

7.3.1. Dissipation factor

A sensitivity analysis of dissipation factor has been carried out as it is presented in Chapter 4. The main conclusion from it is that the dissipation factor affects only the second order forces, in particular at the gap resonance only. In order to quantify the effect of damping factor variation from diffraction database in time domain analysis, the following configuration has been used:

Cases	$SbS_{1.1}$, ϵ_1, d_3, LD_1 **vs** $SbS_{1.1}$, ϵ_2, d_3, LD_1 **vs** $SbS_{1.1}$, ϵ_3, d_3, LD_1 **vs** $SbS_{1.1}$, ϵ_4, d_3, LD_1 **vs** $SbS_{1.1}$, ϵ_5, d_3, LD_1

Table 7.1: Dissipation factor variation for FLNGmax-LNGCmin

Therefore the dissipation factor varies from 0 to 0.4 with step of 0.1 for FLNGmax-LNGCmin configuration, while the other parameters stays constant: gap length of 160m, separation between vessels of 4m.

Relative motions

As it was presented in Chapter 4, the horizontal motions of moored systems in irregular waves is composed from 3 components:

- a mean displacement (new equilibrium position) from a constant load (i.e wind and current) and mean wave drift force (i.e second order wave potential) and mooring system;
- an oscillating displacement generated by the first order wave loads (linear motions) where time-averaged of this component is zero
- an oscillating displacement caused by low-frequency wave drift forces (second order wave loads) and mooring system stiffness characteristics

In Appendix B can be found all these components mentioned above. On this section there are presented only the maximum absolute value of the loading arm relative motions with respect to the initial position (Table 6.3) for the mooring configuration presented in the Table above.

In the figures below there are presented the absolute relative motions with respect to initial location of the loading arm for the environmental condition which has been found a significant change (i.e ME4 [T_p=6.4s] and ME1 [T_p=7s]). In the results which are detailed in the appendix, can be observed that throughout the environmental conditions range the variation of dissipation factor does not influence the relative wave frequency motions, such that with

or without dissipation factor have the same magnitude. Exception makes the environmental condition (i.e ME4 [T_p=6.4s] and ME1 [T_p=7s]) where the moored system is subjected to wave loads periods close to resonant gap frequency. This can be observed only for heave due to increase in draft (wetted surface) such that for the case without dissipation factor is higher with 30% than for the cases with dissipation factor. However the overall magnitude of heave for this specific environmental condition is considerably low compare to the others. This is showed in diffraction chapter where the first order quantities are slightly affected by the presence of the dissipation factor.

Regarding the low frequency relative motions it can be seen that they are highly influenced by the variation of wave elevation in between the vessels. It can be seen that for the governing cases (i.e ME1 and ME4) for the case where there is no damping applied to the water surface between the two vessels, sway and surge reach extreme magnitude compare to the other cases (5-7 times higher). In particular, surge reaches 4.55m maximum above the mean position. This means that the criteria is not satisfied. However, this will be reflected into line and fender loads which will result in extreme values. On the other hand without dissipation factor, the results are not feasible for designing the mooring system.

			Absolute values of relative motion at manifold																					Criteria [m]
			Mean					Max					Min					Stdv					
	DoF	Env.cond	eps=0	eps=0.1	eps=0.2	eps=0.3	eps=0.4	eps=0	eps=0.1	eps=0.2	eps=0.3	eps=0.4	eps=0	eps=0.1	eps=0.2	eps=0.3	eps=0.4	eps=0	eps=0.1	eps=0.2	eps=0.3	eps=0.4	
wave frequency	Relative distance [m]	ME1	0.00	0.00	0.00	0.00	0.00	0.10	0.10	0.10	0.10	0.10	0.11	0.11	0.11	0.11	0.11	0.03	0.03	0.03	0.03	0.03	3.00
		ME4	0.00	0.00	0.00	0.00	0.00	0.10	0.07	0.07	0.07	0.07	0.09	0.06	0.06	0.06	0.06	0.02	0.02	0.02	0.02	0.02	
Low frequency	Sway [m]	ME1	0.08	0.05	0.02	0.01	0.00	0.17	0.22	0.16	0.13	0.11	1.28	0.03	0.02	0.01	0.01	0.10	0.01	0.00	0.00	0.00	4.00
		ME4	0.36	0.08	0.06	0.02	0.03	1.01	0.58	0.23	0.16	0.20	2.99	0.89	0.46	0.25	0.24	0.37	0.12	0.07	0.06	0.05	
	Surge [m]	ME1	0.00	0.14	0.19	0.19	0.18	0.20	0.02	0.01	0.04	0.05	0.51	0.29	0.37	0.38	0.38	0.08	0.04	0.04	0.04	0.04	
		ME4	1.21	0.01	0.07	0.03	0.00	4.55	0.60	0.69	0.58	0.50	0.06	0.39	0.15	0.17	0.18	0.53	0.13	0.08	0.07	0.07	

Figure 7.3: Wave and low frequency relative motions and maximum allowable criteria for dissipation factor variation

Line Tensions

As it presented above there is no big difference in relative motions analyzed under the environmental conditions which are outside the gap resonance. Such that here there are plotted only the results where significant discrepancies between dissipation factor variation has been identified (ME1 and ME4). All the results can be found in the Appendix.

The governing load for the mentioned cases is given by the excitation force from the incoming wave. In both cases the wave period is around the calculated gap resonance. The difference between them is the wave heading (more than 30^o) such that the discrepancy of maximum tension between dissipation factor variation for ME1 is not extreme as for ME4 (head waves). Furthermore it can be seen that the significant wave height for ME1 is half meter higher than for ME4. Even though, for the latter mentioned it can be seen that for $\epsilon = 0$ the maximum tension exceeds the SWL and also MBL. In reality such cases could not occur as there are many sources of dissipation (i.e viscosity, wind drag, current, etc.). For the other environmental conditions analyzed there is no influence at all whether is considered or not the dissipation factor.

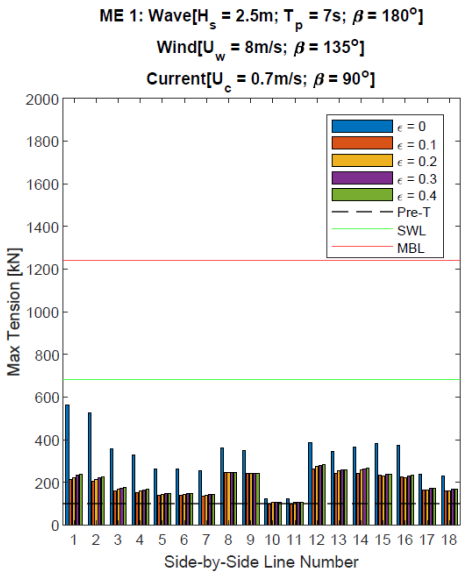

Figure 7.4: Maximum tension for side-by-side lines under ME1 environmental condition [dissipation factor variation]

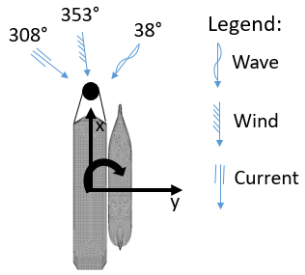

Figure 7.5: Relative angle of attack for wind, wave and current wrt. the bow of the vessels at the equilibrium position under mean environmental loads (ME1)

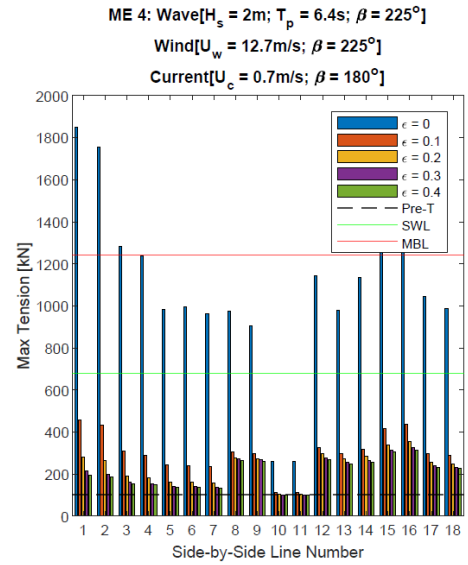

Figure 7.6: Maximum tension for side-by-side lines under ME4 environmental condition [dissipation factor variation]

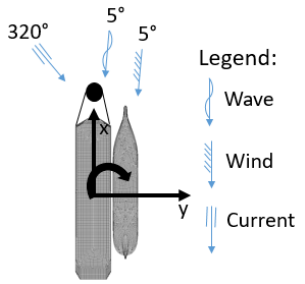

Figure 7.7: Relative angle of attack for wind, wave and current wrt. the bow of the vessels at the equilibrium position under mean environmental loads (ME4)

Fender Reaction Loads

Same impact on fender reaction forces can be expected. The results are presented below. It can be seen that for ME1 the difference is visible only when is not applied dissipation factor in between the two vessels, but the overall contribution is not significant. On the other hand as it is observed from the relative motions and mooring line tension under ME4 environmental conditions, when no dissipation factor is considered, the magnitude of the force reaches extreme values which exceeds the safe working limit.

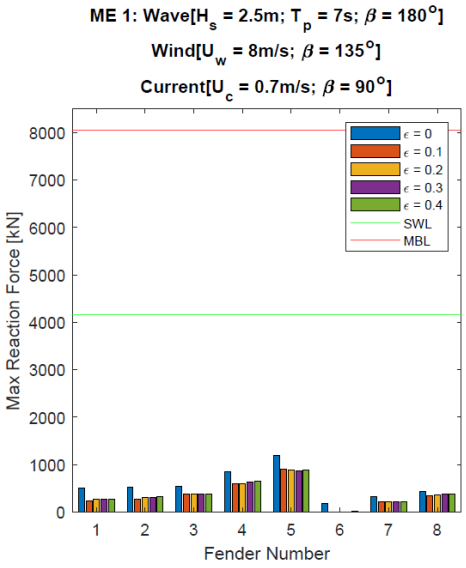

Figure 7.8: Maximum Reaction Force for fenders under ME1 environmental condition [dissipation factor variation]

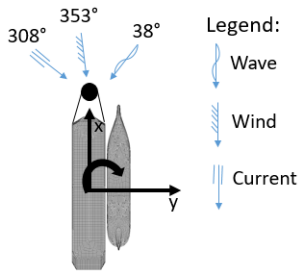

Figure 7.9: Relative angle of attack for wind, wave and current wrt. the bow of the vessels at the equilibrium position under mean environmental loads (ME1)

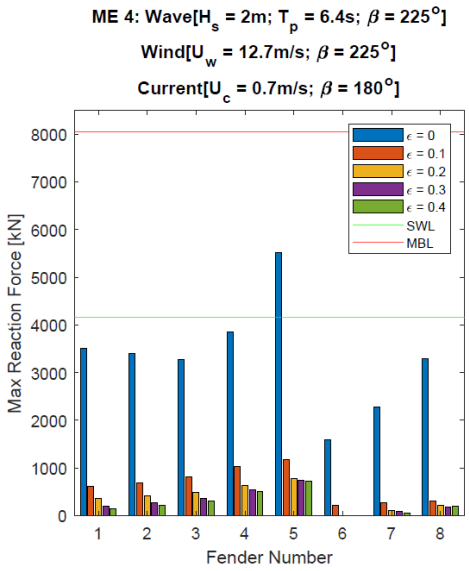

Figure 7.10: Maximum Reaction force for fenders under ME4 environmental condition [dissipation factor variation]

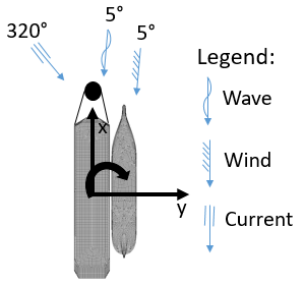

Figure 7.11: Relative angle of attack for wind, wave and current wrt. the bow of the vessels at the equilibrium position under mean environmental loads (ME4)

7.3.2. Gap length

For this comparison the length of the gap where it is applied the dissipation factor has been varied. The hydrodynamic input is based on the following configurations from diffraction database:

Cases	$SbS_{1.1}$, ϵ_3, d_3, LD_1 **vs** $SbS_{1.1}$, ϵ_3, d_3, LD_2 **vs** $SbS_{1.1}$, ϵ_3, d_3, LD_3

Table 7.2: Gap length variation for FLNGmax-LNGCmin configuration

Relative Motions

Relative motions for each case are presented in the table below. As it can be seen there is no major impact on relative motions when the length of the gap is varied. However this becomes important when the moored system is subjected to waves around 7seconds (ME4 and ME1) such that the low frequency relative motions decrease if a bigger gap length is used.

			Absolute values of relative motion at manifold												Criteria [m]
			Mean			Max			Min			Stdv			
	DoF	Env.cond	L160m	L200m	L285m	L160m	L200m	L285m	L160m	L200m	L285m	L160m	L200m	L285m	
wave frequency	Relative distance [m]	ME1	0.00	0.00	0.00	0.10	0.10	0.10	0.11	0.11	0.11	0.03	0.03	0.03	3.00
		ME4	0.00	0.00	0.00	0.07	0.06	0.06	0.06	0.06	0.05	0.02	0.02	0.01	
Low frequency	Sway [m]	ME1	0.02	0.01	0.00	0.16	0.15	0.14	0.02	0.03	0.03	0.00	0.00	0.00	4.00
		ME4	0.06	0.04	0.03	0.23	0.16	0.19	0.46	0.29	0.23	0.07	0.06	0.05	
	Surge [m]	ME1	0.19	0.19	0.20	0.01	0.01	0.01	0.37	0.37	0.38	0.04	0.04	0.04	
		ME4	0.07	0.06	0.02	0.69	0.62	0.47	0.15	0.13	0.14	0.08	0.07	0.06	

Figure 7.12: Wave and low frequency relative motions and maximum allowable criteria for gap length variation

Line Tensions

Line tensions are influenced by the variation of the gap length between the vessels only at the gap resonance.

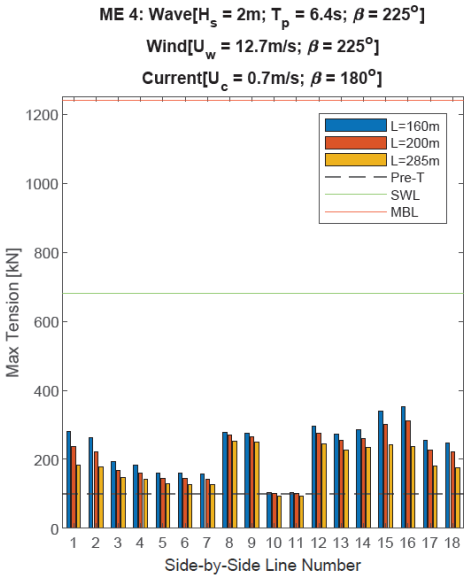

Figure 7.13: Maximum tension for side-by-side lines under ME4 environmental condition [gap length variation]

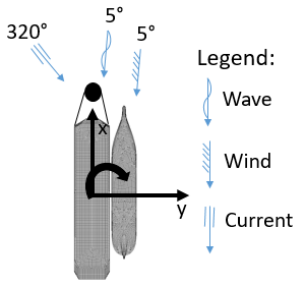

Figure 7.14: Relative angle of attack for wind, wave and current wrt. the bow of the vessels at the equilibrium position under mean environmental loads (ME4)

Fender Reaction Loads

Fenders are very low affected by the variation of the gap length between the vessels. This can be seen in the Figure below.

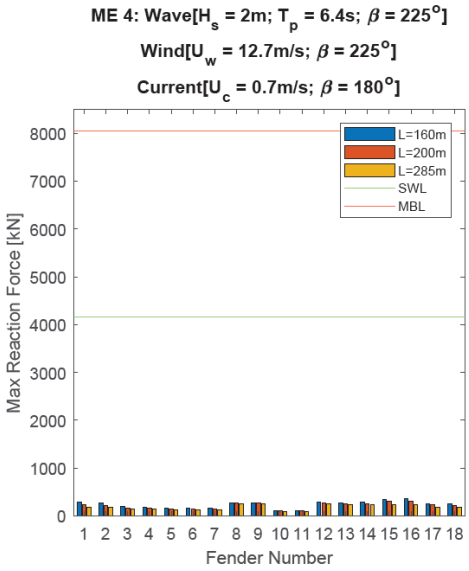

Figure 7.15: Maximum Reaction Force for fenders under ME4 environmental condition [gap length variation]

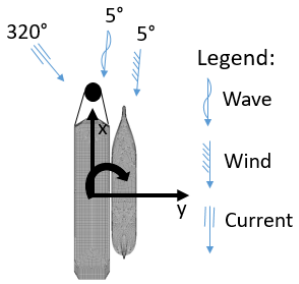

Figure 7.16: Relative angle of attack for wind, wave and current wrt. the bow of the vessels at the equilibrium position under mean environmental loads (ME4)

7.3.3. Separation distance

Relative Motions

This section presents the variation of the distance between the vessels. As it can be seen throughout the tables, only the relative low frequency relative motions are affected and only at the gap resonance.

			Absolute values of relative motion at manifold																Criteria [m]
			Mean				Max				Min				Stdv				
	DoF	Env.cond	d1=3m	d2=3.5m	d3=4m	d4=4.5m	d1=3m	d2=3.5m	d3=4m	d4=4.5m	d1=3m	d2=3.5m	d3=4m	d4=4.5m	d1=3m	d2=3.5m	d3=4m	d4=4.5m	
wave frequency	Relative distance [m]	ME1	0.00	0.00	0.00	0.00	0.10	0.10	0.10	0.11	0.12	0.12	0.11	0.11	0.03	0.03	0.03	0.03	3.00
		ME4	0.00	0.00	0.00	0.00	0.07	0.07	0.07	0.07	0.07	0.06	0.06	0.07	0.02	0.02	0.02	0.02	
Low frequency	Sway [m]	ME1	0.02	0.00	0.02	0.02	0.13	0.15	0.16	0.15	0.04	0.03	0.02	0.02	0.01	0.01	0.00	0.00	4.00
		ME4	0.02	0.06	0.06	0.05	0.44	0.30	0.23	0.18	0.87	0.66	0.46	0.32	0.09	0.08	0.07	0.06	
	Surge [m]	ME1	0.20	0.20	0.19	0.19	0.02	0.00	0.01	0.01	0.36	0.34	0.37	0.38	0.04	0.04	0.04	0.04	
		ME4	0.01	0.06	0.07	0.07	0.79	0.74	0.69	0.64	0.25	0.19	0.15	0.14	0.10	0.09	0.08	0.07	

Figure 7.17: Wave and low frequency relative motions and maximum allowable criteria for separation distance variation

Line Tensions

Tension of the line increases as the distance between the vessels decreases. Here it is presented a variation of separation distance between 3m and 4.5m with a step of 0.5m. As it is expected, the biggest impact on line tensions is the case of 3m. However, this distance is not reliable as the diameter of the fender is 4.5m. Thus a minimum distance that can be considered is 4m in diffraction analysis such that to account for the effect of the initial pretension in lines.

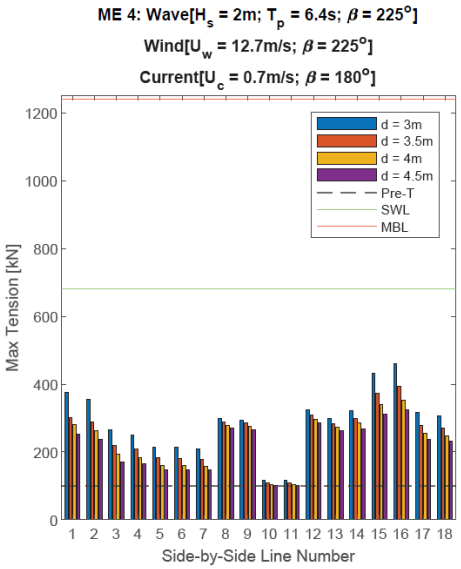

Figure 7.18: Maximum tension for side-by-side lines under ME4 environmental condition [separation distance variation]

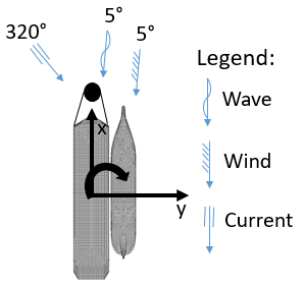

Figure 7.19: Relative angle of attack for wind, wave and current wrt. the bow of the vessels at the equilibrium position under mean environmental loads (ME4)

Fender Reaction Loads

Due to the fact the tension in lines is higher for a separation distance of 3m, this means that the forces in the mooring system are higher which means higher oscillations of the vessels. This is reflected on the fender's reaction forces also. The results are presented in the figure below.

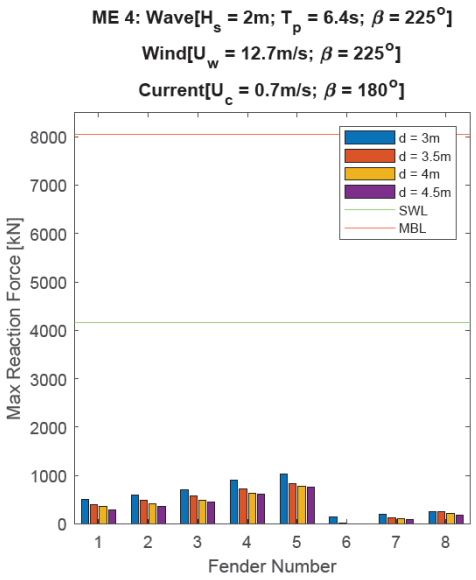

Figure 7.20: Maximum Reaction Force for fenders under ME4 environmental condition [separation distance variation]

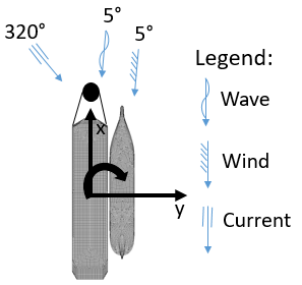

Figure 7.21: Relative angle of attack for wind, wave and current wrt. the bow of the vessels at the equilibrium position under mean environmental loads (ME4)

7.3.4. Summary and recommendations

The main conclusion of this section is that the variation of gap parameters either dimensions (length and separation distance) either dissipation factor which is applied on the water surface to suppress the wave elevation, are important only when the moored system is excited by an incoming wave with a natural period equal or in the same range with the resonant frequency of the gap. Another aspect is the incidence angle of the incoming wave such that if it is approaching against bow, the effects are more predominant. This has been shown as well on the Chapter 4.

Furthermore the wave frequency relative motions are not dependent on those factors, except of heave which is dependent on the wave elevation, but the overall magnitude can be considered small. In general, considering no dissipation factor for diffraction calculations is not reliable and thus is not applicable for designing the mooring systems. On the other hand for a range between 0.2-0.4 brings similar results for all environments considered. The maximum allowable criteria is not exceeded for none of the cases whether is considered or not the dissipation factor.

Regarding the physical dimensions of the gap between the vessels are more important but does not bring major difference in results. Overall, the most appropriate configuration for more conservative results can be as follows: a dissipation factor of 0.2, separation distance of 4 meters to account for the effect of line pretension and a gap length equal to the length where the width between vessels is constant. However, if the site conditions are governed by the long waves (i.e above 12seconds) then these parameters are no longer important, having no impact on relative motions or line tensions.

This specific mooring configuration is governed by long waves as it can be seen in the relative motions tables and thus higher tensions in mooring lines are expected.

7.4. Mooring line forces and optimization for each side-by-side configuration

This section presents the results of time domain simulations for both mooring configurations FLNG-LNGC and respectively FLNG-LPGC for initial mooring arrangement and for optimized configuration. Optimization is done with respect to the quick release hook location (on board of FLNG). The new location of quick release hook is lowered down such that the relative vertical distance between quick release hook (FLNG) and fairlead (carrier) to be zero thus also the vertical angle with horizontal plane becomes zero. This helps to maximize the holding capacity of the mooring lines.

In **??** and **??** are presented the initial relative distances between quick release hook and fairlead for each line. This gives an impression on the required distance to lower down the quick release hooks on board of FLNG. It can be seen that the difference increase when carriers are fully loaded, as the freeboard decreases. In particular for FLNG-LPGC is quite significant, such that the connection points of the lines from the forward part are approximately 10 meters elevation apart from each other. Therefore extremely high loads are expected for this configuration. Optimization should bring significant reduction in line tension. Negative values of the relative vertical distance means that the fairlead is located above the quick release hook location.

7.4.1. FLNG-LNGC

Relative Motions

Relative motions are not affected by the optimization of mooring lines. This can be observed also in the tables below. This configuration is governed by wave periods above 10 seconds, as it can be seen in Figure 7.2. In particular for carrier in ballast condition the governing sea-states are ME2 and squalls conditions where the wave period is close to roll period of the vessel. On the other hand when the carrier is fully loaded, the governing case is ME3 which has the wave period close to the roll of FLNG. In terms of low frequency relative motions, the squall conditions are governing due to the rapid changes of the wind magnitude and direction which ultimately exceeds the maximum allowable criteria.

			Absolute values of relative motion at manifold								Criteria [m]
			Mean		Max		Min		Stdv		
	DoF	Env.cond	FLNGmax-LNGCmin	FLNGmin-LNGCmax	FLNGmax-LNGCmin	FLNGmin-LNGCmax	FLNGmax-LNGCmin	FLNGmin-LNGCmax	FLNGmax-LNGCmin	FLNGmin-LNGCmax	
wave frequency	Relative distance [m]	ME1	0.00	0.00	0.10	0.10	0.11	0.10	0.03	0.03	3.00
		ME2	0.00	0.00	0.92	0.70	1.51	0.62	0.21	0.11	
		ME3	0.00	0.00	0.42	1.18	0.45	1.54	0.13	0.35	
		ME4	0.00	0.00	0.07	0.06	0.06	0.05	0.02	0.01	
		ME5	0.00	0.00	0.35	0.42	0.56	0.32	0.07	0.07	
		Squall1	0.00	0.00	0.23	0.23	0.97	0.40	0.05	0.05	
		Squall2	0.00	0.00	0.43	0.36	1.46	0.25	0.06	0.05	
Low frequency	Sway [m]	ME1	0.02	0.15	0.16	0.03	0.02	0.28	0.00	0.00	4.00
		ME2	0.02	0.01	0.06	0.02	0.05	0.01	0.00	0.00	
		ME3	0.03	0.00	0.00	0.03	0.06	0.01	0.00	0.00	
		ME4	0.06	0.10	0.23	0.33	0.46	0.03	0.07	0.05	
		ME5	0.01	0.03	0.04	0.06	0.05	0.06	0.00	0.00	
		Squall1	2.56	2.56	5.90	5.69	0.02	0.02	1.77	1.76	
		Squall2	2.27	2.27	6.65	6.47	0.43	0.43	1.55	1.55	
	Surge [m]	ME1	0.19	0.02	0.01	0.22	0.37	0.09	0.04	0.04	
		ME2	0.01	0.00	0.10	0.09	0.15	0.19	0.02	0.02	
		ME3	0.02	0.05	0.08	0.00	0.06	0.01	0.01	0.01	
		ME4	0.07	0.18	0.69	0.80	0.15	0.08	0.08	0.07	
		ME5	0.03	0.01	0.16	0.12	0.10	0.12	0.04	0.04	
		Squall1	3.17	3.15	1.92	1.53	4.95	4.90	1.98	2.03	
		Squall2	4.47	4.35	5.21	4.14	6.77	6.68	1.25	1.43	

Figure 7.22: Wave and low frequency relative motions and maximum allowable criteria for FLNG-LNGC configuration

Line Tensions

This section presents the line tensions for the governing cases of the moored system. Throughout the figures it can be observed that the optimization does not bring significant improvement such that initial location can be considered as a good option by default. Exception makes ME3 and Squall2 where multiple lines from forward part exceeds the SWL and the new location diminish the tension but still not sufficient for line 15 and 16 to drop below SWL. On the other hand for Squall1 and ME2 optimization gives tensions slightly higher for Line 15 and 16. A first recommendation is to determine the most probable maximum for at least 20 realizations. From statistical point of view the results are more reliable. In case if the tensions are still higher than SWL, it needs to reconsider the mooring line material. Furthermore in case if happens to have tensions higher for optimized case than for initial design, it needs to be considered another calculation tool for further investigations.

The least loaded lines are forward spring lines (Line 10 and Line 11) while the most loaded are the forward breast lines. This is caused by a steep vertical angle (α) compare to the other lines (Figure **??**).

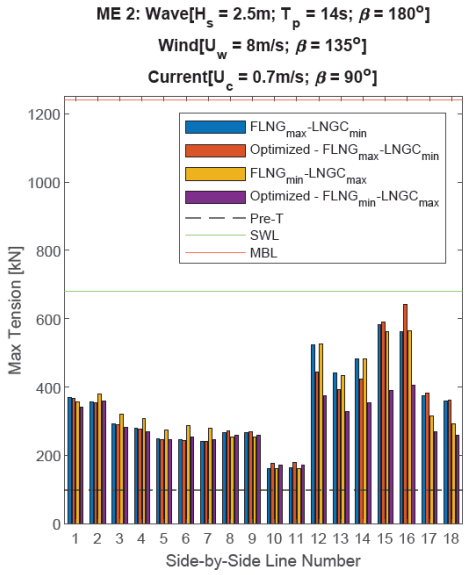

Figure 7.23: Maximum tension for side-by-side lines under ME2 environmental condition [FLNG-LNGC configuration]

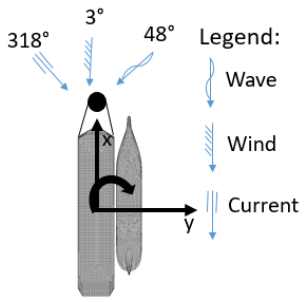

Figure 7.24: Relative angle of attack for wind, wave and current wrt. the bow of the vessels at the equilibrium position under mean environmental loads (ME2)

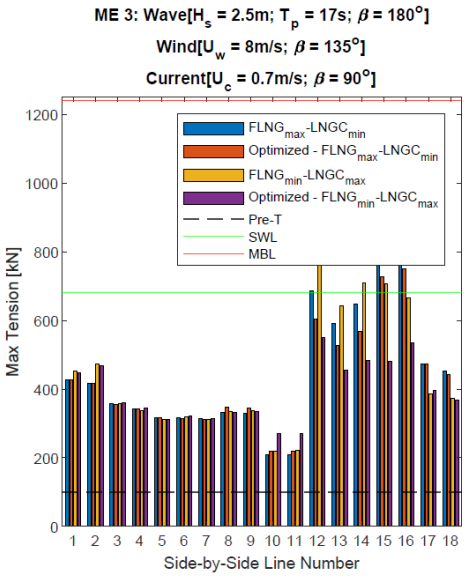

Figure 7.25: Maximum tension for side-by-side lines under ME3 environmental condition [FLNG-LNGC configuration]

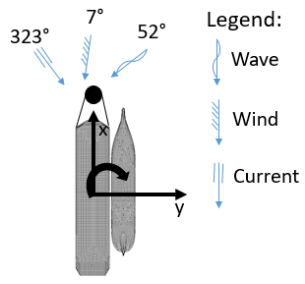

Figure 7.26: Relative angle of attack for wind, wave and current wrt. the bow of the vessels at the equilibrium position under mean environmental loads (ME3)

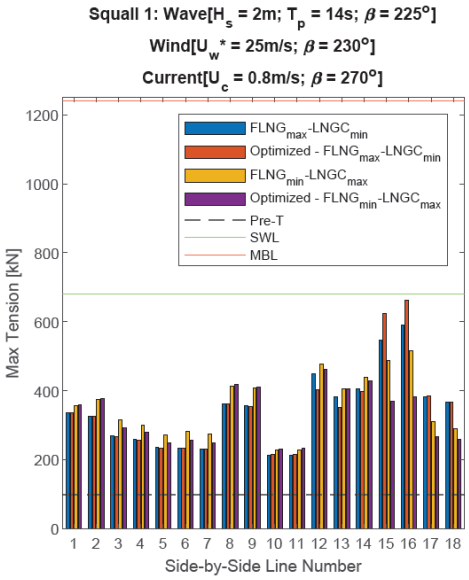

Figure 7.27: Maximum tension for side-by-side lines under Squall1 environmental condition [FLNG-LNGC configuration]

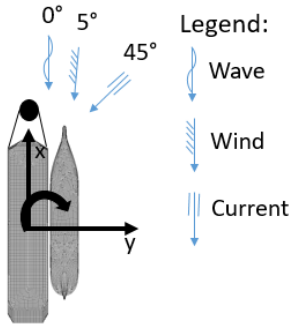

Figure 7.28: Relative angle of attack for wind, wave and current wrt. the bow of the vessels at the equilibrium position under mean environmental loads (Squall1)

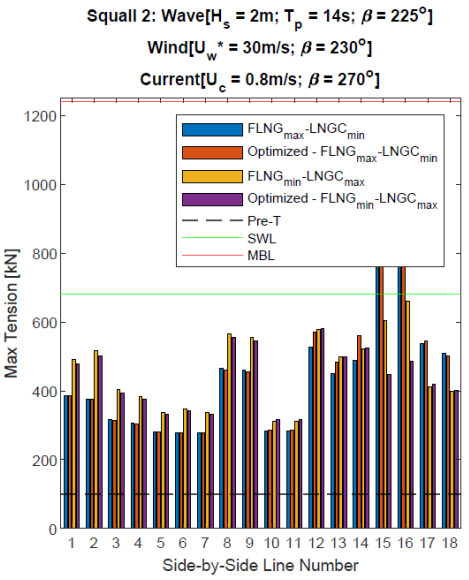

Figure 7.29: Maximum tension for side-by-side lines under Squall2 environmental condition [FLNG-LNGC configuration]

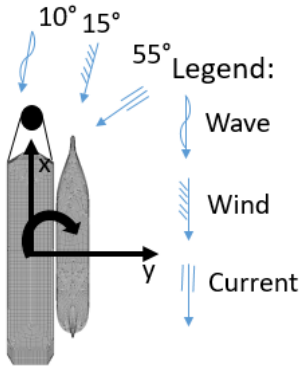

Figure 7.30: Relative angle of attack for wind, wave and current wrt. the bow of the vessels at the equilibrium position under mean environmental loads (Squall2)

Fender Reaction Loads

Regarding fenders, the most loaded are the middle ones (Fender4 and Fender5) as it is expected. Below it is presented the results for Squall2 where the highest line loads are recorded. No extreme are found throughout the results, so fenders are way below the SWL. Regarding the optimization this not bring any influence into fender's loads as they can be scaled with the vessels weight which does not change.

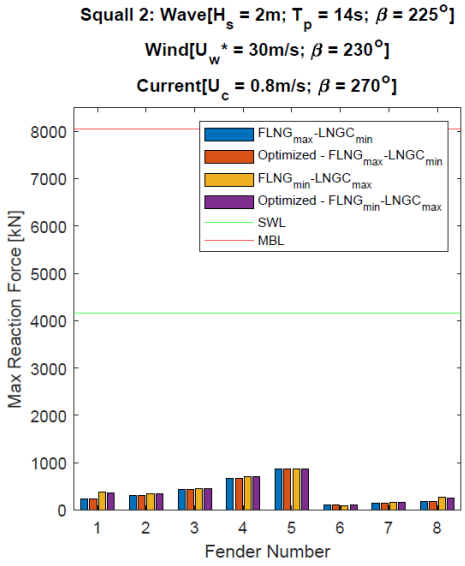

Figure 7.31: Maximum Reaction Force for fenders under Squall2 environmental condition [FLNG-LNGC configuration]

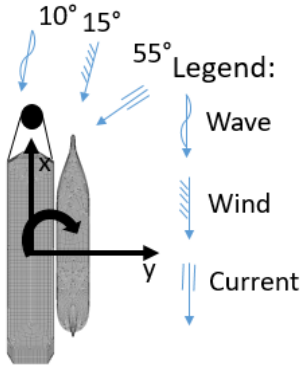

Figure 7.32: Relative angle of attack for wind, wave and current wrt. the bow of the vessels at the equilibrium position under mean environmental loads (Squall2)

7.4.2. FLNG-LPGC

Relative Motions

Relative motions for FLNG-LPGC are governed by wave frequency loads, in particular with significant heave response for the majority of the sea-states considered. This is caused by the fact that the heave natural period of the carrier is close to the incoming wave period. Regarding the low frequency motions, these are governed by the squall phenomena due to the rapid changes in the wind direction. In particular the criteria is not satisfied for squall conditions where extreme relative motions are registered. For the mentioned cases it is expected to occur high tension in lines.

			Absolute values of relative motion at manifold								Criteria [m]
			Mean		Max		Min		Stdv		
	DoF	Env.cond	FLNGmax-LPGCmin	FLNGmin-LPGCmax	FLNGmax-LPGCmin	FLNGmin-LPGCmax	FLNGmax-LPGCmin	FLNGmin-LPGCmax	FLNGmax-LPGCmin	FLNGmin-LPGCmax	
wave frequency	Relative distance [m]	ME1	0.00	0.00	0.36	0.48	0.47	0.45	0.11	0.13	3.00
		ME2	0.00	0.00	1.21	1.37	1.51	1.55	0.34	0.36	
		ME3	0.00	0.00	0.53	0.70	0.83	0.95	0.20	0.22	
		ME4	0.00	0.00	0.21	0.23	0.21	0.24	0.05	0.06	
		ME5	0.00	0.00	1.02	1.04	1.01	1.03	0.30	0.29	
		Squall1	0.00	0.00	0.81	0.76	1.02	0.98	0.17	0.18	
		Squall2	0.00	0.00	0.65	0.86	0.95	1.05	0.13	0.15	
Low frequency	Sway [m]	ME1	0.18	0.43	0.22	0.09	0.00	0.52	0.01	0.01	4.00
		ME2	0.00	0.14	0.02	0.07	0.01	0.05	0.02	0.01	
		ME3	0.01	0.08	0.01	0.04	0.01	0.03	0.01	0.01	
		ME4	0.01	0.52	0.12	0.26	0.46	0.25	0.02	0.03	
		ME5	0.01	0.10	0.08	0.05	0.05	0.06	0.00	0.00	
		Squall1	2.07	4.66	4.84	2.76	0.39	1.89	1.32	1.42	
		Squall2	1.12	4.27	4.59	3.34	0.49	0.93	0.99	1.10	
	Surge [m]	ME1	0.27	0.50	0.06	0.25	0.53	0.23	0.05	0.05	
		ME2	0.02	0.41	0.12	0.20	0.16	0.11	0.02	0.03	
		ME3	0.03	0.15	0.12	0.07	0.05	0.08	0.01	0.01	
		ME4	0.03	0.94	0.41	0.47	0.15	0.11	0.03	0.04	
		ME5	0.01	0.18	0.08	0.09	0.03	0.08	0.02	0.03	
		Squall1	3.62	1.52	2.74	0.77	6.02	2.29	2.12	2.18	
		Squall2	5.01	3.20	5.19	0.27	8.15	2.93	1.01	1.11	

Figure 7.33: Wave and low frequency relative motions and maximum allowable criteria for FLNG-LPGC configuration

Line Tensions

In this section there are presented the governing cases for FLNG-LPGC configuration. It can be seen throughout the results that the line tensions are a lot higher than SWL, in particular for some cases (ME2 ME3), exceeds also the MBL. Optimization brings a significant tension reduction especially for the most tensioned lines (forward lines) but not enough to drop below SWL. Overall the worse case scenario is under Squall2 where majority of the lines exceeds SWL. It is obvious that mooring line material has to be changed.

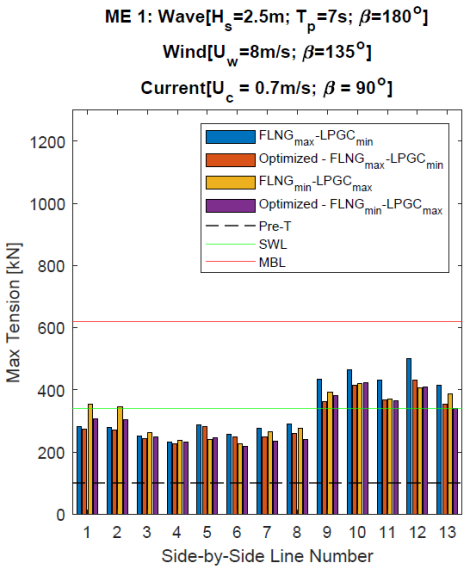

Figure 7.34: Maximum tension for side-by-side lines under ME1 environmental condition [FLNG-LPGC configuration]

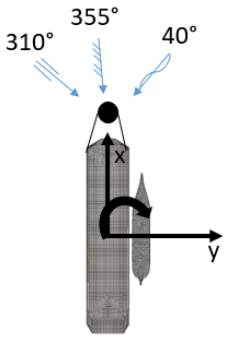

Figure 7.35: Relative angle of attack for wind, wave and current wrt. the bow of the vessels at the equilibrium position under mean environmental loads (ME1)

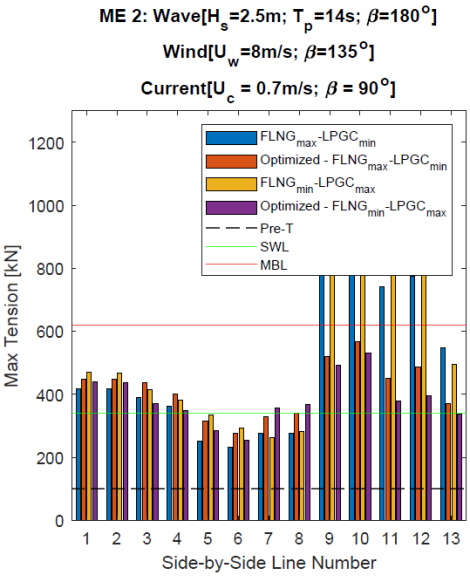

Figure 7.36: Maximum tension for side-by-side lines under ME2 environmental condition [FLNG-LPGC configuration]

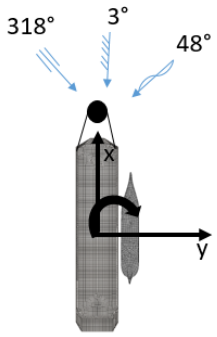

Figure 7.37: Relative angle of attack for wind, wave and current wrt. the bow of the vessels at the equilibrium position under mean environmental loads (ME2)

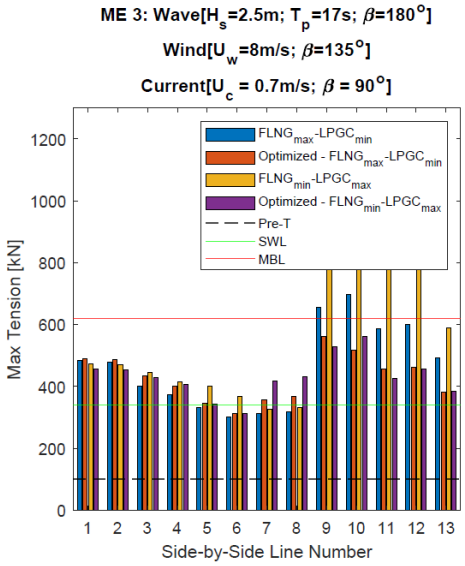

Figure 7.38: Maximum tension for side-by-side lines under ME3 environmental condition [FLNG-LPGC configuration]

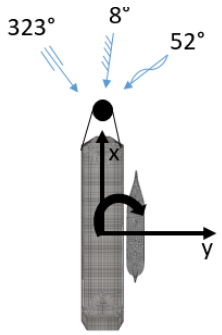

Figure 7.39: Relative angle of attack for wind, wave and current wrt. the bow of the vessels at the equilibrium position under mean environmental loads (ME3)

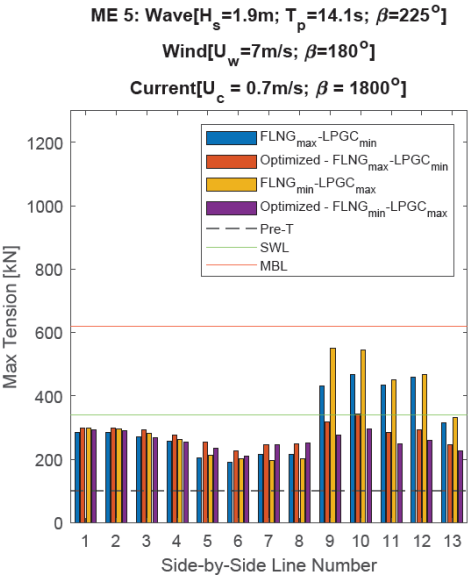

Figure 7.40: Maximum tension for side-by-side lines under ME5 environmental condition [FLNG-LPGC configuration]

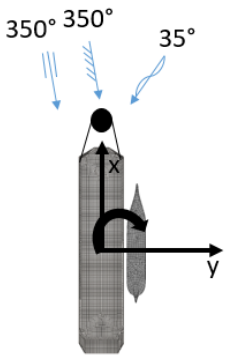

Figure 7.41: Relative angle of attack for wind, wave and current wrt. the bow of the vessels at the equilibrium position under mean environmental loads (ME5)

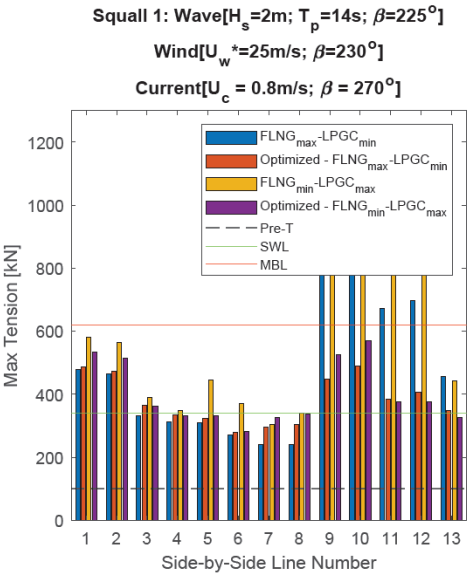

Figure 7.42: Maximum tension for side-by-side lines under Squall1 environmental condition [FLNG-LPGC configuration]

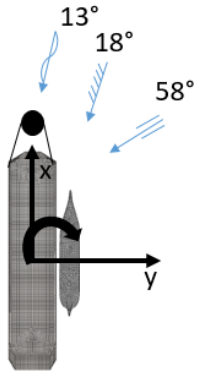

Figure 7.43: Relative angle of attack for wind, wave and current wrt. the bow of the vessels at the equilibrium position under mean environmental loads (Squall1)

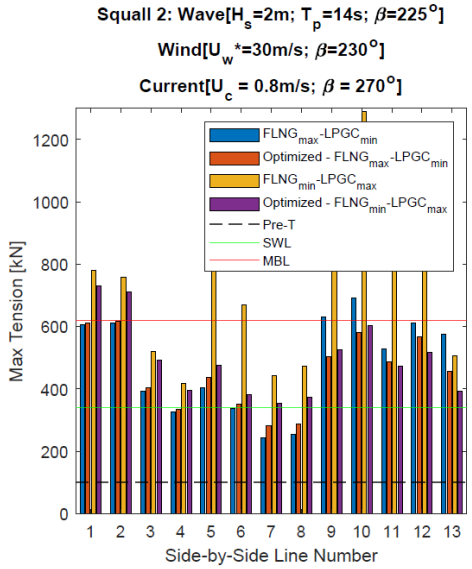

Figure 7.44: Maximum tension for side-by-side lines under Squall2 environmental condition [FLNG-LPGC configuration]

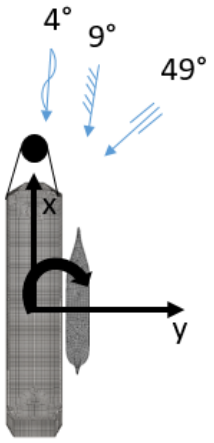

Figure 7.45: Relative angle of attack for wind, wave and current wrt. the bow of the vessels at the equilibrium position under mean environmental loads (Squall2)

Fender Reaction Loads

Fenders are loaded almost the same for each sea-state. In general the most affected are fenders placed on the middle. Overall the impact on fenders is below 1000 kN which means that is way below SWL.

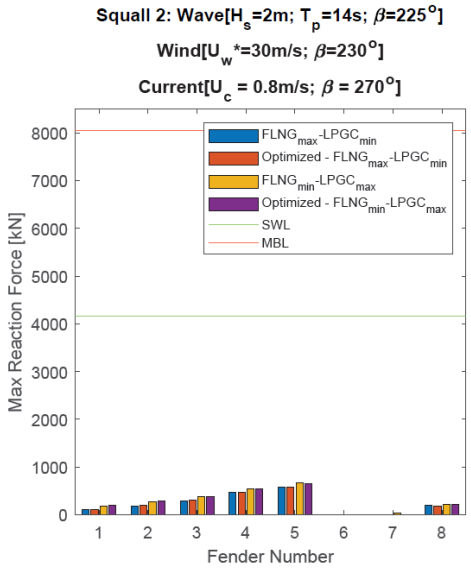

Figure 7.46: Maximum Reaction Force for fenders under Squall2 environmental condition [FLNG-LPGC configuration]

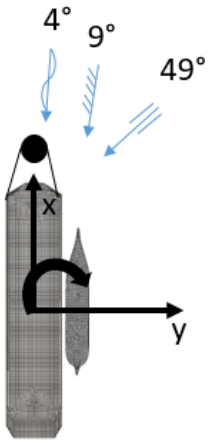

Figure 7.47: Relative angle of attack for wind, wave and current wrt. the bow of the vessels at the equilibrium position under mean environmental loads (Squall2)

7.4.3. Summary and recommendations

The main conclusion from this section is that the squall phenomena is the governing sea-state for both configurations. For FLNG-LNGC there are only two cases(ME3 and Squall2) where the line tension exceeds the SWL, while for FLNG-LPGC this happens for the majority of the analyzed cases. However the results shown throughout the graphs consists in only one peak during 3hours simulation. In general, for more reliable results value of the maximum line tension with the highest probability of occurring in 3hours sea-state needs to be considered. Thus a minimum of 20 wave realizations as recommended by API has to be taken into account. If by doing this, the line tensions are still above SWL it means that the mooring lines needs to be redesigned.

Another fact observed is that for certain cases, the optimized mooring line had a higher tension. This should be checked as well by doing more wave realization. In case if it is still the case, then another tool needs to be used in order to validate the results.

7.4.4. Newman current-wave interaction vs QTFC

Ariane7 is capable to determine the low-frequency loads using different formulations. It is known that these loads are the main source of excitation for the moored systems. It is important to asses the mooring line tension accurately. In particular, for side-by-side applications, Newman current-wave interaction and full QTFC formulation are used. The main advantage of Newman's formulation is due to the fact that only requires the diagonal terms of the QTF (Quadratic Transfer Function) matrix. Therefore less computational effort needed as the time series reconstruction is done using only single summation. Most of the time this approximation gives satisfactory results for the moored systems in deep water, while towards shallow water conditions can highly underestimates the drift loads. The side-by-side systems analyzed here (FLNG-LNGC and FLNG-LPGC) are located on site with approximately 50m water depth which represents intermediate water regime. In this case, the full QTF matrix may gives better estimates [5]. One big disadvantages of this method is that requires more computational time as the reconstruction is done by double summation.

Therefore here it presented the difference between Newman wave-current formulation and QTFC formulation. This is highlighted using comparison between relative motions and line tensions for the moored system between FLNGmax and LNGCmin.

It can be seen that the wave frequency relative motions are not affected by the change in drift type formulation, while low frequency motions are influenced. Two conclusions can be drawn such as:

- if the incoming wave has the same resonant frequency as the wave elevation between the vessels, the interaction wave-current plays an important role in estimating the second order drift forces; thus Newman-wave-current (heading correction) formulation gives better estimates

- outside the gap resonance frequency range, QTFC(complete matrix) formulation gives slightly higher relative motions thus also line and fender tensions;

			Absolute values of relative motion at manifold								Criteria [m]
			Mean		Max		Min		Stdv		
	DoF	Env.cond	cur/wave	QTFC	cur/wave	QTFC	cur/wave	QTFC	cur/wave	QTFC	
wave frequency	Relative distance [m]	ME1	0.00	0.00	0.10	0.10	0.11	0.09	0.10	0.12	3.00
		ME2	0.00	0.00	0.92	0.88	1.51	1.40	0.13	0.13	
		ME3	0.00	0.00	0.42	0.32	0.45	0.53	0.13	0.12	
		ME4	0.00	0.00	0.07	0.07	0.06	0.06	0.03	0.09	
		ME5	0.00	0.00	0.35	0.39	0.56	0.48	0.11	0.12	
		Squall1	0.00	0.00	0.23	0.23	0.97	0.97	0.05	0.05	
		Squall2	0.00	0.00	0.43	0.41	1.46	1.63	0.06	0.03	
Low frequency	Sway [m]	ME1	0.02	0.01	0.16	0.04	0.02	0.04	0.00	0.01	4.00
		ME2	0.02	0.06	0.06	0.05	0.05	0.22	0.00	0.00	
		ME3	0.03	0.03	0.00	0.08	0.06	0.33	0.00	0.01	
		ME4	0.06	0.02	0.23	0.08	0.46	0.09	0.07	0.02	
		ME5	0.01	0.00	0.04	0.01	0.05	0.02	0.00	0.00	
		Squall1	2.56	2.56	5.90	5.90	0.02	0.02	1.77	1.73	
		Squall2	2.27	2.06	6.65	6.47	0.43	0.48	1.55	1.47	
	Surge [m]	ME1	0.19	0.03	0.01	0.21	0.37	0.15	0.04	0.04	
		ME2	0.01	0.01	0.10	0.17	0.15	0.08	0.02	0.02	
		ME3	0.02	0.01	0.08	0.07	0.06	0.14	0.01	0.02	
		ME4	0.07	0.02	0.69	0.27	0.15	0.06	0.08	0.03	
		ME5	0.03	0.03	0.16	0.15	0.10	0.11	0.04	0.03	
		Squall1	3.17	3.17	1.92	1.92	4.95	4.95	1.98	2.01	
		Squall2	4.47	4.84	5.21	5.95	6.77	7.29	1.25	0.89	

Figure 7.48: Wave and low frequency relative motions and maximum allowable criteria[FLNGmax-LNGCmin configuration]

For exemplification, time trace of low frequency tension of line 7 for ME3 and ME4 has been plotted. This emphasis the statement mentioned above. Such that the QTFC formulation gives better estimates than Newman-wave-current formulation for low frequency motions outside the gap resonance period. In order to cover all the frequency ranges, a QTFC wave-current formulation can be suitable for all the analyzed cases. This formulation is available within Ariane8 version.

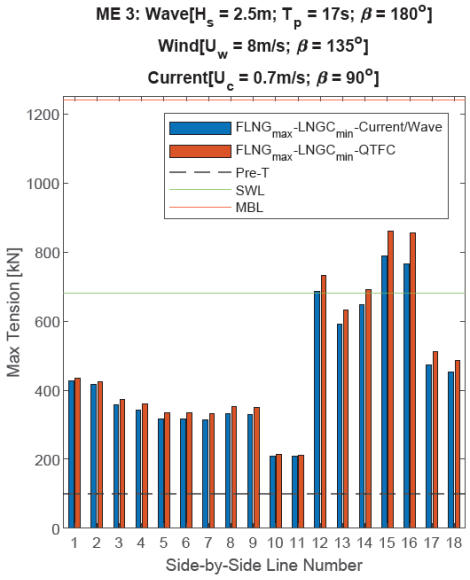

Figure 7.49: Maximum tension for side-by-side lines under ME3 environmental condition [FLNGmax-LNGCmin configuration]

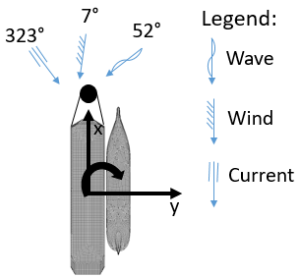

Figure 7.50: Relative angle of attack for wind, wave and current wrt. the bow of the vessels at the equilibrium position under mean environmental loads (ME3)

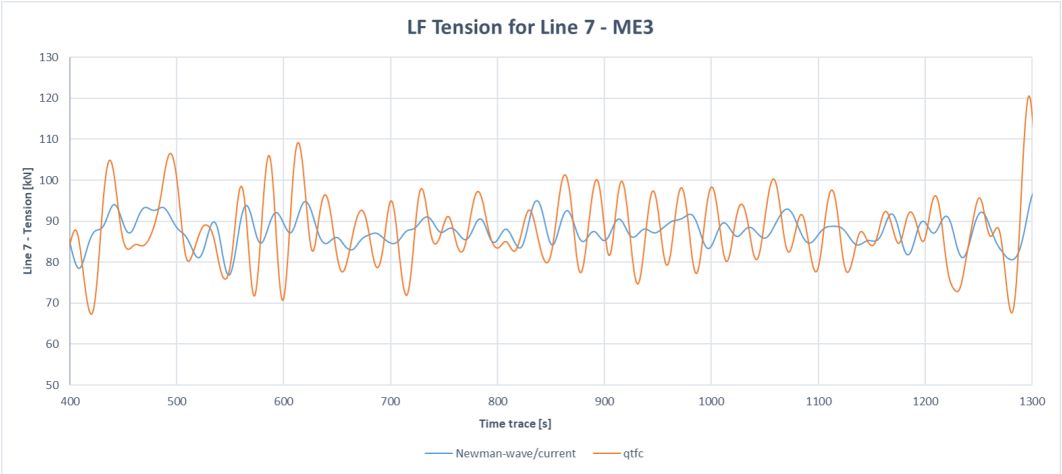

Figure 7.51: Low frequency component for Line 7 under ME3 (T_p=7s) environmental conditions

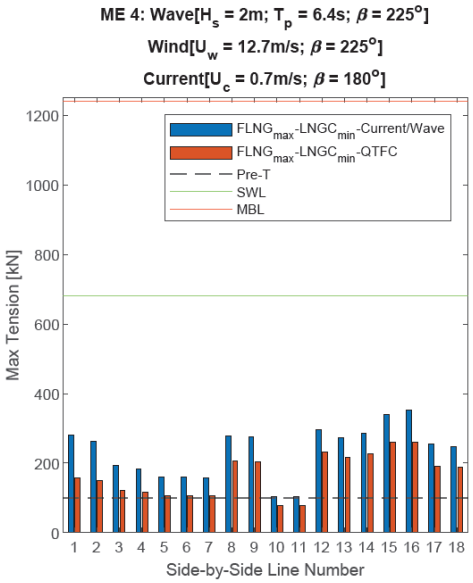

Figure 7.52: Maximum tension for side-by-side lines under ME4 environmental condition [FLNGmax-LNGCmin configuration]

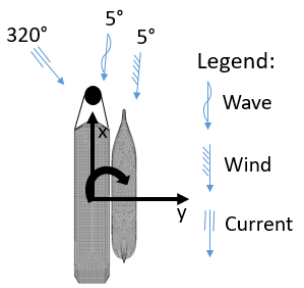

Figure 7.53: Relative angle of attack for wind, wave and current wrt. the bow of the vessels at the equilibrium position under mean environmental loads (ME4)

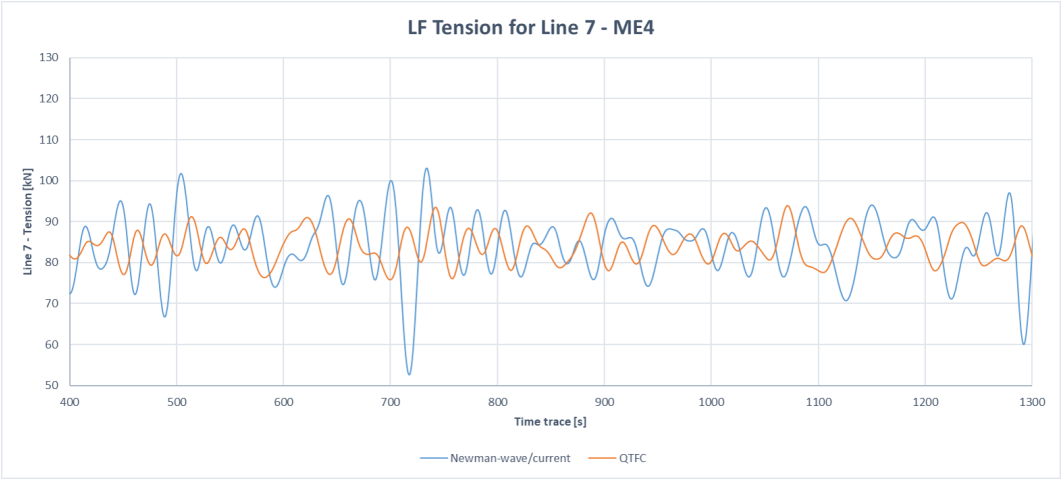

Figure 7.54: Low frequency component for Line 7 under ME4 (T_p=6.4s) environmental conditions

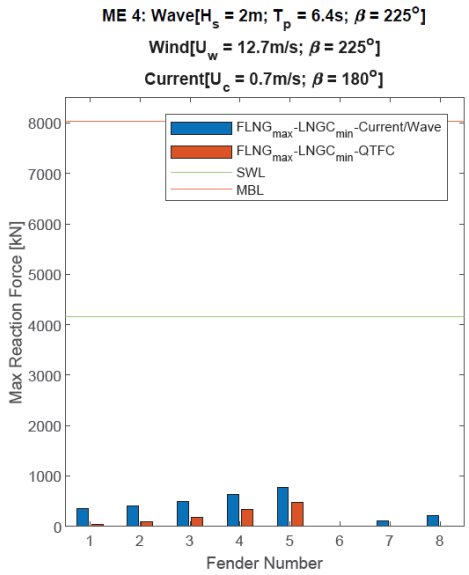

Figure 7.55: Maximum Reaction Force for fenders under ME4 environmental condition

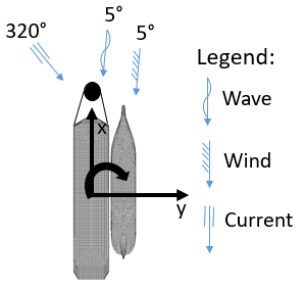

Figure 7.56: Relative angle of attack for wind, wave and current wrt. the bow of the vessels at the equilibrium position under mean environmental loads (ME4)

7.5. Comparison between Ariane8 and Ariane7 using two different integration methods

With the available version of Ariane8 in SBM office, the simulations with longer wave periods than 10 seconds did not converge. Therefore only 2 out of 7 environmental cases successfully succeed. At this moment, version8 of Ariane is important to be validated, as this do not provide enough confidence due to multiple errors. However a conclusion can be made out of the available results. Beside the convergence problem, this version encounter post-processing errors, such that it was needed to retrieve the data manually. The results are presented in terms of relative motions and line tensions.

Based on Ariane7 calculation method (de-coupled schema), the wave and low frequency response due to different time scale do not affect each other. This can be noticed from the table below. Furthermore, the time-average of the wave-frequency response which is oscillating around the loading arm position is zero. On the other hand Ariane8 (coupled schema) is solving simultaneously both responses taking into account the memory effect of the free surface. This can be noticed on the wave frequency mean response which is no longer zero. The diffracted wave field between the vessels (memory effect) brings significant additional loads into the system (especially for heave and sway) which should not be neglected as Ariane7 assumption does. This become more important when the diffracted and radiated waves have higher magnitudes. As it can be seen in the table of results the impact is higher for ME1 (incoming wave is 40deg. offset from vessel's bow) than for ME4 (incoming wave is 5deg offset from vessel's bow). This can be seen also from line tension perspective. The coupled analysis gives higher results (i.e 50% for ME1) if the diffraction-radiated waves have higher magnitude.

Based on these results it can be concluded that:

- there is an interdependence between low and wave frequency, especially for side-by-side moored vessels, where the resonance of the moored system can be close to the vessel resonant frequencies as presented in Figure 7.2;

- the incidence of the incoming wave is very important such that if the influence of diffracted and radiated waves is small (ie ME4), then the coupled method gives similar results compare to the de-coupled analysis

7.5.1. Relative Motions

			Relative motion at manifold [m]				
	DoF	Env.cond	Mean absolute value		Max absolute value		Criteria [m]
			A7	A8	A7	A8	
wave frequency	Heave	ME1	0.000	0.090	0.097	0.601	1.5
		ME4	0.000	0.265	0.069	0.701	
	Surge	ME1	0.000	0.025	0.035	0.191	2.0
		ME4	0.000	0.283	0.001	0.356	
	Sway	ME1	0.000	0.285	0.001	0.705	1.5
		ME4	0.000	0.237	0.006	0.395	
	Relative distance	ME1	0.000	0.300	0.103	0.946	3.0
		ME4	0.000	0.454	0.069	0.880	

Figure 7.57: Wave frequency relative motions and maximum allowable criteria[FLNGmax-LNGCmin configuration]

	DoF	Env.cond	Relative motion at manifold [m]				Criteria [m]
			Mean absolute value		Max absolute value		
			A7	A8	A7	A8	
Low frequency	Sway	ME1	0.016	0.011	0.144	0.407	4.0
		ME4	0.060	0.164	0.348	0.387	
	Surge	ME1	0.187	0.050	0.193	0.359	
		ME4	0.074	0.043	0.616	0.252	

Figure 7.58: Low frequency relative motions and maximum allowable criteria [FLNGmax-LNGCmin configuration]

7.5.2. Line Tensions

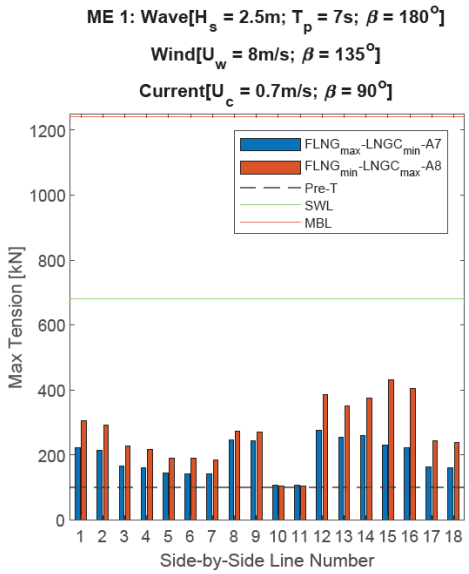

Figure 7.59: Maximum tension for side-by-side lines under ME4 environmental condition

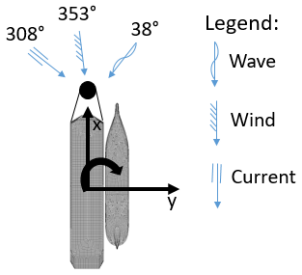

Figure 7.60: Relative angle of attack for wind, wave and current wrt. the bow of the vessels at the equilibrium position under mean environmental loads (ME1)

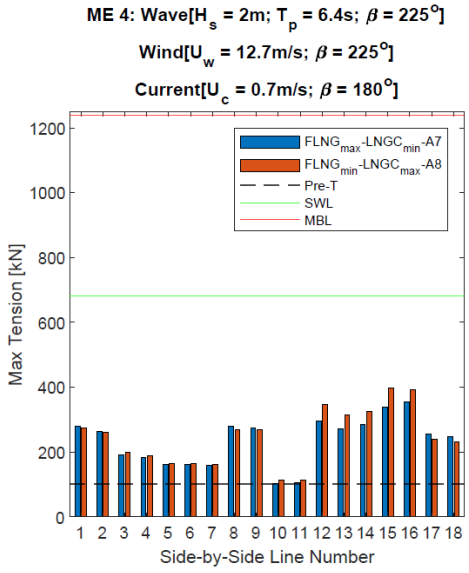

Figure 7.61: Maximum tension for side-by-side lines under ME4 environmental condition

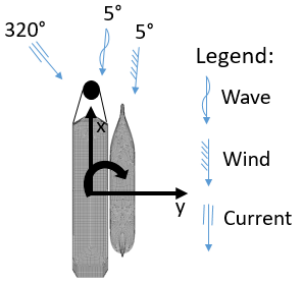

Figure 7.62: Relative angle of attack for wind, wave and current wrt. the bow of the vessels at the equilibrium position under mean environmental loads (ME4)

8

Concluding remarks and recommendations

The diffraction analysis shows that the hydrodynamic interactions effects of the moored systems in side-by-side configuration are complex problems and strongly coupled. A main characteristic of side-by-side system is that the sway added mass become negative at the resonant frequency for both vessels involved. This is generated by the presence of the second ship which acts as a reflecting wall. In general the FLNG is less affected by the presence of the carrier. In particular, interaction effects could be identified only for FLNG's heave. It can be clearly identified that there is a heave-roll coupling between FLNG and carrier. Radiated waves from the rolling carrier are travelling towards FLNG's side which cause a significant decrease in FLNG's heave. Regarding the second order quantities the effect is more visible, affecting all degrees of freedom. However, this depends on the carrier's size. As it is presented, when the FLNG is moored in side-by-side configuration with a smaller vessel (i.e LPGC) the interaction is insignificant compare to the single vessel case. Furthermore there are no shielding effects for FLNG in fully loading condition, while for ballast condition they are visible. This is caused by the increase of the carrier volume (LNGC) and respectively the draft which will tend to act like a rigid wall and shelter the FLNG against the incoming waves. The gap resonance highly affects the drifts forces, in particular yaw and sway under beam waves conditions.

The behaviour of the carrier in side-by-side configuration revealed important aspects. In general sway and roll for single vessel is zero for head and following waves due to the symmetry. However in multi-body, the carrier response is significant. For instance rolling of the LNG is 2deg/m while for LPGC approximately 10deg/m. Thus smaller ships are more sensitive due to interaction effect and thus their seakeeping performances become weaker.

An unexpected event regarding roll motions from bow quartering waves has been noticed. Such that the roll of the carrier is two times higher from the lee-side than weather side. This can be explained that the radiated waves from the FLNG have higher amplitudes which impact the bow of the carrier with a higher force than on the opposite side due to the incoming wave (unit amplitude).

The variation of the FLNG sizes does not have a big impact on the first order loads of the carrier. It is notices a small shifting in the resonance period. The same conclusion regarding the roll of the carrier in bow-quartering waves is drawn. This emphasises the statement made above and shows that no matter the size of the FLNG (larger FLNG = higher sheltered area), the roll of the carrier due to the incoming wave from the exposed side is still smaller compare to the sheltered area. On the other hand the drift forces of the carrier are highly influenced by the presence of a the second vessel and its dimensions (length and displacement). The tendency is to expect higher carrier's drift forces when is moored in side-by-side configuration with larger vessel and especially towards higher frequencies.

The variation of the loading condition in terms of drift force no significant difference neither for FLNG nor for carriers has been found. Even though the change in draft for the carrier is

not negligible and thus some impact could have been expected.

The variation of the gap damping length shows that there is a small impact, but negligible on the first order quantities, while second order are more sensitive and they are affected towards higher frequencies.

Dissipation factor is not influencing at all the first order loads weather is considering or not. On the other hand the second order forces are extremely affected, except of surge which is not dependent on the pumping mode resonance. Furthermore this shows the importance of the wave heading. Such that if there are beam waves extremely huge peaks can be identified for the case without dissipation factor and important differences between the other values used. However due to the diffraction effects, for quartering waves, the difference in force magnitude of using the range of dissipation factors is not significant.

Varying the separation distance between the vessels has no impact on the first order motions. However on the drift loads the effect is visible at the gap resonance mainly. As the distance decrease, the peak frequency is shifted towards higher frequency range.

All in all the parameters which are dependent on dissipation factor are not influencing the first order quantities as the pressure integration is done with respect to the mean water level, while the second order forces become sensitive due to the changes on the fluctuating water level.

Overall, in terms of wave loading, beam waves are the most dangerous and needs to be avoided for this kind of moored systems. However, due to the turret system which has the capability to weather vane, the bow quartering waves can be considered as the governing sea states.

The influence of diffraction database into time domain simulations has been presented. The hydrodynamic parameters which play an important role in diffraction calculations for multi-body configuration such as: dissipation factor and defined area (length and separation distance) between the vessels does bring a contribution only if the considered sea-state is within the natural period range of the gap elevation. Outside this region there is no influence as has been demonstrated on diffraction calculations. In particular for first order loads for which the integration is done with respect to the mean wetted surface of the vessels there is no visible influence. On the other hand considering the second order quantities which are dependent on the fluctuating part of the wetted surface significant influence can be found. This is also reflected into time domain analysis where the motions are determined by the summation of the low frequency and wave frequency at each time step. Furthermore the incidence of the incoming wave is very important. Due to the fact that there is no mechanism to damp the wave elevation in between the vessels (i.e for the case with no dissipation factor) for head waves (i.e ME4) extreme relative motions and line tensions are identified which exceeds the allowable criteria. This is caused mainly due to low frequency component. For incoming waves with an offset of 40deg (i.e ME4) damping mechanism are due to the rolling of the vessels such that a significant reduction of the relative motions and line tensions can be noticed. Overall, in terms of relative motions and line tensions, similar results are found for all the environments considered. However the cases with no dissipation is not considered feasible for the mooring design.

Regarding the mooring line design, the focus has been on the hydrodynamic and mechanical interactions between two vessels using two configurations (FLNG-LNGC, FLNG-LPGC) analysed for two loading conditions. The modal analysis of the moored system is a priority and can be assessed for different positions such that to establish the suitable methodology for second order loads evaluation. With this respect, two methods are presented which are used within Ariane7, respectively Newman-wave-interaction and QTFC formulation. It has been shown that Newman significantly underestimates the low frequency loads which are outside the gap resonance, thus smaller tension in lines. This is caused by the fact that the integration method uses only mean drift component which is proportional to the wave elevation squared. Moreover this approach takes into account the interaction between current speed and instantaneous heading. On the other hand, the complete quadratic transfer (QTFC) formulation provides the integration of the all components not only zero order terms as Newman formulation does. However, does not count for heading changes due to current-wave interaction which can bring major changes in drift loads especially for squall conditions.

The QTFC formulation can be a good alternative, but not within the gap resonance range. However in the new released version (Ariane8) it is implemented the QTFC formulation with the correction for wave-current interaction, such that can be applicable for entire range of wave frequencies used and for any water depth.

The mooring configuration between FLNG and LNGC is governed by long waves (ie. 17s) and squall phenomena. The other configuration FLNG with LPGC is more sensitive, as the seakeeping behavior of the carrier is less favourable. The results show that the current mooring configuration, is not capable to sustain the loads and most of the the line tensions are exceeding the MBL. With this respect, the mooring line optimization is proposed. This is done by leveling the quick release hook with the fairlead on the same z location. This should bring a significant reduction in line tension. In particular for forward lines of the FLNGmin-LPGCmax where the initial relative vertical distance is approximately 10m. In terms of relative motions this action should not have any impact. With the aid of optimization, a significant decrease of tension is visible for the most loaded lines, but still not enough to drop below SWL, in particular for FLNG-LPGC. An unexpected result has been recorded for FLNG-LNGC under squall conditions. Apparently the optimization for the most loaded lines (i.e 15 and 16) shows an increase in load rather than reduction. As a recommendation is important to obtain the statistical results for at least 20 realizations for 3hours simulations. In this way it can be determined whether is only a singular peak with this magnitude throughout the wave realization or whether is a trend. In general, having a vertical angle with horizontal plane zero, should be favourable, thus less tension in lines.

Unified (Ariane8) versus non-unified integration scheme (Ariane7) method results are presented. Due to the convergence problems with the version 8 of Ariane, is not possible to capture the full picture which includes comparison with all the environmental conditions used as in Ariane7. Thus, this might represent a premature conclusion based only on the results of the simulation which successfully succeed. Furthermore, due to the fact that this new version of Ariane8 is still under developing, validation with another tool is vital. The main conclusion of this investigation is that the surface memory effect is more important when the diffracted-radiated wave field has higher magnitudes such that the lines are more tensioned due to the low and wave frequency response of the vessel. The coupled method shows that there is an interdependence between low and wave frequency response in particular for side-by-side vessels. This can be observed on the mean wave frequency response which does not oscillate around zero anymore.

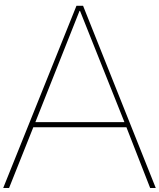

Appendices

B

Time-domain results

B.1. Legends and Environmental conditions

B.1.1. Legend for FLNG-LNGC configuration

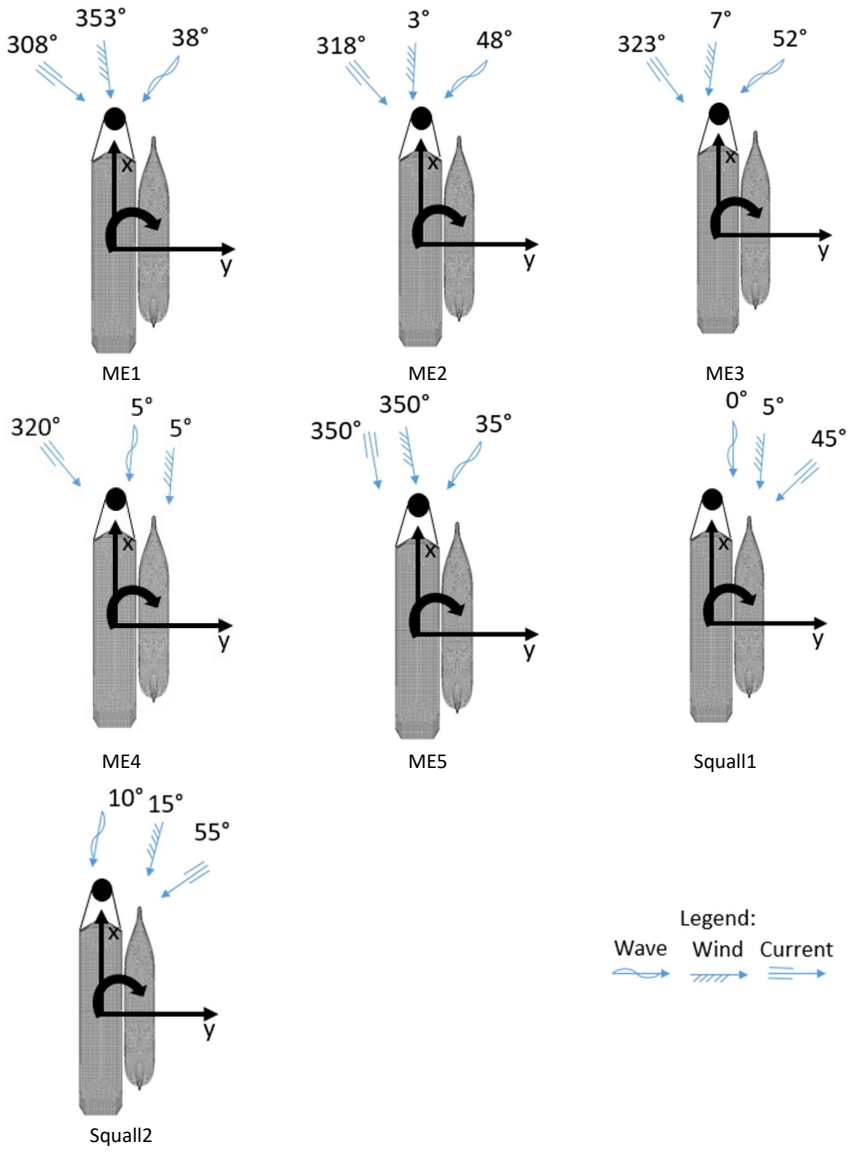

Figure B.1: Relative angle of attack for wind, wave and current of the FLNG-LNGC configuration at static equilibrium position under mean forces for each environmental condition

B.1.2. Legend for FLNG-LPGC configuration

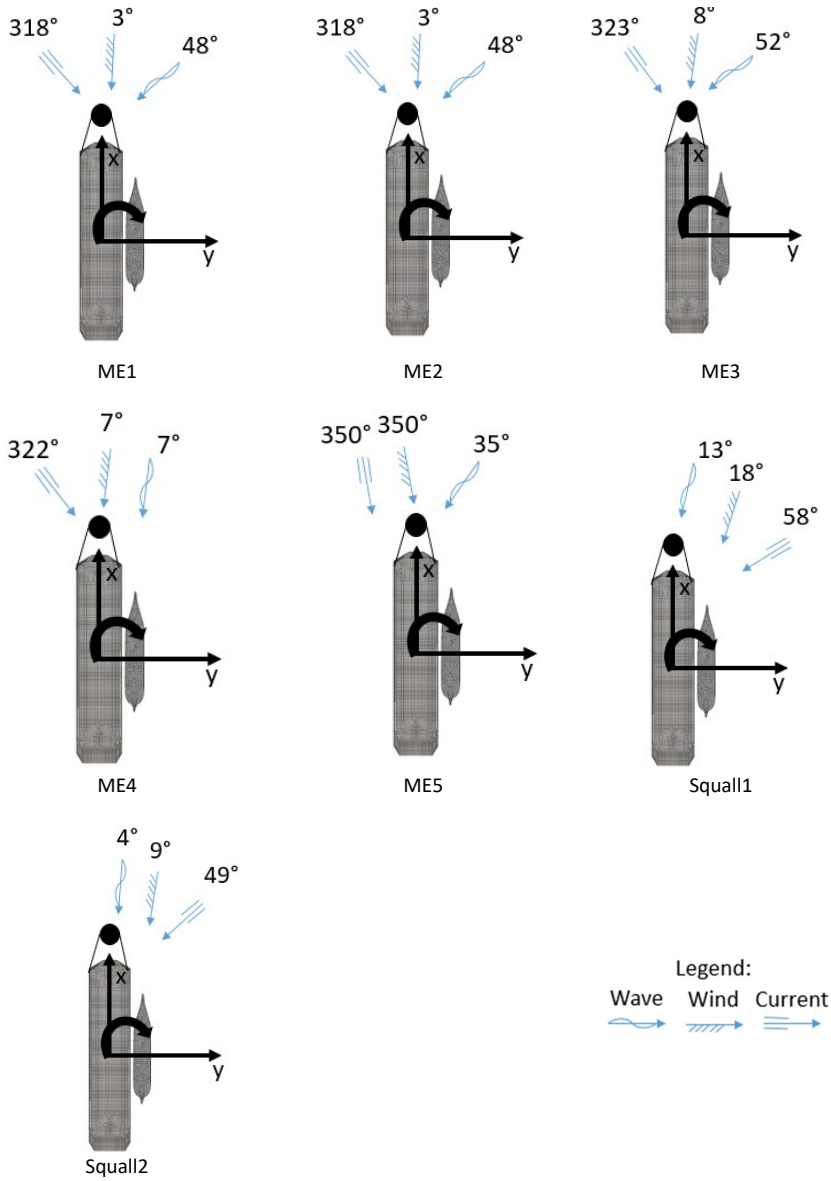

Figure B.2: Relative angle of attack for wind, wave and current of the FLNG-LPGC configuration at static equilibrium position under mean forces for each environmental condition

B.2. Dissipation factor variation

B.2.1. Relative motions for dissipation factor variation

			Absolute values of relative motion at manifold																				Criteria[m]
			Mean					Max					Min					Stdv					
	DoF	Env.cond	eps=0	eps=0.1	eps=0.2	eps=0.3	eps=0.4	eps=0	eps=0.1	eps=0.2	eps=0.3	eps=0.4	eps=0	eps=0.1	eps=0.2	eps=0.3	eps=0.4	eps=0	eps=0.1	eps=0.2	eps=0.3	eps=0.4	
	Heave [m]	ME1	0.00	0.00	0.00	0.00	0.00	0.10	0.09	0.09	0.10	0.10	0.10	0.10	0.10	0.11	0.11	0.03	0.03	0.03	0.03	0.03	1.50
		ME2	0.00	0.00	0.00	0.00	0.00	0.27	0.26	0.26	0.26	0.26	0.26	0.26	0.26	0.26	0.26	0.07	0.07	0.07	0.07	0.07	
		ME3	0.00	0.00	0.01	0.01	0.00	0.23	0.22	0.22	0.22	0.22	0.12	0.12	0.12	0.12	0.12	0.05	0.05	0.05	0.05	0.05	
		ME4	0.00	0.00	0.00	0.00	0.00	0.09	0.07	0.07	0.07	0.07	0.09	0.06	0.06	0.06	0.06	0.02	0.02	0.02	0.02	0.02	
		ME5	0.00	0.00	0.00	0.00	0.00	0.29	0.29	0.29	0.29	0.30	0.23	0.23	0.23	0.23	0.23	0.06	0.06	0.06	0.06	0.06	
		Squall1	0.00	0.00	0.00	0.00	0.00	0.22	0.22	0.22	0.22	0.22	0.17	0.17	0.17	0.17	0.17	0.05	0.05	0.05	0.05	0.05	
		Squall2	0.00	0.00	0.00	0.00	0.00	0.41	0.41	0.41	0.41	0.41	0.35	0.34	0.34	0.34	0.34	0.06	0.06	0.06	0.06	0.06	
	Surge [m]	ME1	0.00	0.00	0.00	0.00	0.00	0.01	0.03	0.03	0.03	0.03	0.05	0.02	0.01	0.01	0.01	0.00	0.00	0.00	0.00	0.00	2.00
		ME2	0.00	0.00	0.00	0.00	0.00	0.87	0.84	0.84	0.84	0.84	1.12	1.12	1.12	1.12	1.12	0.16	0.16	0.16	0.16	0.16	
		ME3	0.00	0.00	0.00	0.00	0.00	0.32	0.31	0.31	0.31	0.31	0.00	0.02	0.02	0.02	0.02	0.08	0.08	0.08	0.08	0.08	
		ME4	0.00	0.00	0.00	0.00	0.00	0.02	0.00	0.00	0.00	0.01	0.01	0.01	0.00	0.01	0.01	0.00	0.00	0.00	0.00	0.00	
		ME5	0.00	0.00	0.00	0.00	0.00	0.01	0.00	0.01	0.01	0.00	0.02	0.01	0.01	0.01	0.01	0.00	0.00	0.00	0.00	0.00	
		Squall1	0.00	0.00	0.00	0.00	0.00	0.03	0.02	0.02	0.01	0.01	0.31	0.32	0.31	0.31	0.30	0.00	0.00	0.00	0.00	0.00	
		Squall2	0.00	0.00	0.00	0.00	0.00	0.12	0.12	0.11	0.11	0.12	0.42	0.42	0.43	0.43	0.44	0.00	0.00	0.00	0.00	0.00	
	Sway [m]	ME1	0.00	0.00	0.00	0.00	0.00	0.03	0.00	0.00	0.01	0.01	0.01	0.03	0.04	0.03	0.03	0.00	0.00	0.00	0.00	0.00	1.50
		ME2	0.00	0.00	0.00	0.00	0.00	0.26	0.26	0.26	0.26	0.25	0.96	0.98	0.98	0.99	0.99	0.11	0.11	0.11	0.11	0.11	
		ME3	0.00	0.00	0.00	0.00	0.00	0.18	0.18	0.18	0.18	0.17	0.44	0.43	0.43	0.43	0.43	0.08	0.08	0.09	0.09	0.09	
		ME4	0.00	0.00	0.00	0.00	0.00	0.03	0.01	0.01	0.01	0.01	0.00	0.01	0.01	0.02	0.02	0.00	0.00	0.00	0.00	0.00	
		ME5	0.00	0.00	0.00	0.00	0.00	0.21	0.19	0.19	0.19	0.19	0.48	0.50	0.50	0.50	0.51	0.04	0.04	0.04	0.04	0.04	
		Squall1	0.00	0.00	0.00	0.00	0.00	0.02	0.05	0.06	0.05	0.05	0.89	0.90	0.90	0.90	0.90	0.01	0.01	0.01	0.01	0.01	
		Squall2	0.00	0.00	0.00	0.00	0.00	0.05	0.05	0.05	0.05	0.06	1.33	1.35	1.36	1.35	1.35	0.02	0.01	0.02	0.02	0.02	
	Heading [deg]	ME1	0.00	0.00	0.00	0.00	0.00	0.00	0.02	0.04	0.02	0.02	0.02	0.01	0.02	0.02	0.01	0.00	0.00	0.00	0.00	0.00	-
		ME2	0.00	0.00	0.00	0.00	0.00	0.06	0.06	0.06	0.07	0.06	0.05	0.05	0.05	0.05	0.06	0.00	0.00	0.00	0.00	0.00	
		ME3	0.00	0.00	0.00	0.00	0.00	0.12	0.12	0.11	0.11	0.12	0.17	0.17	0.17	0.17	0.18	0.00	0.00	0.00	0.00	0.00	
		ME4	0.00	0.00	0.00	0.00	0.00	0.00	0.01	0.00	0.00	0.01	0.04	0.01	0.01	0.02	0.02	0.00	0.00	0.00	0.00	0.00	
		ME5	0.00	0.00	0.00	0.00	0.00	0.08	0.09	0.09	0.09	0.09	0.00	0.01	0.01	0.00	0.01	0.00	0.00	0.00	0.00	0.00	
		Squall1	0.00	0.00	0.00	0.00	0.00	0.07	0.04	0.04	0.04	0.02	0.04	0.04	0.04	0.03	0.04	0.00	0.00	0.00	0.00	0.00	
		Squall2	0.00	0.00	0.00	0.00	0.00	0.02	0.03	0.03	0.03	0.03	0.03	0.01	0.01	0.01	0.00	0.00	0.00	0.00	0.00	0.00	
	Relative distance [m]	ME1	0.00	0.00	0.00	0.00	0.00	0.10	0.10	0.10	0.10	0.10	0.11	0.11	0.11	0.11	0.11	0.03	0.03	0.03	0.03	0.03	3.00
		ME2	0.00	0.00	0.00	0.00	0.00	0.94	0.92	0.92	0.92	0.92	1.50	1.51	1.51	1.52	1.52	0.20	0.20	0.21	0.21	0.21	
		ME3	0.00	0.00	0.00	0.00	0.00	0.43	0.43	0.42	0.42	0.42	0.45	0.45	0.45	0.45	0.45	0.13	0.13	0.13	0.13	0.13	
		ME4	0.00	0.00	0.00	0.00	0.00	0.10	0.07	0.07	0.07	0.07	0.09	0.06	0.06	0.06	0.06	0.02	0.02	0.02	0.02	0.02	
		ME5	0.00	0.00	0.00	0.00	0.00	0.36	0.35	0.35	0.35	0.35	0.54	0.55	0.56	0.55	0.56	0.07	0.07	0.07	0.07	0.07	
		Squall1	0.00	0.00	0.00	0.00	0.00	0.22	0.22	0.23	0.22	0.22	0.96	0.97	0.97	0.97	0.96	0.05	0.05	0.05	0.05	0.05	
		Squall2	0.00	0.00	0.00	0.00	0.00	0.43	0.43	0.43	0.43	0.43	1.43	1.46	1.46	1.46	1.46	0.06	0.06	0.06	0.06	0.06	
Low frequency	Sway [m]	ME1	0.08	0.05	0.02	0.01	0.00	0.17	0.22	0.16	0.13	0.11	1.28	0.03	0.02	0.01	0.01	0.10	0.01	0.00	0.00	0.00	4.00
		ME2	0.03	0.02	0.02	0.02	0.02	0.05	0.06	0.06	0.06	0.06	0.05	0.05	0.05	0.05	0.05	0.00	0.00	0.00	0.00	0.00	
		ME3	0.03	0.03	0.03	0.03	0.03	0.00	0.00	0.00	0.00	0.00	0.06	0.06	0.06	0.06	0.06	0.00	0.00	0.00	0.00	0.00	
		ME4	0.36	0.08	0.06	0.02	0.03	1.01	0.58	0.23	0.16	0.20	2.99	0.89	0.46	0.25	0.24	0.37	0.12	0.07	0.06	0.05	
		ME5	0.01	0.01	0.01	0.01	0.01	0.04	0.03	0.04	0.04	0.03	0.05	0.05	0.05	0.05	0.04	0.00	0.00	0.00	0.00	0.00	
		Squall1	2.62	2.57	2.56	2.57	2.56	5.90	5.90	5.90	5.90	5.90	0.05	0.02	0.02	0.02	0.02	1.78	1.77	1.77	1.77	1.77	
		Squall2	2.28	2.27	2.27	2.27	2.27	6.65	6.65	6.65	6.65	6.66	0.41	0.43	0.43	0.43	0.43	1.55	1.55	1.55	1.55	1.55	
	Surge [m]	ME1	0.00	0.14	0.19	0.19	0.18	0.20	0.02	0.01	0.04	0.05	0.51	0.29	0.37	0.38	0.38	0.08	0.04	0.04	0.04	0.04	
		ME2	0.02	0.01	0.01	0.01	0.01	0.10	0.10	0.10	0.10	0.10	0.15	0.16	0.15	0.15	0.15	0.02	0.02	0.02	0.02	0.02	
		ME3	0.02	0.02	0.02	0.03	0.03	0.08	0.08	0.08	0.08	0.08	0.06	0.06	0.06	0.06	0.06	0.01	0.01	0.01	0.01	0.01	
		ME4	1.21	0.01	0.07	0.03	0.00	4.55	0.60	0.69	0.58	0.50	0.06	0.39	0.15	0.17	0.18	0.53	0.13	0.08	0.07	0.07	
		ME5	0.03	0.03	0.03	0.03	0.03	0.17	0.16	0.16	0.16	0.16	0.11	0.10	0.10	0.10	0.10	0.04	0.04	0.04	0.04	0.04	
		Squall1	3.22	3.18	3.17	3.17	3.16	1.91	1.92	1.92	1.92	1.91	5.00	4.96	4.95	4.95	4.94	2.02	1.98	1.98	1.97	1.97	
		Squall2	4.51	4.48	4.47	4.46	4.45	5.20	5.21	5.21	5.20	5.17	6.78	6.77	6.77	6.76	6.76	1.29	1.26	1.25	1.25	1.25	
	Heading [deg]	ME1	0.40	0.32	0.32	0.32	0.32	0.25	0.17	0.22	0.25	0.24	0.88	0.38	0.44	0.46	0.46	0.04	0.02	0.02	0.02	0.02	-
		ME2	0.30	0.30	0.30	0.30	0.29	0.15	0.16	0.17	0.17	0.18	0.44	0.43	0.43	0.43	0.44	0.01	0.01	0.01	0.01	0.01	
		ME3	0.30	0.29	0.30	0.30	0.30	0.20	0.20	0.21	0.21	0.21	0.37	0.37	0.37	0.37	0.37	0.01	0.01	0.01	0.01	0.01	
		ME4	0.67	0.34	0.28	0.26	0.26	0.07	0.17	0.13	0.08	0.11	1.36	0.82	0.77	0.63	0.54	0.17	0.07	0.05	0.04	0.04	
		ME5	0.30	0.29	0.30	0.29	0.30	0.21	0.20	0.20	0.20	0.20	0.38	0.37	0.37	0.37	0.37	0.01	0.01	0.01	0.01	0.01	
		Squall1	0.32	0.30	0.31	0.31	0.31	0.16	0.18	0.18	0.18	0.19	0.31	0.31	0.31	0.31	0.31	0.01	0.00	0.00	0.00	0.00	
		Squall2	0.33	0.31	0.32	0.31	0.32	0.26	0.26	0.25	0.25	0.25	0.32	0.30	0.30	0.29	0.29	0.02	0.01	0.01	0.01	0.01	

Figure B.3: Relative motions at the manifold location and maximum allowable criteria for dissipation factor variation [mooring configuration used: FLNGmax-LNGCmin]

B.2.2. Line Tensions

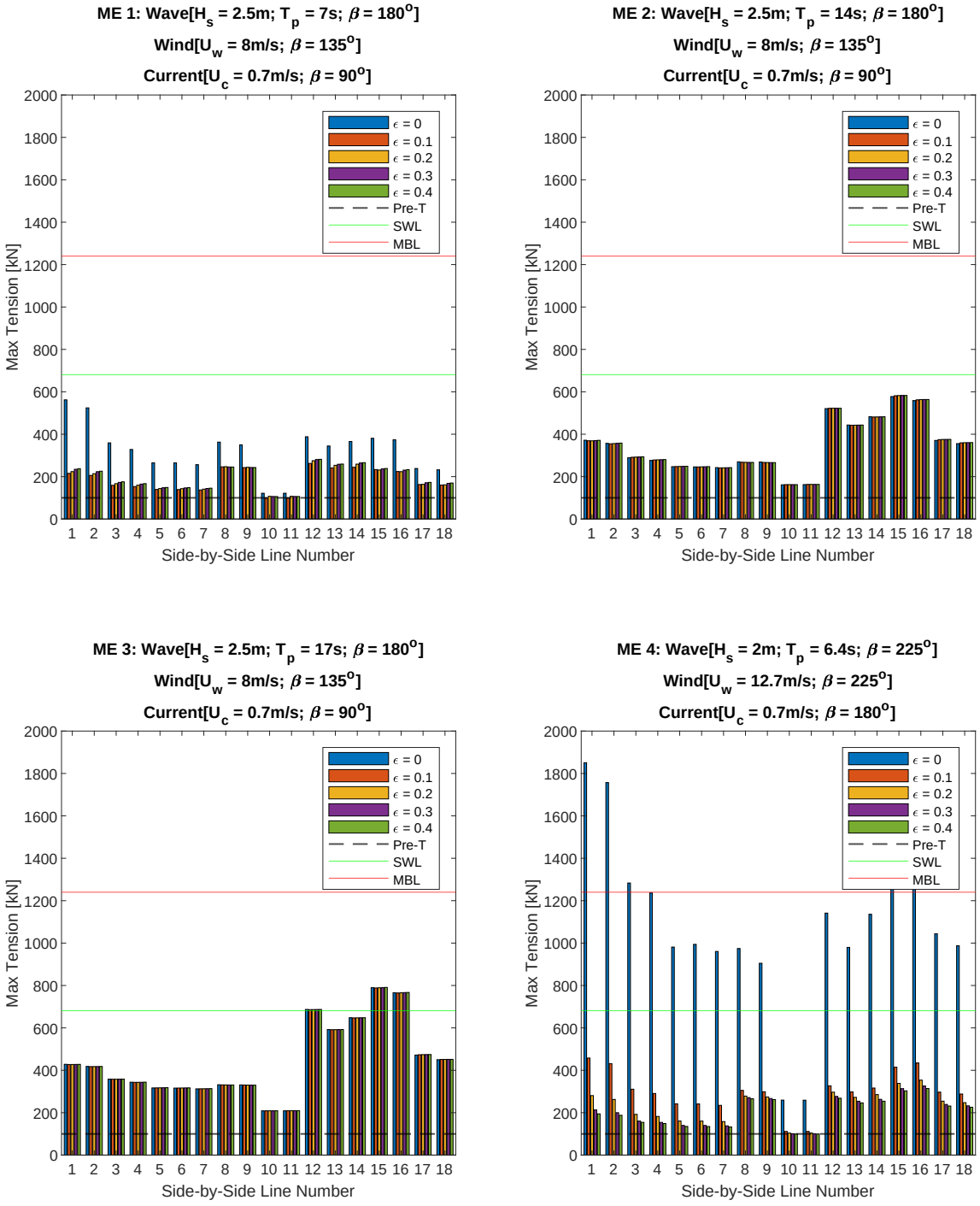

Figure B.4: Line tensions for environmental conditions from ME1 to ME4 using the range of dissipation factors [mooring configuration used: FLNGmax-LNGCmin]

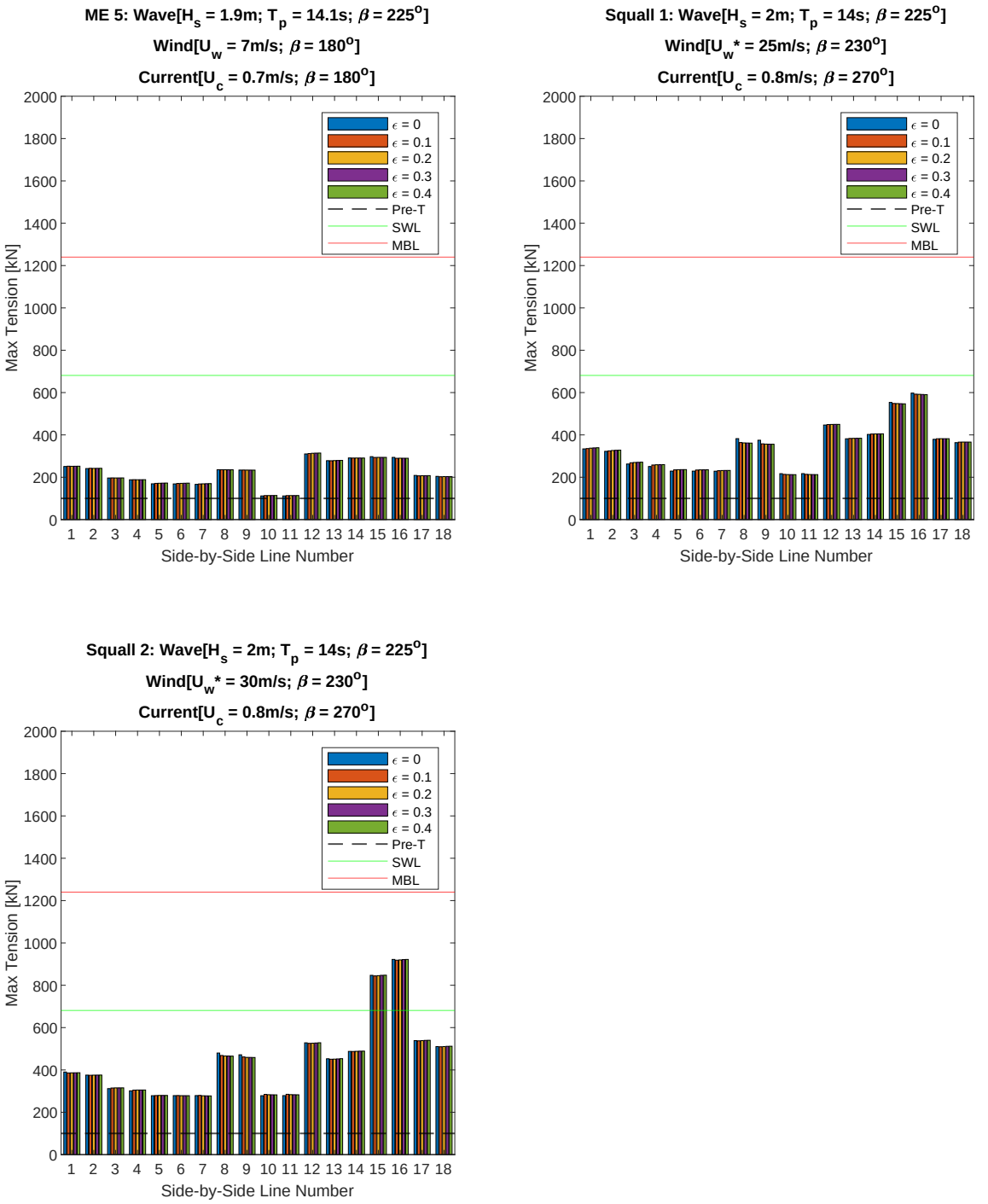

Figure B.5: Line tensions for environmental conditions from ME5 to Squall2 using the range of dissipation factors [mooring configuration used: FLNGmax-LNGCmin]

B.2.3. Fender Reaction Loads

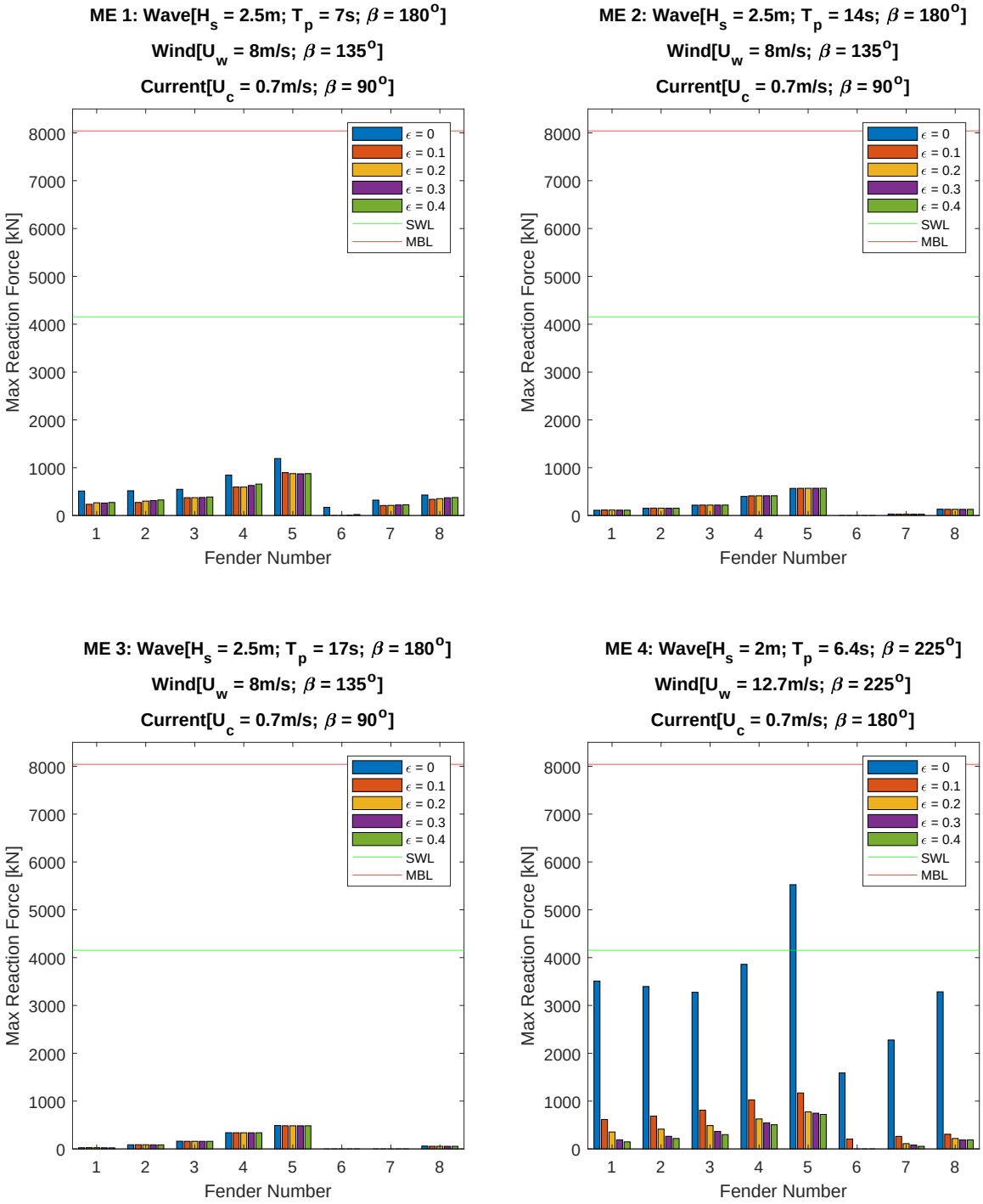

Figure B.6: Fender reaction forces for environmental conditions from ME1 to ME4 using the range of dissipation factors [mooring configuration used: FLNGmax-LNGCmin]

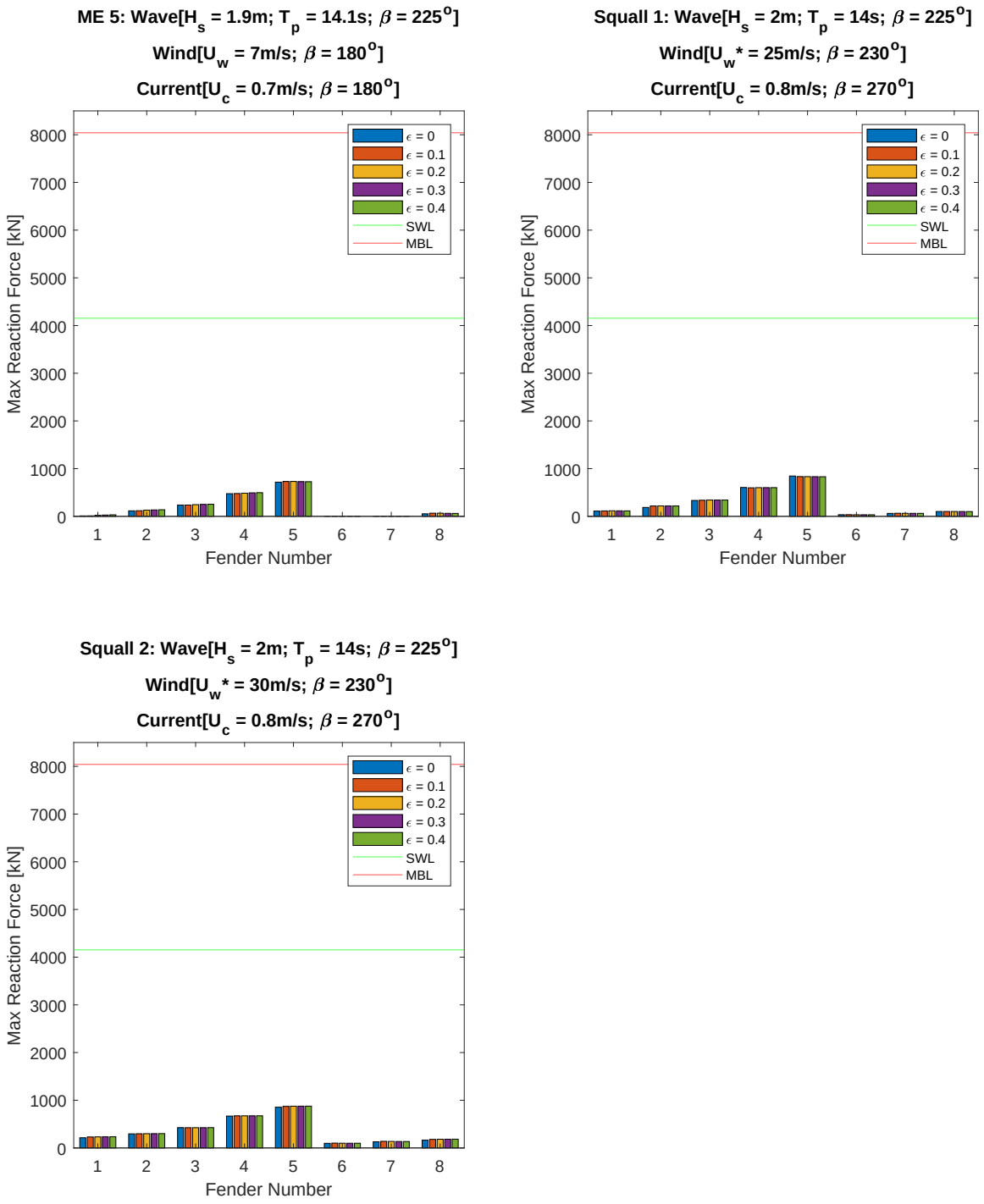

Figure B.7: Fender reaction forces for environmental conditions from ME5 to Squall2 using the range of dissipation factors [mooring configuration used: FLNGmax-LNGCmin]

B.3. Gap length variation

B.3.1. Relative motions for gap length variation

			Absolute values of relative motion at manifold												Criteria[m]
			Mean			Max			Min			Stdv			
	DoF	Env.cond	L160m	L200m	L285m	L160m	L200m	L285m	L160m	L200m	L285m	L160m	L200m	L285m	
wave frequency	Heave [m]	ME1	0.00	0.00	0.00	0.09	0.09	0.09	0.10	0.11	0.10	0.03	0.03	0.03	1.50
		ME2	0.00	0.00	0.00	0.26	0.26	0.26	0.26	0.26	0.26	0.07	0.07	0.07	
		ME3	0.00	0.00	0.00	0.22	0.22	0.22	0.12	0.12	0.12	0.05	0.05	0.05	
		ME4	0.00	0.00	0.00	0.07	0.06	0.06	0.06	0.06	0.05	0.02	0.02	0.01	
		ME5	0.00	0.00	0.00	0.29	0.29	0.29	0.23	0.23	0.23	0.06	0.06	0.06	
		Squall1	0.00	0.00	0.00	0.22	0.22	0.22	0.17	0.17	0.17	0.05	0.05	0.05	
		Squall2	0.00	0.00	0.00	0.41	0.41	0.41	0.34	0.34	0.34	0.06	0.06	0.06	
	Surge [m]	ME1	0.00	0.00	0.00	0.03	0.03	0.03	0.01	0.01	0.01	0.00	0.00	0.00	2.00
		ME2	0.00	0.00	0.00	0.84	0.84	0.84	1.12	1.12	1.12	0.16	0.16	0.16	
		ME3	0.00	0.00	0.00	0.31	0.31	0.31	0.02	0.02	0.02	0.08	0.08	0.08	
		ME4	0.00	0.00	0.00	0.00	0.00	0.00	0.00	0.00	0.00	0.00	0.00	0.00	
		ME5	0.00	0.00	0.00	0.01	0.01	0.01	0.01	0.01	0.02	0.00	0.00	0.00	
		Squall1	0.00	0.00	0.00	0.02	0.02	0.02	0.31	0.31	0.31	0.00	0.00	0.00	
		Squall2	0.00	0.00	0.00	0.11	0.11	0.11	0.43	0.43	0.42	0.00	0.00	0.00	
	Sway [m]	ME1	0.00	0.00	0.00	0.00	0.00	0.01	0.04	0.03	0.03	0.00	0.00	0.00	1.50
		ME2	0.00	0.00	0.00	0.26	0.26	0.27	0.98	0.98	0.98	0.11	0.11	0.11	
		ME3	0.00	0.00	0.00	0.18	0.18	0.18	0.43	0.43	0.43	0.09	0.09	0.09	
		ME4	0.00	0.00	0.00	0.01	0.00	0.01	0.01	0.01	0.02	0.00	0.00	0.00	
		ME5	0.00	0.00	0.00	0.19	0.19	0.18	0.50	0.50	0.50	0.04	0.04	0.04	
		Squall1	0.00	0.00	0.00	0.06	0.06	0.06	0.90	0.90	0.90	0.01	0.01	0.01	
		Squall2	0.00	0.00	0.00	0.05	0.06	0.06	1.36	1.36	1.36	0.02	0.01	0.02	
	Heading [deg]	ME1	0.00	0.00	0.00	0.04	0.04	0.01	0.02	0.01	0.02	0.00	0.00	0.00	-
		ME2	0.00	0.00	0.00	0.06	0.05	0.06	0.05	0.06	0.05	0.00	0.00	0.00	
		ME3	0.00	0.00	0.00	0.11	0.12	0.11	0.17	0.18	0.17	0.00	0.00	0.00	
		ME4	0.00	0.00	0.00	0.00	0.00	0.00	0.01	0.00	0.00	0.00	0.00	0.00	
		ME5	0.00	0.00	0.00	0.09	0.09	0.09	0.01	0.01	0.01	0.00	0.00	0.00	
		Squall1	0.00	0.00	0.00	0.04	0.04	0.03	0.04	0.04	0.04	0.00	0.00	0.00	
		Squall2	0.00	0.00	0.00	0.03	0.03	0.02	0.01	0.01	0.01	0.00	0.00	0.00	
	Relative distance [m]	ME1	0.00	0.00	0.00	0.10	0.10	0.10	0.11	0.11	0.11	0.03	0.03	0.03	3.00
		ME2	0.00	0.00	0.00	0.92	0.92	0.92	1.51	1.51	1.51	0.21	0.21	0.21	
		ME3	0.00	0.00	0.00	0.42	0.42	0.43	0.45	0.45	0.45	0.13	0.13	0.13	
		ME4	0.00	0.00	0.00	0.07	0.06	0.06	0.06	0.06	0.05	0.02	0.02	0.01	
		ME5	0.00	0.00	0.00	0.35	0.35	0.34	0.56	0.55	0.55	0.07	0.07	0.07	
		Squall1	0.00	0.00	0.00	0.23	0.23	0.23	0.97	0.97	0.97	0.05	0.05	0.05	
		Squall2	0.00	0.00	0.00	0.43	0.43	0.43	1.46	1.46	1.46	0.06	0.06	0.06	
Low frequency	Sway [m]	ME1	0.02	0.01	0.00	0.16	0.15	0.14	0.02	0.03	0.03	0.00	0.00	0.00	4.00
		ME2	0.02	0.02	0.02	0.06	0.06	0.06	0.05	0.05	0.05	0.00	0.00	0.00	
		ME3	0.03	0.03	0.03	0.00	0.00	0.00	0.06	0.06	0.06	0.00	0.00	0.00	
		ME4	0.06	0.04	0.03	0.23	0.16	0.19	0.46	0.29	0.23	0.07	0.06	0.05	
		ME5	0.01	0.01	0.01	0.04	0.04	0.03	0.05	0.05	0.04	0.00	0.00	0.00	
		Squall1	2.56	2.57	2.56	5.90	5.90	5.90	0.02	0.02	0.02	1.77	1.77	1.77	
		Squall2	2.27	2.27	2.27	6.65	6.65	6.65	0.43	0.43	0.43	1.55	1.55	1.55	
	Surge [m]	ME1	0.19	0.19	0.20	0.01	0.01	0.01	0.37	0.37	0.38	0.04	0.04	0.04	
		ME2	0.01	0.01	0.01	0.10	0.10	0.10	0.15	0.16	0.16	0.02	0.02	0.02	
		ME3	0.02	0.02	0.03	0.08	0.08	0.08	0.06	0.06	0.06	0.01	0.01	0.01	
		ME4	0.07	0.06	0.02	0.69	0.62	0.47	0.15	0.13	0.14	0.08	0.07	0.06	
		ME5	0.03	0.03	0.03	0.16	0.16	0.16	0.10	0.10	0.10	0.04	0.04	0.04	
		Squall1	3.17	3.17	3.17	1.92	1.92	1.92	4.95	4.95	4.94	1.98	1.98	1.97	
		Squall2	4.47	4.47	4.47	5.21	5.21	5.21	6.77	6.77	6.76	1.25	1.25	1.25	
	Heading [deg]	ME1	0.32	0.32	0.32	0.22	0.24	0.24	0.44	0.44	0.48	0.02	0.02	0.02	-
		ME2	0.30	0.30	0.30	0.17	0.17	0.17	0.43	0.44	0.43	0.01	0.01	0.01	
		ME3	0.30	0.29	0.30	0.21	0.20	0.21	0.37	0.37	0.37	0.01	0.01	0.01	
		ME4	0.28	0.28	0.27	0.13	0.09	0.13	0.77	0.69	0.49	0.05	0.04	0.03	
		ME5	0.30	0.29	0.30	0.20	0.20	0.20	0.37	0.37	0.37	0.01	0.01	0.01	
		Squall1	0.31	0.31	0.31	0.18	0.18	0.19	0.31	0.32	0.31	0.00	0.00	0.00	
		Squall2	0.32	0.32	0.31	0.25	0.25	0.25	0.30	0.30	0.29	0.01	0.01	0.01	

Figure B.8: Relative motions at the manifold location and maximum allowable criteria for gap length variation [mooring configuration used: FLNGmax-LNGCmin]

B.3.2. Line Tension

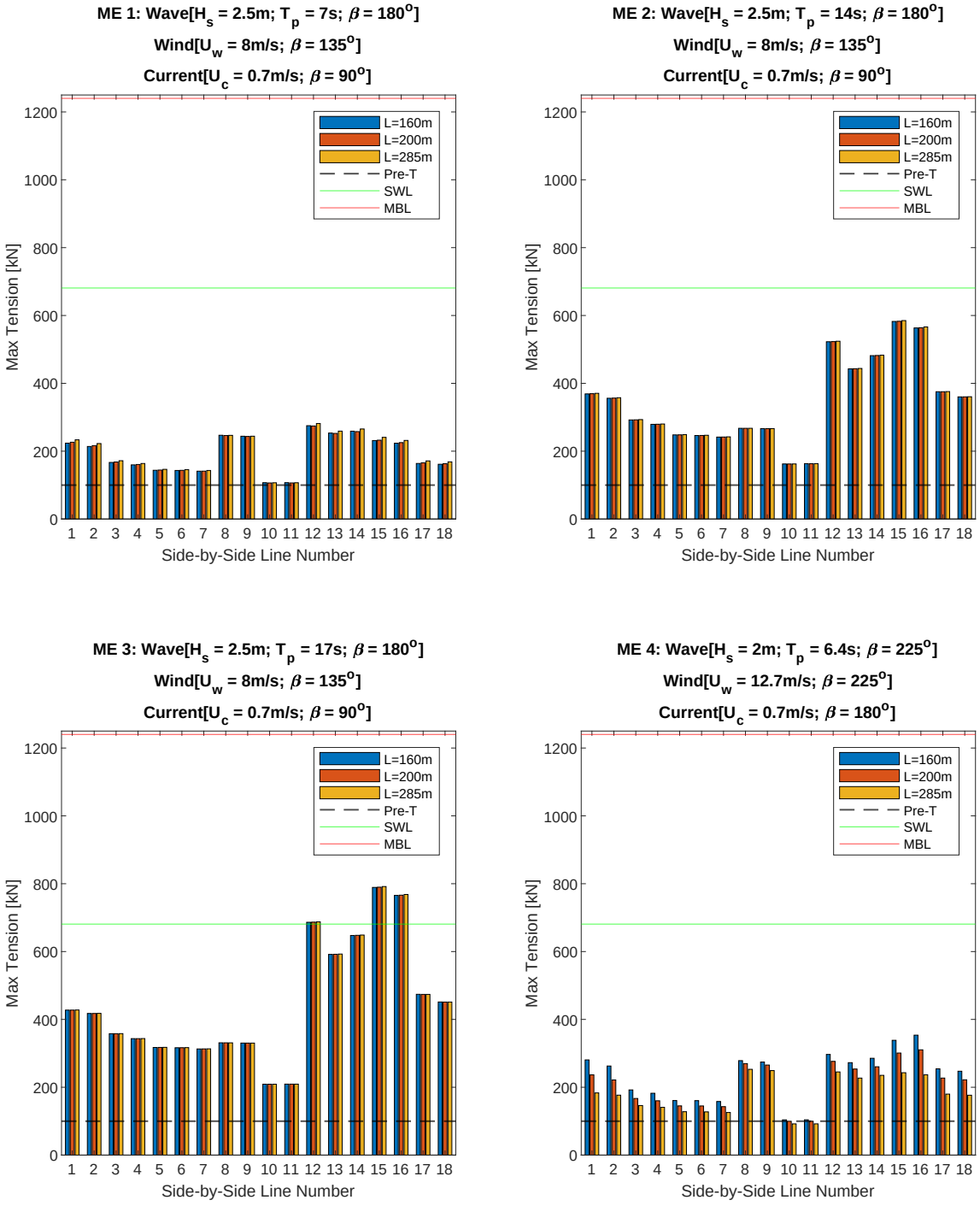

Figure B.9: Line tensions for environmental conditions from ME1 to ME4 using the range of gap length [mooring configuration used: FLNGmax-LNGCmin]

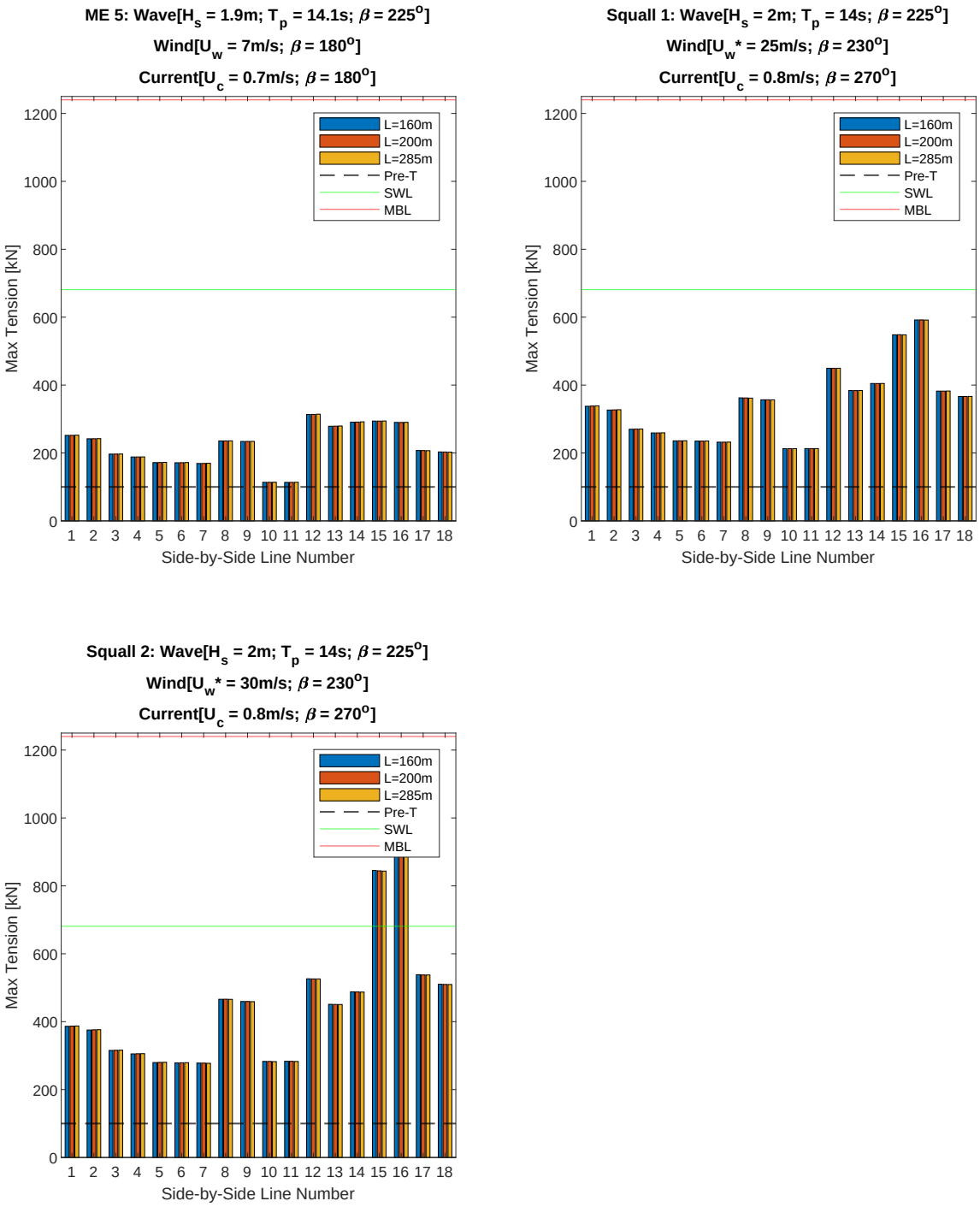

Figure B.10: Line tensions for environmental conditions from ME5 to Squall2 using the range of gap length [mooring configuration used: FLNGmax-LNGCmin]

B.3.3. Fender Reaction Loads

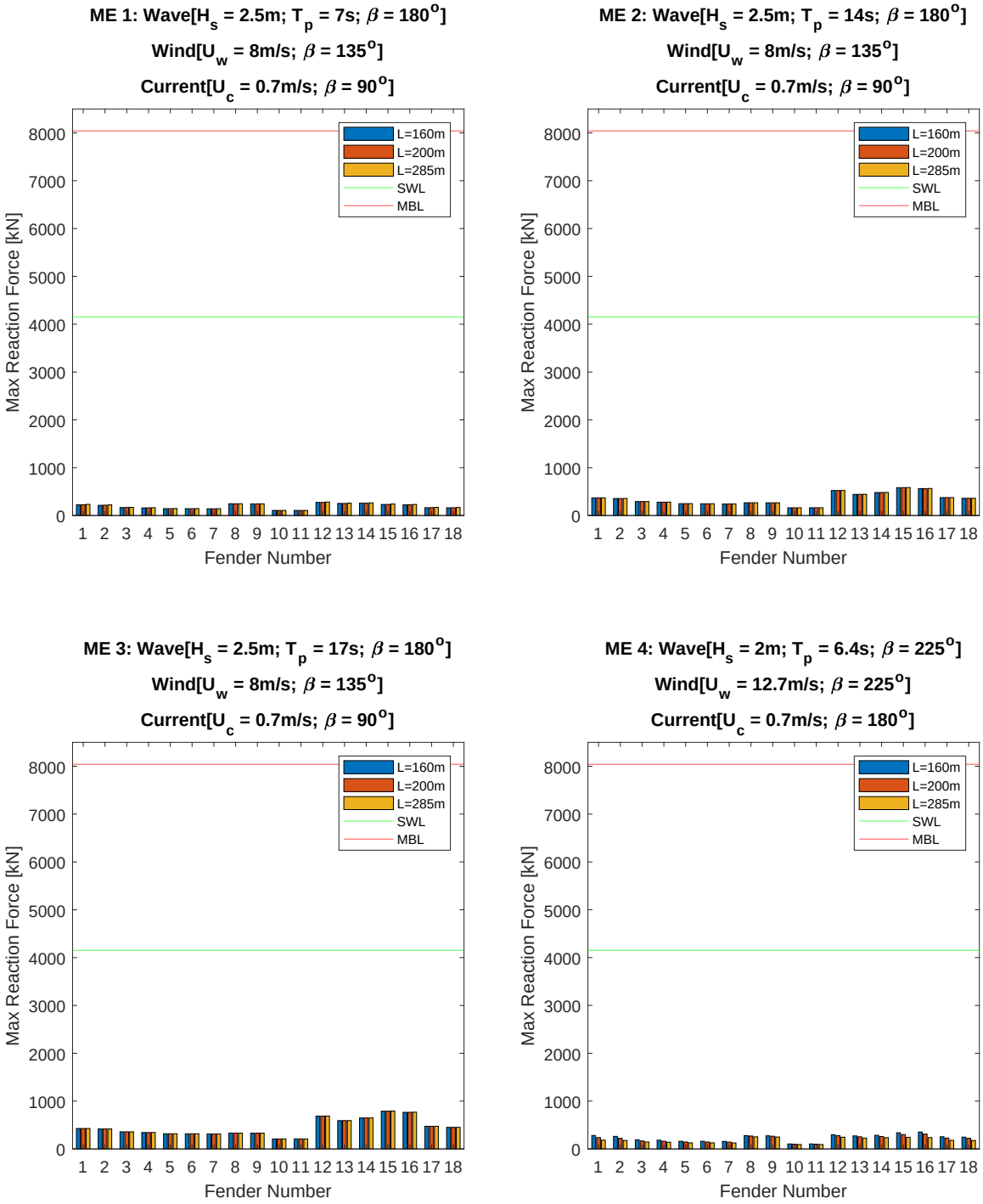

Figure B.11: Fender reaction loads for environmental conditions from ME1 to ME4 using the range of gap length [mooring configuration used: FLNGmax-LNGCmin]

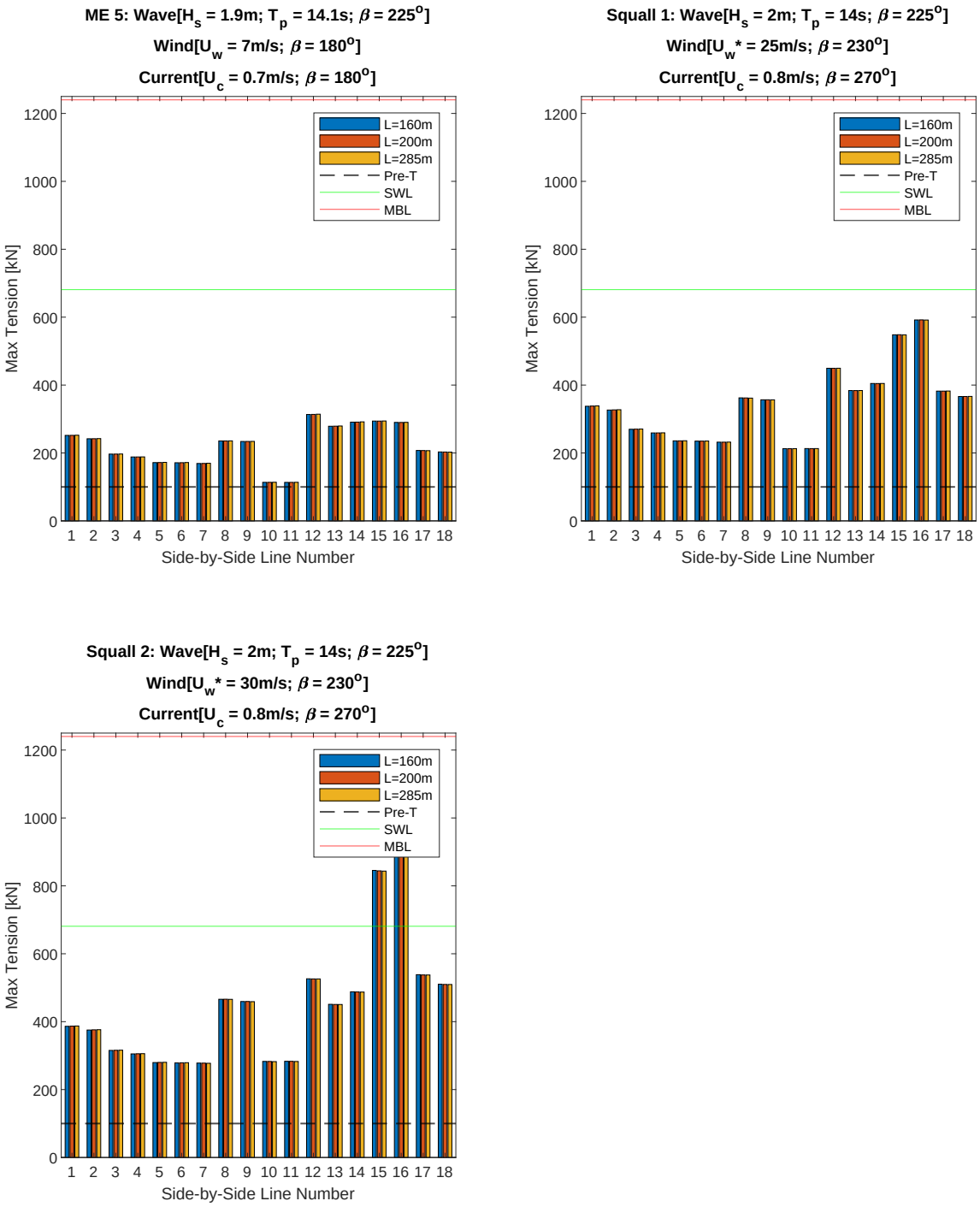

Figure B.12: Fender reaction loads for environmental conditions from ME5 to Squall2 using the range of gap length [mooring configuration used: FLNGmax-LNGCmin]

B.4. Separation distance variation

B.4.1. Relative motions for separation distance variation

			Absolute values of relative motion at manifold																Criteria[m]
			Mean				Max				Min				Stdv				
	DoF	Env.cond	d1=3m	d2=3.5m	d3=4m	d4=4.5m	d1=3m	d2=3.5m	d3=4m	d4=4.5m	d1=3m	d2=3.5m	d3=4m	d4=4.5m	d1=3m	d2=3.5m	d3=4m	d4=4.5m	
wave frequency	Heave [m]	ME1	0.00	0.00	0.00	0.00	0.10	0.09	0.09	0.10	0.12	0.11	0.10	0.10	0.03	0.03	0.03	0.03	1.50
		ME2	0.00	0.00	0.00	0.00	0.27	0.26	0.26	0.26	0.26	0.26	0.26	0.26	0.07	0.07	0.07	0.07	
		ME3	0.00	0.00	0.00	0.00	0.22	0.22	0.22	0.22	0.12	0.12	0.12	0.12	0.05	0.05	0.05	0.05	
		ME4	0.00	0.00	0.00	0.00	0.07	0.07	0.07	0.07	0.06	0.06	0.06	0.06	0.02	0.02	0.02	0.02	
		ME5	0.00	0.00	0.00	0.00	0.30	0.30	0.29	0.29	0.23	0.23	0.23	0.23	0.06	0.06	0.06	0.06	
		Squall1	0.00	0.00	0.00	0.00	0.22	0.22	0.22	0.22	0.17	0.17	0.17	0.18	0.05	0.05	0.05	0.05	
		Squall2	0.00	0.00	0.00	0.00	0.40	0.40	0.41	0.41	0.34	0.34	0.34	0.34	0.06	0.06	0.06	0.06	
	Surge [m]	ME1	0.00	0.00	0.00	0.00	0.03	0.03	0.03	0.04	0.00	0.01	0.01	0.01	0.00	0.00	0.00	0.00	2.00
		ME2	0.00	0.00	0.00	0.00	0.84	0.84	0.84	0.84	1.10	1.12	1.12	1.12	0.16	0.16	0.16	0.16	
		ME3	0.00	0.00	0.00	0.00	0.31	0.31	0.31	0.31	0.04	0.04	0.02	0.01	0.08	0.08	0.08	0.08	
		ME4	0.00	0.00	0.00	0.00	0.01	0.00	0.00	0.00	0.02	0.01	0.00	0.01	0.00	0.00	0.00	0.00	
		ME5	0.00	0.00	0.00	0.00	0.00	0.01	0.01	0.01	0.02	0.02	0.01	0.02	0.00	0.00	0.00	0.00	
		Squall1	0.00	0.00	0.00	0.00	0.03	0.02	0.02	0.01	0.31	0.30	0.31	0.32	0.00	0.00	0.00	0.00	
		Squall2	0.00	0.00	0.00	0.00	0.10	0.11	0.11	0.12	0.36	0.40	0.43	0.46	0.00	0.00	0.00	0.00	
	Sway [m]	ME1	0.00	0.00	0.00	0.00	0.00	0.01	0.00	0.00	0.04	0.03	0.04	0.03	0.00	0.00	0.00	0.00	1.50
		ME2	0.00	0.00	0.00	0.00	0.25	0.25	0.26	0.27	0.97	0.98	0.98	0.99	0.11	0.11	0.11	0.11	
		ME3	0.00	0.00	0.00	0.00	0.19	0.19	0.18	0.18	0.43	0.43	0.43	0.43	0.09	0.09	0.09	0.08	
		ME4	0.00	0.00	0.00	0.00	0.01	0.02	0.01	0.01	0.02	0.02	0.01	0.02	0.00	0.00	0.00	0.00	
		ME5	0.00	0.00	0.00	0.00	0.18	0.19	0.19	0.18	0.50	0.50	0.50	0.50	0.04	0.04	0.04	0.04	
		Squall1	0.00	0.00	0.00	0.00	0.06	0.06	0.06	0.06	0.91	0.90	0.90	0.89	0.01	0.01	0.01	0.01	
		Squall2	0.00	0.00	0.00	0.00	0.06	0.05	0.05	0.06	1.40	1.38	1.36	1.34	0.02	0.01	0.02	0.02	
	Heading [deg]	ME1	0.00	0.00	0.00	0.00	0.05	0.04	0.04	0.04	0.03	0.02	0.02	0.01	0.00	0.00	0.00	0.00	-
		ME2	0.00	0.00	0.00	0.00	0.68	0.67	0.68	0.67	1.04	1.05	1.05	1.04	0.12	0.12	0.12	0.12	
		ME3	0.00	0.00	0.00	0.00	1.20	1.20	1.21	1.21	1.37	1.39	1.39	1.40	0.26	0.26	0.26	0.26	
		ME4	0.00	0.00	0.00	0.00	0.00	0.03	0.02	0.02	0.01	0.02	0.01	0.01	0.00	0.00	0.00	0.00	
		ME5	0.00	0.00	0.00	0.00	0.41	0.41	0.41	0.41	0.64	0.65	0.65	0.64	0.06	0.06	0.06	0.06	
		Squall1	0.00	0.00	0.00	0.00	0.25	0.25	0.26	0.26	0.41	0.40	0.40	0.41	0.00	0.00	0.00	0.00	
		Squall2	0.00	0.00	0.00	0.00	0.49	0.49	0.51	0.50	0.16	0.19	0.19	0.19	0.00	0.00	0.00	0.00	
	Relative distance [m]	ME1	0.00	0.00	0.00	0.00	0.10	0.10	0.10	0.11	0.12	0.12	0.11	0.11	0.03	0.03	0.03	0.03	3.00
		ME2	0.00	0.00	0.00	0.00	0.91	0.91	0.92	0.92	1.49	1.51	1.51	1.52	0.21	0.21	0.21	0.21	
		ME3	0.00	0.00	0.00	0.00	0.43	0.42	0.42	0.42	0.45	0.45	0.45	0.45	0.13	0.13	0.13	0.13	
		ME4	0.00	0.00	0.00	0.00	0.07	0.07	0.07	0.07	0.07	0.06	0.06	0.07	0.02	0.02	0.02	0.02	
		ME5	0.00	0.00	0.00	0.00	0.35	0.35	0.35	0.35	0.55	0.55	0.56	0.55	0.07	0.07	0.07	0.07	
		Squall1	0.00	0.00	0.00	0.00	0.23	0.23	0.23	0.23	0.98	0.97	0.97	0.97	0.05	0.05	0.05	0.05	
		Squall2	0.00	0.00	0.00	0.00	0.41	0.42	0.43	0.43	1.49	1.47	1.46	1.45	0.06	0.06	0.06	0.06	
Low frequency	Sway [m]	ME1	0.02	0.00	0.02	0.02	0.13	0.15	0.16	0.15	0.04	0.03	0.02	0.02	0.01	0.01	0.00	0.00	4.00
		ME2	0.03	0.03	0.02	0.02	0.05	0.06	0.06	0.06	0.06	0.06	0.05	0.05	0.00	0.00	0.00	0.00	
		ME3	0.03	0.03	0.03	0.03	0.00	0.00	0.00	0.00	0.06	0.06	0.06	0.06	0.00	0.00	0.00	0.00	
		ME4	0.02	0.06	0.06	0.05	0.44	0.30	0.23	0.18	0.87	0.66	0.46	0.32	0.09	0.08	0.07	0.06	
		ME5	0.00	0.01	0.01	0.01	0.03	0.03	0.04	0.04	0.05	0.05	0.05	0.04	0.00	0.00	0.00	0.00	
		Squall1	2.56	2.56	2.56	2.57	5.89	5.90	5.90	5.90	0.00	0.01	0.02	0.03	1.77	1.77	1.77	1.77	
		Squall2	2.29	2.28	2.27	2.27	6.67	6.66	6.65	6.65	0.42	0.43	0.43	0.44	1.55	1.55	1.55	1.55	
	Surge [m]	ME1	0.20	0.20	0.19	0.19	0.02	0.00	0.01	0.01	0.36	0.34	0.37	0.38	0.04	0.04	0.04	0.04	
		ME2	0.01	0.01	0.01	0.01	0.11	0.11	0.10	0.10	0.16	0.15	0.15	0.15	0.02	0.02	0.02	0.02	
		ME3	0.03	0.03	0.02	0.02	0.09	0.08	0.08	0.08	0.06	0.06	0.06	0.06	0.01	0.01	0.01	0.01	
		ME4	0.01	0.06	0.07	0.07	0.79	0.74	0.69	0.64	0.25	0.19	0.15	0.14	0.10	0.09	0.08	0.07	
		ME5	0.03	0.03	0.03	0.03	0.16	0.16	0.16	0.16	0.10	0.10	0.10	0.10	0.04	0.04	0.04	0.04	
		Squall1	3.16	3.17	3.17	3.17	1.88	1.90	1.92	1.93	4.93	4.94	4.95	4.97	1.98	1.98	1.98	1.98	
		Squall2	4.47	4.47	4.47	4.47	5.25	5.23	5.21	5.19	6.73	6.75	6.77	6.79	1.26	1.26	1.25	1.25	
	Heading [deg]	ME1	0.31	0.32	0.32	0.32	0.24	0.23	0.22	0.24	0.45	0.43	0.44	0.45	0.02	0.02	0.02	0.02	-
		ME2	0.30	0.30	0.30	0.30	0.17	0.17	0.17	0.16	0.44	0.44	0.43	0.44	0.01	0.01	0.01	0.01	
		ME3	0.29	0.30	0.30	0.30	0.21	0.21	0.21	0.21	0.38	0.37	0.37	0.37	0.01	0.01	0.01	0.01	
		ME4	0.29	0.29	0.28	0.28	0.20	0.18	0.13	0.09	0.87	0.82	0.77	0.72	0.07	0.06	0.05	0.04	
		ME5	0.29	0.29	0.30	0.29	0.20	0.20	0.20	0.20	0.37	0.37	0.37	0.38	0.01	0.01	0.01	0.01	
		Squall1	0.31	0.31	0.31	0.31	0.19	0.19	0.18	0.18	0.31	0.31	0.31	0.31	0.00	0.00	0.00	0.00	
		Squall2	0.31	0.31	0.32	0.32	0.25	0.25	0.25	0.26	0.30	0.30	0.30	0.30	0.01	0.01	0.01	0.01	

Figure B.13: Relative motions at the manifold location and maximum allowable criteria for gap length variation [mooring configuration used: FLNGmax-LNGCmin]

B.4.2. Line Tensions

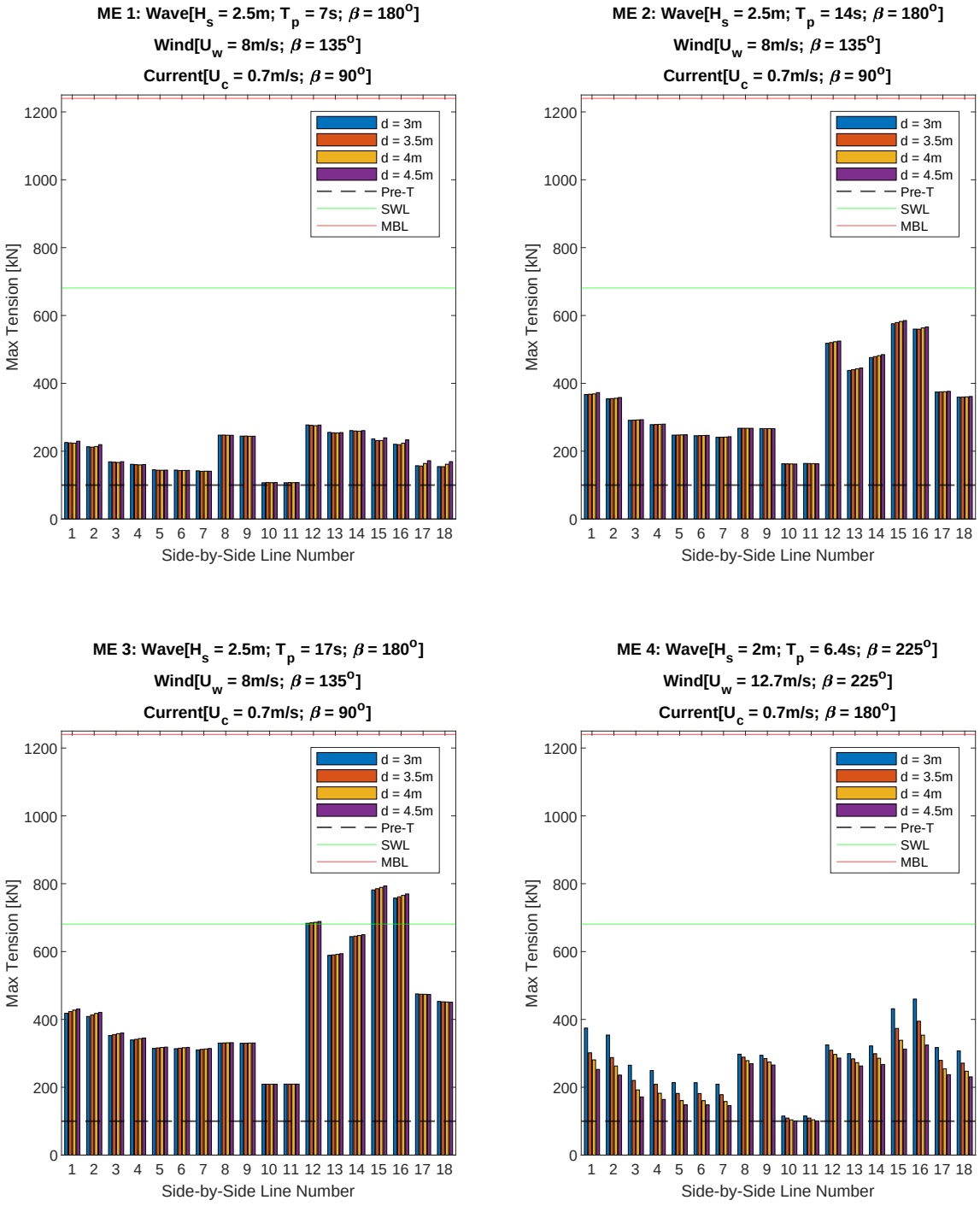

Figure B.14: Line tensions for environmental conditions from ME1 to ME4 using the range of separation distances [mooring configuration used: FLNGmax-LNGCmin]

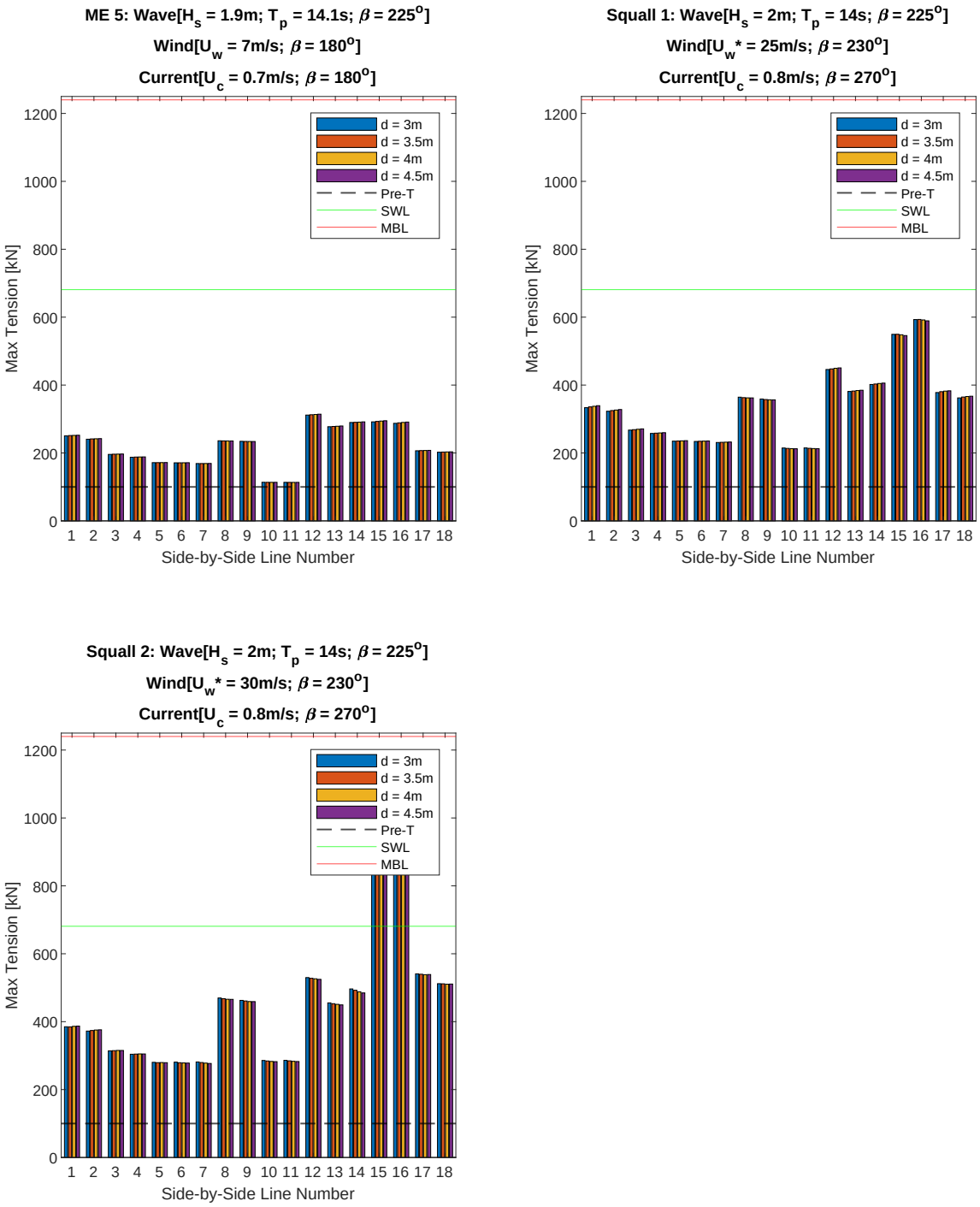

Figure B.15: Line tensions for environmental conditions from ME5 to Squall2 using the range of separation distances [mooring configuration used: FLNGmax-LNGCmin]

B.4.3. Fender Reaction Loads

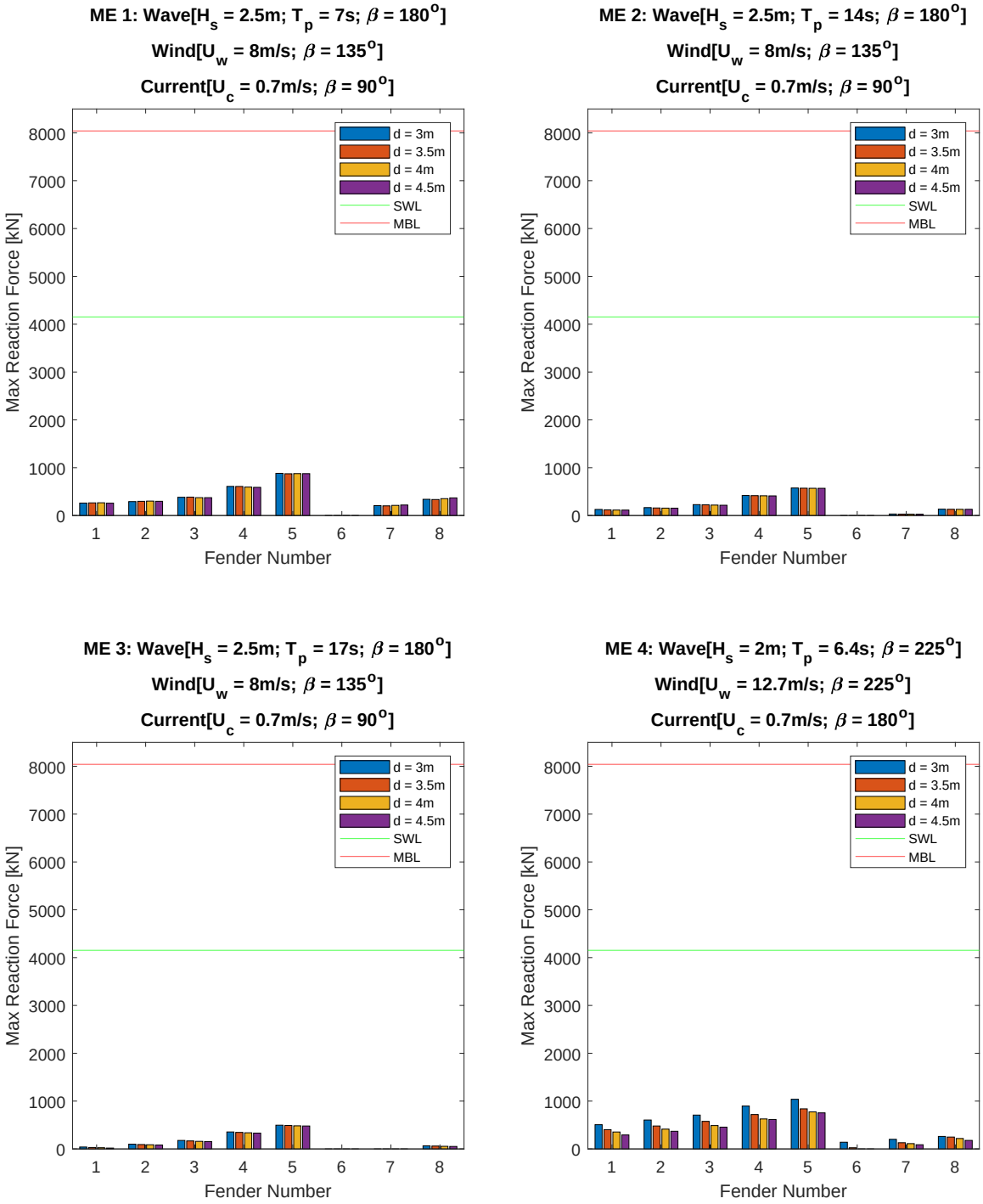

Figure B.16: Fender reaction loads for environmental conditions from ME1 to ME4 using the range of gap length [mooring configuration used: FLNGmax-LNGCmin]

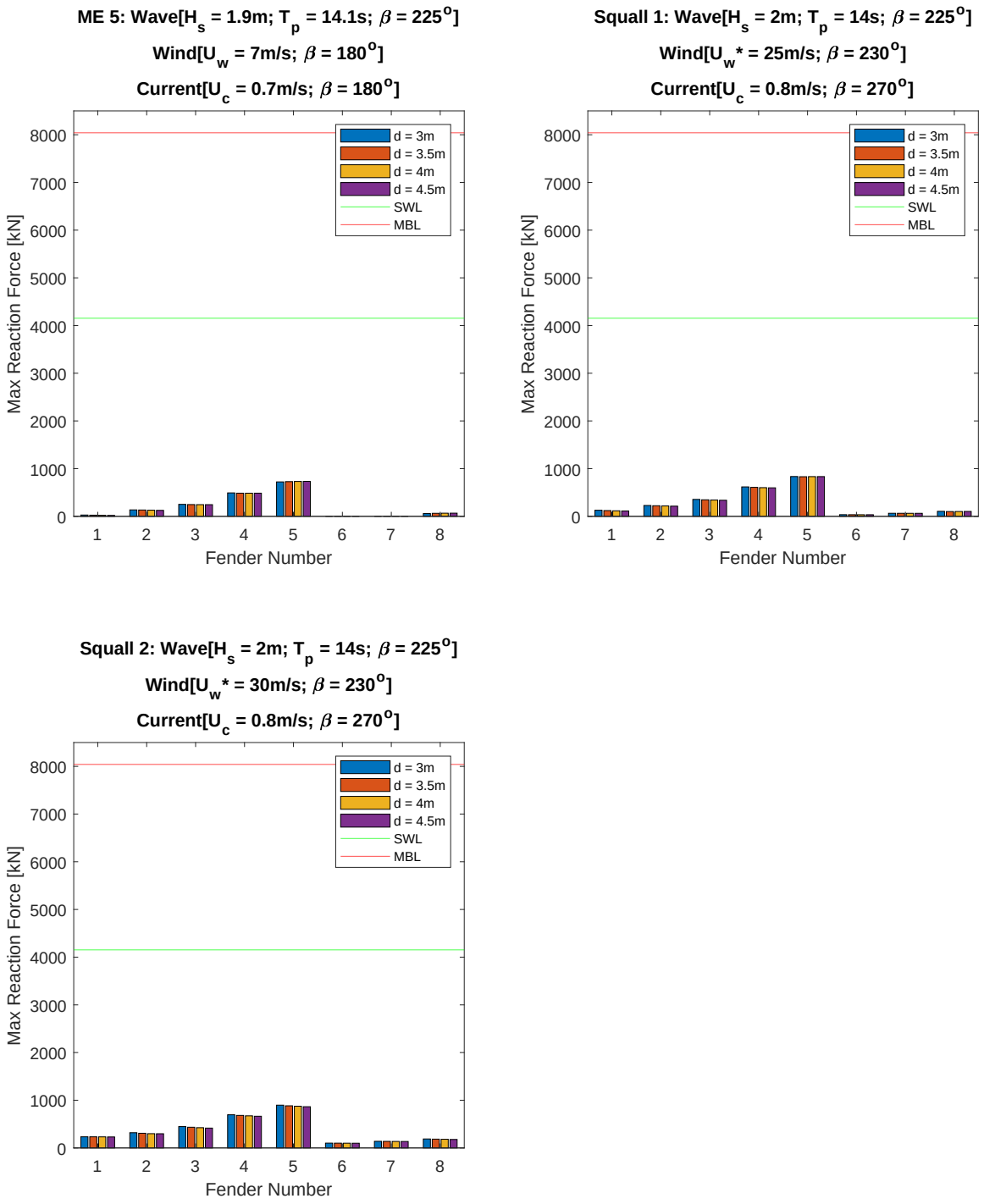

Figure B.17: Fender reaction loads for environmental conditions from ME5 to Squall2 using the range of gap length [mooring configuration used: FLNGmax-LNGCmin]

B.5. Loading condition and carrier size variation. Mooring line optimization

B.5.1. FLNG-LNGC

Relative motions

			Absolute values of relative motion at manifold																Criteria[m]
			Mean				Max				Min				Stdv				
	DoF	Env.cond	FLNGmax-LNGCmin	FLNGmin-LNGCmax	Optimized FLNGmax-LNGCmin	Optimized FLNGmin-LNGCmax	FLNGmax-LNGCmin	FLNGmin-LNGCmax	Optimized FLNGmax-LNGCmin	Optimized FLNGmin-LNGCmax	FLNGmax-LNGCmin	FLNGmin-LNGCmax	Optimized FLNGmax-LNGCmin	Optimized FLNGmin-LNGCmax	FLNGmax-LNGCmin	FLNGmin-LNGCmax	Optimized FLNGmax-LNGCmin	Optimized FLNGmin-LNGCmax	
wave frequency	Heave [m]	ME1	0.00	0.00	0.00	0.00	0.09	0.09	0.09	0.09	0.10	0.09	0.10	0.09	0.03	0.03	0.03	0.03	1.50
		ME2	0.00	0.00	0.00	0.00	0.26	0.34	0.26	0.34	0.26	0.22	0.26	0.22	0.07	0.07	0.07	0.07	
		ME3	0.00	0.00	0.00	0.00	0.22	0.26	0.22	0.26	0.12	0.19	0.12	0.19	0.05	0.06	0.05	0.06	
		ME4	0.00	0.00	0.00	0.00	0.07	0.06	0.07	0.06	0.06	0.05	0.06	0.05	0.02	0.01	0.02	0.01	
		ME5	0.00	0.00	0.00	0.00	0.29	0.30	0.29	0.30	0.23	0.24	0.23	0.24	0.06	0.06	0.06	0.06	
		Squall1	0.00	0.00	0.00	0.00	0.22	0.17	0.22	0.17	0.17	0.17	0.17	0.17	0.05	0.05	0.05	0.05	
		Squall2	0.00	0.00	0.00	0.00	0.41	0.36	0.41	0.36	0.34	0.19	0.34	0.19	0.06	0.05	0.06	0.05	
	Surge [m]	ME1	0.00	0.00	0.00	0.00	0.03	0.02	0.03	0.02	0.01	0.03	0.01	0.03	0.00	0.00	0.00	0.00	2.00
		ME2	0.00	0.00	0.00	0.00	0.84	0.60	0.84	0.60	1.12	0.56	1.12	0.56	0.16	0.08	0.16	0.08	
		ME3	0.00	0.00	0.00	0.00	0.31	1.14	0.31	1.14	0.02	1.43	0.02	1.43	0.08	0.33	0.08	0.33	
		ME4	0.00	0.00	0.00	0.00	0.00	0.01	0.00	0.01	0.00	0.00	0.00	0.00	0.00	0.00	0.00	0.00	
		ME5	0.00	0.00	0.00	0.00	0.01	0.03	0.01	0.03	-0.01	0.02	0.01	0.02	0.00	0.00	0.00	0.00	
		Squall1	0.00	0.00	0.00	0.00	0.02	0.16	0.02	0.16	0.31	0.13	0.31	0.12	0.00	0.00	0.00	0.00	
		Squall2	0.00	0.00	0.00	0.00	0.11	0.00	0.11	0.00	0.43	0.11	0.43	0.12	0.00	0.00	0.00	0.00	
	Sway [m]	ME1	0.00	0.00	0.00	0.00	0.00	0.00	0.00	0.00	0.04	0.04	0.03	0.04	0.00	0.00	0.00	0.00	1.50
		ME2	0.00	0.00	0.00	0.00	0.26	0.07	0.26	0.07	0.98	0.15	0.98	0.15	0.11	0.02	0.11	0.02	
		ME3	0.00	0.00	0.00	0.00	0.18	0.18	0.18	0.18	0.43	0.54	0.43	0.54	0.09	0.13	0.09	0.13	
		ME4	0.00	0.00	0.00	0.00	0.01	0.02	0.01	0.02	0.01	0.01	0.00	0.01	0.00	0.00	0.00	0.00	
		ME5	0.00	0.00	0.00	0.00	0.19	0.30	0.19	0.30	0.50	0.21	0.50	0.21	0.04	0.03	0.04	0.03	
		Squall1	0.00	0.00	0.00	0.00	0.06	0.01	0.06	0.01	0.90	0.34	0.90	0.34	0.01	0.00	0.01	0.00	
		Squall2	0.00	0.00	0.00	0.00	0.05	0.02	0.04	0.01	1.35	0.11	1.35	0.11	0.02	0.00	0.02	0.01	
	Heading [deg]	ME1	0.00	0.00	0.00	0.00	0.04	0.04	0.04	0.04	0.02	0.01	0.02	0.01	0.00	0.00	0.00	0.00	-
		ME2	0.00	0.00	0.00	0.00	0.06	0.03	0.06	0.02	0.05	0.03	0.05	0.03	0.00	0.01	0.00	0.01	
		ME3	0.00	0.00	0.00	0.00	0.11	0.08	0.11	0.08	0.17	0.05	0.17	0.05	0.00	0.02	0.00	0.02	
		ME4	0.00	0.00	0.00	0.00	0.00	0.02	0.00	0.02	0.01	0.01	0.01	0.01	0.00	0.00	0.00	0.00	
		ME5	0.00	0.00	0.00	0.00	0.09	0.03	0.09	0.02	0.01	0.01	0.01	0.01	0.00	0.01	0.00	0.01	
		Squall1	0.00	0.00	0.00	0.00	0.04	0.02	0.03	0.02	0.04	0.01	0.04	0.01	0.00	0.00	0.00	0.00	
		Squall2	0.00	0.00	0.00	0.00	0.03	0.10	0.02	0.11	0.01	0.02	0.01	0.02	0.00	0.00	0.00	0.00	
	Relative distance [m]	ME1	0.00	0.00	0.00	0.00	0.10	0.10	0.10	0.10	0.11	0.10	0.11	0.11	0.03	0.03	0.03	0.03	3.00
		ME2	0.00	0.00	0.00	0.00	0.92	0.70	0.92	0.70	1.51	0.62	1.51	0.62	0.21	0.11	0.21	0.11	
		ME3	0.00	0.00	0.00	0.00	0.42	1.18	0.42	1.18	0.45	1.54	0.45	1.54	0.13	0.35	0.13	0.35	
		ME4	0.00	0.00	0.00	0.00	0.07	0.06	0.07	0.06	0.06	0.05	0.06	0.05	0.02	0.01	0.02	0.01	
		ME5	0.00	0.00	0.00	0.00	0.35	0.42	0.35	0.42	0.56	0.32	0.56	0.32	0.07	0.07	0.07	0.07	
		Squall1	0.00	0.00	0.00	0.00	0.23	0.23	0.23	0.23	0.97	0.40	0.97	0.40	0.05	0.05	0.05	0.05	
		Squall2	0.00	0.00	0.00	0.00	0.43	0.36	0.43	0.36	1.46	0.25	1.46	0.25	0.06	0.05	0.06	0.05	
Low frequency	Sway [m]	ME1	0.02	0.15	0.01	0.13	0.16	0.03	0.16	0.02	0.02	0.28	0.02	0.26	0.00	0.00	0.00	0.00	4.00
		ME2	0.02	0.01	0.02	0.01	0.06	0.02	0.06	0.03	0.05	0.01	0.05	0.01	0.00	0.00	0.00	0.00	
		ME3	0.03	0.00	0.03	0.00	0.00	0.03	0.00	0.03	0.06	0.01	0.06	0.02	0.00	0.00	0.00	0.00	
		ME4	0.06	0.10	0.06	0.09	0.23	0.33	0.23	0.32	0.46	0.03	0.45	0.03	0.07	0.05	0.07	0.05	
		ME5	0.01	0.03	0.01	0.03	0.04	0.06	0.04	0.06	0.05	0.06	0.05	0.07	0.00	0.00	0.00	0.00	
		Squall1	2.56	2.56	2.56	2.55	5.90	5.69	5.90	5.67	0.02	0.02	0.02	0.02	1.77	1.76	1.77	1.75	
		Squall2	2.27	2.27	2.27	2.26	6.65	6.47	6.64	6.44	0.43	0.43	0.43	0.43	1.55	1.55	1.55	1.54	
	Surge [m]	ME1	0.19	0.02	0.19	0.02	0.01	0.22	0.01	0.22	0.37	0.09	0.36	0.09	0.04	0.04	0.04	0.04	
		ME2	0.01	0.00	0.01	0.00	0.10	0.09	0.10	0.09	0.15	0.19	0.15	0.19	0.02	0.02	0.02	0.02	
		ME3	0.02	0.05	0.03	0.04	0.08	0.00	0.08	0.00	0.06	0.01	0.06	0.01	0.01	0.01	0.01	0.01	
		ME4	0.07	0.18	0.07	0.17	0.69	0.80	0.68	0.78	0.15	0.08	0.15	0.08	0.08	0.07	0.08	0.07	
		ME5	0.03	0.01	0.03	0.00	0.16	0.12	0.16	0.12	0.10	0.12	0.10	0.12	0.04	0.04	0.04	0.04	
		Squall1	3.17	3.15	3.17	3.15	1.92	1.53	1.92	1.54	4.95	4.90	4.95	4.90	1.98	2.03	1.98	2.03	
		Squall2	4.47	4.35	4.47	4.35	5.21	4.14	5.21	4.14	6.77	6.68	6.77	6.68	1.25	1.43	1.25	1.43	
	Heading [deg]	ME1	0.32	0.28	0.32	0.28	0.22	0.18	0.23	0.18	0.44	0.35	0.44	0.35	0.02	0.02	0.02	0.02	-
		ME2	0.30	0.25	0.30	0.25	0.17	0.16	0.17	0.16	0.43	0.34	0.43	0.34	0.01	0.01	0.01	0.01	
		ME3	0.30	0.24	0.30	0.24	0.21	0.19	0.21	0.19	0.37	0.27	0.37	0.27	0.01	0.01	0.01	0.01	
		ME4	0.28	0.24	0.28	0.24	0.13	0.20	0.13	0.20	0.77	0.52	0.77	0.53	0.05	0.04	0.05	0.04	
		ME5	0.30	0.25	0.30	0.25	0.20	0.20	0.20	0.20	0.37	0.33	0.37	0.33	0.01	0.01	0.01	0.01	
		Squall1	0.31	0.27	0.31	0.28	0.18	0.17	0.19	0.17	0.31	0.25	0.31	0.25	0.00	0.01	0.00	0.01	
		Squall2	0.32	0.28	0.32	0.27	0.25	0.19	0.25	0.18	0.30	0.23	0.30	0.23	0.01	0.02	0.01	0.02	

Figure B.18: Relative motions at the manifold location and maximum allowable criteria for FLNG-LNGC configuration

Line Tensions

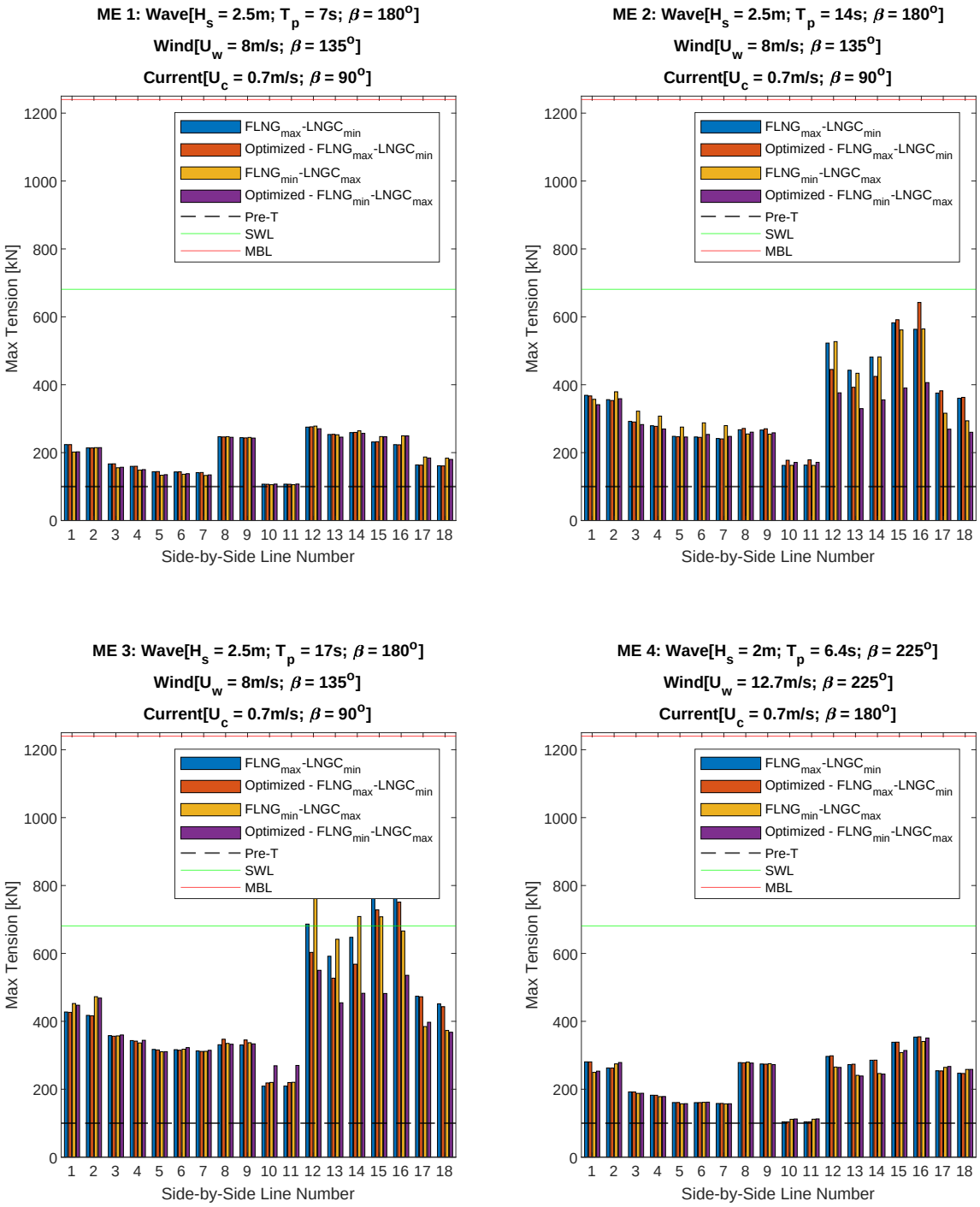

Figure B.19: Line tensions for environmental conditions from ME1 to ME4 for FLNG-LNGC initial and optimized configuration

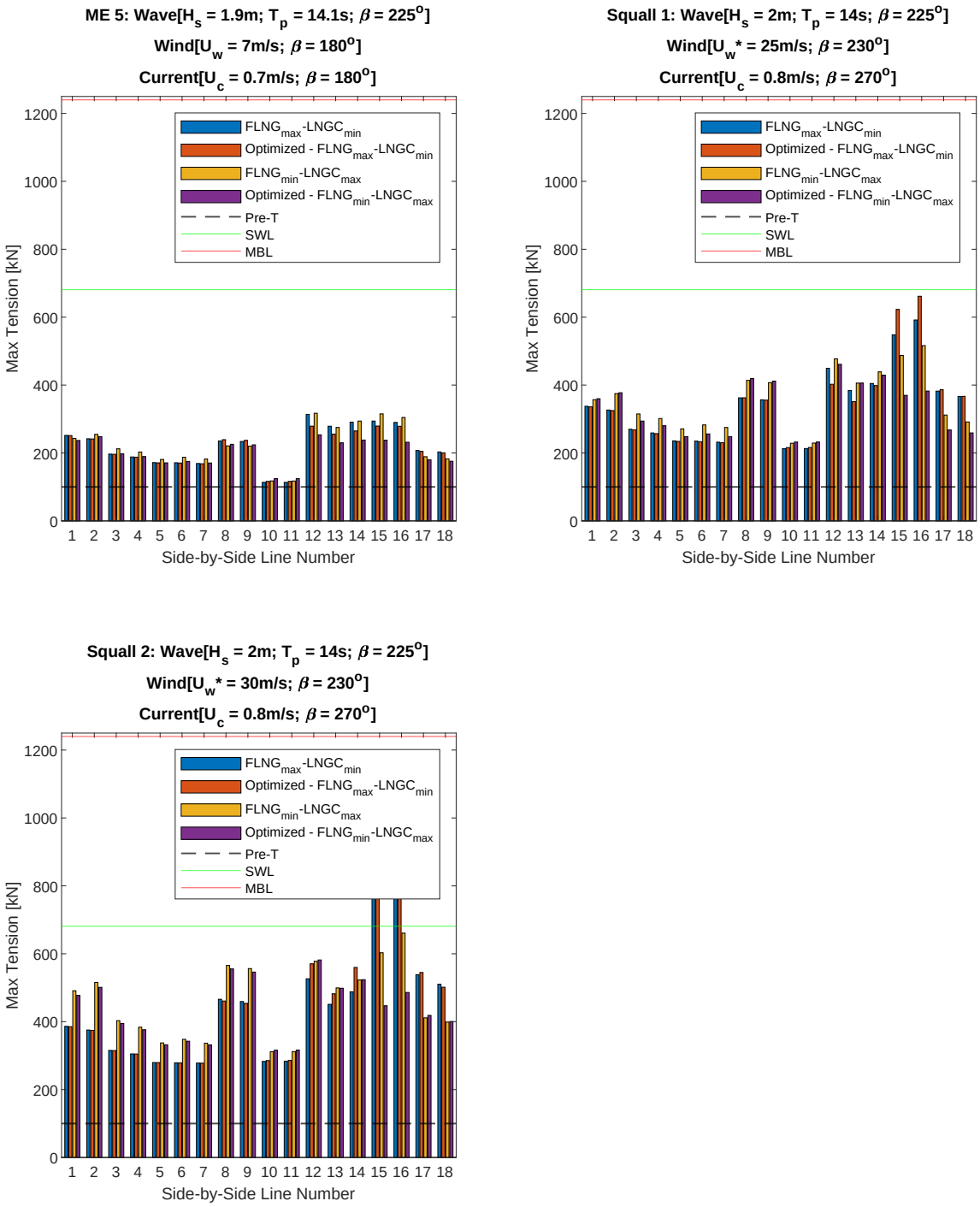

Figure B.20: Line tensions for environmental conditions from ME5 to Squall2 for FLNG-LNGC initial and optimized configuration

Fender Reaction Forces

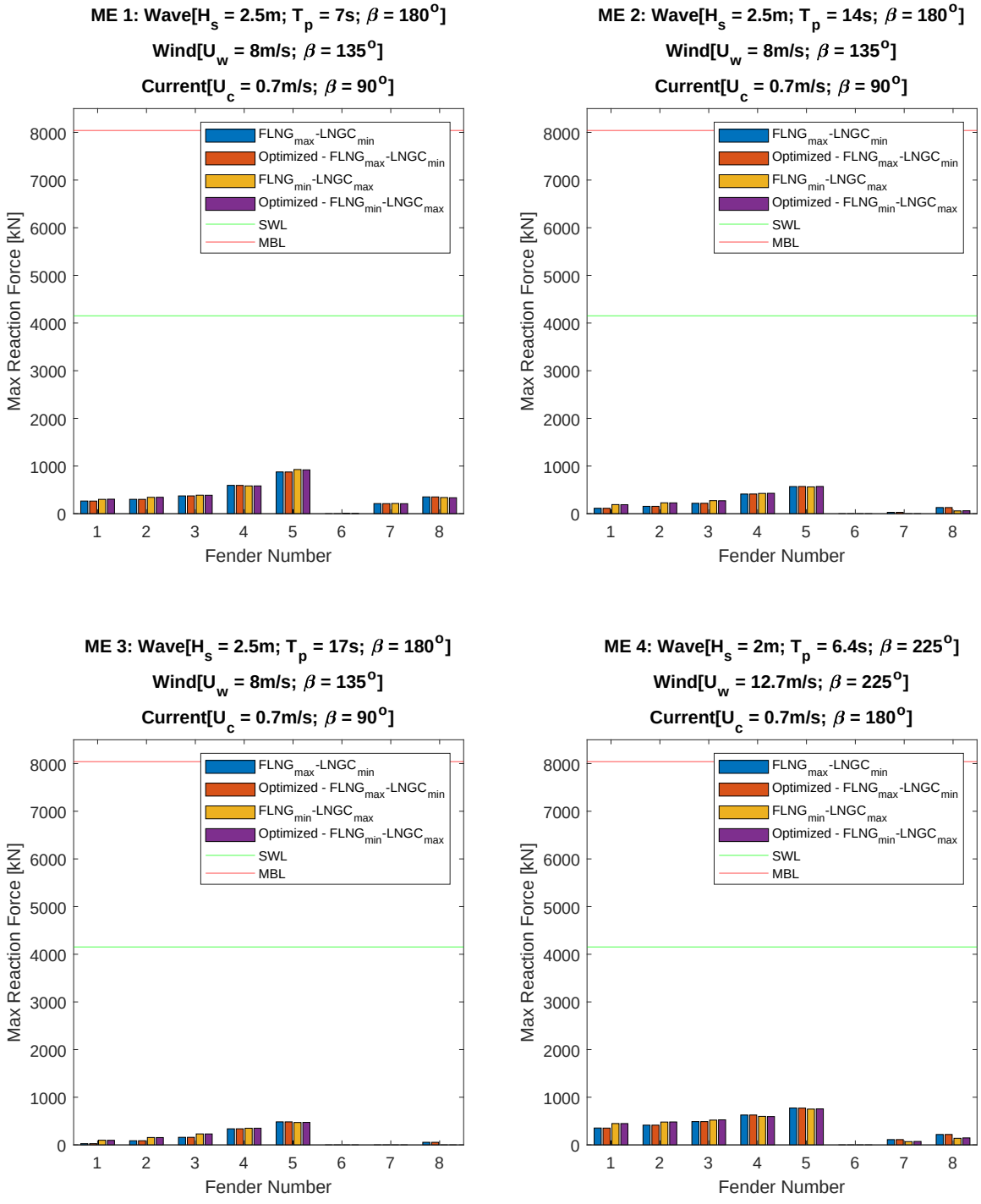

Figure B.21: Fender reaction forces for environmental conditions from ME1 to ME4 for FLNG-LNGC initial and optimized configuration

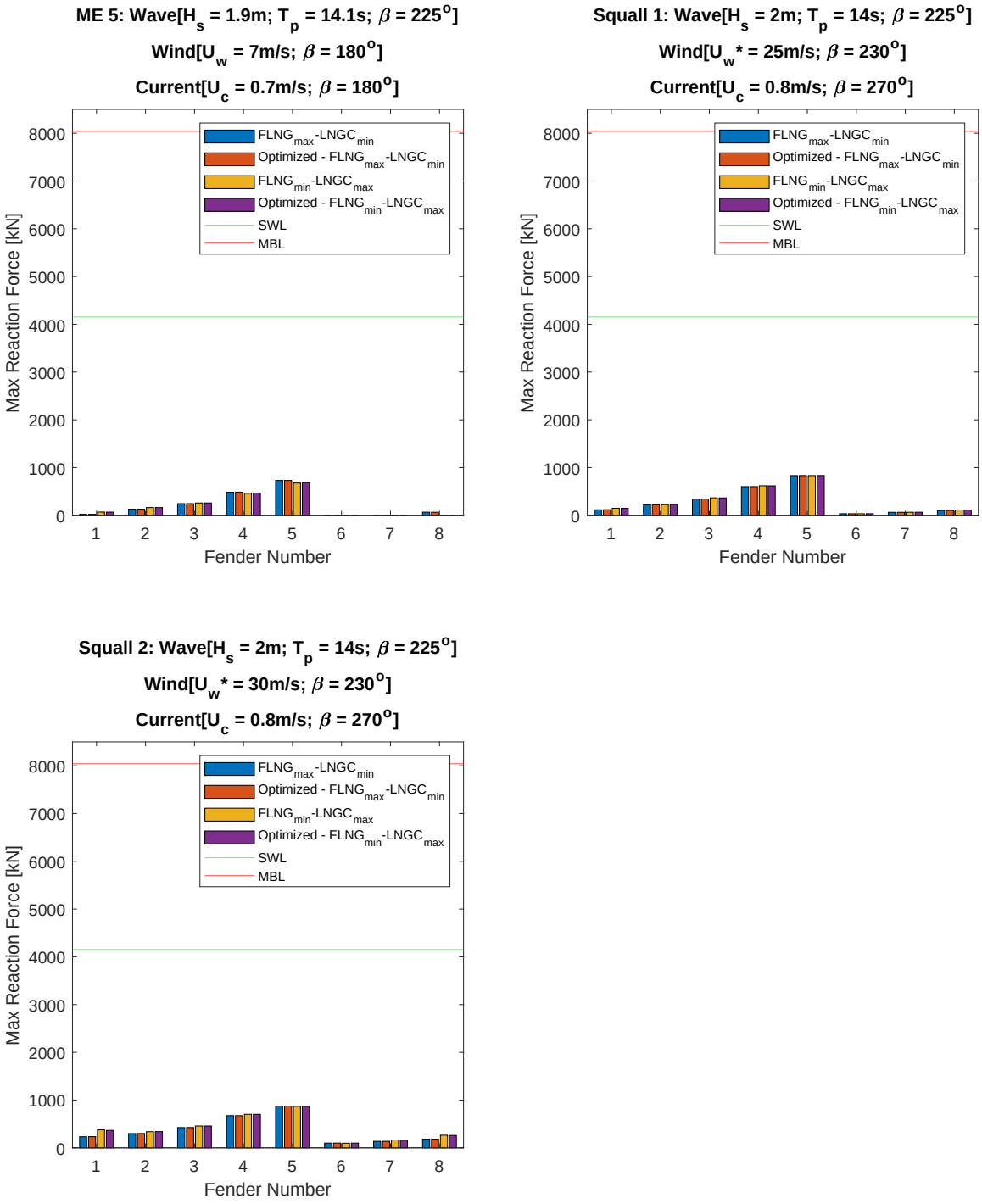

Figure B.22: Fender reaction forces for environmental conditions from ME5 to Squall2 for FLNG-LNGC initial and optimized configuration

B.5.2. FLNG-LPGC

Relative motions

			Absolute values of relative motion at manifold																
			Mean				Max				Min				Stdv				Criteria[m]
	DoF	Env.cond	FLNGmax-LPGCmin	FLNGmin-LPGCmax	Optimized FLNGmax-LPGCmin	Optimized FLNGmin-LPGCmax	FLNGmax-LPGCmin	FLNGmin-LPGCmax	Optimized FLNGmax-LPGCmin	Optimized FLNGmin-LPGCmax	FLNGmax-LPGCmin	FLNGmin-LPGCmax	Optimized FLNGmax-LPGCmin	Optimized FLNGmin-LPGCmax	FLNGmax-LPGCmin	FLNGmin-LPGCmax	Optimized FLNGmax-LPGCmin	Optimized FLNGmin-LPGCmax	
wave frequency	Heave [m]	ME1	0.00	0.00	0.00	0.00	0.35	0.48	0.35	0.48	0.40	0.45	0.39	0.45	0.11	0.13	0.11	0.13	1.50
		ME2	0.00	0.00	0.00	0.00	1.18	1.21	1.18	1.22	1.19	1.13	1.19	1.13	0.33	0.34	0.33	0.34	
		ME3	0.00	0.00	0.00	0.00	0.52	0.63	0.52	0.63	0.81	0.91	0.81	0.91	0.19	0.21	0.19	0.21	
		ME4	0.00	0.00	0.00	0.00	0.20	0.23	0.20	0.23	0.21	0.23	0.21	0.23	0.05	0.06	0.05	0.06	
		ME5	0.00	0.00	0.00	0.00	0.96	0.97	0.96	0.97	0.93	0.91	0.93	0.91	0.28	0.28	0.28	0.28	
		Squall1	0.00	0.00	0.00	0.00	0.63	0.73	0.63	0.73	0.81	0.74	0.81	0.74	0.17	0.17	0.17	0.17	
		Squall2	0.00	0.00	0.00	0.00	0.62	0.78	0.62	0.78	0.90	0.98	0.90	0.98	0.13	0.15	0.13	0.15	
	Surge [m]	ME1	0.00	0.00	0.00	0.00	0.06	0.04	0.06	0.05	0.25	0.07	0.12	0.09	0.00	0.00	0.00	0.00	2.00
		ME2	0.00	0.00	0.00	0.00	0.18	0.64	0.19	0.66	0.69	0.99	0.68	0.98	0.04	0.10	0.04	0.10	
		ME3	0.00	0.00	0.00	0.00	0.05	0.31	0.04	0.31	0.20	0.25	0.19	0.26	0.02	0.07	0.02	0.07	
		ME4	0.00	0.00	0.00	0.00	0.06	0.03	0.01	0.03	0.00	0.06	0.01	0.06	0.00	0.00	0.00	0.00	
		ME5	0.00	0.00	0.00	0.00	0.34	0.24	0.33	0.26	0.36	0.19	0.35	0.21	0.09	0.07	0.09	0.07	
		Squall1	0.00	0.00	0.00	0.00	0.30	0.01	0.30	0.02	0.03	0.37	0.03	0.37	0.00	0.00	0.00	0.00	
		Squall2	0.00	0.00	0.00	0.00	0.08	0.34	0.06	0.35	0.14	0.35	0.14	0.33	0.00	0.00	0.00	0.00	
	Sway [m]	ME1	0.00	0.00	0.00	0.00	0.06	0.05	0.06	0.03	0.01	0.01	0.03	0.02	0.00	0.00	0.00	0.00	1.50
		ME2	0.00	0.00	0.00	0.00	0.17	0.03	0.17	0.03	0.61	0.37	0.61	0.37	0.04	0.04	0.04	0.04	
		ME3	0.00	0.00	0.00	0.00	0.03	0.04	0.03	0.04	0.06	0.11	0.06	0.08	0.01	0.01	0.01	0.01	
		ME4	0.00	0.00	0.00	0.00	0.01	0.00	0.01	0.03	-0.01	0.06	0.02	0.03	0.00	0.00	0.00	0.00	
		ME5	0.00	0.00	0.00	0.00	0.07	0.30	0.08	0.30	0.18	0.44	0.18	0.43	0.01	0.04	0.01	0.04	
		Squall1	0.00	0.00	0.00	0.00	0.41	0.20	0.40	0.25	0.61	0.52	0.61	0.54	0.01	0.01	0.00	0.01	
		Squall2	0.00	0.00	0.00	0.00	0.19	0.15	0.19	0.16	0.28	0.16	0.28	0.19	0.01	0.02	0.02	0.02	
	Heading [deg]	ME1	0.00	0.00	0.00	0.00	0.11	0.10	0.12	0.12	0.06	0.24	0.09	0.17	0.00	0.00	0.01	0.00	-
		ME2	0.00	0.00	0.00	0.00	0.07	0.20	0.07	0.22	0.09	0.36	0.08	0.34	0.04	0.03	0.08	0.03	
		ME3	0.00	0.00	0.00	0.00	0.03	0.21	0.03	0.20	0.16	0.19	0.15	0.19	0.10	0.01	0.09	0.01	
		ME4	0.00	0.00	0.00	0.00	0.06	0.09	0.06	0.09	0.06	0.04	0.03	0.01	0.00	0.01	0.01	0.01	
		ME5	0.00	0.00	0.00	0.00	0.05	0.20	0.06	0.20	0.14	0.26	0.14	0.24	0.02	0.02	0.06	0.02	
		Squall1	0.00	0.00	0.00	0.00	0.03	0.15	0.02	0.15	0.13	0.22	0.13	0.24	0.00	0.00	0.00	0.00	
		Squall2	0.00	0.00	0.00	0.00	0.03	0.12	0.03	0.12	0.01	0.08	0.01	0.12	0.00	0.00	0.00	0.00	
	Relative distance [m]	ME1	0.00	0.00	0.00	0.00	0.36	0.48	0.36	0.48	0.47	0.45	0.42	0.46	0.11	0.13	0.11	0.13	3.00
		ME2	0.00	0.00	0.00	0.00	1.21	1.37	1.21	1.38	1.51	1.55	1.50	1.54	0.34	0.36	0.34	0.36	
		ME3	0.00	0.00	0.00	0.00	0.53	0.70	0.53	0.70	0.83	0.95	0.83	0.95	0.20	0.22	0.20	0.22	
		ME4	0.00	0.00	0.00	0.00	0.21	0.23	0.20	0.23	0.21	0.24	0.21	0.24	0.05	0.06	0.05	0.06	
		ME5	0.00	0.00	0.00	0.00	1.02	1.04	1.02	1.05	1.01	1.03	1.01	1.03	0.30	0.29	0.30	0.29	
		Squall1	0.00	0.00	0.00	0.00	0.81	0.76	0.81	0.78	1.02	0.98	1.02	0.99	0.17	0.18	0.17	0.18	
		Squall2	0.00	0.00	0.00	0.00	0.65	0.86	0.65	0.87	0.95	1.05	0.95	1.05	0.13	0.15	0.13	0.15	
Low frequency	Sway [m]	ME1	0.18	0.43	0.17	0.32	0.22	0.09	0.18	0.03	0.00	0.52	0.03	0.35	0.01	0.01	0.01	0.00	4.00
		ME2	0.00	0.14	0.00	0.10	0.02	0.07	0.01	0.05	0.01	0.05	0.01	0.07	0.02	0.01	0.02	0.01	
		ME3	0.01	0.08	0.01	0.04	0.01	0.04	0.01	0.02	0.01	0.03	0.01	0.03	0.01	0.01	0.01	0.01	
		ME4	0.01	0.52	0.01	0.51	0.12	0.26	0.10	0.26	0.46	0.25	0.41	0.19	0.02	0.03	0.02	0.03	
		ME5	0.01	0.10	0.01	0.09	0.08	0.05	0.07	0.05	0.05	0.06	0.05	0.06	0.00	0.00	0.00	0.00	
		Squall1	2.07	4.66	2.04	4.43	4.84	2.76	4.79	2.66	0.39	1.89	0.40	1.78	1.32	1.42	1.30	1.35	
		Squall2	1.12	4.27	1.09	3.99	4.59	3.34	4.51	3.19	0.49	0.93	0.50	0.80	0.99	1.10	0.96	1.03	
	Surge [m]	ME1	0.27	0.50	0.25	0.32	0.06	0.25	0.04	0.16	0.53	0.23	0.56	0.12	0.05	0.05	0.05	0.05	
		ME2	0.02	0.41	0.01	0.36	0.12	0.20	0.12	0.18	0.16	0.11	0.17	0.11	0.02	0.03	0.02	0.02	
		ME3	0.03	0.15	0.03	0.14	0.12	0.07	0.11	0.07	0.05	0.08	0.05	0.08	0.01	0.01	0.01	0.01	
		ME4	0.03	0.94	0.03	0.76	0.41	0.47	0.37	0.38	0.15	0.11	0.15	0.06	0.03	0.04	0.02	0.03	
		ME5	0.01	0.18	0.01	0.18	0.08	0.09	0.08	0.09	0.03	0.08	0.03	0.04	0.02	0.03	0.02	0.02	
		Squall1	3.62	1.52	3.63	1.37	2.74	0.77	2.70	0.96	6.02	2.29	6.05	2.33	2.12	2.18	2.13	2.20	
		Squall2	5.01	3.20	5.00	2.90	5.19	0.27	5.10	0.07	8.15	2.93	8.16	2.97	1.01	1.11	1.02	1.14	
	Heading [deg]	ME1	0.08	0.07	0.09	0.09	0.01	0.04	0.03	0.07	0.29	0.16	0.36	0.15	0.01	0.00	0.01	0.00	-
		ME2	0.12	0.10	0.12	0.12	0.06	0.02	0.06	0.05	0.21	0.16	0.22	0.19	0.01	0.01	0.01	0.01	
		ME3	0.11	0.10	0.12	0.11	0.08	0.05	0.08	0.06	0.18	0.15	0.18	0.16	0.00	0.00	0.00	0.00	
		ME4	0.10	0.08	0.10	0.10	0.16	0.06	0.13	0.01	0.44	0.20	0.42	0.22	0.01	0.01	0.01	0.01	
		ME5	0.11	0.10	0.11	0.12	0.07	0.05	0.08	0.07	0.12	0.13	0.13	0.15	0.00	0.00	0.00	0.00	
		Squall1	0.13	0.13	0.13	0.14	0.09	0.07	0.09	0.09	0.16	0.14	0.17	0.13	0.01	0.01	0.01	0.01	
		Squall2	0.14	0.14	0.14	0.15	0.07	0.06	0.08	0.07	0.18	0.14	0.19	0.14	0.01	0.01	0.01	0.01	

Figure B.23: Relative motions at the manifold location and maximum allowable criteria for FLNG-LPGC configuration

Line Tensions

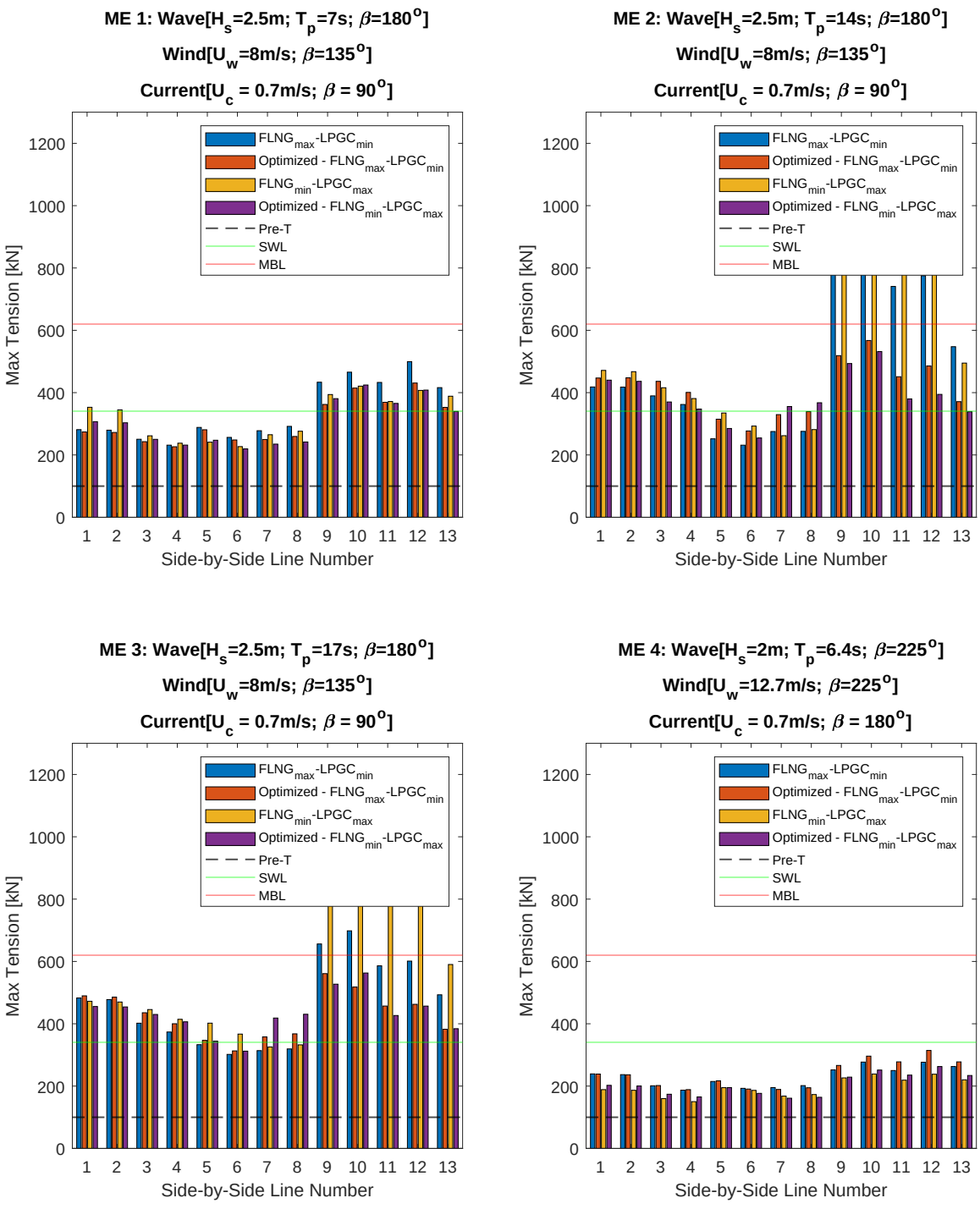

Figure B.24: Line tensions for environmental conditions from ME1 to ME4 for FLNG-LPGC initial and optimized configuration

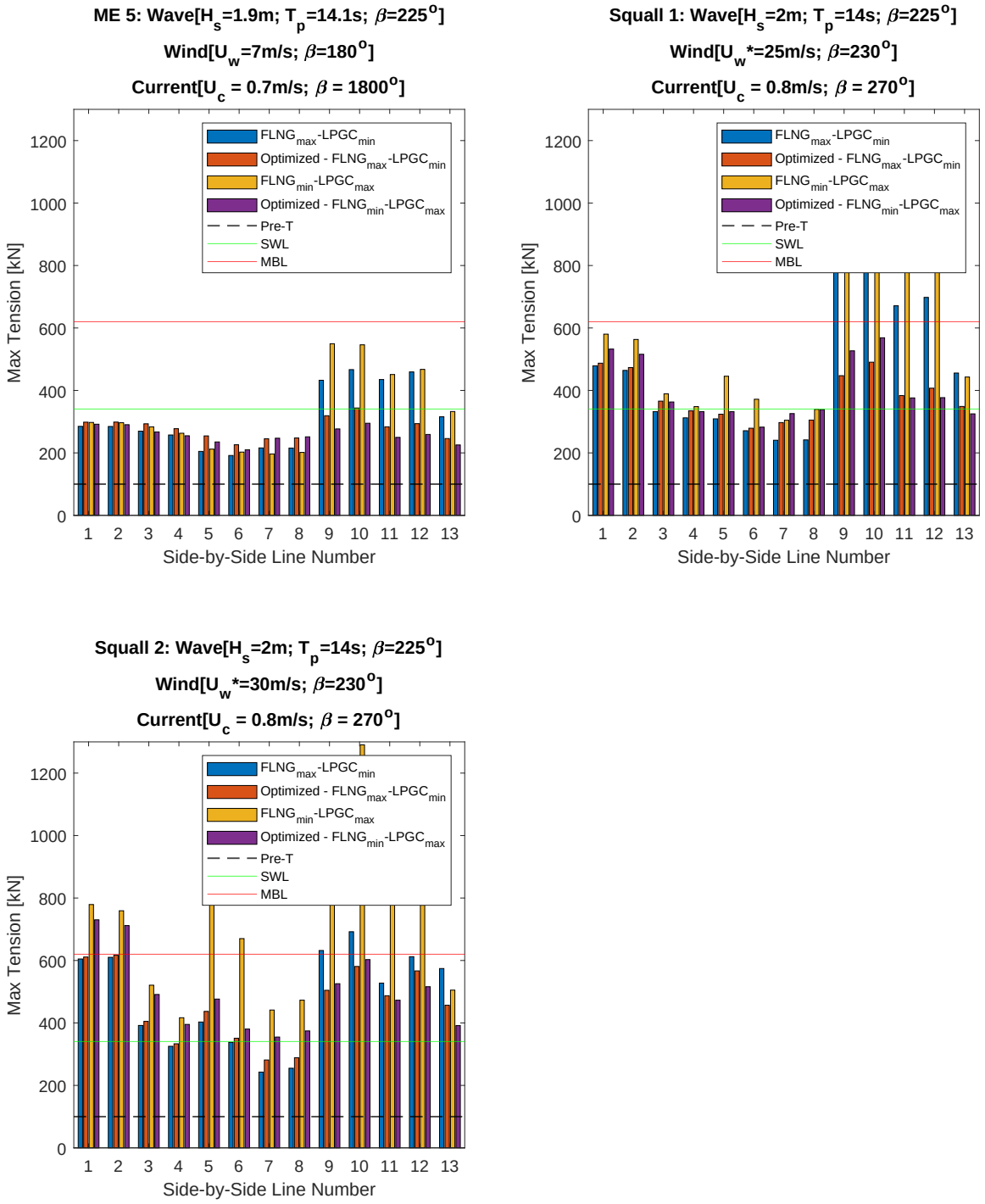

Figure B.25: Line tensions for environmental conditions from ME5 to Squall2 for FLNG-LPGC initial and optimized configuration

Fender Reaction Forces

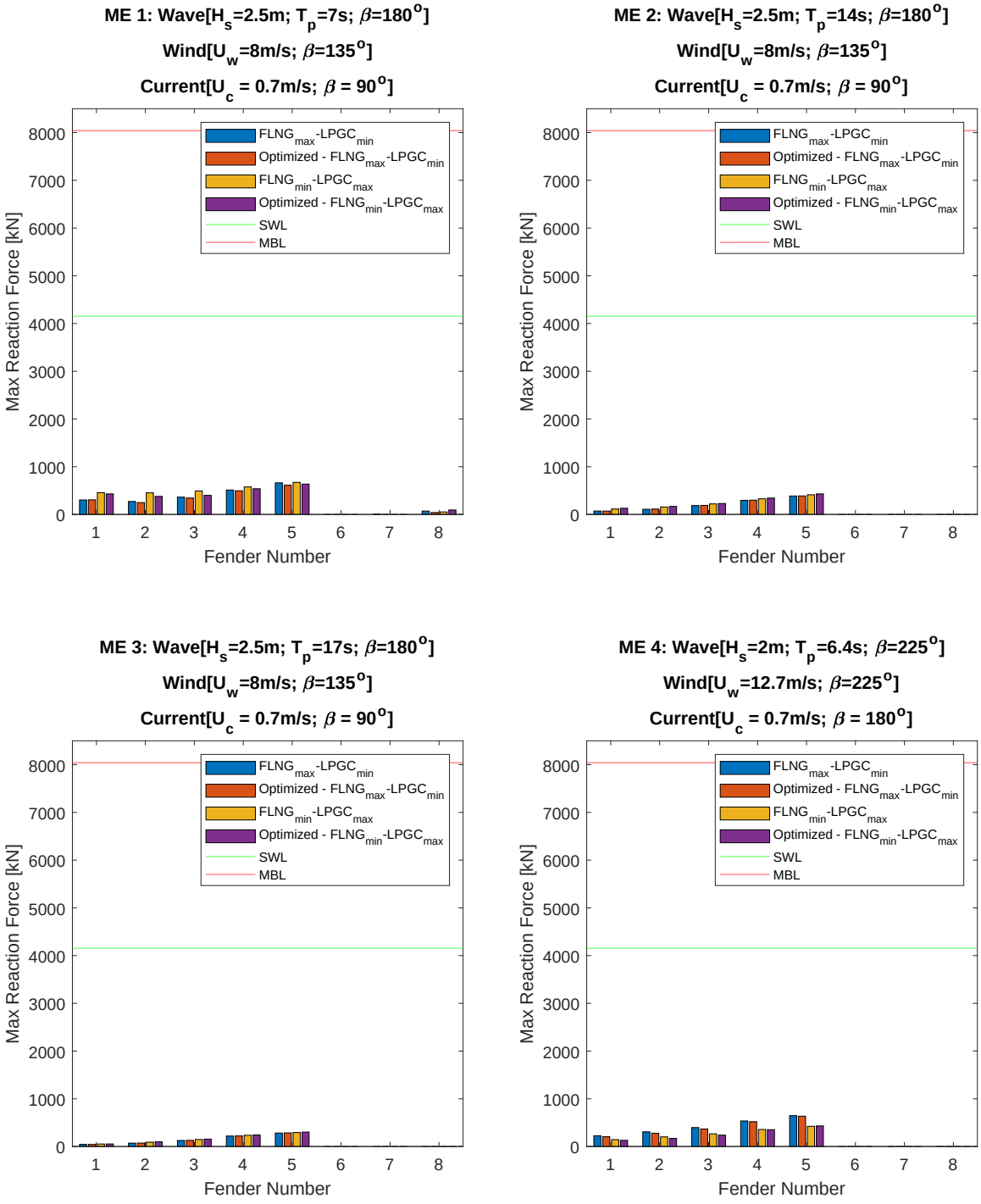

Figure B.26: Fender reaction forces for environmental conditions from ME1 to ME4 for FLNG-LPGC initial and optimized configuration

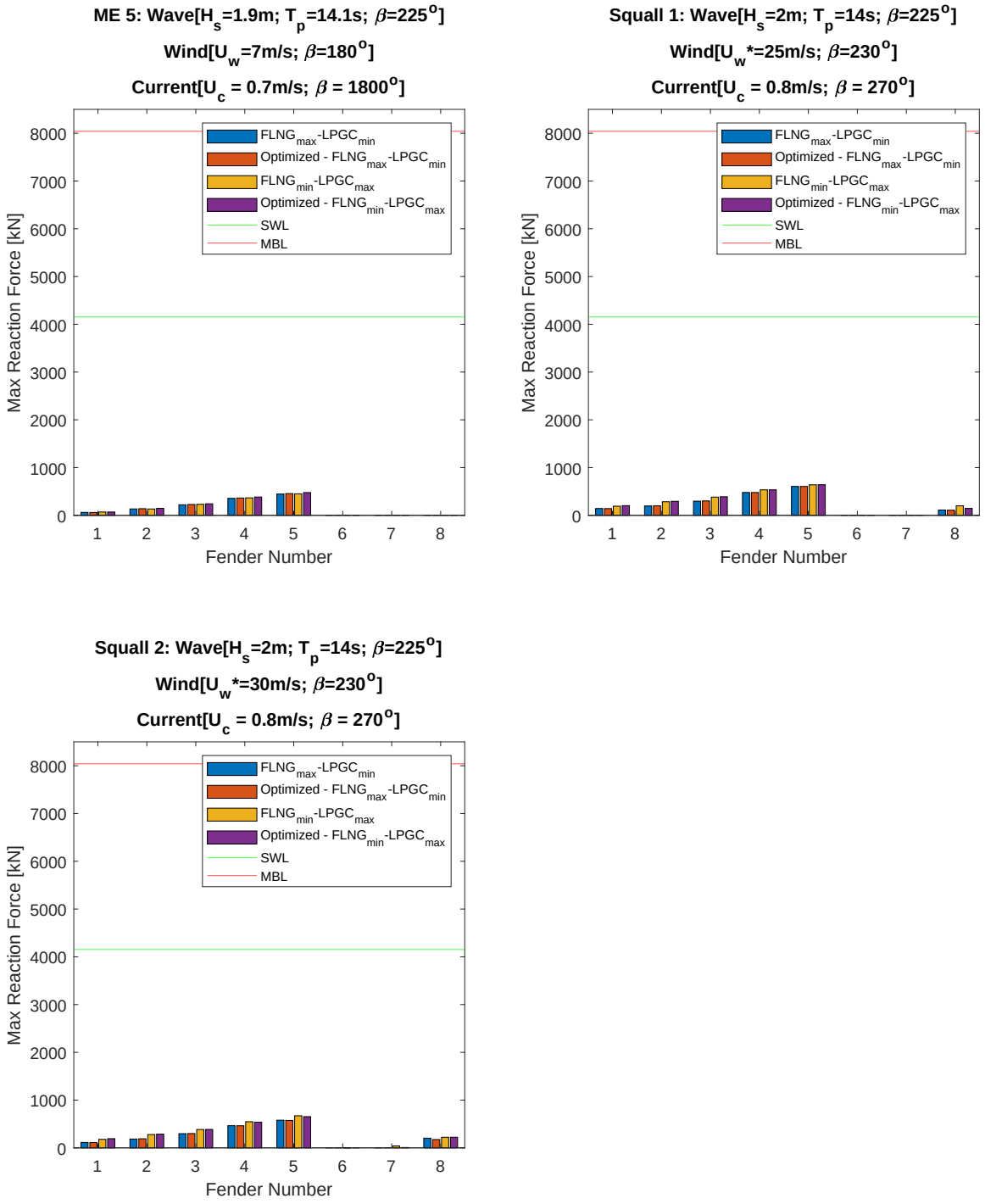

Figure B.27: Fender reaction forces for environmental conditions from ME5 to Squall2 for FLNG-LPGC initial and optimized configuration

B.6. QTFC formulation vs Newman-wave-current formualtion

B.6.1. FLNG-LNGC

Relative motions

			Absolute values of relative motion at manifold								Criteria[m]
			Mean		Max		Min		Stdv		
	DoF	Env.cond	cur/wave	QTFC	cur/wave	QTFC	cur/wave	QTFC	cur/wave	QTFC	
wave frequency	Heave [m]	ME1	0.00	0.00	0.09	0.10	0.10	0.09	0.03	0.03	1.50
		ME2	0.00	0.00	0.26	0.26	0.26	0.25	0.07	0.07	
		ME3	0.00	0.00	0.22	0.23	0.12	0.13	0.05	0.05	
		ME4	0.00	0.00	0.07	0.07	0.06	0.06	0.02	0.02	
		ME5	0.00	0.00	0.29	0.29	0.23	0.23	0.06	0.06	
		Squall1	0.00	0.00	0.22	0.22	0.17	0.17	0.05	0.05	
		Squall2	0.00	0.00	0.41	0.37	0.34	0.46	0.06	0.06	
	Surge [m]	ME1	0.00	0.00	0.03	0.01	0.01	0.02	0.04	0.03	2.00
		ME2	0.00	0.00	0.84	0.82	1.12	1.04	0.06	0.05	
		ME3	0.00	0.00	0.31	0.16	0.02	0.20	0.06	0.06	
		ME4	0.00	0.00	0.00	0.01	0.00	0.01	0.00	0.04	
		ME5	0.00	0.00	0.01	0.02	0.01	0.02	0.04	0.04	
		Squall1	0.00	0.00	0.02	0.02	0.31	0.31	2.05	2.08	
		Squall2	0.00	0.00	0.11	0.16	0.43	0.49	1.33	0.97	
	Sway [m]	ME1	0.00	0.00	0.00	0.03	0.04	0.02	0.09	0.11	1.50
		ME2	0.00	0.00	0.26	0.18	0.98	0.89	0.10	0.10	
		ME3	0.00	0.00	0.18	0.15	0.43	0.47	0.10	0.09	
		ME4	0.00	0.00	0.01	0.01	0.01	0.00	0.03	0.08	
		ME5	0.00	0.00	0.19	0.26	0.50	0.42	0.09	0.09	
		Squall1	0.00	0.00	0.06	0.06	0.90	0.90	1.67	1.63	
		Squall2	0.00	0.00	0.05	0.07	1.35	1.48	1.45	1.37	
	Heading [deg]	ME1	0.00	0.00	0.04	0.01	0.02	0.09	0.00	0.00	-
		ME2	0.00	0.00	0.06	0.07	0.05	0.03	0.00	0.00	
		ME3	0.00	0.00	0.11	0.02	0.17	0.31	0.00	0.01	
		ME4	0.00	0.00	0.00	0.04	0.01	0.00	0.00	0.00	
		ME5	0.00	0.00	0.09	0.06	0.01	0.04	0.00	0.00	
		Squall1	0.00	0.00	0.04	0.03	0.04	0.01	0.00	0.00	
		Squall2	0.00	0.00	0.03	0.06	0.01	0.03	0.00	0.00	
	Relative distance [m]	ME1	0.00	0.00	0.01	0.01	0.01	0.01	0.01	0.01	3.00
		ME2	0.00	0.00	0.84	0.78	2.29	1.95	0.02	0.02	
		ME3	0.00	0.00	0.18	0.10	0.20	0.28	0.02	0.01	
		ME4	0.00	0.00	0.00	0.01	0.00	0.00	0.00	0.01	
		ME5	0.00	0.00	0.12	0.15	0.31	0.23	0.01	0.01	
		Squall1	0.00	0.00	0.05	0.05	0.93	0.93	7.01	7.01	
		Squall2	0.00	0.00	0.18	0.17	2.14	2.64	3.88	2.82	
Low frequency	Sway [m]	ME1	0.02	0.01	0.16	0.04	0.02	0.04	0.00	0.01	4.00
		ME2	0.02	0.06	0.06	0.05	0.05	0.22	0.00	0.00	
		ME3	0.03	0.03	0.00	0.08	0.06	0.33	0.00	0.01	
		ME4	0.06	0.02	0.23	0.08	0.46	0.09	0.07	0.02	
		ME5	0.01	0.00	0.04	0.01	0.05	0.02	0.00	0.00	
		Squall1	2.56	2.56	5.90	5.90	0.02	0.02	1.77	1.73	
		Squall2	2.27	2.06	6.65	6.47	0.43	0.48	1.55	1.47	
	Surge [m]	ME1	0.19	0.03	0.01	0.21	0.37	0.15	0.04	0.04	
		ME2	0.01	0.01	0.10	0.17	0.15	0.08	0.02	0.02	
		ME3	0.02	0.01	0.08	0.07	0.06	0.14	0.01	0.02	
		ME4	0.07	0.02	0.69	0.27	0.15	0.06	0.08	0.03	
		ME5	0.03	0.03	0.16	0.15	0.10	0.11	0.04	0.03	
		Squall1	3.17	3.17	1.92	1.92	4.95	4.95	1.98	2.01	
		Squall2	4.47	4.84	5.21	5.95	6.77	7.29	1.25	0.89	
	Heading [deg]	ME1	0.32	0.30	0.22	0.14	0.44	0.39	0.02	0.01	-
		ME2	0.30	0.30	0.17	0.17	0.43	0.43	0.01	0.01	
		ME3	0.30	0.30	0.21	0.24	0.37	0.44	0.01	0.01	
		ME4	0.28	0.25	0.13	0.20	0.77	0.33	0.05	0.01	
		ME5	0.30	0.30	0.20	0.22	0.37	0.41	0.01	0.01	
		Squall1	0.31	0.31	0.18	0.18	0.31	0.30	0.00	0.00	
		Squall2	0.32	0.32	0.25	0.20	0.30	0.30	0.01	0.00	

Figure B.28: Relative motions at the manifold location and maximum allowable criteria for FLNG-LNGC configuration using QTFC and Newman-wave formulation for assessing second order drift forces

Line Tensions

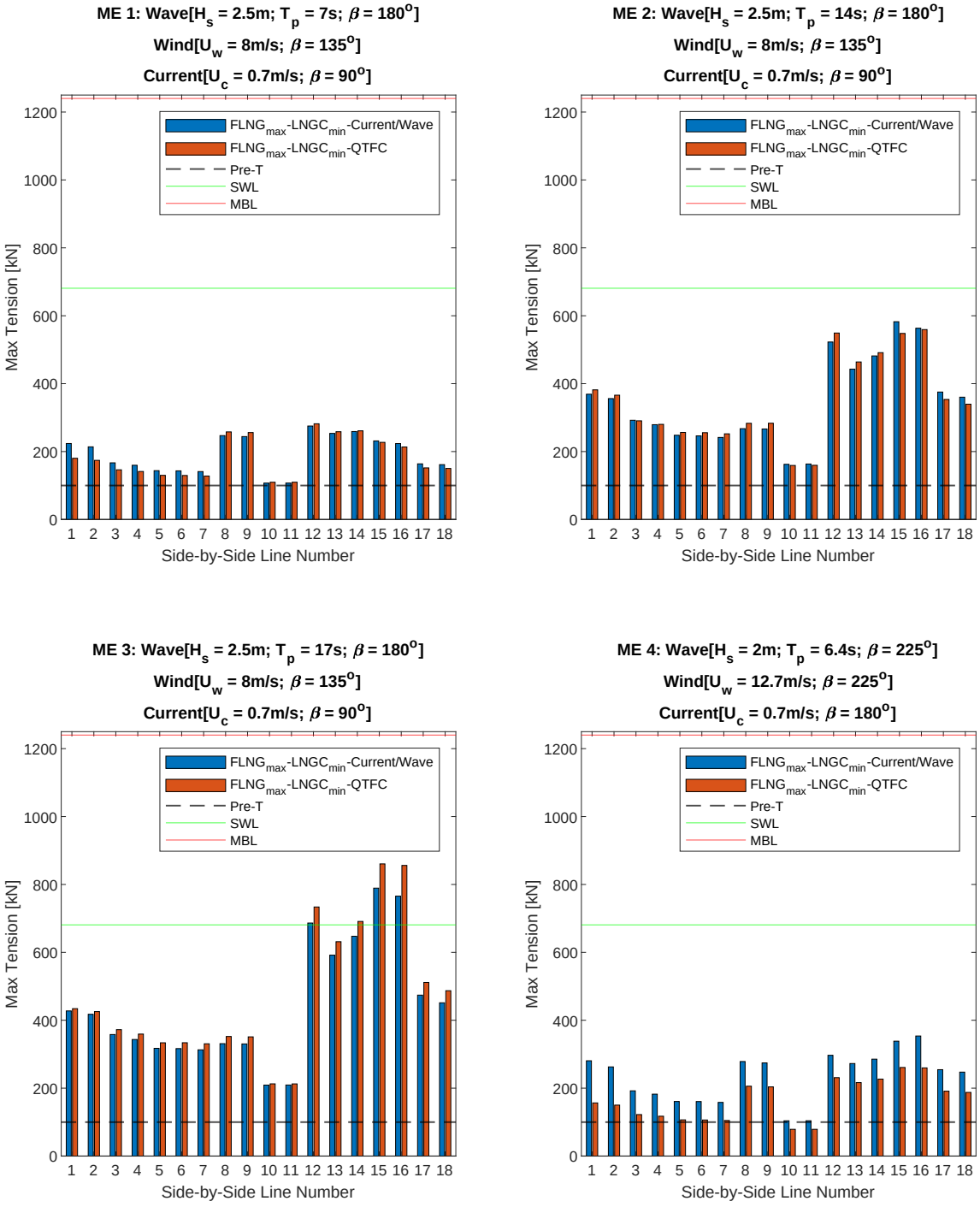

Figure B.29: Line tensions for environmental conditions from ME1 to ME4 for FLNG-LNGC configuration using QTFC and Newman-wave formulation for assessing second order drift forces

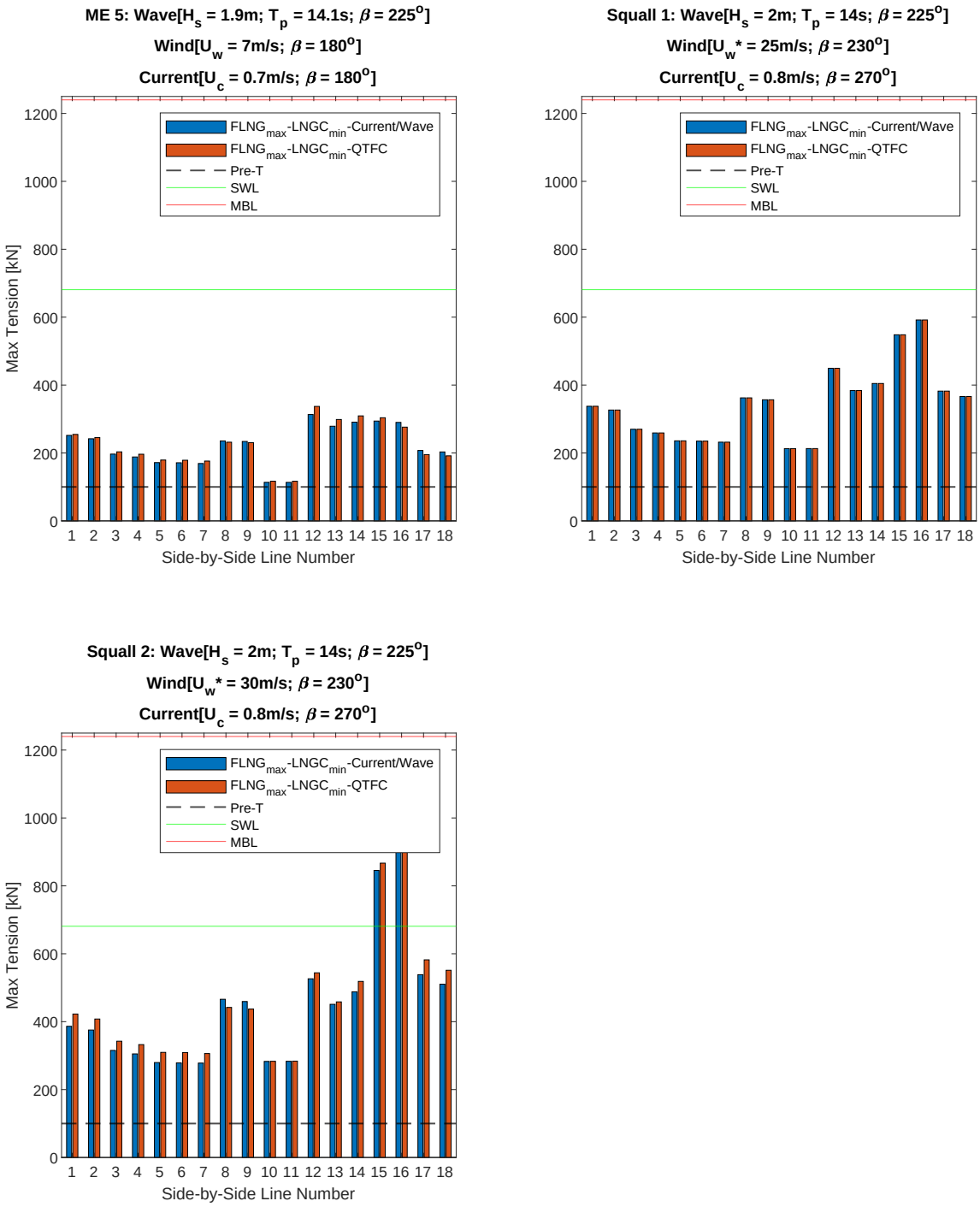

Figure B.30: Line tensions for environmental conditions from ME5 to Squall2 for FLNG-LNGC configuration using QTFC and Newman-wave formulation for assessing second order drift forces

Fender Reaction Forces

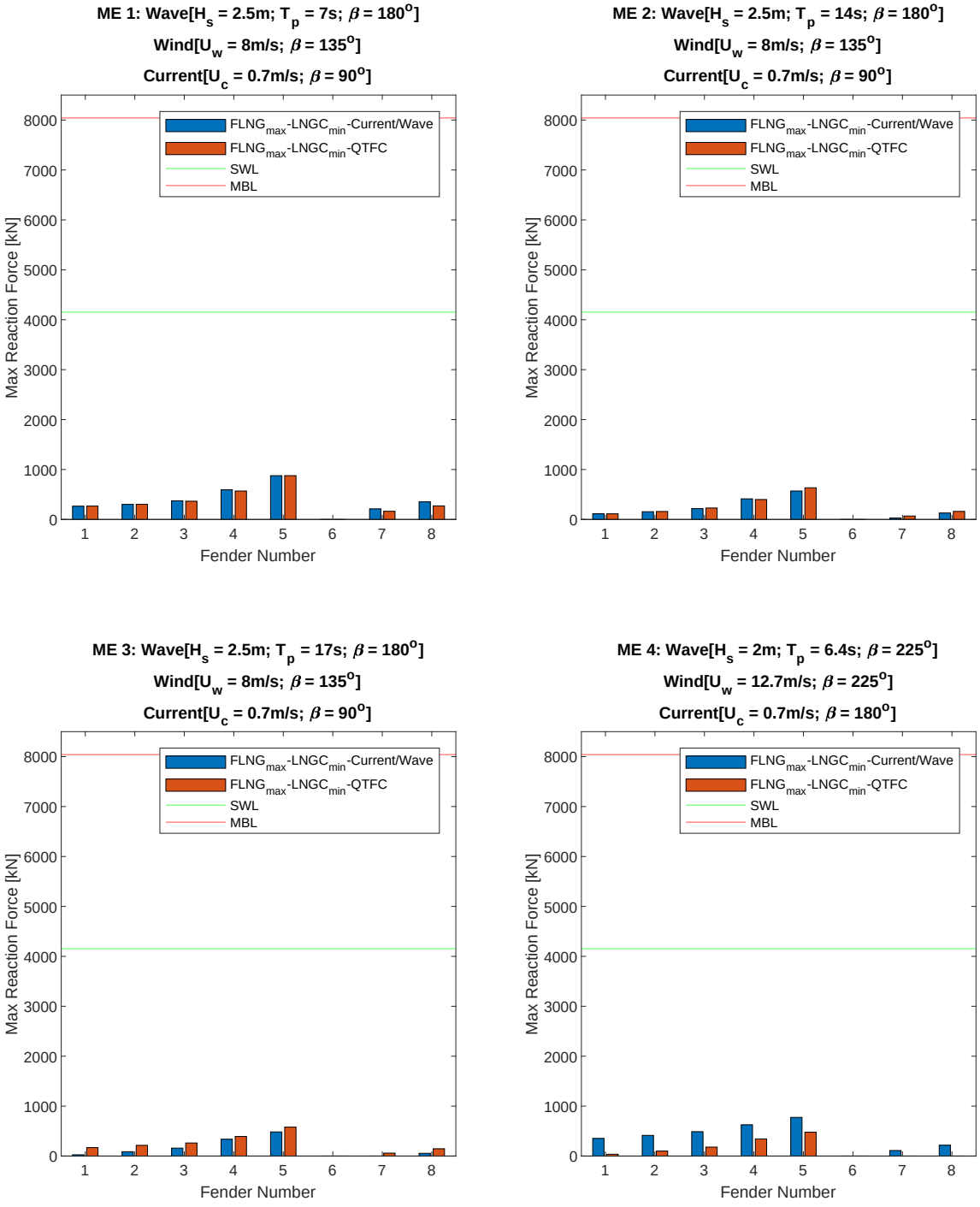

Figure B.31: Fender reaction forces for environmental conditions from ME1 to ME4 for FLNG-LNGC configuration using QTFC and Newman-wave formulation for assessing second order drift forces

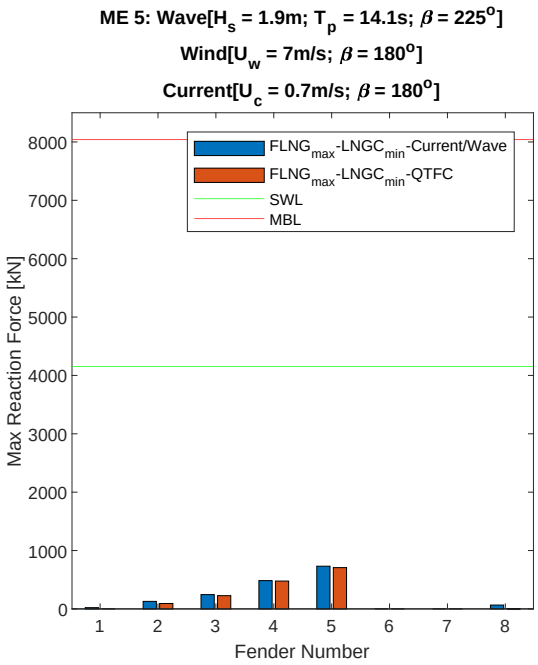

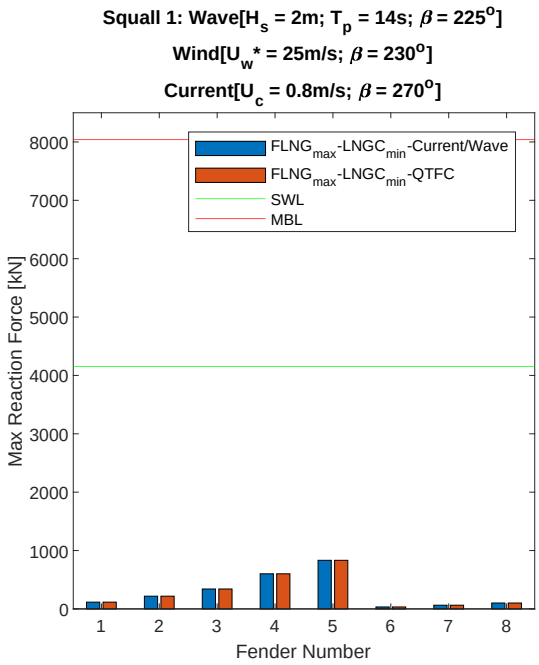

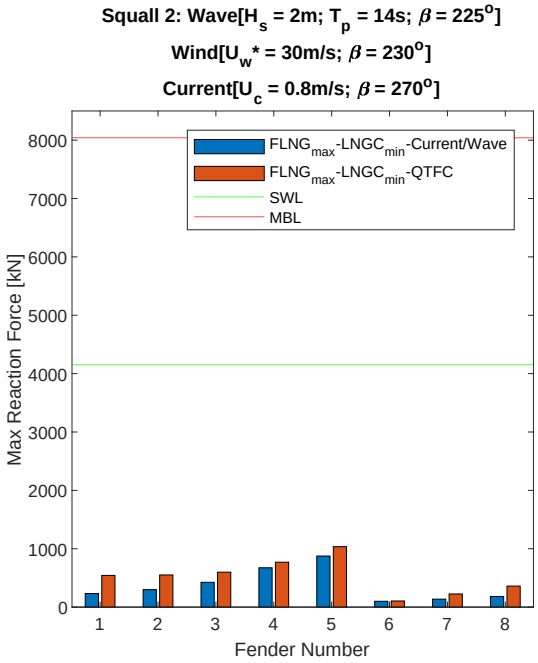

Figure B.32: Fender reaction forces for environmental conditions from ME5 to Squall2 for FLNG-LNGC configuration using QTFC and Newman-wave formulation for assessing second order drift forces

Bibliography

[1] Hielke Brugts Arjan Voogt. Numerical simulations to optimize offshore offloading operations. *Offshore Technology Conference*, pages 5–7, 2010.

[2] Molin B. On the piston and sloshing modes in moonpools. *Journal of Fluid Mechanics*, 2001.

[3] Adri van Dijk Bas Buchner and Jaap de Wilde. Numerical multiple-body simulations of side-by-side mooring to an fpso. *Maritime Research Institute Netherlands*, 2001.

[4] Adri van Dijk Bas Buchner and Jaap de Wilde. The interaction effects of mooring in close proximity of other structures. *Maritime Research Institute Netherlands*, 2004.

[5] F. Rezende C. Brun, D. Coache. Advanced computation of mooring systems.

[6] Yokohama Fender Catalogue. yokohama.com.

[7] Chakrabarti. Handbook of offshore engineering. *Elsevier Ocean Engineering*, 2005.

[8] C.B Chen. Hydrodynamic analysis for offshore lng terminals. *2nd Offshore Hydrodynamics Symposium*, 2005.

[9] DNV-OS-E301. Position mooring. *Offshore Standard*, 2013.

[10] DNV-RP-H103. Modelling and analysis of marine operations. April 2011.

[11] Cummins W. E. The impulse response function and ship motions. *Schiffstechnik*, 9, 1962.

[12] A. K. Ernst & Young and H. A. M. S. ter Tisha. Global lng - will new demand and new supply mean new pricing? page 4, 2013.

[13] Shell International Exploration and BV Production. West africa swell project. May 2004.

[14] Ogilvie T. F. Recent progress toward the understanding and prediction of ship motions. *Proc. 5th Symposium on Naval Hydrodynamics*, 1964.

[15] M. Francois S. Le-Guennec F.Legerstee, C. Morandini. Squall: Nightmare for designers of deepwater west african mooring systems. *International Conference on Offshore Mechanics and Arctic Engineering*, June 2006.

[16] Georgios Gkikas. Seakeeping behavior of an innovative, twin-hull lngfpso design during side by side offloading operations. a numerical and experimental investigation.

[17] Hohn Gould. Hydrodynamic uncertainties associated with flng side by side off take. 2016.

[18] J.A. Pinkster Huijsmans R.H.M. and J.J. de Wilde. Diffraction and radiation of waves around side by side moored vessels. 2001.

[19] Mampaey Offshore Industries. Quick release mooring systems. *The Netherlands*.

[20] Xiao-Bo Chen Jean-Robert Fournier, Mamoun Naciri. Hydrodynamics of two side-by-side vessels experiments and numerical simulations. *Fournier*, page 1, 2004.

[21] W.W.Massie J.M.J. Journee and R.H.M.Huijsmans. Offshore hydromechanics. *Delft University of Technology*, Third Edition:736–739, 2015.

[22] Newman J.N. Application of generalized modes for the simulation of free surface patches in multiple body interactions. *WAMIT Consortium Report*, 2003.

[23] X.B. Chen J.R. Fournier, M.Naciri. Hydrodynamics of two side-by-side vessels - experiments and numerical simulations. 2006.

[24] Fukuda K. Behavior of water in vertical well with bottom opening of ship and its effects ship-motion. *Journal of the Society of Naval Architects of Japan*, 141:107–122, 1977.

[25] KE Kaasen and Mo K. Efficient time-domain model for frequency-dependent added mass and damping. *Proceedings of* 23^{rd} *International Conference on Offshore Mechanics and Arctic Engineering*, 2004.

[26] Thomas Gazzola Louis Diebold and Eric Baudin. Methodology for lng terminals (flng, fsru & lngrv). *The* 6^{th} *Asia-Pacific Workshop on Marine Hydrodymics*, 2012.

[27] Jaap de Wilde Mamoun Naciri, Olaf Waals. Time domain simulations of side-by-side moored vessels lessons learnt from a benchmark test. 2007.

[28] Mun Keun Ha Mun Sung Kim and Byung Woo Kim. Relative motions between lng-fpso and side-by-side positioned lng carrier in waves. *International Offshore and Polar Engineering Conference*, 2003.

[29] Newman N. Marin hydrodynamics. *The MIT Press, Cambridge*, 1977.

[30] OCIMF. Mooring equipment guidelines. 3^{rd} Edition, 2008.

[31] Inga Lehmann R. Barreto Portella, M. de Abreu Grove. Deepwater mooring system design and analysis. a practical overview of various calculation methods.

[32] Massel Stanislaw Ryszard. Ocean surface waves: Their physics and prediction (third edition). pages 3–4, 2017.

[33] sbmoffshore.com. Fleet and operations performances record.

[34] C.A.C. van der et. al. Valk. Chiksan lng marine loading arm enhanced for application in exposed areas. 2004.

[35] C.A.C. van der et. al. Valk. Offloading operability analysis of side-by-side moored lng fpso. *The International Society of Offshore and Polar Engineers*, 2010.

[36] Bureau Veritas.

[37] Bureau Veritas. Ariane theoretical manual. Version 8, 2015.

[38] Malenica . and Chen X.B. On the irregular frequencies appearing in wave diffraction-radiation solutions. *International Offshore and Polar Engineering*, 3:275–294, 1998.

[39] Hong-Chao Wang and Lei Wang. Horizontal hydrodynamic coupling between shuttle tanker and fpso arranged side-by-side. *Ocean Systems Engineering*, 3:275–294, 2013.

[40] Rene H.M.Huijsmans Willemijn H. Pauw and Arjan Voogt. Advances in the hydrodynamics of side-by-side moored vessels. *International Conference on Offshore Mechanics and Arctic Engineering*, 2007.

[41] www.researchimpact.uwa.edu.au. Side by side: offloading lng on the open seas.

[42] Yan S. Ma Q.W. Cheng X. Fully nonlinear simulation of two floating structures in close proximity subjected to oblique waves. 2011.

[43] S. Malenica & J.R.Fournier X.B. Chen, F. Rezende. Advanced hydrodynamic analysis of lng terminals.

[44] Johanna Evans Xiaosen Xu, Prasanta Sahoo and Yanwu Tao. Hydrodynamic performances of fpso and shuttle tanker during side-by-side offloading operation. *Ships and Offshore Structures*, 2019.

[45] HongGun YunHo Kim and SeokKyu Cho. Methodology for lng terminals (flng, fsru & lngrv). *Energy and Power Engineering II*, 2017.

[46] HU Zhi-qiang Zhao Wen-hua, Yang Jian-min. Hydrodynamic interaction between flng vessel and lng carrier in side by side configuration. 2012.